Sérgio Ricardo Pais Carvalho Leite

MODULATING ACTIN DYNAMICS DURING AXONAL FORMATION, GROWTH AND REGENERATION: THE IMPORTANCE OF ADDUCIN AND PROFILIN-1

Tese de Candidatura ao grau de Doutor em Ciências Biomédicas submetida ao Instituto de Ciências Biomédicas Abel Salazar da Universidade do Porto.

Orientadora – Doutora Mónica Mendes Sousa
Categoria – Investigadora Principal
Afiliação – Instituto de Biologia Molecular e Celular, Instituto de Investigação e Inovação em Saúde – Porto

Este trabalho foi financiado pela Fundação para a Ciência e Tecnologia, SFRH/BD/72240/2010 e pela International Foundation for Research in Paraplegia (IRP), Research Grant P140.

Ignoranti quem portum petat, nullus suus ventus est.

If one does not know to which port one is sailing, no wind is favourable.

Lucius Annaeus Seneca

Aos meus Pais.

Ao meu Irmão.

Foram utilizados nesta Tese os artigos publicados ou em vias de publicação:

Leite SC and Sousa MM. The neuronal commitment: why do neurons need a ring? Invited review, Cytoskeleton, *In preparation*

Liz MA*, **Leite SC***, Juliano L, Saraiva MJ, Damas AM, Bur D, Sousa MM. Transthyretin is a metallopeptidase with an inducible active site (2012). Biochem J., 1;443(3):769-78

Leite SC, Sampaio S, Sousa V, Nogueira-Rodrigues J, Pinto-Costa R, Peters LL, Brites P, Sousa MM. The actin-binding protein α-adducin is required for maintaining axon diameter. *Submitted*

Leite SC*, Costa R*, Mendes R, Liz MA, Mar FM, Sousa MM. Profilin is a key mediator in regulating actin dynamics and axon growth. *In preparation*

* Authors contributed equally

Table of contents

Acknowledgements / Agradecimentos

Chegado o final desta aventura resta agradecer a todas as pessoas que tornaram esta tarefa possível. Isto porque apesar do título ser individual, o trabalho final é sempre resultado de uma equipa. Como tal tenho que agradecer à chefe dessa mesma equipa, quem põe toda a máquina a funcionar e que sofre e exalta com todos os planos e resultados que surgem. O meu muito obrigado à Mónica, minha orientadora de há 6 anos e que me aceitou receber no seu grupo e sempre me permitiu explorar a minha veia científica e me forneceu todas as ferramentas para que nascesse esta tese. Obrigado por sempre demonstrar apoio, pela atenção, pela paciência e por ser a pessoa séria que é. Para além de tudo isso, tenho que agradecer também pela excelente companhia nas viagens ao hemisfério sul! Muito obrigado!

Devo também agradecer aos dois companheiros mais sénior desta caminhada, o já Dr(^{2}). Fernando Mar e o futuro Dr. Tiago Silva, que sem dúvida não só são competentes cientistas, mas são sobretudo grandes amigos, grandes companheiros e sempre dispostos a ajudar. Para além do tempo útil de laboratório que partilhámos, também não esquecerei o tempo "inútil", desde as espetaculares partidas até às mais filosóficas discussões sobre os temas mais profundos! Muito obrigado.

Gostaria de agradecer à Márcia Liz, com quem iniciei a minha caminhada científica e que foi sempre não só uma impecável colega de bancada e secretária mas também uma espetacular amiga, companheira de refeições e cafés, com quem dava sempre para discutir todos os assuntos e que foi minha *confidant* boa parte das vezes. Muito obrigado. Como extra, também quero muito agradecer aos restantes membros ND, por ser dos grupos mais bem compostos do mundo da ciência!

Um agradecimento à Vera Sousa, Filipa Franquinho e Ana Rita Malheiro, as restantes companheiras desde o sempre, e que não só são ótimas colegas de bancada mas também boas amigas e que tornaram a viagem bem mais agradável.

Ao Pedro Brites também gostaria de agradecer pela ajuda e pelo apoio, já que é sempre a pessoa a recorrer quando não se sabe algo! É garantido que se volta com resposta garantida, para além de ter sempre uma visão mais além sobre os assuntos,

Não podia deixar de agradecer às meninas que fizeram parte do seu percurso académico comigo, Rita, Joana, Carla, que sempre foram não só interessadas mas também excelentes companheiras.

Aos restantes membros do Nerve, assim como os *former members* (das quais teria de destacar a Telma e Marta, minhas antigas colegas académicas, à Marlene, Catarina Miranda e Carla Teixeira) que foram continuar suas carreiras por esse mundo fora, o meu agradecimento e o voto de futuros sucessos!

Devo também um grande agradecimento à Paula Sampaio, a mais extraordinária *expert* de microscopia de Portugal (e suponho que do planeta!), que sem dúvida foi crucial para conseguir boa parte da data que obtivemos. O meu muito obrigado por toda a ajuda, e também pelos momentos sempre divertidos fora de portas!

Aos restantes serviços e pessoas, nomeadamente o CCGen e o Biotério, o meu muito obrigado.

Gostaria também de agradecer à minha co-orientadora Professora Doutora Maria João Saraiva assim como ao diretor do programa doutoral, o Professor Doutor Eduardo Rocha por toda a ajuda e disponibilidade.

Para além de todos os agradecimentos dentro de portas gostaria de agradecer a uma série de pessoas que partilharam algum do tempo que sobra, quer caríssimos amigos quer de Vila Real quer de Ovar, que obviamente desemprenharam um papel importantíssimo na nobre atividade de sair e beber uns copos, tão necessários!

Para terminar, gostaria de agradecer àqueles que me acompanham não só nestes últimos 6 anos, mas uns 22 anos mais do que isso. Há minha família, sempre preocupada e interessada, o meu muito obrigado pelo apoio e por acharem sempre que o que faço é importante e poderá ser útil para alguém.

À Fabiana eu quero agradecer porque apesar dos altos e baixos que possa existir na vida eu sei que no fundo parte significativa destas 190 páginas tiveram o seu contributo. Talvez não na forma mais óbvia, mas sei que no fundo sempre torce por mim e que aconteça o que acontecer. Se não fosse por mais nada, eu já teria muito a agradecer. O meu muito obrigado.

Por fim, não só o agradecimento mas também a quem dedico esta tese. Por um lado aos meus pais, a quem não devo só os espetaculares 46 cromossomas e nutrientes (que a avaliar pelo fenótipo, foram muitos) que me deram mas também por aquilo que é mais intangível e que me fizeram o que eu sou. O outro agraciado é o meu irmão. Apesar de 9 anos mais novo eu sei que é alguém com quem posso contar para tudo, que pode ser ainda um jovem sonhador mas será um dia um grande homem. E a quem ler esta tese (sem ser obrigado), em parte ou na totalidade, o meu agradecimento!

Summary

The regenerative capacity of the central and peripheral nervous system (CNS and PNS, respectively) is fundamentally different, due to both neuronal intrinsic properties and also to the different environments that CNS and PNS neurons experience. In a generalized way, PNS axons regenerate (successfully) whereas CNS neurons fail to exhibit this ability. Understanding the reasons that result in this differential regrowth capacity is fundamental to design future approaches aimed at promoting robust and everlasting axon regeneration, with the restoration of the original neuronal functions. The conditioning injury model, in which a priming lesion to the peripheral branch of dorsal root ganglia neurons enhances the regenerative capacity of the central branch, is an elegant paradigm to study the neuron-dependent mechanisms that are elicited to promote axon regeneration. Using this model, we identified two actin binding proteins differentially regulated after conditioning, profilin and adducin, which we studied in detail as presented and discussed in this Thesis.

Adducins are a family of actin binding proteins, known for their plus tip capping activity and for enhancing the spectrin/actin interactions, having an overall stabilizer effect towards the actin cytoskeleton. To study the consequences of adducin inactivation in the nervous system, we used α-adducin KO mice as a model of complete adducin absence. Here we show that the lack of adducin leads to progressive axon enlargement and axonal loss. Moreover, α-adducin KO axon actin rings – the recently described submembraneous axonal cytoskeleton composed of actin, spectrin and adducin – were enlarged, although distributed with a regular periodicity. This data raises the exciting prospect that adducins regulate axon diameter and that alterations in this regulation may result in axon degeneration.

In the context of axon regeneration, we show using the conditioning lesion model that adducins are inhibited in the growth cone of regenerating axons. Analysis of the cytoskeleton in this neuronal compartment revealed an increased dynamics/instability when adducin is depleted, with an enhancement of both actin retrograde flow and microtubule growth speed. *In vitro*, this increased cytoskeleton dynamics in the growth cone was translated into a higher regenerative capacity, both in the presence of permissive and non-permissive substrates. Moreover, *in vivo* the absence of adducin increased the regeneration of dorsal column axons after spinal cord injury.

Profilins are small actin binding proteins that catalyze the exchange of ADP to ATP bound G-actin, enabling its incorporation in the barbed end of actin filaments. Our data shows

that profilin-1 activity is significantly increased in regenerating growth cones in the conditioning lesion model, suggesting that this protein positively modulates axon growth. Corroborating this hypothesis, we show that *in vitro*, in the absence of profilin-1, neurons either fail to extend neurites or extend shorter neurites. Moreover, *in vivo*, in two well-established models where successful axon regeneration occurs, the sciatic nerve injury and the conditioning lesion paradigm, the absence of profilin-1 inhibited axon regeneration. Besides, we show that a constitutively active profilin-1 mutant significantly increased axon growth. Finally, our data suggests that profilin-1 acts not only via actin modulation but also possibly by regulating the microtubule cytoskeleton through the GSK3β pathway.

In summary in this Thesis we provide important evidence strongly supporting that the regulation of two actin binding proteins, adducin and profilin, is pivotal to modulate axon growth and regeneration. In the case of adducin, we provide further evidence of its relevance in the control of axon diameter. These findings will certainly be explored in the future to further our understanding of axon biology, and of axon growth and regeneration.

Sumário

A capacidade regenerativa do sistema nervoso central (SNC) e periférico (SNP) é fundamentalmente diferente, quer devido às propriedades neuronais intrínsecas quer ao diferente ambiente que os neurónios do SNC e SNP experienciam. De uma maneira geral os neurónios do SNP regeneram com sucesso enquanto neurónios do SNC falham esse processo. Perceber quais as razões que determinam esta diferencial capacidade de crescimento é fundamental para futuras abordagens que conduzam a uma robusta e bem-sucedida regeneração axonal. O modelo da lesão condicionante, no qual uma lesão primária no ramo periférico dos neurónios dos gânglios das raízes dorsais aumenta a capacidade do ramo central regenerar, é um elegante paradigma para o estudo dos mecanismos neuronais que promovem a regeneração axonal. Utilizando este modelo identificámos duas proteínas ligantes da actina, a profilina e a aducina, as quais foram avaliadas em detalhe, como apresentado e discutido nesta Tese.

As aducinas são uma família de proteínas ligantes da actina conhecidas pela sua função de limitação de incorporação de monómeros da extremidade positiva dos filamentos de actina e por aumentar a interação entre a actina e a espectrina, tendo portanto um efeito de estabilização do citoesqueleto de actina. De forma a avaliar o efeito da sua inativação no sistema nervoso, utilizámos murganhos α-aducina KO como modelo de total ausência de aducina. Neste trabalho demonstrámos que a ausência de aducina leva a um progressivo cenário de alargamento e perda axonal. Para além disso os anéis de actina – que compõem o recentemente descrito citoesqueleto submembranar axonal, composto por actina, espectrina e aducina – estão alargados, apesar de distribuídos com a mesma periodicidade. Estes resultados levantam a interessante hipótese de que a aducina regula o calibre axonal e que alterações nessa regulação podem levar a um cenário de degeneração.

No contexto da regeneração axonal demonstrámos que no modelo de lesão condicionante as aducinas estão inibidas nos cones de crescimento dos axónios a regenerar. A análise do citoesqueleto no cone de crescimento demonstrou que existe um aumento da dinâmica/instabilidade da actina com a depleção da aducina, com um aumento do transporte retrogrado da actina e da velocidade de crescimento dos microtúbulos. Análises *in vitro* revelaram que o aumento da dinâmica do citoesqueleto traduz-se num aumento de capacidade de crescimento dos axónios, quer em condições permissivas quer não permissivas. Para além do aumento do crescimento *in vitro*, a análise à regeneração *in vivo* demonstrou que a ausência de aducina leva a um aumento

da capacidade de crescimento dos axónios do trato dorsal após lesão da espinhal medula.

As profilinas são pequenas proteínas ligantes da actina que catalisam a conversão da actina ligada ao ADP para actina ligada ao ATP, permitindo a incorporação dos monómeros na extremidade positiva dos filamentos de actina. A nossa análise demonstrou que a atividade da profilina-1 está claramente aumentada nos cones de crescimento dos axónios regenerantes no modelo de lesão condicionante, sugerindo um efeito modulador positivo para a regeneração axonal. Confirmando esta hipótese, neurónios depletados *in vitro* de profilina-1 falham a estender neurites, ou estendem em menor escala. Para além disso, a análise *in vivo* de dois modelos de regeneração bem-sucedida, a lesão do nervo ciático e a lesão condicionante na espinhal medula demonstraram que a ausência de profilina-1 inibe a regeneração axonal. Para além do mais, demonstrámos que a forma constitutivamente ativa da profilina-1 aumenta significativamente o crescimento axonal. Por fim, os nossos dados indicam também que a profilina não exerce o seu efeito pró-neuritogénico apenas via actina, mas também através da modulação do citoesqueleto dos microtúbulos, via GSK3β.

Em resumo, nesta Tese obtivemos importantes evidências que suportam que a regulação de duas diferentes proteínas ligantes da actina, profilina e aducina, são boas candidatas para modularem o crescimento axonal e a regeneração. No caso da aducina demonstrámos também que terá um papel importante no controlo do diâmetro axonal. Estes resultados irão certamente ser explorados no futuro para perceber melhor a biologia axonal, o crescimento axonal e regeneração.

Abbreviations List

ABP(s) – Actin Binding Protein(s)

ADF – Actin Depolymerizing Factor

AIS – Axon Initial Segment

AKT - Protein Kinase B

ALS – Amyotrophic Lateral Sclerosis

cAMP – Cyclic Adenosine Monophosphate

Cfl1 – Cofilin-1

CL – Conditioning Lesion

CNS – Central Nervous System

CSF - Cerebrospinal fluid

CSPGs - Chondroitin Sulphate Proteoglycans

CST – Corticospinal tract

CT-B – Cholera Toxin subunit B

DIV – Day(s) *in vitro*

DRG – Dorsal Root Ganglia

EB3 – End-Binding protein 3

ERK - Extracellular signal Regulated Kinase

Fl – Floxed

GAN – Giant Axon Neuropathy

GFP – Green Fluorescence Protein

GSK3β – Glycogen Synthase Kinase 3 β

HDAC – Histone Deacetylase

KO – Knock-out

MAG - Myelin-Associated Glycoprotein

MAI - Myelin Associated Inhibitors

MAP – Microtubule Associated Protein

Abbreviations List

MARCKS – Myristoylated Alanine-Rich C kinase Substrate

MT – Microtubules

ND – Non detected

NF – Neurofilaments

NMJ – Neuromuscular Junction

NS – Not statistic

OMgp - Oligodendrocyte Myelin Glycoprotein

PDK1 - Phosphoinositide-dependent kinase-1

Pfn – Profilin

PI3K - Phosphoinositide 3-kinase

PIP_2 - $PI(4,5)P_2$

PKA – Protein Kinase A

PKC – Protein Kinase C

PLL – Poly-L-Lysine

PLP – Poly-L-Proline

PNS – Peripheral Nervous System

PTM – Post Transcriptional Modifications

RAG – Regeneration Associated Genes

RBC – Red Blood Cells

RFP – Red Fluorescence Protein

ROCK – Rho-associated kinase

SCI – Spinal Cord Injury only (In opposition to CL)

ShRNA - Small Hairpin RNA

SiR-Actin - Silicon Rhodamine Actin

SLICK - Single-Neuron Labeling with Inducible Cre-mediated Knock-out

SMA – Spinal Muscle Atrophy

STED – Stimulated Emission Depletion

STORM – Stochastic Optical Reconstruction Microscopy

TTR - Transthyretin

WD – Wallerian Degeneration

WT – Wild Type

YFP – Yellow Fluorescence Protein

Introduction

I- The neuronal cytoskeleton

1- Neuronal polarization and axon formation

Neurons are the basic unit of the nervous system and rely on their shape, and on their high polarization, to perform their functions. Most neurons have a typical organization where a round cell body has initially thin processes extending: several usually branched and small processes – the dendrites; and a long and less branched process, the axon. The neuron morphology is fundamental for the information flow. Dendrites receive synaptic input that is latter integrated at the cell body and propagated through the axon, being transmitted to the next neuron/cell through the synapses (Neukirchen and Bradke, 2011). What exact processes drive this polarization is a matter of high debate, although some key events are already established. Hippocampal neuron cultures are a great tool to study the events of process extension and neuronal polarization (Kaech and Banker, 2006), as is depicted in figure 1.

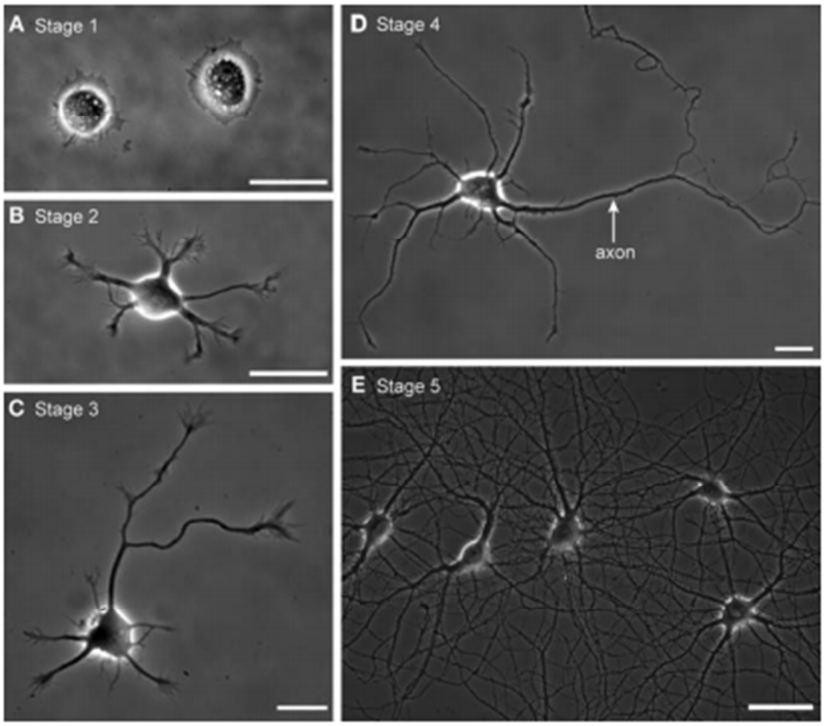

Figure 1. The polarization process in cultured hippocampal neurons. Just after plating neurons adhere to the substrate and start attempting to extend small processes called neurites (A-B). These neurites will generate then an axon and several dendrites (C-D), which will eventually develop synapses *in vitro* (E). For that reason the characteristic capacity of hippocampal neurons to recapitulate the polarization steps *in vitro* is useful in several studies as in studies of axon regeneration, polarization and synapse dynamics. From (Kaech and Banker, 2006).

Embryonic hippocampal neurons in culture undergo 5 robust stages of differentiation. In the first 6 hours after plating neurons are spherical cells that extend lamellipodia, generating the known fried-egg shape – stage 1. The transition to stage 2 is characterized by the initiation of small and thin processes called the neurites that are the precursors of the future axon and dendrites. For symmetry to be broken, the local instability in the actin cytoskeleton is fundamental (Bradke and Dotti, 1999; Flynn et al., 2012). Recent studies revealed the crucial role of actin retrograde flow in the cortical cytoskeleton to generate the gaps in which microtubules are able to protrude towards the cell membrane (Flynn et al., 2012). For the early steps of neuritogenesis the activity of the actin binding proteins (ABPs) Actin Depolymerizing Factor (ADF)/Cofilin, which are responsible for depolymerizing and severing the actin filaments (F-actin), is fundamental (Flynn et al., 2012). Reinforcing the importance of the destabilization of the cortical actin cytoskeleton in neurite generation and extension, the addition of the actin depolarizing agent latrunculin B allows the increased formation of neurites, as it promotes the capacity of microtubules to protrude (Bradke and Dotti, 1999; Flynn et al., 2012). Conversely, the addition of jasplakinolide, which inhibits actin dynamics, abolishes the process of extension (Flynn et al., 2012).

The stage 2 processes are highly dynamic and present several rounds of extension and retraction. In the second day *in vitro* (DIV) one of the processes increases dramatically in size while the others arrest their growth – this event is the beginning of stage 3. At this point neurons establish the process that will elongate and generate the axon and the dendrites. Interestingly, if the growing axon is severed at this stage, another process will be assumed as the axon and will start elongation (Gomis-Ruth et al., 2008). During the elongation process, growth cone like waves enriched in actin move from the cell body to the axon tip, resulting in the supply of actin and associated proteins to the extending process (Flynn et al., 2009). Stages 4 and 5 are characterized by the outgrowth of dendrites and synapse formation (Kaech and Banker, 2006).

It is important however to keep in mind that the embryonic cultures of hippocampal neurons are performed with polarized post-mitotic cells, which at the time of plating were already expressing proteins that are involved in the polarization program and for that reason these cells may keep some aspects of the original polarization (Polleux and Snider, 2010). Although hippocampal neuron cultures are suitable to understand the cell biology events that lead to polarization, they do not reflect exactly the different environment that neurons face during development. In nervous system development, for polarization to occur, there are three main relevant factors: extracellular cues, intracellular signaling and the subcellular organelle localization (Lewis et al., 2013). *In vivo* axonal

initiation is different from what occurs *in vitro* in hippocampal culture models (Polleux and Snider, 2010). Usually neurons migrate long distances after exiting the cell cycle. While migrating, cortical neurons start extending the processes that will generate the axon and dendrites, as shown in figure 2. In the case of the retinal ganglion neurons and bipolar cells from the retina, they inherit the polarization program from progenitor cells (Barnes and Polleux, 2009). In the case of long migrating cerebellar granule neurons and hippocampal pyramidal neurons, the polarity is achieved during migration (Polleux and Snider, 2010).

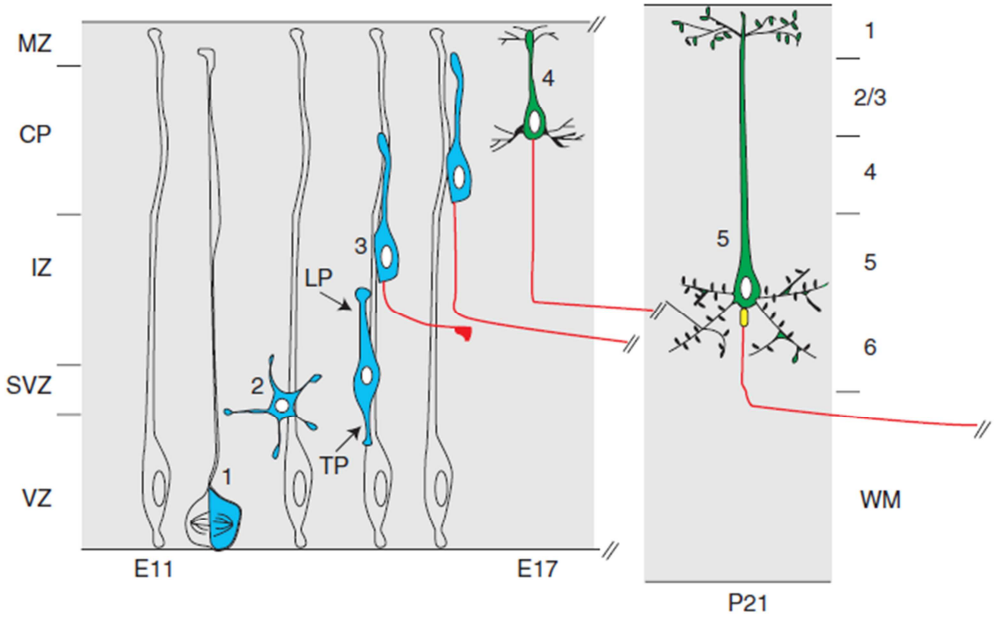

Figure 2. *In vivo* neuronal polarization. The polarization of pyramidal neurons is established during the migratory process, in the late embryonic stage. The trailing process (TP) and the leading process (LP) are then converted in axon and dendrites, respectively. The neuron is only fully matured in the first weeks after birth, exhibiting then the typical axon initial segment (AIS) (in yellow) and the dendritic spines (in grey). Taken from (Polleux and Snider, 2010).

2- The components of the neuronal cytoskeleton

The neuronal cytoskeleton is fundamental for the polarization process. The neuronal cytoskeleton is composed by microtubules, actin filaments and neurofilaments. Regulation of each of these components is crucial for polarization and for axonal extension.

a. Neurofilaments

Neurofilaments (NF) are intermediate filaments with approximately 10nm, abundant in neurons. NFs are fundamental for several neuronal processes: they mediate radial growth of axons, the development and maintenance of the axon caliber and they are fundamental

for electric impulses (Yuan et al., 2012). NFs are composed by 4 different forms: neurofilament heavy, medium and light, and either α-internexin or peripherin, in the central nervous system (CNS) or peripheral nervous system (PNS), respectively (Yuan et al., 2012). NFs are mostly synthetized in the cell body and transported by the slow component of axonal transport, although no detailed mechanism is known (Yuan et al., 2012). NFs are regulated by post-translational modifications such as phosphorylation, glycosylation, nitration oxidation and ubiquitination (Yuan et al., 2012).

Supporting their importance in neuron biology, dysregulation in NF organization is present in several neurodegenerative disorders such amyotrophic lateral sclerosis (ALS) (Manetto et al., 1988), Charcot-Marie-Tooth disease (Abe et al., 2009), neurofilament inclusion disease (Perrot and Eyer, 2009), giant axonal neuropathy (GAN) (Ganay et al., 2011; Monaco et al., 1985), diabetic neuropathy (Fernyhough and Schmidt, 2002), spinal muscular atrophy (SMA) (Cifuentes-Diaz et al., 2002), spastic paraplegia (Wang and Brown, 2010), Alzheimer's disease (Perrot and Eyer, 2009) and Parkinson's disease (Goldman et al., 1983).

b. Microtubules

Microtubules (MT) are fundamental for the neuronal cytoskeleton. MT stabilization and dynamics s is crucial for the axon/dendrite specification and intracellular transport (Janke, 2014; Janke and Kneussel, 2010). MTs are composed by cylinders of 13 protofilaments, composed of polarized α/β heterodimers. While α-tubulin is always bound to GTP, in β-tubulin GTP is converted to GDP after incorporation into the filament (Desai and Mitchison, 1997). MTs are intrinsically dynamic and polarized structures, with a plus and a minus end. Polymerization and depolymerization occurs preferentially in the plus tip. Depolymerization in the plus tip occurs in the form of catastrophe events that lead to shrinkage of MTs (Desai and Mitchison, 1997). The MT net growth is the result of cycles of polymerization and catastrophe. Therefore the regulation of these two events is crucial and is depicted in figure 3.

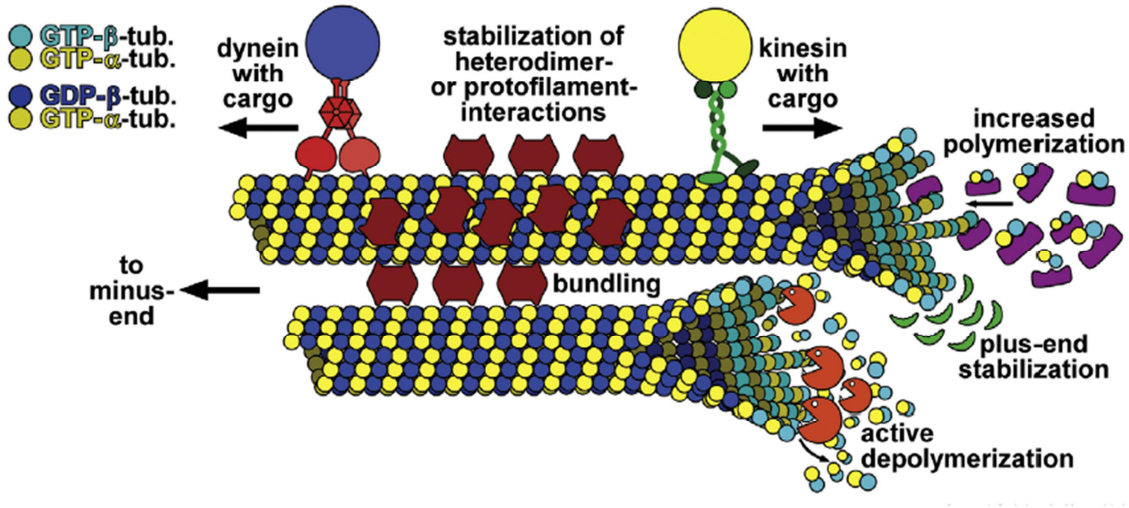

Figure 3. Structure and regulation of microtubules. Microtubules are dynamic structures with increased polymerization and depolymerization in the plus tip. The balance between the two events will determine the net increase or decrease in filament size. The regulation of the different microtubule binding proteins, as well as its post-transcriptional regulation will impact filament size and transport through the MTs (Witte and Bradke, 2008).

In neurons, MTs have an important role in the polarization process. MTs in the axon are more stable than in dendrites, with the exception of the microtubules present in the tip of the axon, the growth cone (Witte and Bradke, 2008). Several proteins are responsible for this duality in the axon and dendrites. Collapsin response mediator 2 is a protein involved in the polymerization of MTs: its overexpression leads to increased number of axons and dominant-negative mutants abolish axon formation (Kimura et al., 2005). In axons the plus tip of the MT is the place of increased instability. The plus-end binding proteins are good candidates for mediating the growth rate of MTs and thereby axonal extension (Neukirchen and Bradke, 2011). Indeed, plus-end binding proteins such as adenomatous polyposis complex and cytoplasmatic linker protein 170 are responsible for decreasing the catastrophe rate and increase rescue (Neukirchen and Bradke, 2011).

Microtubule associated proteins (MAPs) are important for the regulation of MTs in neurons, where MAPs are heavily expressed (Dehmelt and Halpain, 2005). Tau and MAP2 stabilize and bundle MTs and also interact with actin (Tahirovic and Bradke, 2009). Tau and MAP2 are fundamental for axon formation, as suggested by knockdown experiments (Caceres and Kosik, 1990; Caceres et al., 1992). However, as suggested in Tau and MAP2 KO animals where no neuronal polarity deficits exist, the function of MAPs is probably redundant in this context (Dehmelt and Halpain, 2005).

MTs are more dynamic in dendrites than in the axon shaft. Thereby, another process to regulate the axon/dendrite specification is to increase the instability in dendritic MTs.

Stathmin/Op18 is a MT destabilizing protein that is active in all neurites with exception of the axon (Watabe-Uchida et al., 2006; Wittmann et al., 2004). Moreover it is inhibited by phosphorylation by the Rac-1-GEF DOCK7, which is axonal specific. Overexpression of DOCK 7 leads to the formation of multiple axons whereas constitutively active Stathmin/Op18 leads to the abolishment of axon formation (Watabe-Uchida et al., 2006).

Besides the regulation by MT binding proteins, MTs have two more different levels of regulation, derived from the expression of different α and β tubulin forms in a cell-specific fashion and as well as of their complex posttranscriptional regulation (Janke, 2014). The expression of the different tubulin isotypes is both cell and temporal diverse. Some cell-specific MTs require the expression of different tubulin forms. This occurs in MTs of the ciliary axonemes (Raff et al., 2008; Renthal et al., 1993); neuronal MTs (Denoulet et al., 1986; Joshi and Cleveland, 1989) and MTs of the marginal band of platelets that have specific β-tubulin forms (Schwer et al., 2001). However the greater level of heterogeneity is conferred by post-transcriptional modifications, represented in figure 4.

Tubulin post-transcriptional modifications (PTM) include polyamination, phosphorylation, acetylation, polyglutamylation, polyglycylation, detyrosination and retyrosination and C-terminal deglutamilation (Janke, 2014; Janke and Kneussel, 2010).

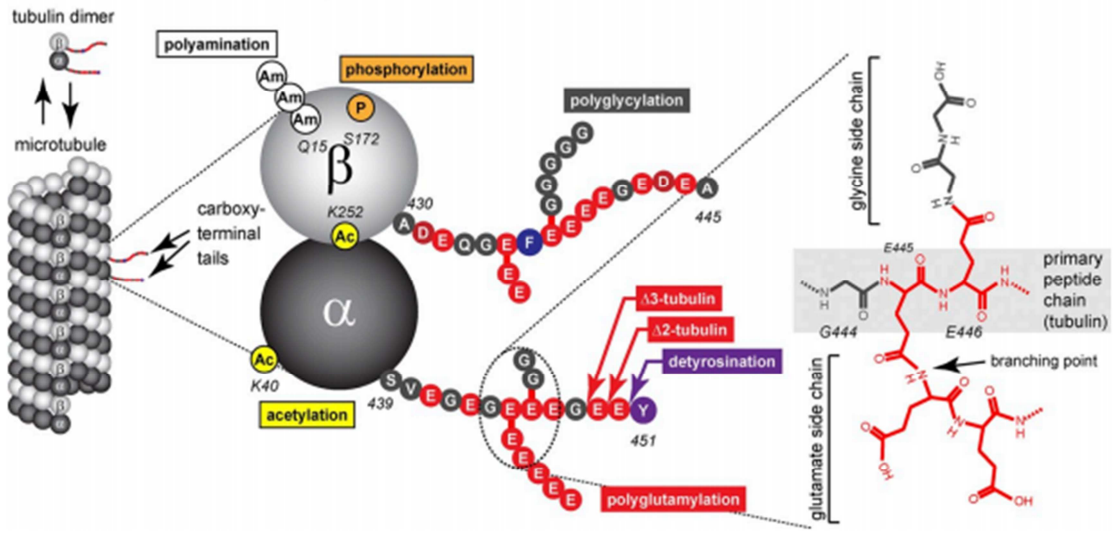

Figure 4. Posttranscriptional modifications in tubulin. Microtubules are composed by αβ tubulin protofilaments. Both α and β residues can be posttranscriptionally modified. As represented, the events of polyamination, phosphorylation and acetylation occur in the MT lattice, whereas the other posttranscriptional modifications are in the tubulin tails, namely polyglutamylation, polyglycylation, detyrosination a C-terminal deglutamilation. From (Janke, 2014)

Tubulin acetylation in Lysine 40 is usually accepted as having a stabilizing effect, since it is enriched in stable MTs, such as those in the axon shaft. Tubulin acetylation has been associated with increased anterograde transport given improved kinesin-1 binding to microtubules. However the mechanism of stabilization is not yet understood since it causes no major ultrastructural changes of the MTs (Howes et al., 2014). The regulation of acetylation is performed by the histone deacetylase family member 6 (HDAC6) (Rivieccio et al., 2009), NAD-dependent deacetylase sirtuin-2 (Maxwell et al., 2011; North et al., 2003) and by the acetyl transferase α-Tat1 (Howes et al., 2014), which specifically acetylates α-tubulin at Lysine 40. In neurons, HDAC6 inhibition is responsible for increased neurite outgrowth, inclusively in the inhibitory presence of myelin (Rivieccio et al., 2009). However, recent and contradictory data suggests that inhibitors of tubulin acetylation, as anacardic acid, increase axonal outgrowth in adult Dorsal Root Ganglia (DRG) neurons (Lin et al., 2015). Tubulin acetylation is associated with axon-dendrite differentiation (Witte et al., 2008). During the axonal extension period the axonal MTs are more acetylated than dendritic MTs, as is visible in figure 5. Interestingly, the administration of taxol, a microtubule stabilizing drug leads to the growth of multiple axon like processes (Witte et al., 2008), and facilitates the outgrowth of neuronal processes in adult DRG neurons (Sengottuvel et al., 2011).

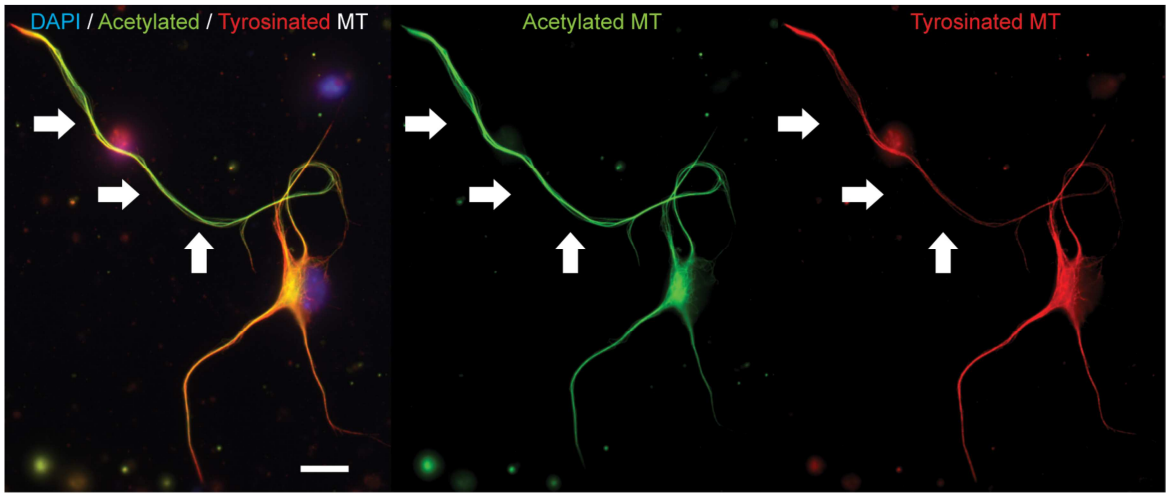

Figure 5. Microtubule acetylation is enriched in axons of polarized (DIV3) mouse hippocampal neurons. Axons (highlighted with white arrows) have increased levels of acetylated tubulin (in green) when compared to dendrites (smaller processes). Tyrosinated (more dynamic, in red) tubulin is found in all neurons, namely in the growth cone of the axon. Scale: 10µm.

Tubulin detyrosination and re-tyrosination are reversible reactions (Arce et al., 1975; Hallak et al., 1977). Tyrosinated MTs are usually associated with a dynamic cytoskeleton, whereas detyrosinated MTs are stable. The C-terminal deglutamylation is an irreversible

PTM, since no retyrosination can occur (Janke, 2014). Reversibly, for deglutamylation to occur, detyrosination of tubulin is required. The C-terminal deglutamylation, also known as Δ2-tubulin given the lack of the two last amino acids, is particularly enriched in aged neurons (Paturle-Lafanechere et al., 1994) and cytosolic carboxypeptidases are the enzymes responsible for this reaction (Kalinina et al., 2007). In neurons, polyglutamylation - when secondary glutamate side chains are formed on γ-carboxyl groups of glutamate residues in a protein (Janke, 2014) - can also occur, namely during differentiation (Audebert et al., 1993). Despite the enrichment of polyglutamylation in neurons, mice lacking polyglutamylase in the brain have no major impairments (Ikegami et al., 2010). Conversely in mice with impaired deglutamylase function (deglutamylases are proteins from the cytosolic carboxypeptidase family), as is the case of the *pcd* (Purkinge cell degeneration) mouse (Mullen et al., 1976), that has mutations in cytosolic carboxypeptidase 1, neurodegeneration, related with the perturbation of axonal transport occurs (Maas et al., 2009). The other PTM are thought to have no major roles in neurons (Janke, 2014; Janke and Kneussel, 2010).

c. Actin

Actin is a major component of the neuronal cytoskeleton, specially enriched in subcellular components such as the growth cone, dendritic spines and the AIS. Actin cytoskeleton dynamics plays a crucial role in neurons, mediating cellular structures such as lamellipodia, filopodia, stress fibers and focal adhesions (Neukirchen and Bradke, 2011). An important characteristic in all these processes is the dynamic transition between monomeric and filamentous actin and the asymmetry of the filament. Actin polymerization occurs preferentially at the fast growing end, the “barbed end”, when it is in the ATP-globular-actin state (ATP-G-actin), and depolymerization occurs in the opposite site of the filament, the “pointed end”, which is usually in the ADP-bound state (Carlier et al., 1987; Korn et al., 1987). These dynamics are regulated by the intrinsic proprieties of actin, its interaction with the environment and by the presence of the ABPs. ABPs closely interfere with the polymerization/depolymerization rates, severing, capping, nucleation and crosslinking of filamentous actin (Lee and Dominguez, 2010). Figure 6 represents the dynamic regulation of the actin filaments.

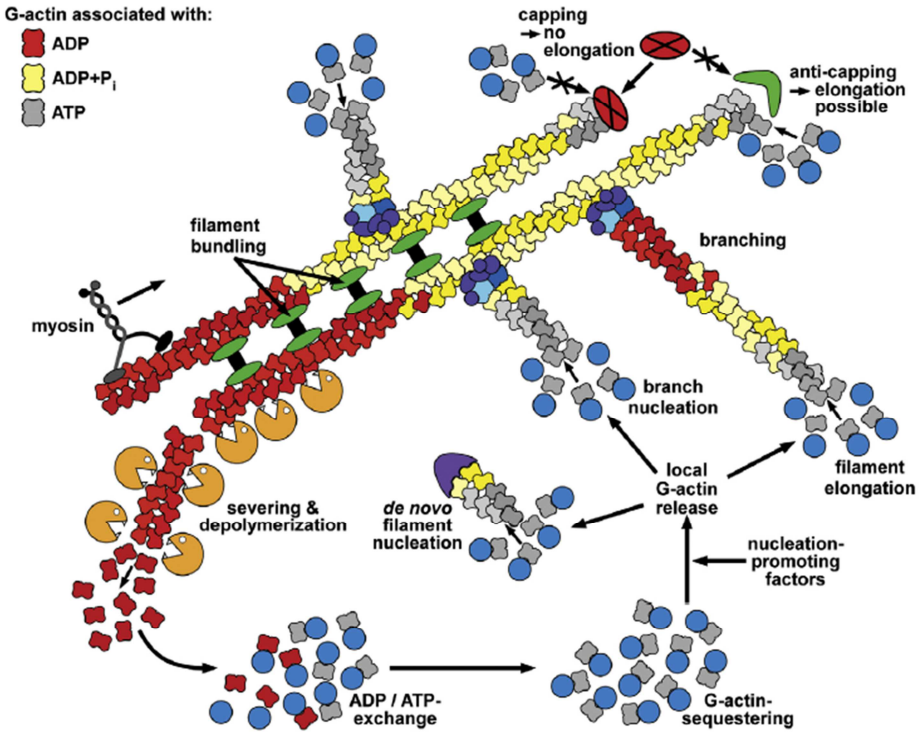

Figure 6. Actin regulation by actin binding proteins. Actin is present both in the form of monomers and filaments. The regulation of filament stability or severing, polymerization and depolymerization or branching, or monomer availability for nucleation determines how the actin cytoskeleton is controlled and assembled. Neurons critically depend on the actin binding proteins to the polarization process (Witte and Bradke, 2008).

3- The growth cone

The growth cone is the structure found at the tip of extending axons, characterized by its enrichment in actin and its dynamic properties. Although actin enrichment is the hallmark of the growth cone, MTs also play a very important function, in both maintaining its structure and dynamism. The growth cone is composed by three different domains, the peripheral domain (P-domain), the transition domain (T-domain) and the central domain (C-domain), as is depicted in figure 7.

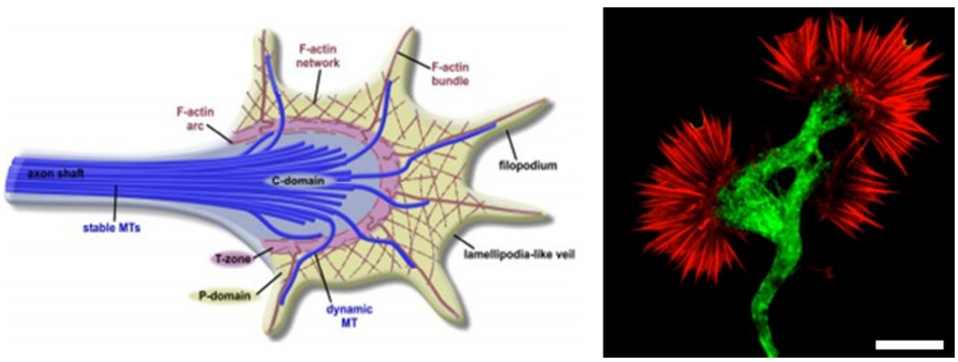

Figure 7. The growth cone. The growth cone is the structure responsible for the extension and guidance of the axon. The organization of the growth cone in three different domains is based in its composition. (Left) In

the most peripheral part, the P-domain, actin is enriched in the form of both filopodia and lamellipodia and few but highly dynamic (tyrosinated) MTs protrude along filopodia. Conversely the central domain, C-domain, as the rest of the axon, is composed by bundled and stable MTs and serves as a track to the vesicles and organelles travelling to and from the growth cone. In the intermediate part there is the transition zone, T-domain, where actin is organized in the form of a hemicircumferential ring, perpendicular to the F-actin bundles. The contractility of this structure in the T-domain is fundamental for the movement of the growth cone. (Right) An *in vitro* hippocampal neuron growth cone stained with phalloidin, in red (which stains filamentous actin) and βIII-tubulin, in green (the specific neuronal β tubulin form). Scale bar 2µm. From (Lowery and Van Vactor, 2009)

The role of the growth cone in neurons is to control both the rate and the direction of growth. In these mechanisms MTs and actin, have a crucial role. Actin in the growth cone is extremely abundant, with a concentration of up to 100 µM (Gomez and Letourneau, 2014), 1000-fold higher than the critical concentration required for polymerization (Pollard and Borisy, 2003). Interestingly, half of the actin in the growth cone is not polymerized (Letourneau, 2009). It is noteworthy that in developing neurons, *in vitro*, the growth cone from the future axon is more dynamic and larger than the growth cones on dendrites (Stiess and Bradke, 2011). In the P-domain, filamentous actin (F-actin) is present in the form of lamellipodia and filopodia. These two forms of actin are the ones responsible for pushing the membrane forward during axonal extension (Gomez and Letourneau, 2014). For filament growth the supply of G-actin monomers is required as well as free barbed ends for monomer incorporation.

For the supply of G-actin, two proteins are crucial: profilin, a protein that is required for the conversion of ADP-G-actin to ATP-G-actin and β-thymosin, which sequesters actin but releases it when the concentration of free G-actin decreases, refreshing the actin pool for dynamics (Lee et al., 2013). Interestingly, profilin-1 (Pfn1) knockdown mice have decreased actin retrograde flow in the growth cones (Lee et al., 2013). Besides the availability of G-actin in the leading edge, actin barbed ends must be available for monomer incorporation. As such, the capping of barbed ends is a limiting event for the actin dynamics of the growth cone (Dent et al., 2011). The capping activity of capZ is known to block incorporation of new monomers (Xu et al., 1999), to impair motility and promote P-domain addition (Dent et al., 2011). Proteins such as ena, Vasp and Ev1 inhibit the capping of F-actin, creating continuously protruding filopodia (Gomez and Letourneau, 2014). The increase in barbed ends can also be generated by the Arp2/3 complex and formins, in two different mechanisms. Arp2/3 complex nucleates a new filament from a pre-existing one. The new actin filament is generated as a 70º branch. Formins nucleate actin monomers from the freely G-actin pool (Mellor, 2010). For that reason, Arp2/3

complex is related with lamellipodia formation and formins with filopodia growth (Mellor, 2010). Even the ADF/cofilin family that depolymerizes and severs the actin filaments can, together with ARP 2/3 complex, generate new barbed ends that will lead to lamellipodia formation (Tania et al., 2013). In the growth cone, ezrin-radixin-moesin proteins are responsible to bind filopodia and lamellipodia to the plasmalemmal proteins (Letourneau, 2009), namely L1, a neuronal adhesion molecule. In the absence of ezrin-radixin-moesin proteins, F-actin is greatly diminished in the growth cones (Marsick et al., 2012).

When extending, the depolarization and polarization rates are not even in the growth cone (Dent and Gertler, 2003). During extension, the polarization and depolarization cycles have increased rates in the leading margin of the growth cone, whereas in the lateral parts of the leading edge only depolymerization, but not polymerization, occurs. In fact, the extending growth cones turnover their actin cytoskeleton in minutes (Van Goor et al., 2012). In that process the ADF/Cofilin family has a critical role in degrading F-actin and in increasing the pool of G-actin. Gelsolin, another F-actin severing protein has a minor role in growth cones (Dent et al., 2011).

4- Actin retrograde flow

The actin filaments in the growth cone are transported backwards from the leading edge to the T-domain, in a process called actin retrograde flow. Actin protrusions are resultant of the balance of both protrusive activities, such as the incorporation of new monomers in the barbed-ends, and actin crosslinking by ABPs, and anti-protrusive activities, such ADF/Cofilin mediated depolarization and the forces generated by the myosin motors, in the so called actin retrograde flow (Gomez and Letourneau, 2014). This mechanism allows the growth cone to control its progression. If the protrusive forces are increased, actin polymerizes and pushes the membrane forward, whereas if the anti-protrusive forces are increased the actin filaments are withdrawn. If the polymerization rate exceeds retrograde flow (which averages 3–6 mm/min), then the growth cone protrudes (Dent et al., 2011). The molecules responsible for the retrograde flow are the myosin motors (Lin et al., 1996). From the myosin family, myosin II is the form that is more enriched in the P-domain. Myosin II is a barbed-end directed motor protein that is responsible for limiting and guiding growth (Medeiros et al., 2006). Interestingly myosin II is regulated by Rho kinase, a known inhibitor of axonal extension (Gallo, 2006). Knockdown of myosin II results in increased axonal outgrowth, namely in non-adherent substrates (Yu et al., 2012). Some myosin II activity is however required for supplying the inner P-domain with

F-actin to be severed and recycled (Gomez and Letourneau, 2014). The filaments retrogradely transported are from the protrusions that lack adherence to other cells or matrices. The accumulation of transported filaments can however block the protrusion of MTs. The actin filament extension and consequent protrusions is represented in figure 8.

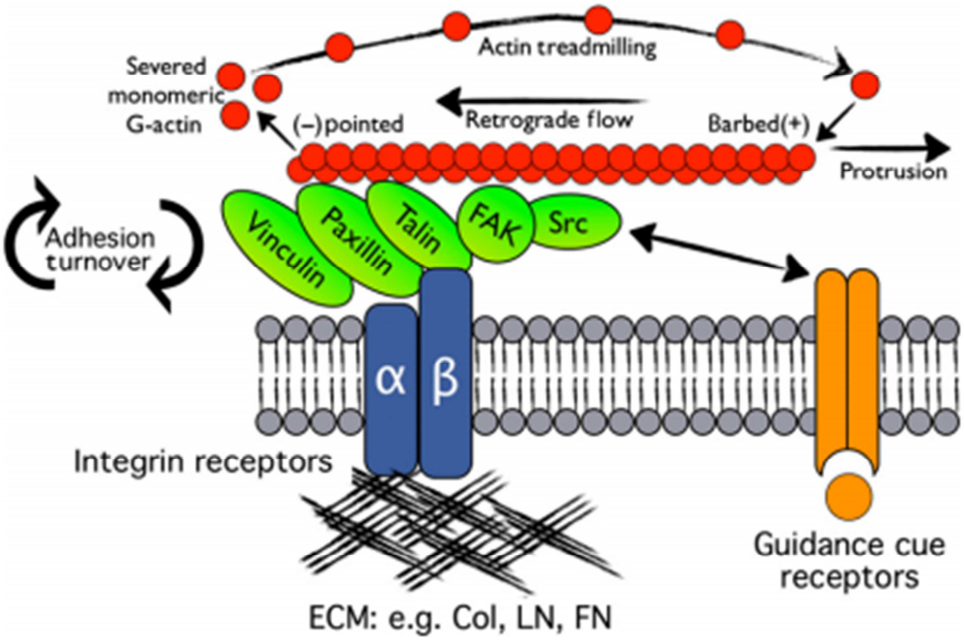

Figure 8. The actin protrusions in the growth cone and their interaction with substrates. In response to the guidance cues, and under permissive substrates such as collagen, laminin or fibronectin αβ, integrin assembly occurs. Integrin then binds to a series of scaffolding proteins, such as talin, paxilin and viculin, focal adhesion kinases (FAK) and the Proto-oncogene tyrosine-protein kinase Src (Src), which are regulators of the process. In an adherent substrate actin incorporation in the barbed end will generate motion against the cell membrane and protrusions will extend the growth cone forward. If the substrate is not permissive the reaction force generated by the cell membrane with the activity of myosin II will increase the actin retrograde flow, and protrusion velocity will decrease. From (Gomez and Letourneau, 2014).

The growth cone regulation is fundamental for the steering process, is required to the proper migration of the axon while extending, and for the enervation of the proper destination. The process that controls the extension direction is summarized in figure 9.

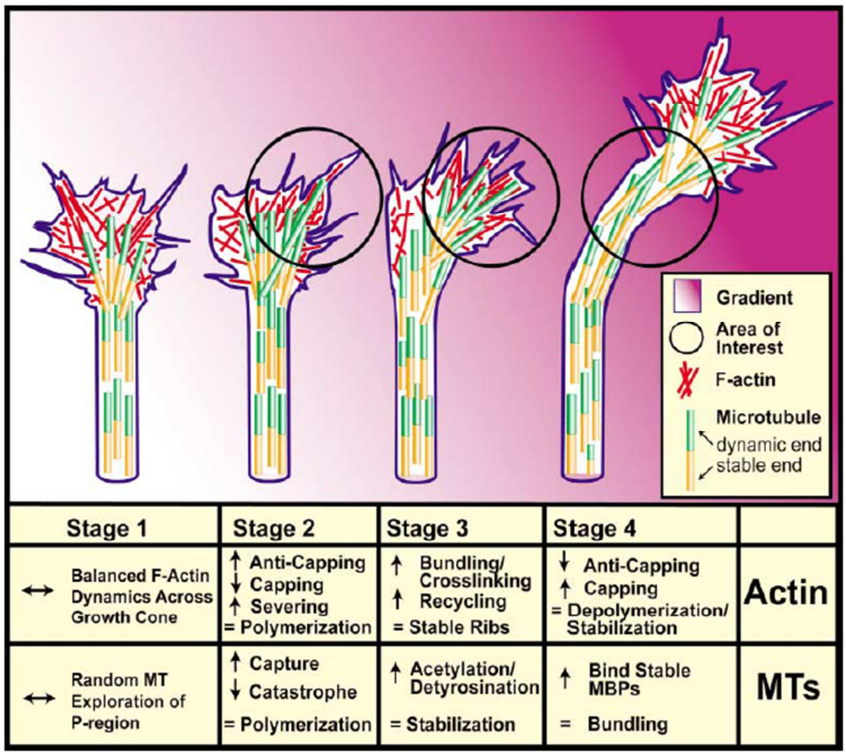

Figure 9. Axonal guidance is an orchestrated balance between actin and MT dynamics. The growth cone steering is divided in 4 stages, with several dynamic regulations in the steering side. The increase in actin and MT dynamics in the side attracted by the guidance molecule leads to an increase in protrusive actin filaments and MTs. The axon is then extended in the direction of the guidance cue, in the case of a neuronal chemoattractant. From (Dent and Gertler, 2003).

Actin, several ABPs and receptors have a fundamental role in the migratory process of the growth cone. When neurons are plated in a homogeneous substrate neurites tend to grow straight, with a minor curvature. However, the creation of a chemical gradient of a chemoatractant or chemorepulsive substance creates a curvature in the axon growth, growing in or off the chemical gradient, respectively. The reactiveness to the chemical gradient depends on the ABPs present in the P-domain (Dent and Gertler, 2003). Chemoattractans for the neuronal growth cones include nerve growth factor (NGF) and netrin, whereas the repulsive cues include semaphoring-3A, slit3 and ephrin-A2 (Bashaw and Klein, 2010; Dent and Gertler, 2003). The repulsive cues act via increasing the retrograde flow or through the removal or inactivation of the adhesion molecules (Dent and Gertler, 2003).

5- The Axon Initial Segment

The AIS is a fundamental component of the mature neuron as it regulates action potential initiation and axon-dendritic polarity (Rasband, 2010; Yoshimura and Rasband, 2014). Therefore, the establishment of the AIS and its activity are key steps in the maturation process of the axon. Typically, this structure is found in the first 20-50 µm of the axon and is characterized by a dense actin and microtubule cytoskeleton, similar to the spectrin-based membrane cytoskeleton found in Red Blood Cells (RBC) (Jones et al., 2014). Recent studies suggest that actin is organized in two different fashions in the AIS: either small-sized and stable actin filaments (as in the RBC) or long and dynamic filaments (Jones et al., 2014). Actin in the AIS is suggested to act as a filter to allow only either axon-targeted vesicles or non-specific localized protein vesicles to enter the axon, inhibiting dendritic-specific cargos to proceed (Al-Bassam et al., 2012). Interestingly, dendritic-specific protein vesicles have similar rates of entering both the axon and dendrites, although they are halted and reverse at the AIS. The filter mechanism acts via myosin Va, which interacts with the actin filaments that are present in the AIS (Al-Bassam et al., 2012). How the actin cytoskeleton is organized in the AIS is a subject of debate. In 2012 Watanabe *et al* proposed that actin is organized in the form of patches, with a 2-3µm distribution along the AIS. These actin patches are enriched (80%) in barbed ends facing the cell body (Watanabe et al., 2012). Therefore, dendritic vesicles, by interaction with myosin Va (which moves from pointed to barbed ends) would be stopped and engage in the reverse orientation (Watanabe et al., 2012). There are, however, new insights that suggest that only a small fraction of these patch-filaments are in such orientation (25%), whereas almost half were neutrally orientated and the rest were distally orientated (Jones et al., 2014). Nevertheless, actin dynamics is known to be crucial for the proper AIS assembly and maintenance (Nakada et al., 2003; Song et al., 2009; Winckler et al., 1999).

The AIS is the site of anchoring of several proteins, namely ion channels, fundamental for the development of its activity (Grubb et al., 2011), as represented in figure 10.

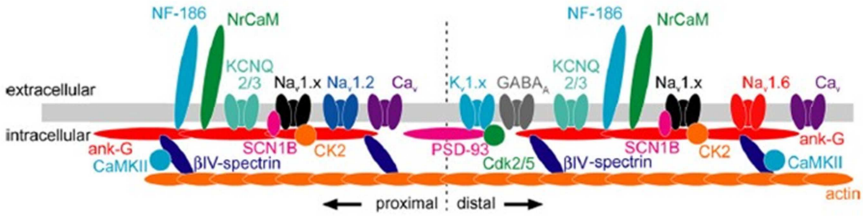

Figure 10. The AIS allocates several ion channels, responsible for the generation of the action potentials. The AIS is composed by several transmembrane proteins and ion channels which are anchored by ankyrinG and βIV spectrin, which interacts with actin. Adhesion molecules such as NrCAM, NF186 and ADAM22 are

fundamental in the AIS. Interestingly, AIS and the Ranvier Nodes have similar biochemical structures (Grubb et al., 2011).

AnkyrinG is a spectrin-related protein that is specifically found in the AIS. Contrarily to the nodes of Ranvier, where the recruitment of Na^+ channels requires glial derived signals, the AIS is neuronal intrinsic and it does not require any extracellular cues to be assembled (Rasband, 2010). AnkyrinG is pivotal in the assembly process since channels have to bind it (Hedstrom et al., 2008). Channels that are not bound to ankyrinG are removed by endocytosis (Fache et al., 2004). AnkyrinG removal from cells results in the disappearance of the polarized distribution of the Na^+ channels, K^+ channels, cell adhesion molecules and of the scaffold protein βIV spectrin (Hedstrom et al., 2008). As such, ankyrinG is not only crucial for the AIS assembly but also for its maintenance, since the removal of ankyrinG from mature neurons, with an established AIS, results in the loss of AIS markers (Hedstrom et al., 2008).

The AIS is a dynamic and plastic component of neurons. The plasticity of the AIS has been clearly demonstrated in hippocampal neuron cultures and in the avian auditory brainstem (Grubb and Burrone, 2010; Grubb et al., 2011; Kuba et al., 2010). In rat hippocampal cultures, the AIS is relocated distally from the cell body under chronic neuronal activity driven by elevated extracellular potassium, returning to its original position after the potassium levels return to baseline (Grubb and Burrone, 2010). Interestingly, the AIS maintains its ion channel distribution after relocation (Grubb and Burrone, 2010). The relocation mechanism occurs through the increase in intracellular Ca^{2+}, since blocking the AIS L-type Ca^{2+} channels inhibits relocation (Grubb and Burrone, 2010). The avian auditory system is an *in vivo* example of AIS plasticity, not through relocation but by regulating AIS size. Deprivation of the auditory stimuli in chicken causes an AIS elongation, which causes increased neuronal excitability (Kuba et al., 2010). The available data on AIS plasticity suggests that it could have an important role in some diseases such as epilepsy (Buffington and Rasband, 2011).

6- Why Adducin and Profilin?

In this thesis we focused specifically in the study of two different ABPs, adducin and profilin-1. These two proteins were selected based on preliminary data from our group supporting their relevance in the context of axon formation and (re)growth, as will be expanded in detail in the Results section. In the following sections of this Introduction I will summarize and discuss the state-of-the-art on their structure and function.

II- Adducin

1- Gene and Protein

a. The spectrin-based membrane cytoskeleton

Adducin, as most of the components of the spectrin-actin cytoskeleton, was first identified in the erythrocyte membrane (Gardner and Bennett, 1986). Erythrocytes have a unique biconcave disk shape, which is crucial for their activity. Moreover, and despite they lack a nuclei, they survive around 120 days in the circulatory system and undergo several shape remodeling. The typical shape and incredible deformability that these cells undergo depends critically of the spectrin cytoskeleton and of its associated proteins (Baines, 2009).

The erythrocyte spectrin-based membrane skeleton has been extensively studied by electronic microscopy after extraction with non-ionic detergents (Schwoch and Passow, 1973). This method that promotes the removal of the membrane lipids leaving only a dense meshwork of protein that retains the original cell shape, allowed the deep study of the structural and biochemical proprieties of the erythrocyte membranes. This procedure originates what is known as the RBC 'ghosts' (Schwoch and Passow, 1973; Yu et al., 1973). The analysis of these RBC 'ghosts' allowed understanding how their membrane cytoskeleton is organized. The main components of the membrane-based cytoskeleton have been identified as actin, organized either in filaments or present in the form of monomers (Bennett and Baines, 2001); spectrin (from the Latin word *spectre*, which means ghost) organized in α β heterotetramers; and its associated proteins, ankyrin, protein 4.1 and adducin (Baines, 2009; Bennett and Baines, 2001).

The spectrin-based membrane cytoskeleton was originally considered to be unique to erythrocytes, although subsequent analysis revealed it to be ubiquitous in all the metazoan (Baines, 2009). Spectrin is fundamental for the cellular shape and function. In erythrocytes, spectrin and actin are the main components of the membrane-associated cytoskeleton, creating a 2D lattice of α1/β1 spectrin tetramers (composed by two α1/β1 heterodimers), attached to small actin filaments (of 12-17 monomer length), which are capped by α- and β-adducin (in the barbed end). Besides their capping activity, α- and β-adducins are fundamental for stabilizing the actin-spectrin junctions (Li et al., 1998; Matsuoka et al., 1998). The spectrin-based membrane cytoskeleton in erythrocytes is depicted in figure 11.

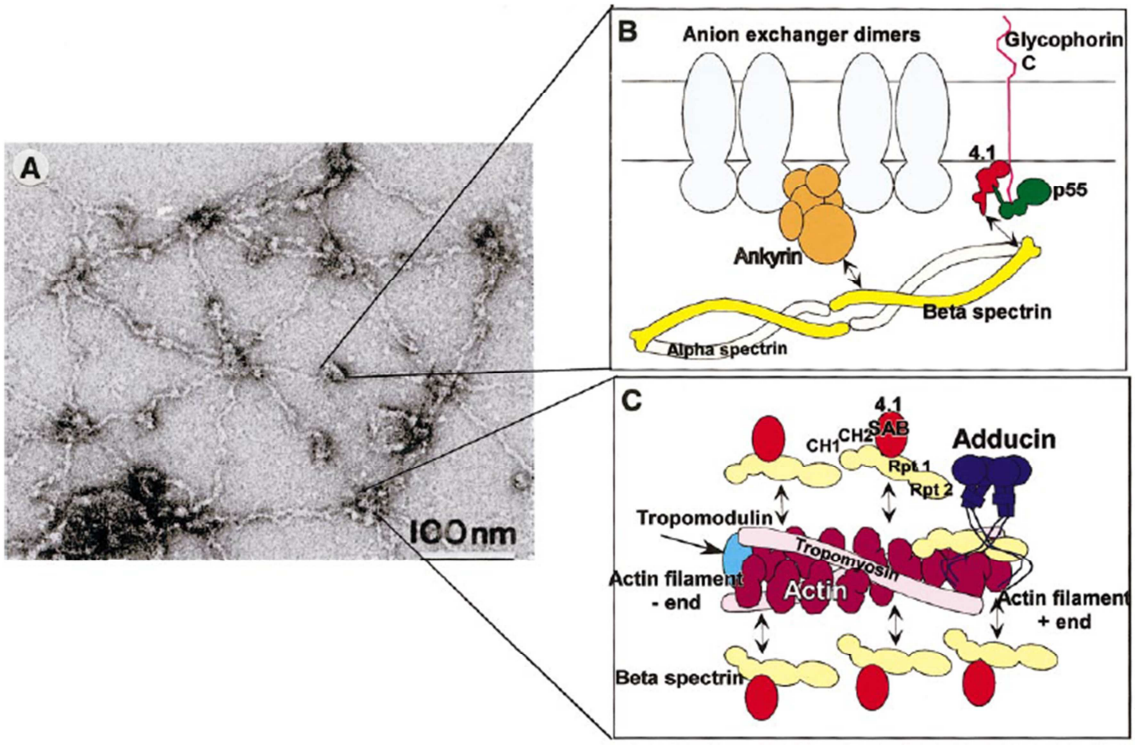

Figure 11. The organization of the spectrin-based membrane cytoskeleton in erythrocytes. (A) Electron microscopy of the erythrocyte membrane, revealing the hexagonal lattice of the α/β spectrin dimer cytoskeleton, where each spectrin is connected to other 6 spectrin dimers. (B) membrane-cytoskeleton connections in erythrocytes. Ankyrin is linked to dimers of the anion exchanger. Each ankyrin is capable of cross-linking two anion exchanger dimers and β-spectrin (yellow) interacts with ankyrin. At the NH_2-terminal region of β-spectrin is a binding site for 4.1 (red). 4.1 forms a ternary complex with the transmembrane protein glycophorin C and the membrane-associated guanylate kinase p55 (green). (C) Spectrin-actin junction organization. Actin filaments are capped in the pointed (-) end by tropomodulin (light blue) and in the barbed (+) end by adducin (dark blue). Besides the capping activity, adducin (and protein 4.1 – in red) also interacts with β-spectrin (yellow), promoting it interaction with actin. Nonmuscle tropomyosin (in pink) lies along the filament. From (Bennett and Baines, 2001)

In the RBC it is particularly distinguishable the phenotypic consequences of the disruption of the spectrin-based membrane cytoskeleton. Dysregulations in spectrin, ankyrin (-R) or adducin (α and β) result in hemolytic anemia hereditary spherocytosis, that leads to abnormal shaped RBC with decreased deformability and stability (Bennett and Baines, 2001). The decreased capacity of the RBC to sustain morphological adaptations results in decreased survival in circulation and leads to disease in mammals (Bennett and Baines, 2001).

b. Adducins: Genes and proteins

Adducins are a family of actin binding proteins, encoded by three different genes: ADD1, ADD2 and ADD3, resulting in α-, β- and γ-adducin proteins, respectively. Adducins were first purified from human erythrocytes, in 1986 by Gardner and Bennett. The original given name of adducin, calmodulin binding protein 103/97 ($CaM\text{-}BP_{103/97}$), resulted from its binding capability to calmodulin and its molecular weight. Gel filtration was the first suggestion of the heterodimer configuration, with a proposed stoichiometry of 1:1 of α- and β-adducin monomers in the erythrocytes (Gardner and Bennett, 1986). Only by using the crosslinker ethylene glycol bis(succinimidylsuccinate) (EGS) it was later found that adducin is organized in cells in the form of an heterotetramer, composed by two heterodimers (Matsuoka et al., 1996).

The third form of adducin, γ-adducin, was found 10 years later by screening of a rat kidney cDNA library. Given its resemblance to α- and β-adducin and binding capabilities, γ-adducin was found to be the α-adducin dimer pair in tissues that lacked β-adducin (Dong et al., 1995). Extensive analysis of the expression pattern of the three forms of adducin (Gilligan et al., 1999), as well as the generation of the KO mice for the α (Robledo et al., 2008), β (Gilligan et al., 1999) or γ adducin (Sahr et al., 2009) revealed the distribution of the different adducin forms in different tissues: α-adducin is ubiquitous, β-adducin is restricted to the RBC, and brain and γ-adducin although ubiquitous, is absent from erythrocytes (Gilligan et al., 1999). The α-adducin KO mice also revealed that α-adducin is the fundamental dimer subunit, since the RBC 'ghosts' did not have βγ-adducin heterodimers (Robledo et al., 2008), whereas the double βγ-adducin KO still had α-adducin (Sahr et al., 2009). This evidence raised the possibility of the existence of $\alpha_2$homodimers (Sahr et al., 2009). Of note, the depletion of either β or γ-adducin alone leads to the compensation of the complementary forms (Sahr et al., 2009).

As referred to above, in mammals, adducin exists in three different forms: α, β and γ. These three proteins are encoded by ADD1, ADD2 and ADD3 genes, respectively. ADD1 gene is located in chromosome 4 in humans (5 in mice and 14 in rats) leading to a 737 amino acids long protein (735 in both mice and rat); ADD2 gene is located in chromosome 2 in humans (6 in mice and 4 in rats) leading to a 726 amino acids long protein (725 in mice, 725 in rats); and ADD3 gene is located in chromosome 10 in humans (16 in mice and 1 in rats) leading to a 674 amino acids long protein (674 in mice, 673 in rats) (Matsuoka et al., 2000; Suriyapperuma et al., 2000). All adducin genes present two splicing variants. In the α2 and β2 splicing variants it is noticeable the absence of the spectrin-actin binding domain suggesting different functions apart from the well described functions of the variants α1 and β1. Adducins have a conserved structure, presenting a

distinctive globular and protease resistant head (39kDa) connected by a neck (9kDa) to the C-terminus protease sensitive tail domain (33kDa). A comparative alignment of the 3 human adducin forms is represented in figure 12.

The primary, secondary and tertiary structure of adducin is fundamental for its function and regulation, and adducin is highly conserved through different species, suggesting a role in basic cellular functions (Bianchi et al., 2005). In nematodes and in insects adducin has only one form (Ohler et al., 2011; Pielage et al., 2011; Vukojevic et al., 2012).

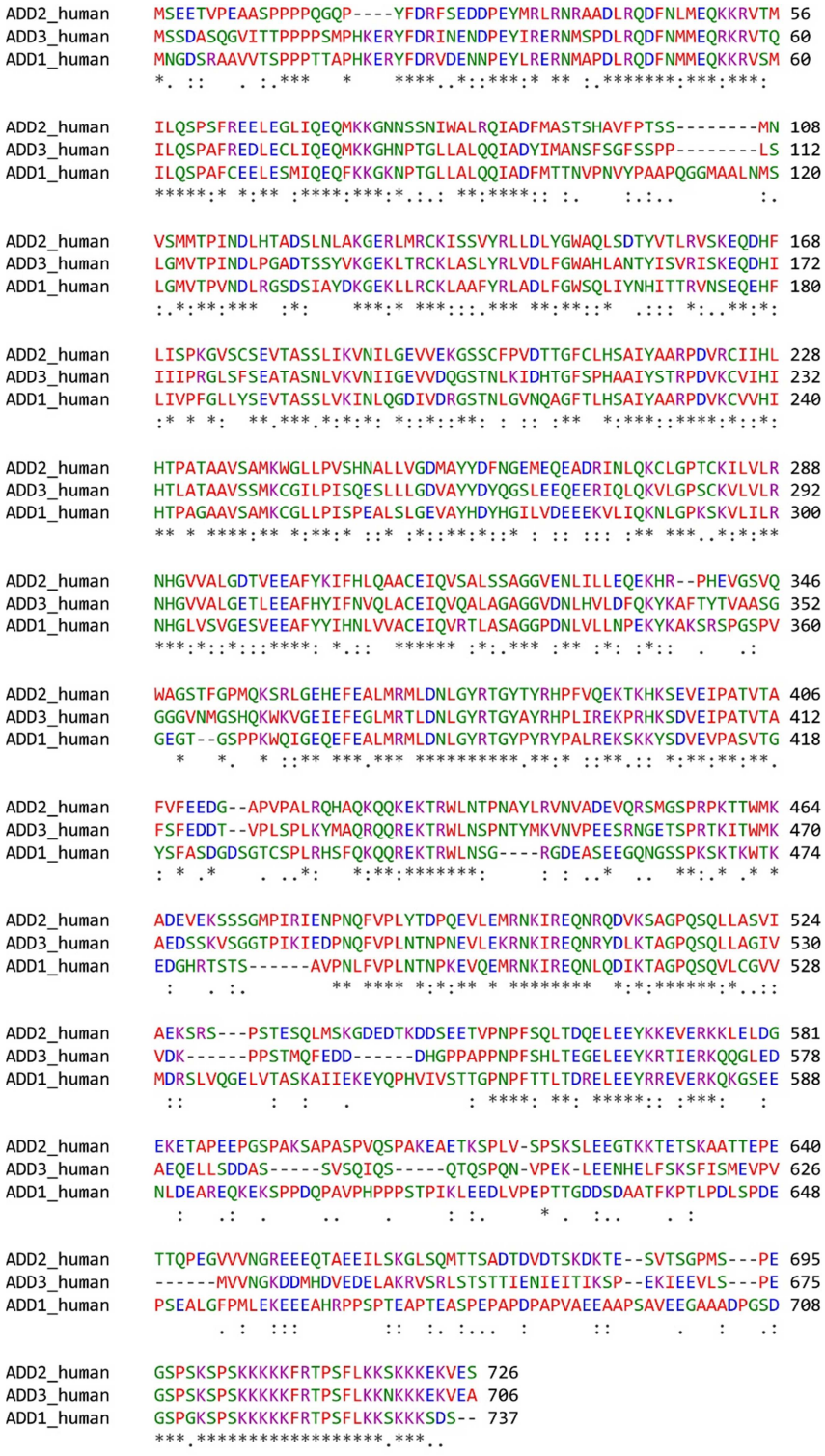

Figure 12. Alignment of different adducin forms. Human α, β and γ-adducin (isoform A) were aligned with ClustalW2 (http://www.ebi.ac.uk/Tools/msa/clustalw2/). Correspondence: Symbols - '*' fully conserved residue; ':' residue with high similarity; '.' residue with low similarity; no symbol, no similarity. Color code: red, small residue; blue, acidic residue; magenta, basic residue; green, Hydroxyl + sulfhydryl + amine + G.

c. Adducin: function and regulation

The adducin tetramer has three main functions related to the actin filaments. It promotes the bundling of actin filaments and also by capping their barbed ends, it inhibits the incorporation of new monomers into the filament (Gardner and Bennett, 1986). Adducin is also involved in the recruitment of spectrin to the ends of the filaments (Hughes and Bennett, 1995; Mische et al., 1987). For the actin and spectrin related functions, both the neck and the C-terminus tail domain of adducin are fundamental (Matsuoka et al., 1998). In the last 22 residues of the tail domain there is a MARCKS-related domain, with high homology to the myristoylated alanine-rich C kinase substrate (MARKS) protein (Hughes and Bennett, 1995; Joshi et al., 1991). Current data suggests that the neck domain is fundamental for the oligomerization (Li et al., 1998) and the tail domain, namely the MARCKS related domain, for its interaction with actin (Li et al., 1998). The loss of each of these domains abolishes both the capping activity, and the recruitment of spectrin (Li et al., 1998). It is from its ability to bind and bundle actin that adducin got its name, derived from the Latin word *adducere*, which means 'to bring together' (Mische et al., 1987). In figure 13 is represented the actin binding to its partners actin and spectrin.

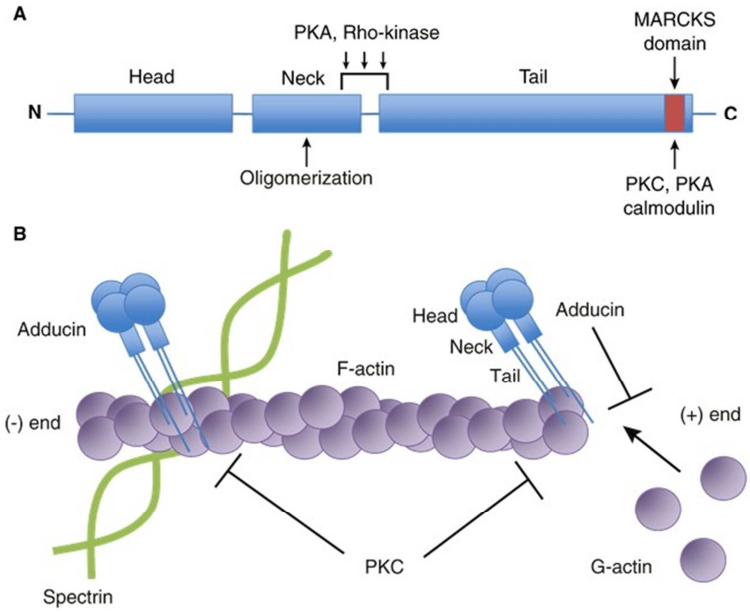

Figure 13. Schematic representation of adducin and its interaction with spectrin and actin. (A) Adducin is composed by three different domains, the head, neck and tail that contains the MARCKS-related domain. Adducin has several phosphorylation sites, being highlighted with black arrows the well characterized ones. (B) Adducin interacts with actin and spectrin via MARCKS domain and it is regulated by PKC phosphorylation, which decreased the affinity of adducin towards its interactors (Stevens and Littleton, 2011).

The affinity of adducin to actin and spectrin is regulated by phosphorylation. Several different kinases regulate this interaction, such as protein kinase C (PKC), cyclic-adenosine monophosphate (cAMP) dependent protein kinase (PKA) and Rho-associated kinase (ROCK), as well as by calmodulin binding (Matsuoka et al., 1996; Matsuoka et al., 1998; Mische et al., 1987). PKC and PKA phosphorylation of Serine residues in the MARCKS domain (in humans: Serine 726, 713 and 662 in α, β and γ-adducin, respectively), as well as calmodulin binding, results in loss of affinity for actin and spectrin, promoting a more dynamic actin cytoskeleton (Matsuoka et al., 1998). This C-terminus Serine phosphorylation is visible in many dynamic cellular processes such as in dendritic spines of hippocampal neurons (Matsuoka et al., 1998), in the leading edge of the lamellipodia of activated platelets (Matsuoka et al., 1998) and also in the growth cone of DRG neurons. Adducin phosphorylation by PKC has been proposed as an important step for events of cell shape modulation, cell migration (Chen et al., 2011), tissue rearrangements (Rotzer et al., 2014; Wu et al., 2015), neuronal plasticity (Babic and Zinsmaier, 2011; Bednarek and Caroni, 2011; Ruediger et al., 2011), among others. Moreover, phosphorylation of Serine 726 is the only conserved phosphorylated site in both vertebrates and non-vertebrates, suggesting a critical role of adducin regulation in this specific residue (Gruenbaum et al., 2003).

Besides the Serine residues of the C-terminus of adducin, PKA also phosphorylates the neck domain Serine residues 408, 438 and 481 of α-adducin, but the functional meaning of this phosphorylation is yet to be known (Matsuoka et al., 1996). Adducin interaction with actin is also regulated by ROCK. Contrarily to the PKA/PKC C-terminus Serine phosphorylation, phosphorylation of the adducin residues Threonine 445 and 480 by ROCK is associated with an increased affinity to actin, impacting cellular processes as membrane ruffling and cell migration (Fukata et al., 1999), the survival of retina cells under adverse conditions (Tura et al., 2009) and also the outer hair cell electromotility, which is crucial for the proper function of the mammals ear (Zhang et al., 2003). Adducin phosphorylation by ROCK is regulated by myosin phosphatase (Zhang et al., 2003). All together, the above findings suggest a double regulation of adducin, either by increasing its affinity to actin or by decreasing it. The regulation by PKC is, however, more extensively studied.

Besides regulation that impacts the actin cytoskeleton, other kinases such as glycogen synthase kinase 3β (GSK3β) and Fyn kinase are able to phosphorylate several residues of adducin. GSK3β was predicted to phosphorylate β-adducin in the tail domain Serine residues 600, 613 and 697 (Farghaian et al., 2011). This was proven to occur in cortical neuron cultures. In the case of Fyn kinase, its interaction with β-adducin was shown by

immunoprecipitation and by immunocytochemistry, where they were co-localized at the membrane of COS7 cells (Gotoh et al., 2006; Shima et al., 2001).

Recently α-adducin was suggested to interact with microtubules, via binding to the non-conventional myosin-X (Chan et al., 2014). In this work adducin was localized at the mitotic spindle and this interaction required α-adducin head domain and phosphorylation of Serine 12 and Serine 355 by cyclin-dependent kinase (Chan et al., 2014). Either phospho-resistant or phospho-mimetic mutants for each of these residues resulted in loss of affinity to the spindle. Moreover, depletion of α-adducin caused aberrant congression and segregation of chromosomes in HeLa mitotic cells. This data suggests a new role for adducin, which would not only be a regulator of the actin cytoskeleton but would also impact the microtubule cytoskeleton (Chan et al., 2014).

A list of regulators of adducin interaction with actin and microtubules is shown in table 1:

Table 1- List of known regulators of the adducin.

Protein	Residue (of human α-adducin)	Function	Reference(s)
Calmodulin	MARCKS-related motif	Loss of affinity towards actin and spectrin	(Matsuoka et al., 1996; Mische et al., 1987)
PKA / PKC	Serine 726	Loss of affinity towards actin and spectrin	(Matsuoka et al., 1996)
PKA	Serines 408, 438 and 481	Not known	(Matsuoka et al., 1996)
Rho Kinase	Threonines 445 and 480	Increased affinity to actin	(Fukata et al., 1999; Kimura et al., 1998)
Fyn Kinase	Tyrosine 489 (β-adducin)	Relocation of β-adducin to the plasma membrane	(Shima et al., 2001)
GSK3β	Serines 600/613/697 (β-adducin)	Role in the axon outgrowth	(Farghaian et al., 2011)
cyclin-dependent kinase 1	Serines 12 and 355	Required for interaction with unconventional myosin X and the mitotic spindle	(Chan et al., 2014)

2- Physiological roles of adducin:

a. Red blood cells

Adducin was first identified in the RBC, as part of the membrane associated spectrin-actin cytoskeleton (Gardner and Bennett, 1986). The knowledge on the role of adducin in this particular cytoskeleton and consequently in the RBC, was greatly improved by the development of KO mice for each of the three forms of adducin. Besides other phenotypes (that will be described below) both α and β adducin KO animals displayed a very critical hemolytic anemia hereditary spherocytosis, characterized by abnormally shaped RBC, with decreased deformability and stability (Gilligan et al., 1999; Robledo et al., 2008). Interestingly, a similar phenotype occurs in humans with known mutations in spectrin and R-ankyrin (Bennett and Baines, 2001; Winkelmann and Forget, 1993). β-adducin KO mice were the first adducin KOs generated (Gilligan et al., 1999). Although in erythrocytes these mice had a small decrease in the levels of α-adducin and a 5-fold increase in those of γ-adducin, they presented a decreased deformability and lower resistance to osmotic stress. In order to further understand the organization of adducin in cells, namely in the RBC, α-adducin KO mice were also generated (Robledo et al., 2008). Similarly to the β-adducin KO mice, the ablation of α-adducin resulted in severe hemolytic anemia with spherocytosis. Interestingly β and γ-adducin were not present in RBC membranes of β-adducin KO mice, whereas EcapZ, the homolog of capping protein in erythrocytes was enriched, suggesting a compensatory mechanism by another actin barbed-end capping protein, that is however unable to increase the spectrin-actin junction stability (Robledo et al., 2008). The double βγ-adducin KO mice have also been generated (Sahr et al., 2009). Interestingly, in the erythroid cells of these animals, the levels of α-adducin were greatly diminished (less than 1% in relation to controls), whereas in non-erythroid cells the reduction of α-adducin was not as striking (decrease of 25-50%). This suggests that erythroid and non-erythroid cells have a different membrane organization of adducin and also supports the possibility that, at least in non-erythroid cells, α-adducin homodimers can be formed and be functional (Sahr et al., 2009).

b. Cell and tissue rearrangements

The spectrin-based membrane cytoskeleton plays a crucial role in maintaining the cell morphology and function. In respect to epithelia, spectrin-adducin complexes are fundamental for the proper apical and tight junction formation, which plays crucial roles in epithelial cell adhesion, polarity and differentiation (Naydenov and Ivanov, 2011). Spectrin

rods are linked to the actin cytoskeleton through ankyrin and protein 4.1, which also have affinity for the cytoplasmatic domains of channels and transmembrane transporters (Baines, 2009; Bennett and Baines, 2001). The association of spectrin with actin filaments is enhanced by several other proteins, namely adducin (Bennett and Baines, 2001). α- and γ-adducins are enriched in the apical and tight junctions and the knockdown of each of the adducin forms delayed the reformation of these structures (Naydenov and Ivanov, 2010), resulting in less stable cell-to-cell contacts (Abdi and Bennett, 2008). The exposure of epithelial cells to phorbol esters (PKC activators) results in the loss of cell-to-cell contacts by the internalization of AJ and TJ proteins, with increasing levels of phosphorylated adducin (Naydenov and Ivanov, 2011). Adducin has also been associated with the keratinocyte cell-to-cell adhesions (Rotzer et al., 2014; Wu et al., 2015; Zhao et al., 2013; Zhao et al., 2011).

c. Renal tubular cells

Point mutations in α-adducin have been suggested as an important risk factor for hypertension (Hopkins and Hunt, 2003), namely in the Italian (Cusi et al., 1997; Lanzani et al., 2005; Manunta et al., 1998), Japanese (Iwai et al., 1997; Tamaki et al., 1998) and Chinese (Zhang et al., 2013) populations. Particularly in humans, the polymorphism G460W in α-adducin is associated with increased blood pressure (Cusi et al., 1997; Manunta et al., 1998). The first observations linking adducin and hypertension came however from the studies of the Milan Hypertensive rat strain (MHS) (Bianchi et al., 2005). The MHS has a single nucleotide polymorphism in the three adducin forms, F316Y in α-adducin, Q529R in β-adducin and Q572K in the γ-adducin (Bianchi et al., 2005; Torielli et al., 2008). The cellular mechanism by which mutations in adducin are linked with hypertension is not fully understood but some key events are described: in rat cells, mutant α-adducin F316Y increases the Na-K pump activity and rearrangements in the actin cytoskeleton in renal tubular cells. This is due to the fact that mutated α-adducin has increased affinity to the Na-K pump, and impairs pump endocytosis (Efendiev et al., 2004). Interestingly, β-adducin KO mice also develop a hypertension phenotype (Marro et al., 2000). These abnormal Na-K exchanges in renal tubular cells lead to sodium reabsorption and subsequently to the development of hypertension (Bianchi et al., 2005; Bianchi and Tripodi, 2003).

d. Nervous system

Over the last 10 years adducin has been widely associated with the nervous system. These studies ranged from the use of simple animal models such as nematodes to more complex mammalian organisms, including humans.

e. The Axon Initial Segment

Using hippocampal neurons cultures, the analysis of their AIS revealed that, contrarily to ankyrin-G and spectrin βIV, the levels of adducin in this structure are decreased after the DIV 6 (Jones et al., 2014), as is depicted in figure 14. Moreover, in the rest of the axon the levels of adducin remained enriched and comparable to those present in dendrites (Jones et al., 2014). This data suggests that adducin is not required for AIS formation and maintenance, but could have an important role in regulating actin dynamics in the neighboring regions of the AIS.

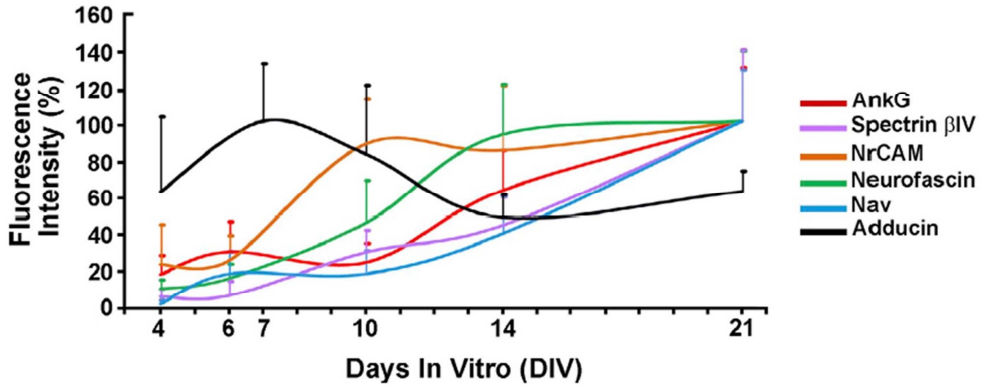

Figure 14. The different components of the AIS have a differential accumulation profile. Adducin is present in the initial stages of AIS establishment, with a maximum intensity at DIV6. However its levels are depressed after the accumulation of the mature AIS components such ankyrinG and spectrin βIV. From (Jones et al., 2014).

f. A new axonal cytoarchitecture: adducin and the Actin Rings

In 2013 a revolutionary model for the organization of actin in axons was proposed. Using either DIV5-12 rat hippocampal neuron cultures (when the axon/dendrite specification is occurring) or hippocampal slices (Xu et al., 2013) and super-resolution microscopy techniques (3D-Stochastic Optical Reconstruction Microscopy – STORM – and STimulated Emission Depletion – STED) a very unique axonal cytoskeleton organization was observed (depicted in figure 15). The super-resolution techniques revealed the

formation of a series of actin rings along the axons, distributed in a conserved periodicity of 190 nm (Xu et al., 2013). These actin rings were formed from the cell body towards the axon tip (Zhong et al., 2014). Further analysis of the biochemical structure of the rings by immunocytochemistry revealed that the periodicity was spatially regulated by parallel spectrin heterotetramers along the axon (Xu et al., 2013). Of interest, the interaction of spectrin and actin rings was mediated by adducin, as observed by immunocytochemistry (Xu et al., 2013).

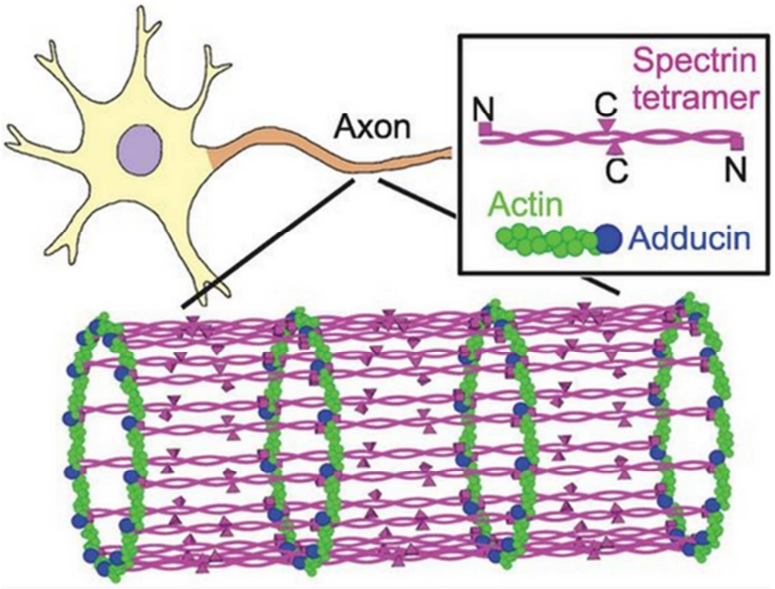

Figure 15: The axonal actin rings. The actin rings are a novel level of organization of actin in axons. Super-resolution microscopy revealed actin rings (green) distributed along the axons of cultured hippocampal neurons, with a 190 nm periodicity. The periodicity is regulated by spectrin tetramers (purple) and adducin heterotetramers mediate the actin-spectrin junctions and actin filament size (blue). From (Xu et al., 2013)

The inner dynamic nature of this structure has been a matter of great interest. Treatment with lantruculin A results in loss of the actin rings (Xu et al., 2013). Latrunculin A binds to globular actin inhibiting its incorporation in filaments thereby the above results suggest that the rings are dynamic, undergoing incorporation and removal of actin subunits from the filaments (Gallo, 2013). However, data obtained by βII spectrin-GFP fluorescence recovery after photo bleaching (FRAP) suggests that this structure is very stable presenting low levels of turnover (Zhong et al., 2014). Interestingly, the latrunculin A treatment not only disrupts actin rings but also the associated spectrin βII pattern. This further suggests that actin and spectrin association is interdependent (Zhong et al., 2014), although the dynamic proprieties of the two components are different. Moreover, besides actin and spectrin, adducin is also a putative regulator of the dynamic proprieties of the

rings. Adducin is not co-localized with the actin rings until DIV6 (Zhong et al., 2014). Since adducin is a stabilizer of the actin cytoskeleton (by capping and bundling actin filaments and by crosslinking them with spectrin), it is possible that its localization in actin rings is important for stabilization of the actin filaments of the rings and therefore, of the cortical cytoskeleton itself.

Recently, the advent of new cell permeable silicon-rhodamine (SiR) derivatived probes, namely SiR-actin (which is conjugated with desbromo-desmethyl-jasplakinolide) allowed the visualization of actin rings in neurons by STED and live imaging, without the requirement of extraction processes for labelling the actin cytoskeleton (which is mandatory when using phalloidin staining) (D'Este et al., 2015; Lukinavicius et al., 2014). Surprisingly, with this new technique the actin rings were visible much earlier that with phalloidin (from DIV2 and DIV5, respectively) (D'Este et al., 2015). Moreover, not only axons developed these structures but also dendrites, although later (DIV5 on) (D'Este et al., 2015), although only about 1/3 of the dendrites analyzed revealed the presence of actin rings.

The current knowledge on the new cortical cytoskeleton organization suggests that it might be dependent on the establishment of the axon/dendrite polarity:

i) Although both axons and (some) dendrites have actin rings, in axons they are formed earlier (D'Este et al., 2015);

ii) 3D-STORM failed to revealed actin rings in dendrites (Xu et al., 2013; Zhong et al., 2014). This was probably due to the fact that after DIV6 actin rings in axons are more resistant (and stable) to detergent extraction after fixation (Zhong et al., 2014). MT stabilization, using Taxol, that is known to lead to multiple axon formation (Witte et al., 2008),leads to the appearance of actin rings in all neuronal processes (Zhong et al., 2014).

Interestingly, βII spectrin is excluded from the mature AIS, by exchange with spectrin βIV (Zhong et al., 2014). This suggests that particularly in the AIS, and Ranvier nodes (D'Este et al., 2015), the structure of the actin rings could be different from the one present in the rest of the axon. The current model for the assembly and maturation of these structures is depicted in figure 16.

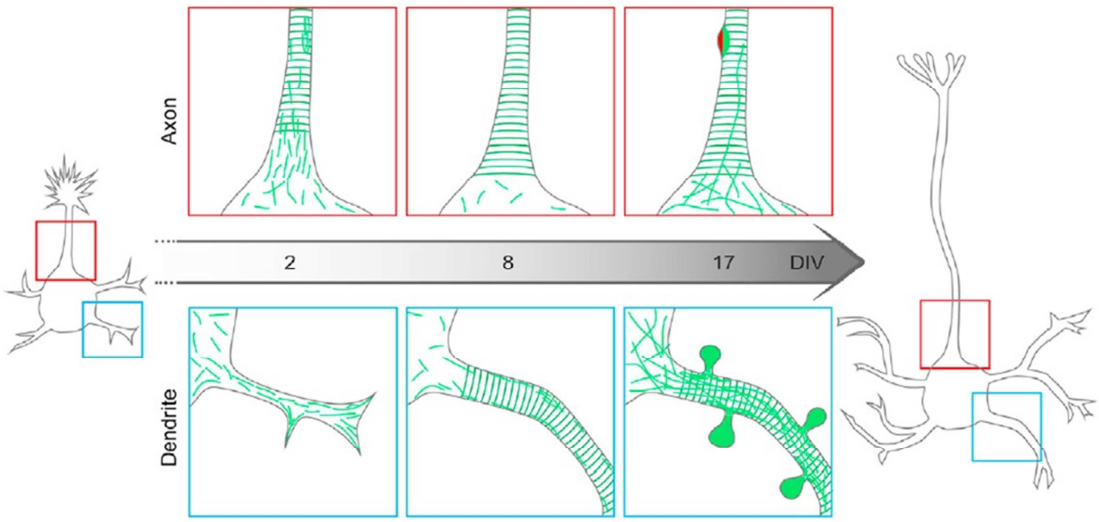

Figure 16. Current model for the assembly and maturation of actin rings in hippocampal neuron cultures. In axons the actin rings begin to be assembled at DIV2, in a proximal-to-distal fashion. At that time point, actin rings are not visible in dendrites, where they only appear at approximately DIV8. As neuronal maturation progresses axons start to present actin accumulations, in the form of actin patches (that co-localize with the presynaptic marker Bassoon) and longitudinal actin filaments, namely in the AIS. Interestingly, dendrites start to develop dendritic spines (enriched in actin) and longitudinal actin filaments. These structures in dendrites make it challenging to visualize actin rings, which can underlie the fact that dendrites failed to reveal these structures in the original descriptions (D'Este et al., 2015).

Until actin rings were described, axons were thought to depend on microtubules and neurofilaments (Perrot and Eyer, 2009; Perrot et al., 2007; Yuan et al., 2012) to be maintained and to have a defined caliber. Nevertheless it had been already suggested that the spectrin-based membrane cytoskeleton, is important for axonal integrity. In *C. elegans*, the knockdown of the spectrin homologue unc-70 results in impaired axon morphology (Hammarlund et al., 2000) and spontaneous axon break as a consequence of movement, leading to a series of injury and regrowth attempts (Hammarlund et al., 2007). In *Drosophila*, adducin homolog (*hu-li tai shao*- HTS, 'too little nursing') mutants display axonal growth and guidance deficits in photoreceptor (R) axons, leading to impaired innervation of the eye (Ohler et al., 2011). In other model systems, adducin has also been proposed to have a role in the regulation of neurite outgrowth. GSK3β regulation of β-adducin was suggested to be fundamental for the neuritogenic effect of GSK3β, though phosphorylation of three adducin Serine residues, 600, 613 and 697 (Farghaian et al., 2011). Besides β-adducin, γ-adducin was also proposed to have a role in neuritogenesis. In fibroblast COS7 cells over-expressing γ-adducin lead to increased ability of extending neurites (Lou et al., 2013). However, the over-expression of its C-terminus domain, that interacts with actin, in neuroblastoma N2A cells, decreased the percentage of cells with

neurites (Lou et al., 2013). Therefore, the role of adducin in neuritogenesis is still not fully understood, although the protein is known to be present both in the axon shaft (Gumy et al., 2011; Xu et al., 2013) and in growth cones (Estrada-Bernal et al., 2012; Matsuoka et al., 2000).

g. Synapses and Memory

The role of adducin in neurons is most studied in the process of synapse formation and activity. The first demonstration of its role in synapses was made in 1995 when Siedel *et al,* in a screening for the different constituents of the synaptic junctions in the rat brain, detected α-adducin cDNA (Seidel et al., 1995). In that report, the presence of adducin in synapses was confirmed by immunohistochemistry, including immuno-electron microscopic analysis in a subset of dendritic spines of the CA1 and CA3 region of the hippocampus (Seidel et al., 1995). Besides neurons, adducin was also identified in astroglia (Seidel et al., 1995). In 1999, Matsuoka *et al*, confirmed that adducin was not only present in dendritic spines of hippocampal neurons grown *in vitro* but also that it was phosphorylated. This phosphorylation of the C-terminus Serine residue of adducin in dendritic spines further suggested a role of this protein in the dynamics of synapse formation and function (Matsuoka et al., 2000). The first *in vivo* evidence of the role of adducin in synapses was made in *Aplysia californica*, where the homolog of adducin was found to have increased phosphorylation levels in a model for long-term facilitation (Gruenbaum et al., 2003). Long-term facilitation leads to the formation of new spines on postsynaptic hippocampal dendrites and to the appearance of multiple spine synapses between a single axon terminal and a dendrite (Engert and Bonhoeffer, 1999; Klintsova and Greenough, 1999; Maletic-Savatic et al., 1999; Toni et al., 1999). This process was is mediated in part by adducin phosphorylation, which was proposed to destabilize the spectrin-actin membrane cytoskeleton leading to increased actin polymerization (Gruenbaum et al., 2003).

The advent of the β-adducin KO mice allowed the study of the role of adducin in the vertebrate brain, where β-adducin is enriched (Gilligan et al., 1999). In the original screening for the expression levels of the different adducin forms, whereas α- and γ-adducin were found to be ubiquitous (with the exception of the lack of γ-adducin in erythrocyte precursors), β-adducin was only present in the brain and in the RBC (Gilligan et al., 1999). However, it was only in 2005 (and after the establishment of adducin as an important mediator of LTF in *Aplysia*) that the role of adducin in synaptogenesis in mammals was dissected. Rabenstein *et al*, using β-adducin KO mice observed that although their dendritic spines were similar to controls, an impairment in short-term and

long-term synaptic plasticity was present, including generalized learning deficits, namely in the Morris water maze and in the fear conditioning tests (Rabenstein et al., 2005). Interestingly, α-adducin expression analysis by *in situ* hybridization revealed no differences between controls and β-adducin KO mice (Rabenstein et al., 2005). Subsequent studies revealed, however, that in the β-adducin KO mice the protein levels of γ-adducin were increased (3-fold in the brain). Moreover, western blot analysis revealed that not only the total levels of α-adducin but also the levels of its phosphorylated form were decreased, both to half the levels of controls (Porro et al., 2010). The dysregulation in the levels of the different adducin forms and in their regulatory phosphorylation were then associated with the motor coordination deficits of the β-adducin KO mice, that present a poorer performance in the open field and in the rotarod tests (Porro et al., 2010). This dysregulation in the total protein levels may be related to the specific requirement of β-adducin in neurons. The inability to form the correct tetramer may then lead to degradation of α-adducin monomers,

Recently, PKC was found to be the *in vivo* kinase required for adducin phosphorylation in synapses, namely in the context of environmental enrichment (Bednarek and Caroni, 2011). Under standard conditions, CA3 hippocampal neurons of β-adducin KO mice have normal active zone densities at the large mossy fiber terminals but present increased synapse turnover, suggesting loss of synaptic stability (Bednarek and Caroni, 2011). Environmental enrichment exacerbates the turnover of synapses, increasing the rate of assembly and disassembly of synapses. Either inhibition of adducin phosphorylation by the PKC inhibitor chelerythrine, or absence of β-adducin in the β-adducin KO mouse brain, resulted in a worse performance upon environmental enrichment, suggesting that the process of synapse turnover is dependent on adducin and on its regulation (Bednarek and Caroni, 2011). It has been suggested that for synapse disassembly adducin inactivation by phosphorylation is required, whereas active adducin is fundamental for synapse assembly (Babic and Zinsmaier, 2011; Bednarek and Caroni, 2011). Interestingly, in synapses in the nucleus accumbens (NAc), β-adducin was also found to be crucial for remodelling after cocaine exposure (Lavaur et al., 2009). Cocaine, promotes increased remodeling of brain synapses, inducing an increase in spine density, in part through increased β-adducin phosphorylation, via PKC activation (Lavaur et al., 2009). In β-adducin KO mice the exposure to cocaine results in an even greater increase of mushroom spine density, reinforcing the role of adducin as a stabilizer of spines (Jung et al., 2013). Of interest, rearrangement of the actin cytoskeleton in synapses was recently proposed to be regulated via mTORC2, by the canonical PKC pathway and its downstream targets, such as adducin (Angliker and Ruegg, 2013).

Adducin has also been associated with synapse formation in other organisms such as the nematode *C. elegans* and *Drosophila*. Studies with the *C. elegans* adducin homolog mutant *tm3760* (a loss of function mutant) revealed no impairment in learning but impairments in short- and long-term aversive memory (Vukojevic et al., 2012). The actin capping adducin function was favored for memory consolidation since cytochalasin B (a drug that inhibits actin polymerization and therefore is analogous to the capping activity of adducin) restored the short- and long-term aversive memory, similarly to the rescue through expression of human α-adducin (Vukojevic et al., 2012). The same study associated α-adducin polymorphisms and hippocampus-dependent memory (Vukojevic et al., 2012). A subsequent study proposed a mechanism for the acquisition of memory and forgetting, based on the role of adducin and *musashi*, respectively (Hadziselimovic et al., 2014). In this study, a model on how adducin and *musashi* impact the retention or elimination of dendritic spines (and therefore, memories), was proposed. According to this model, in the learning process new dendritic spines are formed by Arp2/3 complex activity, leading to increased actin polimerization and subsequent stabilization by adducin. Conversely, the forgetting process was proposed to occur by the inhibition of translation by *musashi*, reducing actin branching and inhibiting the formation/maintenance of dendritic synapses (Hadziselimovic et al., 2014).

The *Drosophila* neuromuscular junction (NMJ) has also been used as a model for the study of the role of adducin in synaptogenesis. Of note, in *C. elegans* and *Aplysia,* the *Drosophila* adducin homolog Hts is expressed by a single gene. Hts is an important regulator of the stability and growth of the NMJ. In *Drosophila*, downregulation of neuronal, but not muscular, Hts-M (the splicing variant equivalent to full length α-adducin with the MARCKS-related motif) results in increased levels of retraction and elimination of synapses (Pielage et al., 2011). Interestingly, removal of Hts-M results in aberrant synapses, with long filopodia-like structures in the pre-synaptic compartment, leading to an increased sized NMJ (Pielage et al., 2011). In contrast, over-expression of Hts-M results in the restriction of synapse formation and growth. The phosphorylation of the C-terminus Serine residue 703 (equivalent to the Serine 726 in human α-adducin) is fundamental for the proper regulation of synapse growth and regulation (Pielage et al., 2011). As in *C. elegans,* the role of adducin as a capping protein is favored to be responsible for the phenotypes described above (Pielage et al., 2011).

Besides β-adducin KO mice, α-adducin KO mice also have impairments at the level of the nervous system, as expected given the knockdown of both β and γ forms, resulting in a true adducin KO mice – although the expression levels of β and γ-adducin forms remain similar to wt animals (Robledo et al., 2008). The α-adducin KO mice develop a lethal

hydrocephaly dependent on the genetic background (Robledo et al., 2008; Robledo et al., 2012). The hydrocephaly rate is 50% in B6/129 mixed background (Robledo et al., 2008) whereas in a pure 129 background the hydrocephaly rate is 3% and in the pure B6 background it is 80% (Robledo et al., 2012). The hydrocephaly cause remains unknown. Actually, only 6% of the human hydrocephalies have a well-known genetic cause. One possible reason that could explain this phenotype is function of adducin in mediating cell-cell contacts and cell polarity (Ma et al., 2007; Rolf et al., 2001; Yamamoto et al., 2013). Cells lacking adducin or with unbalanced phosphorylation of adducin result in abnormal shape (Rotzer et al., 2014; Wu et al., 2015; Zhao et al., 2013; Zhao et al., 2011), therefore it is possible that adducin knockdown in the α-adducin KO mice could result in weakened cell-cell interactions and tissue remodeling and less strength to resist the Cerebrospinal fluid (CSF) pressure. The α-adducin KO mice also revealed decreased density of myelinated fibers in femoral nerve axons, suggesting a peripheral nervous system involvement (Robledo et al., 2012). Analysis of the α-adducin KO mice also suggested a putative muscular impairment, since these animals develop hyperkyphosis that usually results from muscle wasting and/or a defect in peripheral enervation (Robledo et al., 2012).

h. Association of adducin with cerebral palsy and amyotrophic lateral sclerosis

Recently several insights on adducin dysregulation in disease have been published. Cerebral palsy is a neuromotor disability that affects 1 in 500 live births, in which 20% of the cases have no identifiable etiology for their symptoms suggesting a heritable nature (Leonard et al., 2011). From the known genetic studies some genes were already associated with this disorder, including the actin capping protein KANK1 (Lerer et al., 2005) and α-adducin polymorphisms (Wu et al., 2011). Recently γ-adducin was suggested to be a genetic cause in cases of quadriplegic cerebral palsy. The G367D mutation in γ-adducin causes impairments in actin oligomerization given the decreased actin capping activity that ultimately leads to impairments in cell migration (Kruer et al., 2013). Confirmation of the deleterious effects of the G367D γ-adducin mutation were visible in *Drosophila*, where mutants displayed neuromotor deficits as impaired locomotion and malformations of the brain lamina and medulla (Kruer et al., 2013).

Adducin is also deregulated in patients and in mouse models of amyotrophic lateral sclerosis (ALS) (Hu et al., 2003; Shan et al., 2005). Phosphorylated adducin is increased in the spinal cord of both ALS mouse models that overexpress mutant superoxide dismutase 1 and in human patients (Hu et al., 2003; Shan et al., 2005), although the

contribution of adducin phosphorylation for disease progression is still unknown. Recently Gallardo *et al* proposed a non-cell autonomous neurodegeneration caused by the α2-Na/K ATPase/α-adducin complex in astrocytes that overexpress mutant superoxide dismutase 1. This study shows that phosphorylation of α-adducin in Serine 436 is increased in astrocytes of mutant superoxide dismutase 1 mice. The authors found that either the knockdown of α-adducin, the heterozygous disruption of the α2-Na/K ATPase, or the usage of digoxin (an inhibitor of the Na/K activity) suppressed degeneration (Gallardo et al., 2014). This suggests that adducin-mediated neurodegeneration might be mechanistically similar to the hypertension phenotype of carriers of adducin polymorphisms, where adducin dysregulates the ion channel activity leading to impaired homeostasis (Gallardo et al., 2014).

In summary, the role if adducin in neurons, although established for a number of different aspects of neurobiology, is still not fully understood. Until recently, its function was mostly explored in the context of memory, where β-adducin was established as a key player in synapse dynamics (critically dependent on actin regulation). The recent discovery of the lattice neuronal cytoskeleton, composed of contiguous actin rings that are spaced by spectrin tetramers and co-localized with adducin, has generated a new interest on actin in the axon shaft, and consequently on the role of adducin in this compartment. For that reason, adducin is a great candidate to study in the context of the development and maintenance of the nervous system, including in the process of axon regeneration: adducin is expressed in neurons; adducin KO animals have defects in the nervous system – in organisms of different *phyla*; and it is downstream of several important pathways involved in cell polarization and axon extension and regeneration.

III- Profilin

1- Gene and Protein

Profilin is a 14-17kDa family of ABPs that are expressed in eukaryotes (Krishnan and Moens, 2009) and in some viruses (Machesky et al., 1994). Profilin is characterized by a conserved protein size and structure within eukaryotes (Krishnan and Moens, 2009) and is one of the most abundant proteins in cells, with a concentration of 10-150 µM (Birbach, 2008). In humans profilin is composed by 4 different forms, I to IV (Birbach, 2008). Although the four forms have medium sequence similarity, their structure and functions are conserved (Birbach, 2008).

The four human profilin forms are very similar in size. Profilin-1 has 140 amino acids and is located in chromosome 17; profilin-2 (Pfn2) has also 140 amino acids and is located in chromosome 3; profilin-3 (Pfn3) has 137 amino-acids and is located in chromosome 5; and profilin-4 (Pfn4) has 129 amino acids and is located in chromosome 2. Pfn1 is ubiquitously expressed, whereas the other three forms are tissue specific. Pfn2 is neuronal, mostly CNS-restricted and Pfn3 and Pfn4 are expressed in germ cells. Pfn2 is known to have two different isoforms, Pfn2 IIa and IIb, both expressed in neurons (Birbach, 2008; Krishnan and Moens, 2009).

Profilins are conserved throughout evolution, both in animals and plants (Birbach, 2008; Krishnan and Moens, 2009). Interestingly, although low sequence homologies exist between species, the tertiary fold of profilins is similar across species, as visible in figure 17.

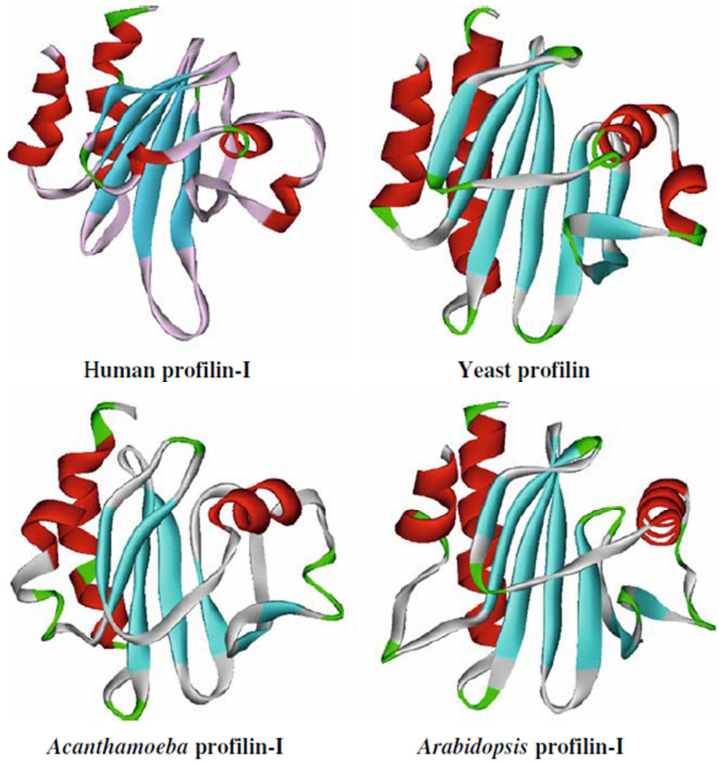

Figure 17. Profilin structure is conserved amongst different kingdoms. Human, yeast, *Acanthamoeba* and *Arabidopsis* profilin-1 structures are represented (PDB database: 1PFL, 1 KOK, 2PRF and 3 NUL, respectively). The helixes are represented in red, strands in cyan and loops in green. From (Krishnan and Moens, 2009)

The ubiquitous distribution of profilin through eukaryotes, as well as the high level of conservation of the structure indicates an important role of profilin in cells (Birbach, 2008;

Krishnan and Moens, 2009). Profilins are usually present in more than one form in different organisms, six in plants and 4 in mammals (Moens, 2008).

2- Profilin activity and regulation

Although small, profilin has several domains that are crucial for its dynamism. Moreover, given their small size the domains are overlapped, generating a greater regulatory complexity (Moens, 2008). Profilin has three main domains, the actin-binding domain, responsible for its interaction with actin; the phosphatidylinositol 4, 5-bisphosphate, $PI(4,5)P_2$ (PIP_2) binding domain; and the poly-L-proline (PLP) binding domain (Birbach, 2008; Krishnan and Moens, 2009; Moens, 2008). Different profilin forms have different abilities to bind to their ligands. Pfn1 and Pfn2 are a good example of these different ligand binding abilities. In humans, Pfn1 has an increased ability to bind actin. Interestingly, the opposite is verified in bovine profilin, suggesting species dependent variations (Lambrechts et al., 1997). The ability to bind to the $PI(4,5)P_2$ and PLP domains is also different amongst different profilin isoforms, but contradictory results are present in the literature (Moens, 2008).

a. Profilin interaction with actin

The actin-binding domain is the most well-known domain of profilin and it was the first described activity of this protein (Carlsson et al., 1977). In humans, the Pfn1 actin-binding domain comprises residues 59-61, 69, 71-74,82, 119, 121, 122, 124, 125, 128 and 129. Mutation of residues Y59, I73, H119, G121 and N124 completely abolishes the actin-binding capability (Krishnan and Moens, 2009), whereas actin residue F375 is the residue required for this interaction (Krishnan and Moens, 2009).

Profilin has two main functions towards actin. It mediates the transition of ADP-G-actin to ATP-G-actin that can be incorporated in the filaments and it is also fundamental for releasing actin in the plus tips of F-actin, thereby leading to an increased filament size/dynamics (Moens, 2008). The transition from ADP to ATP bound G-actin is increased 1000-fold in the presence of profilin (Krishnan and Moens, 2009). The ATP-G-actin conversion is consider to be an end-specific quasi-polymerizable actin monomer. The incorporation of the profilin-actin complex in the barbed ends requires the presence of Mg^{2+} and the hydrolysis of the ATP, which leads to loss of affinity and dissociation from the F-actin tip (Moens, 2008). This will generate the opportunity for the next round of profilin-actin complex incorporation (Moens, 2008).

The ability of profilin to incorporate G-actin into actin barbed ends is dependent on the interaction of F-actin with other ABPs. For instance, presence of capping proteins enhances profilin sequestration of actin monomers. If the capping proteins are not present the sequestering time is reduced and incorporation of monomers can occur (Moens, 2008). Profilin has complementary functions to those of the ADF/cofilin family, as it is responsible for F-actin depolymerization and severing, as shown in figure 18. These contradictory functions cause what is known as the treadmilling movement of actin, in which there is no filament size increase but movement (and thereby force) is created instead. In cells, these continuous cycles of polymerization and depolymerization are enhanced by cofilin and profilin activity. In the presence of these ABPs the rate of F-actin turnover is 400-fold increased (Didry et al., 1998).

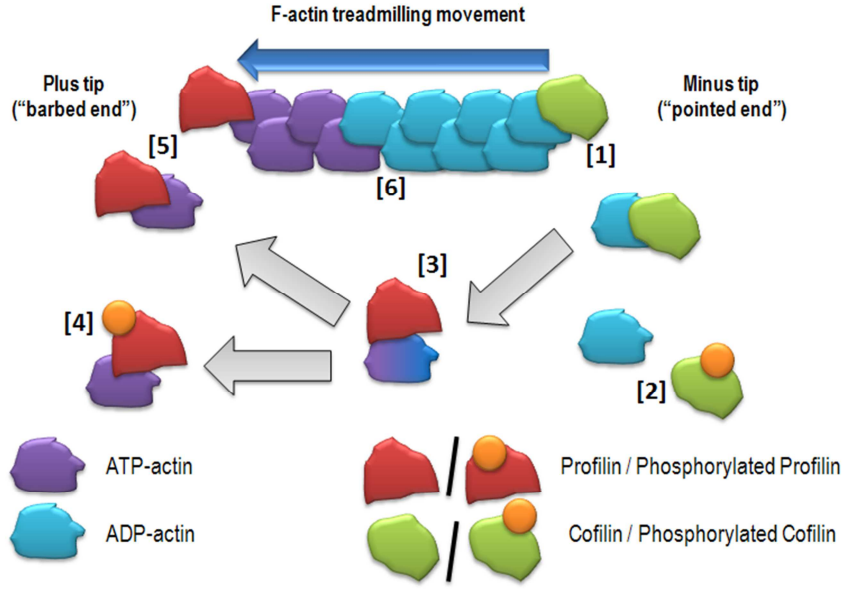

Figure 18. The synergistic action of profilin and cofilin increases the F-actin treadmilling movement. [1] Cofilin depolymerizes F-actin at the minus-tip ends, where ADP-bound actin monomer levels are increased. [2] However, when cofilin is phosphorylated it has no capacity to perform F-actin depolymerization. Profilin has three different functions: [3] it is responsible for the ADP to ATP transition of actin monomers, required to plus end polymerization; [4] for sequestering G-actin, namely when it is phosphorylated and [5] for the polymerization of F-actin at the minus ends. [6] The treadmilling movement of actin is the increased rate of depolymerization and polymerization undertaken by cofilin and profilin respectively. This movement does not increase filament size but it generates a movement, a driving force, instead. Notably, both cofilin and profilin phosphorylation by Rho kinase decreases treadmilling movement. In order to simplify the figure, the other functions of cofilin, such as severing, are not represented.

b. Profilin and the phosphoinositide binding domain

Profilin binds to the phosphoinositide $PI(4,5)P_2$ with high affinity and inhibits the phospholipase C-γ activity, suggesting a role in signaling (Moens, 2008). The residues

responsible for the interaction are not fully known, although residues 126-136 resemble the gelsolin binding domain to $PI(4,5)P_2$ (Schutt et al., 1993) and tryptophan 3 and 31 have also been suggested to be important for this interaction (Moens, 2008). Phosphoinositide, namely $PI(4,5)P_2$, is the only know compound that inhibits profilin binding to actin (Lassing and Lindberg, 1988). The reason for this inhibition is the partial overlap of the actin binding domain and the $PI(4,5)P_2$ binding domain (Lambrechts et al., 2002). The binding of the ligands is therefore mutually exclusive (Lambrechts et al., 2002) and even the binding to PLP is impacted by the binding to $PI(4,5)P_2$, since mutants that lack the binding domain for PLP have increased affinity to $PI(4,5)P_2$ (Krishnan and Moens, 2009). The reason for the incompatibility is the conformational changes caused by $PI(4,5)P_2$ binding, that generate a negative environment at the C-terminus (Lambrechts et al., 2002).

c. Profilin and the poly-L-proline binding domain

Profilins were found to bind PLP stretches (Bjorkegren et al., 1993), with exception of the *Vaccinia* viral profilin (Machesky et al., 1994) and human profilin-IIb (Krishnan and Moens, 2009; Moens, 2008). The interaction of profilin with PLP is extensively studied (Lambrechts et al., 2002) and H133 and W3 are the amino acids involved in binding. Profilin mutants for this interaction are lethal, irrespectively of the $PI(4,5)P_2$ and actin binding activities (Lambrechts et al., 2002). This suggests that PLP binding is crucial for profilin function.

d. Profilin Phosphorylation

Profilin is regulated by phosphorylation, most notably by Rho Kinases (Shao et al., 2008). The phosphorylation site of profilin lies on the C-terminus of the protein, in serine 137 (Shao et al., 2008). This phosphorylation increases the affinity for actin and PLP stretches (Moens, 2008). The increased affinity for actin results in increased sequestering time, which leads to decreased actin incorporation in filaments. The phosphatase activity is performed by protein phosphatase 1 (PP1) (Shao and Diamond, 2012).

3- Profilin in neurons

The role of profilin in neurons has been established in several publications. Given the specific neuronal expression of Pfn2 in mammals, a putative role of Pfn2 was expected in neurons. In 2003, Da Silva and colleagues revealed that Pfn2a is a negative regulator of

neuritogenesis, via ROCK phosphorylation (Da Silva et al., 2003). More recently, Pfn1 was also proposed to have a role in neuritogenesis. Pfn1 knockdown studies revealed that together with thymosin β4, Pfn1 is fundamental for the supply of G-actin in the leading edge of lamellipodia/filopodia in growth cones (Lee et al., 2013). Moreover, Pfn1 KD leads to decreased growth cone extension and actin dynamics (Lee et al., 2013).

Using hippocampal neuron cultures as a model, Michaelsen and colleagues suggested that Pfn1 and Pfn2 have both redundant but also independent functions in neurons (Michaelsen et al., 2010). The proposed model indicates that although both forms operate via actin remodeling, Pfn1 responds in a $PI(4,5)P_2$-mediated pathway, regulating spine density, whereas Pfn2 acts through a formin-based signaling pathway, regulating dendritic complexity (Michaelsen et al., 2010).

These differential roles, together with the different affinities for the ligands could explain the apparent differential role of Pfn1 and Pfn2 in neurite outgrowth. Lambrechts and colleagues explored what Pfn1 ligand interactions are fundamental for the neuritogenesis to occur (Lambrechts et al., 2006). Using PC12 cells as a model, Pfn1 high-level overexpression lead to the abolishment of neurite outgrowth, whereas low-level overexpression suggested increased growth (Lambrechts et al., 2006), indicating that Pfn1 regulation is fundamental for the neuritogenic process. The actin binding mutant lead to decreased growth (Lambrechts et al., 2006), which was later further supported using ALS-associated actin binding incompetent mutants, as discussed below. Interestingly, both the $PI(4,5)P_2$ and PLP binding-defective mutants lead to increased outgrowth capacity (Lambrechts et al., 2006). The authors also suggested that the $PI(4,5)P_2$ binding domain is the one responsible for the ROCK pathway inhibition of neurite outgrowth (Lambrechts et al., 2006).

The role of profilin in neurons has also been studied with the KO animals for either Pfn1 (Kullmann et al., 2012a; Kullmann et al., 2012b) or Pfn2 (Pilo Boyl et al., 2007). Pfn1 KOs are embryonic lethal, in the 2-cell stage due to cytokinesis failure (Witke et al., 2001). In order to dissect the role of Pfn1 in neurons, tissue-specific KOs have been generated with neuronal-specific promoters, such as Nestin-Cre and L7-cre (Kullmann et al., 2012b). Although viable, Nestin-Cre Pfn1 KOs have several impairments in the nervous system, such as decreased brain size, cerebellar hypoplasia, aberrant layer organization in the cerebellum that leads to motor coordination impairments, and defected radial migration of cerebellar granule neurons due to a defect in cell-to-cell contact with glial cells (Kullmann et al., 2012a; Kullmann et al., 2012b). Pfn2 KOs were also generated to study its role in the nervous system (Pilo Boyl et al., 2007). Pfn2 KO mice have no gross defects in development but present behavioral defects (Pilo Boyl et al., 2007), which can be

explained by the presence of Pfn2 in dendritic spines (Michaelsen et al., 2010). It is however interesting to note that although Pfn1 is also present in dendritic spines (Michaelsen et al., 2010), Pfn1 KOs have no deficit in excitatory synapses (Kullmann et al., 2012a). Profilins are, however, proteins with such an overlap in structure and in function that compensatory mechanism are likely. Therefore, an interesting strategy would be a co-knockdown of both Pfn1 and Pfn2 in neurons to avoid any putative compensation by the different profilin isoforms.

4- Profilin in Neuronal Diseases

Recently, Wu and colleagues found that several Pfn1 mutants have been shown to have a role in the development of amyotrophic lateral sclerosis (ALS). Namely Pfn1 mutants C71G, M114T and G118V have decreased affinity for F-actin and neurons carrying these mutants show insoluble and ubiquitinated aggregates, a typical neurodegenerative finding, present in several neurodegenerative diseases such as Parkinson and Alzheimer (Wu et al., 2012). The presence of the above Pfn1 mutants resulted in small sized growth cones with unbalanced (decreased) F/G actin ratio (Wu et al., 2012), as well as decreased neurite outgrowth capacity (Wu et al., 2012).

Besides the actin binding mutants related with ALS, profilin has also been suggested to be important in another neurodegenerative disease, the spinal muscular atrophy (SMN) (Nolle et al., 2011). Profilin involvement in SMN occurs via ROCK hyper-phosphorylation of Pfn2, leading to unbalanced of F/G actin ratio (Nolle et al., 2011).The interaction profilin-actin has other known roles *in vivo,* such as in the control of cell division. Profilin disruption leads to multiple defects in actin dependent processes in *Drosophila* (Verheyen and Cooley, 1994), yeast (Haarer et al., 1990) and mice (Ding et al., 2006; Witke et al., 2001). Interestingly, most of the phenotypes are related with impairments in cell division, namely in the formation of the contractile actin ring during cytokinesis.

IV- Regeneration in the CNS and PNS

1- Regeneration as a recapitulation of development

The regeneration process is, in its principles, similar to what happens during nervous system development. In summary, a neuron with a severed axon must be capable to recapitulate embryonic development and establish a new growth cone in order to regrow the axon and form a competent synapse at the original target, re-enervating it. It is,

however, widely known that regeneration in the adult CNS is limited and usually abortive (Silver, 2009). Many aspects known for axonal growth during development are recapitulated during regeneration. However, several aspects differ greatly. Those differences can be divided in neuronal intrinsic and extrinsic. Interestingly, peripheral nervous system (PNS) regeneration presents more similarities to development, since in the PNS the regeneration process is more efficient.

2- Why is regeneration of the CNS so limited in higher vertebrates?

Nervous system regeneration is remarkably limited in higher vertebrates, namely in mammals, when compared to the lower, and simpler, vertebrates. Moreover, the regeneration potential is drastically decreased with age (Harel and Strittmatter, 2006). In lower vertebrates regeneration of the CNS is very robust, with adult salamanders being able to completely regenerate a transected spinal cord (Ferretti et al., 2003), and *Xenopus laevis* being capable of regenerating the CNS during the larval stages (Ferretti et al., 2003). Even in lower mammals, as the marsupial opossum, fully functional recovery is possible after a spinal cord transection, until the first post-natal week (Saunders et al., 1998).

Therefore, the inability of higher mammals to regenerate the CNS has been related with their increased complexity. From the evolutionary point-of-view, it is possible to hypothesize that natural selection did not favor CNS regeneration, given that the exposure of injured animal to its predators would result in death. Therefore, CNS regeneration was not positively selected (Harel and Strittmatter, 2006). Simultaneously, a more complex CNS was favored during evolution. In this respect, the decreased regenerative capacity could be a by-product of the gain in complexity (Harel and Strittmatter, 2006).

The lack of regenerative capacity of the CNS is not, however, caused by the lack of regeneration attempts. Even in the adult CNS, after an injury, transected axons attempt to regenerate, as shown in figure 19 (Kerschensteiner et al., 2005). This regeneration is, however, slower and less effective than that that occurs in the peripheral counterpart, not only due to the decreased speed of axon growth (4.3µm/h, approximately 30% of the speed observed in peripheral axons growth) but also to the erratic growth direction and increased, but misguided, branching (Kerschensteiner et al., 2005). Most of the regenerating axons do not reach any close to their original targets, creating the axonal bulbs (also known as retraction bulbs or frustrated growth cones) in the point where growth arrests (Kerschensteiner et al., 2005). Interestingly the formation of axonal bulbs

and their non-regenerative behavior was proposed already by Santiago Ramon y Cajal, in 1928 (Bradke and Marin, 2014; Lobato, 2008; Ramon y Cajal and May, 1928).

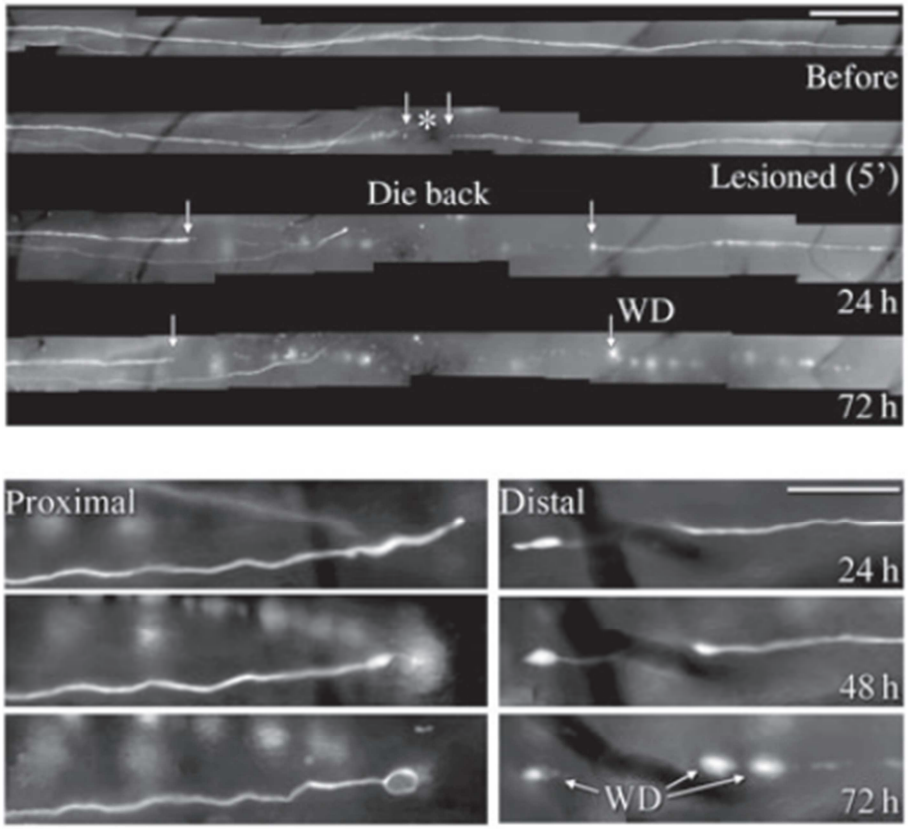

Figure 19: Confocal images of DRG neurons where regeneration attempts are visible in the spinal cord after injury. After injury (highligthed by the asterisk mark) the DRG neurons present a dying back phenotype, caused by AAD (acute axonal degeneration), a process of axonal fragmentation that occurs shortly after injury. Both distally and proximally, the axonal bulb, a hallmark of abortive regeneration, is visible (Kerschensteiner et al., 2005).

3- The neuronal intrinsic mechanisms to axonal growth

Different neurons react differently to injury. Not only neurons from different regions of the nervous system, but also the same neurons in different developmental stages. The intrinsic ability of neurons to undergo regeneration is of the utmost importance.

a. The gene expression profile of axonal growth

After injury, neurons must activate a pro-regenerative program. This is achieved through the expression of the regeneration associated genes (RAG) (Fagoe et al., 2014; Harel and Strittmatter, 2006; Huebner and Strittmatter, 2009), some with a direct role in the regeneration process while others play more indirect roles (Fagoe et al., 2014). RAG

expression is regulated by both transcription factors (Harel and Strittmatter, 2006) and epigenetic modifications of histones (Fagoe et al., 2014). Several RAGs have been identified: GAP43, fos, Gadd45a, CAP23, Itga7, NPY, VIP, galanin, DLK-1, Spirr1a, coronin-b, s100c, p21/waf1, a2 macroglobulin, CLP36, VGF, Fn14, Ddit3, Timm8b, Oazin; including the transcription factors C-jun, ATF3, STAT3, PI3K, SOX11, C/EBP,, Ankrd1, Smad1, KLF4-7, CREB, P53, NFIL3, NFκB, NFAT (Fagoe et al., 2014). Several approaches using microarrays allowed the discovery of RAGs and also suggested that the expression of RAGs is coordinated after injury (Fagoe et al., 2014). Notably, the PNS presents increased capacity to express RAGs after injury, which contributes to the PNS increased regeneration ability (Fagoe et al., 2014).

Recently the epigenetic regulation of axon regeneration was proposed (Cho et al., 2013). The histone deacetylase 5 (HDAC5), that mediates the deacetylation of tubulin, was found to be exported from the nuclei allowing a proregenerative transcription expression program of several RAGs such as c-jun, KLF4, KLF5, Fos and Gadd45a (Cho et al., 2013). The pharmacological inhibition of HDAC leads to histone H4 hyperacetylation, being followed by RAG expression and consequently improvement of axon regeneration in mice (Cho et al., 2013). Conversely, activation of acetyltransferases is also crucial for the transition to a regenerative program with RAG expression. In this respect, the acetyltransferase p300 induces expression of GAP-43, Spirr1a and coronin-b after optic nerve crush (Gaub et al., 2011) and the acetyltransferase p300/CBP-associated factor in association with the acetyltransferase p300 activates GAP-43, galanin and BDNF (Puttagunta et al., 2014).

Complementarily to the expression of RAGs, the intrinsic mechanism of regeneration is also dependent on the inhibition of proteins that antagonize axon regrowth (Fagoe et al., 2014). The knockdown of several of these regeneration inhibitory proteins results in increased axon regeneration/outgrowth capacity. Amongst these inhibitors, the deletion of PTEN, SOCS3 and the co-deletion of both has a great impact in the regenerative capacity of both optic nerve and spinal cord tracts (Fagoe et al., 2014).

b. Signaling and axonal transport mediate regeneration

The severed axon triggers a complex injury signaling in order to reprogram the neuronal cell body to enter a pro-regenerative program. After axon severing the extracellular calcium influx into the axon, leads to cytoskeleton degradation, membrane sealing but also triggers the regeneration machinery fundamental for the establishment of a new growth cone and consequently regeneration (Bradke et al., 2012). The calcium influx is

responsible for the increase in cAMP levels and consequently PKA and DLK-1 expression and activation (Bradke et al., 2012). Although the calcium influx is considered critical for the establishment of the regeneration machinery, the duration and intensity of the influx depends on the neuron type and species (Bradke et al., 2012). Besides calcium signaling, axonal transport, both anterograde and retrograde, is fundamental for regeneration to occur. Indeed, the blockage of axonal transport in DRG neurons by chelerythrine (an inhibitor of PKC) leads to failure in neuritogenesis and neurite retraction (Hiruma et al., 1999). Several injury signals have been established as mediators of axonal regeneration, as is summarized in figure 20.

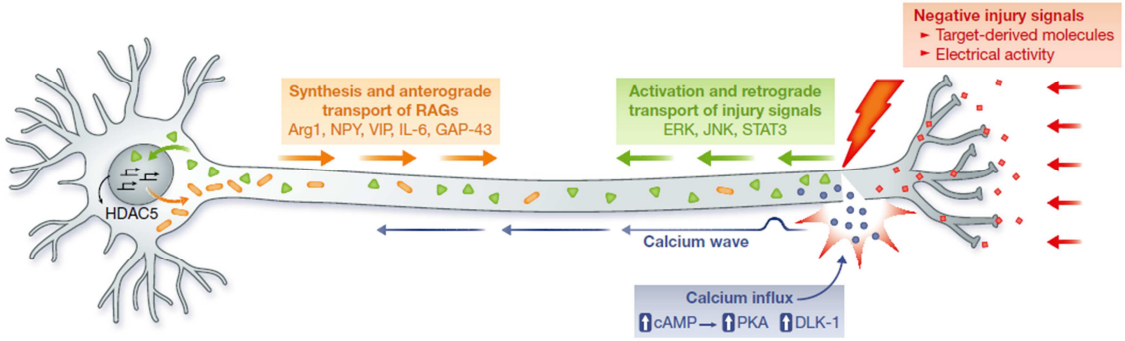

Figure 20. PNS neurons after injury start a regenerative program. After severing the loss of the distal segment of the axon leads to loss of feedback from the enervating cell/tissue. The loss of normal signaling and the activation of several injury signals and their retrograde transport to the cell body generates the expression of RAGs and transport to the lesion site. The export of HDAC5 from the nuclei is also related with increased expression of RAGs (Mar et al., 2014).

Axonal transport is crucial for injury signaling to occur. The retrograde transport of activated injury signals such as extracellular signal-regulated kinase, c-Jun N-terminal kinases, and signal transducer and activator of transcription (Ben-Yaakov et al., 2012), as is visible in the PNS branch of DRG neurons increases the expression of RAGs (Mar et al., 2014). Conversely, the interruption of the normal signals that a mature neuron receives also plays a role in the establishment of the regeneration expression program (Mar et al., 2014).

c. Neurons must generate a competent growth cone

As part of the intrinsic neuronal capacity to regrow, the ability of severed axons to restore a competent growth cone, resembling that of embryonic neurons, is important. Interestingly, whereas peripheral axons can restore a growth cone and start to regrow in the first 24 hours post injury (Kerschensteiner et al., 2005), CNS axons form an

incompetent retraction bulb (Kerschensteiner et al., 2005). The flow of events required for the establishment of a new growth cone is summarized in figure 21.

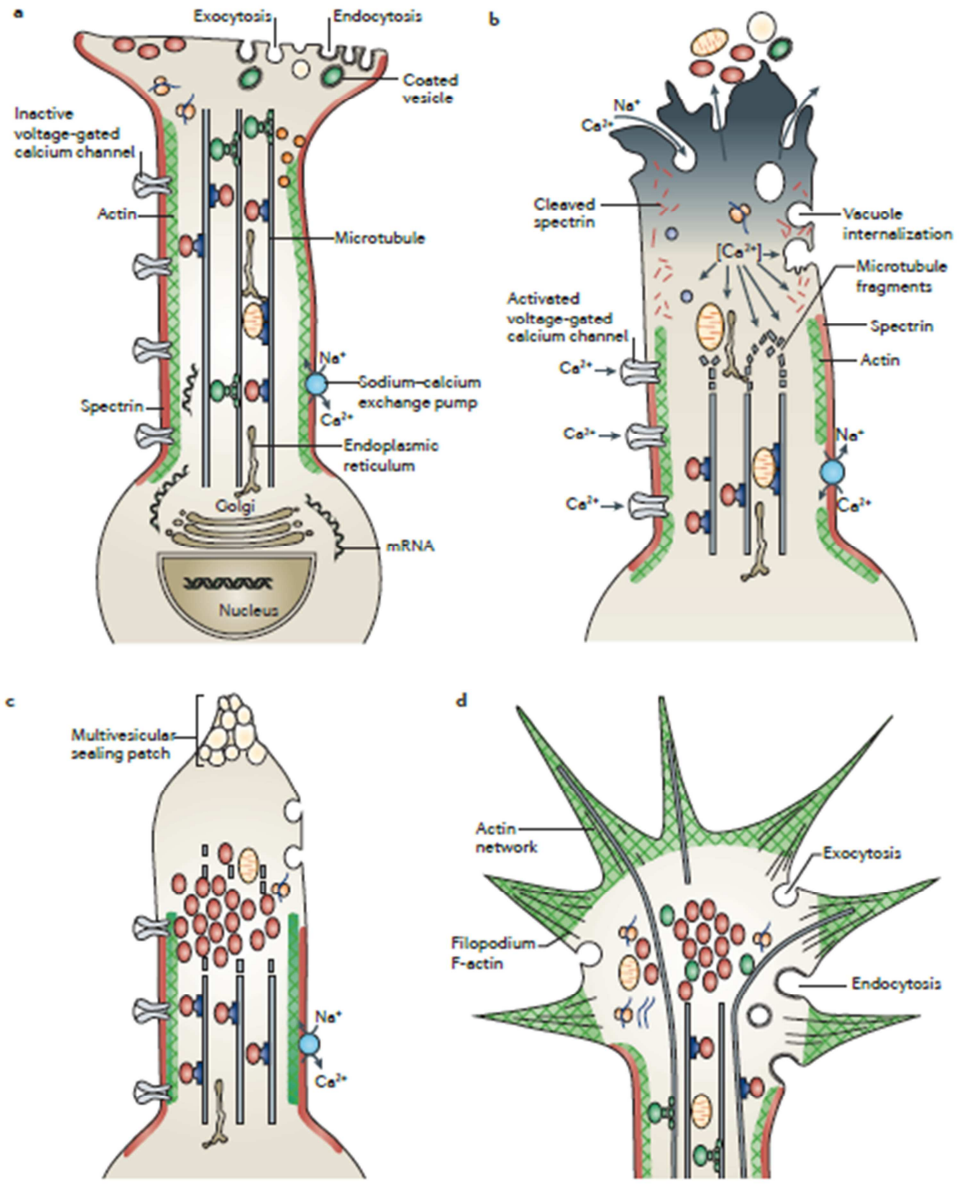

Figure 21. To restore a new and competent growth cone requires several steps. (A) Mature neurons establish synapses with their targets. (B) After axonal severing, both distal and proximal segments become permeable to the extracellular calcium influx that will lead to the activation of axonal proteases and thereby to the degradation of the actin and MT cytoskeleton. (C) The Calcium influx must be transitory to inhibit cell death. For that reason a sealing patch composed of vesicles is generated, to ensure membrane sealing. The membrane sealing allows the decrease of intracellular calcium levels and the restoration of the actin and MT cytoskeleton. (D) After the reorganization of the cytoskeleton, a growth cone can be generated, presenting the actin and MT cytoskeleton in the typical domain division shape. The restored growth cone requires the local expression of proteins as well as axonal transport, via stabilized MT, of vesicles and mitochondria to sustain the regenerative capacity. From (Bradke et al., 2012).

d. Why do CNS neurons intrinsically fail to start regeneration?

There are several differences in CNS and PNS neurons that impact drastically in the outcome of axonal regeneration. Starting by the calcium spikes in the initial moments of the response to axotomy, CNS neurons fail to have high and sustained levels of calcium (Bradke et al., 2012). Moreover, CNS neurons are more sensitive to calcium increase than PNS neurons (Bradke et al., 2012). Besides, CNS neurons usually fail to activate RAGs in contrast to what happens to PNS neurons (Fagoe et al., 2014). In part the lack of histone acetylation can also underlie the lack of regeneration of CNS axons (Puttagunta et al., 2014). Moreover, CNS neurons also express several inhibitors of axonal outgrowth, such as PTEN and SOCS3 (Mar et al., 2014). Furthermore whereas after injury, there is local protein synthesis in the axon of PNS neurons, a similar mechanism is not found in CNS neurons (Mar et al., 2014). All together these factors contribute to the decreased capacity of CNS axons to re-grow after injury.

4- The extrinsic factors

Most of the well-studied factors that impact axon regeneration are part of non-cell autonomous mechanisms. Studies using PNS grafts and CNS neurons showed that despite the decreased intrinsic capacity of CNS neurons to grow, regeneration was possible in a permissive environment, such as that found in the PNS (Mar et al., 2014). Several classes of inhibitors have already been described, namely the myelin associated inhibitors (MAIs) and the chondroitin sulphate proteoglycans (CSPGs).

MAIs are a group of proteins expressed by myelinating cells, namely oligodendrocytes in the CNS. MAIs impair neurite outgrowth *in vitro* and therefore also contribute for regeneration failure *in vivo* (Fagoe et al., 2014). MAIs include Nogo-A, myelin-associated glycoprotein (MAG), oligodendrocyte myelin glycoprotein (OMgp), epherin-B3 and Semaphorin 4D (Huebner and Strittmatter, 2009). Nogo-A, MAG and OMgp inhibit neurite outgrowth via Nogo-66 receptor 1 (Huebner and Strittmatter, 2009). In the PNS only MAG is present, but after injury it is rapidly removed by glial cells (Huebner and Strittmatter, 2009). The genetic ablation of each of the three MAIs that interact with Nogo-66 receptor 1 results in increased neurite outgrowth *in vitro*, whereas Nogo-A KO promotes axon regeneration *in vivo* (Kim et al., 2003; Simonen et al., 2003), although some reports suggest a minimal effect (Lee et al., 2009; Zheng et al., 2003). Interestingly either the triple KO of these proteins, and the Nogo-66 receptor 1 KO and the use of an antagonist peptide for Nogo-66 receptor 1 do not result in an increased axon regeneration capacity

(Lee et al., 2010), although there is a report of robust functional recovery (Cafferty et al., 2010).

Axonal severing results in a proximal and in a distal axonal stump. Whereas the proximal part of the axon will retract and attempt to restore a growth cone and regenerate, the distal part is degraded. The lesion results also in several debris containing myelin proteins that are inhibitory for regeneration. A reason underlying the successful PNS regeneration is Wallerian degeneration (WD) (Rotshenker, 2011). WD results in the clearance of the distal segment of the axon, in the removal of inhibitory debris thereby preparing a permissive environment for regrowth of the severed axons and target re-innervation (Rotshenker, 2011). In the PNS, shortly after injury, Schwann cells become dedifferentiated, reducing the expression of typical markers of differentiated Schwann cells and becoming prone to degrade the debris (Rotshenker, 2011). Interestingly, a great difference between the CNS and the PNS is the fact that the myelinating cells in the CNS, the oligodendrocytes, are not able to dedifferentiate and participate in the removal of myelin debris (Vargas and Barres, 2007). Besides Schwann cells, macrophages are also crucial for the removal of the debris, although they enter the nerve latter than Schwann cells (Rotshenker, 2011), in part as a consequence of the release by Schwann cells of the monocyte chemoattractant protein-1, which is required for macrophage migration (Rotshenker, 2011). After the removal of growth inhibitors, Schwann cells align and start to express pro-regenerative factors such as tropic factors and laminin, generating the proper environment for regrowth (Chen and Strickland, 2003). In the CNS, however, the process is not similar, which is due in part to the difficulty of macrophages to enter the CNS and also to the inability of oligodendrocytes to dedifferentiate, remove debris and secrete pro-regenerative factors (Vargas and Barres, 2007).

The other group of well described inhibitors of axon regeneration in the CNS are CSPGs, expressed by reactive astrocytes present in the glial scar that is formed after injury. The glial scar, besides being a physical barrier also inhibits axon regeneration through its chemical proprieties (Cregg et al., 2014; Silver and Miller, 2004). The CSPGs include neurocan, versican, brevican, phosphacan, aggrecan and NG2 (Galtrey and Fawcett, 2007). The receptors for CSPGs include receptor protein tyrosine phosphatase sigma (RPTPσ) (Garwood et al., 2003; Maurel et al., 1994), NgR1, NgR3 and leukocyte common antigen receptor (LAR) (Fisher et al., 2011). PTPσ and LAR ablation result in increased regenerative capacity (Siebert et al., 2014). Strategies to avoid CSPG inhibition are usually related to the use of chondroitinase ABC, a bacterial enzyme produced by *Proteus vulgaris* (Crespo et al., 2007). The use of chondroitinase ABC leads to improvement in

functional regeneration, probably through increased plasticity but not by increasing axon regeneration (Siebert et al., 2014).

One pathway common to the inhibition of axon regeneration induced by MAIs, CSPGs and repulsive guidance molecules (RGM) is the ROCK pathway (Fujita and Yamashita, 2014), as is depicted in figure 22. RhoA/ROCK is pivotal in the neurodegenerative cascade in several neurological diseases, including traumatic optic nerve and spinal cord injury, stroke and neurodegenerative diseases (Fujita and Yamashita, 2014). Thereby RhoA/ROCK signaling is a good candidate for a therapeutic approach (Fujita and Yamashita, 2014). The inhibition of axon regrowth induced by activation of the RhoA/ROCK pathway acts via cytoskeleton remodeling, both by regulating the actin cytoskeleton, via phosphorylation of cofilin, profilin, adducin and myosin light chain (MLC) amongst others; and also via MT regulation, by phosphorylation of CRMP2 (Fukata et al., 2002). Inhibition of the RhoA/ROCK pathway using C3 transferase (Boato et al., 2010), C3-05 (a cell permeable version of C3) (Lord-Fontaine et al., 2008), Y-27632 (Fournier et al., 2003), Y-39983 (Sagawa et al., 2007) and dimethyl-fasudil (Hara et al., 2000) have been used for spinal cord injury and optic nerve injury models, with promising results with both histological and functional recoveries. Moreover, the RhoA/ROCK inhibitor BA-210, cethrin, is currently being used in clinical trials in patients with acute spinal cord injury, with promising results (Fehlings et al., 2011).

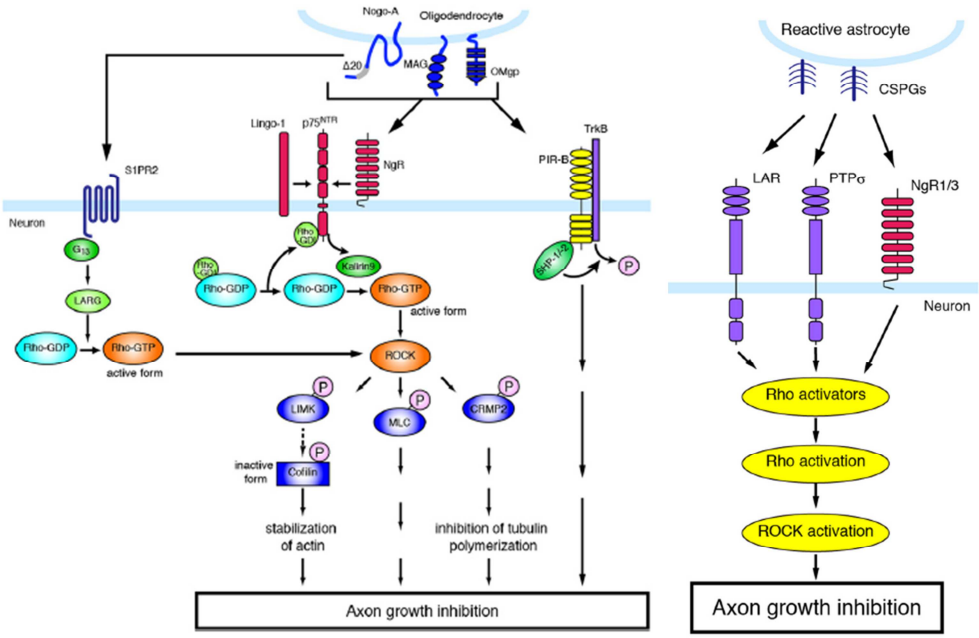

Figure 22. RhoA/ROCK pathway is downstream of both MAIs and CSPG, leading to axon growth inhibition. Both MAIs and CSPGs act via NgR1/3. MAIs act also via NgR2, Lingo-1, $p75^{NTR}$, TrkB and S1PR2 whereas CSPGs act also via LAR and RPTPσ. Downstream effectors of the inhibition cascade are the actin (through the phosphorylation of the ABPs cofilin, profilin and adducin and of myosin light chain, among others) and MT (CRMP2) cytoskeleton. From (Fujita and Yamashita, 2014)

5- How to increase regeneration in the CNS? The conditioning lesion model

The intrinsic neuronal regenerative capacity can be enhanced by several techniques, such as pharmacological treatment and gene overexpression or ablation of both enhancers or inhibitors of axon regeneration, respectively (Silver and Miller, 2004). There is, however an alternative way to increase the intrinsic regenerative capacity of a specific type of neurons, the DRG neurons, which is to perform an injury after a previous injury – conditioning lesion paradigm (McQuarrie and Grafstein, 1973). DRG neurons are a class of sensory neurons which have the particular characteristic of having a peripheral and a central branch, the latest of which enters the spinal cord. As DRG neurons have a peripheral and a central branch, they have been widely used for studies of regeneration, given the possibility of evaluating differences in neuronal behavior depending on the CNS and PNS environment.

In DRG neurons, when injury to the central axon is preceded by a peripheral injury, the central axon gains regenerative capacity and grows beyond the lesion site (Neumann and Woolf, 1999). The priming peripheral injury also enhances neurite growth *in vitro* even in the presence of an inhibitory environment, such as in the presence of myelin (Silver, 2009) – depicted in figure 23. The conditioning lesion model has been a great tool to study the gain of intrinsic regenerative capacity in CNS axons. The enhanced neurite outgrowth following a peripheral injury is related with several factors.

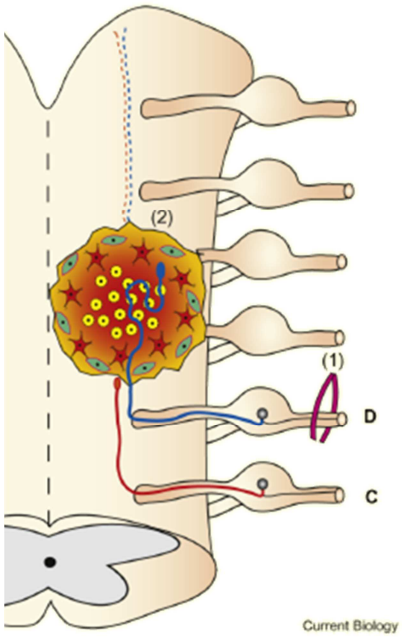

Figure 23. The conditioning lesion model. After a spinal cord injury there is the formation of a glial scar, a mechanical and chemical barrier for axon regeneration (axon in red). However, a previous injury in the peripheral branch enhances the capability of the DRG axons to extend through the CNS injury site (axon in blue). This is an example of gain of regenerative capacity. From (Silver, 2009)

RAG expression is crucial for the conditioning effect and several of the RAGs elicited in this model are already established, as GAP43, CAP23, TC10, Fn14, Sprr1a, integrin α7, Jun, ATF3, as well as the retrograde transport of the signaling molecules STAT3, JNK and ERK1/2 (Fagoe et al., 2014). Interestingly, a peripheral lesion after the central injury also enhances the expression of RAGs in DRG neurons (Ylera et al., 2009). Moreover, after axotomy using a laser that causes an injury with minimal collateral damage and minimal scar formation, the authors suggested that the formation of the glial scar was the limiting factor for the regeneration of conditioned axons (Ylera et al., 2009). Besides RAG expression, several other aspects of axon biology were studied in the context of a conditioning lesion. For instance, the epigenetic control of transcription was also shown to be related to the increased growth capacity promoted by the conditioning lesion (Cho et al., 2013; Lin et al., 2015). HDAC5, the histone H3 deacetylase is exported from the nuclei, in a PKCμ dependent manner, after the axotomy (Cho et al., 2013). Interestingly, the export of HDAC5 from the nuclei mimics the conditioning effect, leading to a pro-regenerative transcriptional program (Cho et al., 2013). The increase of cyclic AMP levels is a hallmark of peripheral injury (Neumann et al., 2002). Inhibition of cAMP degradation by rolipram (an inhibitor of phosphodiesterase) improved regeneration after spinal cord injury in animal models (Costa et al., 2013; Nikulina et al., 2004), but it has limited practical application (Zhu et al., 2001). However, the use of cAMP analogs did not recapitulate the conditioning phenotype (Blesch et al., 2012). Of note, after a conditioning lesion DRG neurons re-gain the capacity to follow a NGF gradient that is restricted to embryonic development (Webber et al., 2008). Transport also plays an important role in the conditioning effect. It is known that a peripheral injury increases the anterograde transport of newly synthesized axonal proteins, organelles and synaptic vesicles (Mar et al., 2014). Another novel insight of the mechanisms underlying the conditioning effect is the fact that electrical silencing of DRG neurons after peripheral injury (Enes et al., 2010) occurs through decrease in the levels of L-type voltage-gated calcium channel. This data suggested that electrical activity could be an important negative factor for regeneration in the CNS (Enes et al., 2010).

References

Abdi, K.M., and Bennett, V. (2008). Adducin promotes micrometer-scale organization of beta2-spectrin in lateral membranes of bronchial epithelial cells. Molecular biology of the cell *19*, 536-545.

Abe, A., Numakura, C., Saito, K., Koide, H., Oka, N., Honma, A., Kishikawa, Y., and Hayasaka, K. (2009). Neurofilament light chain polypeptide gene mutations in Charcot-Marie-Tooth disease: nonsense mutation probably causes a recessive phenotype. Journal of human genetics *54*, 94-97.

Al-Bassam, S., Xu, M., Wandless, T.J., and Arnold, D.B. (2012). Differential trafficking of transport vesicles contributes to the localization of dendritic proteins. Cell reports *2*, 89-100.

Angliker, N., and Ruegg, M.A. (2013). In vivo evidence for mTORC2-mediated actin cytoskeleton rearrangement in neurons. Bioarchitecture *3*, 113-118.

Arce, C.A., Rodriguez, J.A., Barra, H.S., and Caputo, R. (1975). Incorporation of L-tyrosine, L-phenylalanine and L-3,4-dihydroxyphenylalanine as single units into rat brain tubulin. European journal of biochemistry / FEBS *59*, 145-149.

Audebert, S., Desbruyeres, E., Gruszczynski, C., Koulakoff, A., Gros, F., Denoulet, P., and Edde, B. (1993). Reversible polyglutamylation of alpha- and beta-tubulin and microtubule dynamics in mouse brain neurons. Molecular biology of the cell *4*, 615-626.

Babic, M., and Zinsmaier, K.E. (2011). Memory, synapse stability, and beta-adducin. Neuron *69*, 1039-1041.

Baines, A.J. (2009). Evolution of spectrin function in cytoskeletal and membrane networks. Biochemical Society transactions *37*, 796-803.

Barnes, A.P., and Polleux, F. (2009). Establishment of axon-dendrite polarity in developing neurons. Annual review of neuroscience *32*, 347-381.

Bashaw, G.J., and Klein, R. (2010). Signaling from axon guidance receptors. Cold Spring Harbor perspectives in biology *2*, a001941.

Bednarek, E., and Caroni, P. (2011). beta-Adducin is required for stable assembly of new synapses and improved memory upon environmental enrichment. Neuron *69*, 1132-1146.

Ben-Yaakov, K., Dagan, S.Y., Segal-Ruder, Y., Shalem, O., Vuppalanchi, D., Willis, D.E., Yudin, D., Rishal, I., Rother, F., Bader, M.*, et al.* (2012). Axonal transcription factors signal retrogradely in lesioned peripheral nerve. The EMBO journal *31*, 1350-1363.

Bennett, V., and Baines, A.J. (2001). Spectrin and ankyrin-based pathways: metazoan inventions for integrating cells into tissues. Physiological reviews *81*, 1353-1392.

Bianchi, G., Ferrari, P., and Staessen, J.A. (2005). Adducin polymorphism: detection and impact on hypertension and related disorders. Hypertension *45*, 331-340.

Bianchi, G., and Tripodi, G. (2003). Genetics of hypertension: the adducin paradigm. Annals of the New York Academy of Sciences *986*, 660-668.

Birbach, A. (2008). Profilin, a multi-modal regulator of neuronal plasticity. BioEssays : news and reviews in molecular, cellular and developmental biology *30*, 994-1002.

Bjorkegren, C., Rozycki, M., Schutt, C.E., Lindberg, U., and Karlsson, R. (1993). Mutagenesis of human profilin locates its poly(L-proline)-binding site to a hydrophobic patch of aromatic amino acids. FEBS letters *333*, 123-126.

Blesch, A., Lu, P., Tsukada, S., Alto, L.T., Roet, K., Coppola, G., Geschwind, D., and Tuszynski, M.H. (2012). Conditioning lesions before or after spinal cord injury recruit broad genetic mechanisms that sustain axonal regeneration: superiority to camp-mediated effects. Experimental neurology *235*, 162-173.

Boato, F., Hendrix, S., Huelsenbeck, S.C., Hofmann, F., Grosse, G., Djalali, S., Klimaschewski, L., Auer, M., Just, I., Ahnert-Hilger, G*., et al.* (2010). C3 peptide enhances recovery from spinal cord injury by improved regenerative growth of descending fiber tracts. Journal of cell science *123*, 1652-1662.

Bradke, F., and Dotti, C.G. (1999). The role of local actin instability in axon formation. Science *283*, 1931-1934.

Bradke, F., Fawcett, J.W., and Spira, M.E. (2012). Assembly of a new growth cone after axotomy: the precursor to axon regeneration. Nature reviews Neuroscience *13*, 183-193.

Bradke, F., and Marin, O. (2014). Editorial overview: development and regeneration: nervous system development and regeneration. Current opinion in neurobiology *27*, iv-vi.

Buffington, S.A., and Rasband, M.N. (2011). The axon initial segment in nervous system disease and injury. The European journal of neuroscience *34*, 1609-1619.

Caceres, A., and Kosik, K.S. (1990). Inhibition of neurite polarity by tau antisense oligonucleotides in primary cerebellar neurons. Nature *343*, 461-463.

Caceres, A., Mautino, J., and Kosik, K.S. (1992). Suppression of MAP2 in cultured cerebellar macroneurons inhibits minor neurite formation. Neuron *9*, 607-618.

Cafferty, W.B., Duffy, P., Huebner, E., and Strittmatter, S.M. (2010). MAG and OMgp synergize with Nogo-A to restrict axonal growth and neurological recovery after spinal

cord trauma. The Journal of neuroscience : the official journal of the Society for Neuroscience *30*, 6825-6837.

Carlier, M.F., Pantaloni, D., and Korn, E.D. (1987). The mechanisms of ATP hydrolysis accompanying the polymerization of Mg-actin and Ca-actin. The Journal of biological chemistry *262*, 3052-3059.

Carlsson, L., Nystrom, L.E., Sundkvist, I., Markey, F., and Lindberg, U. (1977). Actin polymerizability is influenced by profilin, a low molecular weight protein in non-muscle cells. Journal of molecular biology *115*, 465-483.

Chan, P.C., Hsu, R.Y., Liu, C.W., Lai, C.C., and Chen, H.C. (2014). Adducin-1 is essential for mitotic spindle assembly through its interaction with myosin-X. The Journal of cell biology *204*, 19-28.

Chen, C.L., Lin, Y.P., Lai, Y.C., and Chen, H.C. (2011). alpha-Adducin translocates to the nucleus upon loss of cell-cell adhesions. Traffic *12*, 1327-1340.

Chen, Z.L., and Strickland, S. (2003). Laminin gamma1 is critical for Schwann cell differentiation, axon myelination, and regeneration in the peripheral nerve. The Journal of cell biology *163*, 889-899.

Cho, Y., Sloutsky, R., Naegle, K.M., and Cavalli, V. (2013). Injury-induced HDAC5 nuclear export is essential for axon regeneration. Cell *155*, 894-908.

Cifuentes-Diaz, C., Nicole, S., Velasco, M.E., Borra-Cebrian, C., Panozzo, C., Frugier, T., Millet, G., Roblot, N., Joshi, V., and Melki, J. (2002). Neurofilament accumulation at the motor endplate and lack of axonal sprouting in a spinal muscular atrophy mouse model. Human molecular genetics *11*, 1439-1447.

Costa, L.M., Pereira, J.E., Filipe, V.M., Magalhaes, L.G., Couto, P.A., Gonzalo-Orden, J.M., Raimondo, S., Geuna, S., Mauricio, A.C., Nikulina, E*., et al.* (2013). Rolipram promotes functional recovery after contusive thoracic spinal cord injury in rats. Behavioural brain research *243*, 66-73.

Cregg, J.M., DePaul, M.A., Filous, A.R., Lang, B.T., Tran, A., and Silver, J. (2014). Functional regeneration beyond the glial scar. Experimental neurology *253*, 197-207.

Crespo, D., Asher, R.A., Lin, R., Rhodes, K.E., and Fawcett, J.W. (2007). How does chondroitinase promote functional recovery in the damaged CNS? Experimental neurology *206*, 159-171.

Cusi, D., Barlassina, C., Azzani, T., Casari, G., Citterio, L., Devoto, M., Glorioso, N., Lanzani, C., Manunta, P., Righetti, M.*, et al.* (1997). Polymorphisms of alpha-adducin and salt sensitivity in patients with essential hypertension. Lancet *349*, 1353-1357.

D'Este, E., Kamin, D., Göttfert, F., El-Hady, A., and Hell, S.W. (2015). STED Nanoscopy Reveals the Ubiquity of Subcortical Cytoskeleton Periodicity in Living Neurons. Cell reports *10*.

Da Silva, J.S., Medina, M., Zuliani, C., Di Nardo, A., Witke, W., and Dotti, C.G. (2003). RhoA/ROCK regulation of neuritogenesis via profilin IIa-mediated control of actin stability. The Journal of cell biology *162*, 1267-1279.

Dehmelt, L., and Halpain, S. (2005). The MAP2/Tau family of microtubule-associated proteins. Genome biology *6*, 204.

Denoulet, P., Edde, B., and Gros, F. (1986). Differential expression of several neurospecific beta-tubulin mRNAs in the mouse brain during development. Gene *50*, 289-297.

Dent, E.W., and Gertler, F.B. (2003). Cytoskeletal dynamics and transport in growth cone motility and axon guidance. Neuron *40*, 209-227.

Dent, E.W., Gupton, S.L., and Gertler, F.B. (2011). The growth cone cytoskeleton in axon outgrowth and guidance. Cold Spring Harbor perspectives in biology *3*.

Desai, A., and Mitchison, T.J. (1997). Microtubule polymerization dynamics. Annual review of cell and developmental biology *13*, 83-117.

Didry, D., Carlier, M.F., and Pantaloni, D. (1998). Synergy between actin depolymerizing factor/cofilin and profilin in increasing actin filament turnover. The Journal of biological chemistry *273*, 25602-25611.

Ding, Z., Lambrechts, A., Parepally, M., and Roy, P. (2006). Silencing profilin-1 inhibits endothelial cell proliferation, migration and cord morphogenesis. Journal of cell science *119*, 4127-4137.

Dong, L., Chapline, C., Mousseau, B., Fowler, L., Ramsay, K., Stevens, J.L., and Jaken, S. (1995). 35H, a sequence isolated as a protein kinase C binding protein, is a novel member of the adducin family. The Journal of biological chemistry *270*, 25534-25540.

Efendiev, R., Krmar, R.T., Ogimoto, G., Zwiller, J., Tripodi, G., Katz, A.I., Bianchi, G., Pedemonte, C.H., and Bertorello, A.M. (2004). Hypertension-linked mutation in the adducin alpha-subunit leads to higher AP2-mu2 phosphorylation and impaired Na+,K+-

ATPase trafficking in response to GPCR signals and intracellular sodium. Circulation research *95*, 1100-1108.

Enes, J., Langwieser, N., Ruschel, J., Carballosa-Gonzalez, M.M., Klug, A., Traut, M.H., Ylera, B., Tahirovic, S., Hofmann, F., Stein, V.*, et al.* (2010). Electrical activity suppresses axon growth through Ca(v)1.2 channels in adult primary sensory neurons. Current biology : CB *20*, 1154-1164.

Engert, F., and Bonhoeffer, T. (1999). Dendritic spine changes associated with hippocampal long-term synaptic plasticity. Nature *399*, 66-70.

Estrada-Bernal, A., Sanford, S.D., Sosa, L.J., Simon, G.C., Hansen, K.C., and Pfenninger, K.H. (2012). Functional complexity of the axonal growth cone: a proteomic analysis. PloS one *7*, e31858.

Fache, M.P., Moussif, A., Fernandes, F., Giraud, P., Garrido, J.J., and Dargent, B. (2004). Endocytotic elimination and domain-selective tethering constitute a potential mechanism of protein segregation at the axonal initial segment. The Journal of cell biology *166*, 571-578.

Fagoe, N.D., van Heest, J., and Verhaagen, J. (2014). Spinal cord injury and the neuron-intrinsic regeneration-associated gene program. Neuromolecular medicine *16*, 799-813.

Farghaian, H., Turnley, A.M., Sutherland, C., and Cole, A.R. (2011). Bioinformatic prediction and confirmation of beta-adducin as a novel substrate of glycogen synthase kinase 3. The Journal of biological chemistry *286*, 25274-25283.

Fehlings, M.G., Theodore, N., Harrop, J., Maurais, G., Kuntz, C., Shaffrey, C.I., Kwon, B.K., Chapman, J., Yee, A., Tighe, A.*, et al.* (2011). A phase I/IIa clinical trial of a recombinant Rho protein antagonist in acute spinal cord injury. Journal of neurotrauma *28*, 787-796.

Fernyhough, P., and Schmidt, R.E. (2002). Neurofilaments in diabetic neuropathy. International review of neurobiology *50*, 115-144.

Ferretti, P., Zhang, F., and O'Neill, P. (2003). Changes in spinal cord regenerative ability through phylogenesis and development: lessons to be learnt. Developmental dynamics : an official publication of the American Association of Anatomists *226*, 245-256.

Fisher, D., Xing, B., Dill, J., Li, H., Hoang, H.H., Zhao, Z., Yang, X.L., Bachoo, R., Cannon, S., Longo, F.M.*, et al.* (2011). Leukocyte common antigen-related phosphatase is a functional receptor for chondroitin sulfate proteoglycan axon growth inhibitors. The Journal of neuroscience : the official journal of the Society for Neuroscience *31*, 14051-14066.

Flynn, K.C., Hellal, F., Neukirchen, D., Jacob, S., Tahirovic, S., Dupraz, S., Stern, S., Garvalov, B.K., Gurniak, C., Shaw, A.E.*, et al.* (2012). ADF/cofilin-mediated actin retrograde flow directs neurite formation in the developing brain. Neuron *76*, 1091-1107.

Flynn, K.C., Pak, C.W., Shaw, A.E., Bradke, F., and Bamburg, J.R. (2009). Growth cone-like waves transport actin and promote axonogenesis and neurite branching. Developmental neurobiology *69*, 761-779.

Fournier, A.E., Takizawa, B.T., and Strittmatter, S.M. (2003). Rho kinase inhibition enhances axonal regeneration in the injured CNS. The Journal of neuroscience : the official journal of the Society for Neuroscience *23*, 1416-1423.

Fujita, Y., and Yamashita, T. (2014). Axon growth inhibition by RhoA/ROCK in the central nervous system. Frontiers in neuroscience *8*, 338.

Fukata, Y., Itoh, T.J., Kimura, T., Menager, C., Nishimura, T., Shiromizu, T., Watanabe, H., Inagaki, N., Iwamatsu, A., Hotani, H.*, et al.* (2002). CRMP-2 binds to tubulin heterodimers to promote microtubule assembly. Nature cell biology *4*, 583-591.

Fukata, Y., Oshiro, N., Kinoshita, N., Kawano, Y., Matsuoka, Y., Bennett, V., Matsuura, Y., and Kaibuchi, K. (1999). Phosphorylation of adducin by Rho-kinase plays a crucial role in cell motility. The Journal of cell biology *145*, 347-361.

Gallardo, G., Barowski, J., Ravits, J., Siddique, T., Lingrel, J.B., Robertson, J., Steen, H., and Bonni, A. (2014). An alpha2-Na/K ATPase/alpha-adducin complex in astrocytes triggers non-cell autonomous neurodegeneration. Nature neuroscience *17*, 1710-1719.

Gallo, G. (2006). RhoA-kinase coordinates F-actin organization and myosin II activity during semaphorin-3A-induced axon retraction. Journal of cell science *119*, 3413-3423.

Gallo, G. (2013). More than one ring to bind them all: recent insights into the structure of the axon. Developmental neurobiology *73*, 799-805.

Galtrey, C.M., and Fawcett, J.W. (2007). The role of chondroitin sulfate proteoglycans in regeneration and plasticity in the central nervous system. Brain research reviews *54*, 1-18.

Ganay, T., Boizot, A., Burrer, R., Chauvin, J.P., and Bomont, P. (2011). Sensory-motor deficits and neurofilament disorganization in gigaxonin-null mice. Molecular neurodegeneration *6*, 25.

Gardner, K., and Bennett, V. (1986). A new erythrocyte membrane-associated protein with calmodulin binding activity. Identification and purification. The Journal of biological chemistry *261*, 1339-1348.

Garwood, J., Heck, N., Reichardt, F., and Faissner, A. (2003). Phosphacan short isoform, a novel non-proteoglycan variant of phosphacan/receptor protein tyrosine phosphatase-beta, interacts with neuronal receptors and promotes neurite outgrowth. The Journal of biological chemistry *278*, 24164-24173.

Gaub, P., Joshi, Y., Wuttke, A., Naumann, U., Schnichels, S., Heiduschka, P., and Di Giovanni, S. (2011). The histone acetyltransferase p300 promotes intrinsic axonal regeneration. Brain : a journal of neurology *134*, 2134-2148.

Gilligan, D.M., Lozovatsky, L., Gwynn, B., Brugnara, C., Mohandas, N., and Peters, L.L. (1999). Targeted disruption of the beta adducin gene (Add2) causes red blood cell spherocytosis in mice. Proceedings of the National Academy of Sciences of the United States of America *96*, 10717-10722.

Goldman, J.E., Yen, S.H., Chiu, F.C., and Peress, N.S. (1983). Lewy bodies of Parkinson's disease contain neurofilament antigens. Science *221*, 1082-1084.

Gomez, T.M., and Letourneau, P.C. (2014). Actin dynamics in growth cone motility and navigation. Journal of neurochemistry *129*, 221-234.

Gomis-Ruth, S., Wierenga, C.J., and Bradke, F. (2008). Plasticity of polarization: changing dendrites into axons in neurons integrated in neuronal circuits. Current biology : CB *18*, 992-1000.

Gotoh, H., Okumura, N., Yagi, T., Okumura, A., Shima, T., and Nagai, K. (2006). Fyn-induced phosphorylation of beta-adducin at tyrosine 489 and its role in their subcellular localization. Biochemical and biophysical research communications *346*, 600-605.

Grubb, M.S., and Burrone, J. (2010). Activity-dependent relocation of the axon initial segment fine-tunes neuronal excitability. Nature *465*, 1070-1074.

Grubb, M.S., Shu, Y., Kuba, H., Rasband, M.N., Wimmer, V.C., and Bender, K.J. (2011). Short- and long-term plasticity at the axon initial segment. The Journal of neuroscience : the official journal of the Society for Neuroscience *31*, 16049-16055.

Gruenbaum, L.M., Gilligan, D.M., Picciotto, M.R., Marinesco, S., and Carew, T.J. (2003). Identification and characterization of Aplysia adducin, an Aplysia cytoskeletal protein homologous to mammalian adducins: increased phosphorylation at a protein kinase C consensus site during long-term synaptic facilitation. The Journal of neuroscience : the official journal of the Society for Neuroscience *23*, 2675-2685.

Gumy, L.F., Yeo, G.S., Tung, Y.C., Zivraj, K.H., Willis, D., Coppola, G., Lam, B.Y., Twiss, J.L., Holt, C.E., and Fawcett, J.W. (2011). Transcriptome analysis of embryonic and adult sensory axons reveals changes in mRNA repertoire localization. Rna *17*, 85-98.

Haarer, B.K., Lillie, S.H., Adams, A.E., Magdolen, V., Bandlow, W., and Brown, S.S. (1990). Purification of profilin from Saccharomyces cerevisiae and analysis of profilin-deficient cells. The Journal of cell biology *110*, 105-114.

Hadziselimovic, N., Vukojevic, V., Peter, F., Milnik, A., Fastenrath, M., Fenyves, B.G., Hieber, P., Demougin, P., Vogler, C., de Quervain, D.J.*, et al.* (2014). Forgetting is regulated via Musashi-mediated translational control of the Arp2/3 complex. Cell *156*, 1153-1166.

Hallak, M.E., Rodriguez, J.A., Barra, H.S., and Caputto, R. (1977). Release of tyrosine from tyrosinated tubulin. Some common factors that affect this process and the assembly of tubulin. FEBS letters *73*, 147-150.

Hammarlund, M., Davis, W.S., and Jorgensen, E.M. (2000). Mutations in beta-spectrin disrupt axon outgrowth and sarcomere structure. The Journal of cell biology *149*, 931-942.

Hammarlund, M., Jorgensen, E.M., and Bastiani, M.J. (2007). Axons break in animals lacking beta-spectrin. The Journal of cell biology *176*, 269-275.

Hara, M., Takayasu, M., Watanabe, K., Noda, A., Takagi, T., Suzuki, Y., and Yoshida, J. (2000). Protein kinase inhibition by fasudil hydrochloride promotes neurological recovery after spinal cord injury in rats. Journal of neurosurgery *93*, 94-101.

Harel, N.Y., and Strittmatter, S.M. (2006). Can regenerating axons recapitulate developmental guidance during recovery from spinal cord injury? Nature reviews Neuroscience *7*, 603-616.

Hedstrom, K.L., Ogawa, Y., and Rasband, M.N. (2008). AnkyrinG is required for maintenance of the axon initial segment and neuronal polarity. The Journal of cell biology *183*, 635-640.

Hiruma, H., Maruyama, H., Katakura, T., Simada, Z.B., Nishida, S., Hoka, S., Takenaka, T., and Kawakami, T. (1999). Axonal transport is inhibited by a protein kinase C inhibitor in cultured isolated mouse dorsal root ganglion cells. Brain research *826*, 135-138.

Hopkins, P.N., and Hunt, S.C. (2003). Genetics of hypertension. Genetics in medicine : official journal of the American College of Medical Genetics *5*, 413-429.

Howes, S.C., Alushin, G.M., Shida, T., Nachury, M.V., and Nogales, E. (2014). Effects of tubulin acetylation and tubulin acetyltransferase binding on microtubule structure. Molecular biology of the cell *25*, 257-266.

Hu, J.H., Zhang, H., Wagey, R., Krieger, C., and Pelech, S.L. (2003). Protein kinase and protein phosphatase expression in amyotrophic lateral sclerosis spinal cord. Journal of neurochemistry *85*, 432-442.

Huebner, E.A., and Strittmatter, S.M. (2009). Axon regeneration in the peripheral and central nervous systems. Results and problems in cell differentiation *48*, 339-351.

Hughes, C.A., and Bennett, V. (1995). Adducin: a physical model with implications for function in assembly of spectrin-actin complexes. The Journal of biological chemistry *270*, 18990-18996.

Ikegami, K., Sato, S., Nakamura, K., Ostrowski, L.E., and Setou, M. (2010). Tubulin polyglutamylation is essential for airway ciliary function through the regulation of beating asymmetry. Proceedings of the National Academy of Sciences of the United States of America *107*, 10490-10495.

Iwai, N., Tamaki, S., Nakamura, Y., and Kinoshita, M. (1997). Polymorphism of alpha-adducin and hypertension. Lancet *350*, 369.

Janke, C. (2014). The tubulin code: molecular components, readout mechanisms, and functions. The Journal of cell biology *206*, 461-472.

Janke, C., and Kneussel, M. (2010). Tubulin post-translational modifications: encoding functions on the neuronal microtubule cytoskeleton. Trends in neurosciences *33*, 362-372.

Jones, S.L., Korobova, F., and Svitkina, T. (2014). Axon initial segment cytoskeleton comprises a multiprotein submembranous coat containing sparse actin filaments. The Journal of cell biology *205*, 67-81.

Joshi, H.C., and Cleveland, D.W. (1989). Differential utilization of beta-tubulin isotypes in differentiating neurites. The Journal of cell biology *109*, 663-673.

Joshi, R., Gilligan, D.M., Otto, E., McLaughlin, T., and Bennett, V. (1991). Primary structure and domain organization of human alpha and beta adducin. The Journal of cell biology *115*, 665-675.

Jung, Y., Mulholland, P.J., Wiseman, S.L., Chandler, L.J., and Picciotto, M.R. (2013). Constitutive knockout of the membrane cytoskeleton protein beta adducin decreases mushroom spine density in the nucleus accumbens but does not prevent spine remodeling in response to cocaine. The European journal of neuroscience *37*, 1-9.

Kaech, S., and Banker, G. (2006). Culturing hippocampal neurons. Nature protocols *1*, 2406-2415.

Kalinina, E., Biswas, R., Berezniuk, I., Hermoso, A., Aviles, F.X., and Fricker, L.D. (2007). A novel subfamily of mouse cytosolic carboxypeptidases. FASEB journal : official publication of the Federation of American Societies for Experimental Biology *21*, 836-850.

Kerschensteiner, M., Schwab, M.E., Lichtman, J.W., and Misgeld, T. (2005). In vivo imaging of axonal degeneration and regeneration in the injured spinal cord. Nature medicine *11*, 572-577.

Kim, J.E., Li, S., GrandPre, T., Qiu, D., and Strittmatter, S.M. (2003). Axon regeneration in young adult mice lacking Nogo-A/B. Neuron *38*, 187-199.

Kimura, K., Fukata, Y., Matsuoka, Y., Bennett, V., Matsuura, Y., Okawa, K., Iwamatsu, A., and Kaibuchi, K. (1998). Regulation of the association of adducin with actin filaments by Rho-associated kinase (Rho-kinase) and myosin phosphatase. The Journal of biological chemistry *273*, 5542-5548.

Kimura, T., Watanabe, H., Iwamatsu, A., and Kaibuchi, K. (2005). Tubulin and CRMP-2 complex is transported via Kinesin-1. Journal of neurochemistry *93*, 1371-1382.

Klintsova, A.Y., and Greenough, W.T. (1999). Synaptic plasticity in cortical systems. Current opinion in neurobiology *9*, 203-208.

Korn, E.D., Carlier, M.F., and Pantaloni, D. (1987). Actin polymerization and ATP hydrolysis. Science *238*, 638-644.

Krishnan, K., and Moens, P.D.J. (2009). Structure and functions of profilins. 71-81.

Kruer, M.C., Jepperson, T., Dutta, S., Steiner, R.D., Cottenie, E., Sanford, L., Merkens, M., Russman, B.S., Blasco, P.A., Fan, G.*, et al.* (2013). Mutations in gamma adducin are associated with inherited cerebral palsy. Annals of neurology *74*, 805-814.

Kuba, H., Oichi, Y., and Ohmori, H. (2010). Presynaptic activity regulates Na(+) channel distribution at the axon initial segment. Nature *465*, 1075-1078.

Kullmann, J.A., Neumeyer, A., Gurniak, C.B., Friauf, E., Witke, W., and Rust, M.B. (2012a). Profilin1 is required for glial cell adhesion and radial migration of cerebellar granule neurons. EMBO reports *13*, 75-82.

Kullmann, J.A., Neumeyer, A., Wickertsheim, I., Bottcher, R.T., Costell, M., Deitmer, J.W., Witke, W., Friauf, E., and Rust, M.B. (2012b). Purkinje cell loss and motor coordination defects in profilin1 mutant mice. Neuroscience *223*, 355-364.

Lambrechts, A., Jonckheere, V., Dewitte, D., Vandekerckhove, J., and Ampe, C. (2002). Mutational analysis of human profilin I reveals a second PI(4,5)-P2 binding site neighbouring the poly(L-proline) binding site. BMC biochemistry *3*, 12.

Lambrechts, A., Jonckheere, V., Peleman, C., Polet, D., De Vos, W., Vandekerckhove, J., and Ampe, C. (2006). Profilin-I-ligand interactions influence various aspects of neuronal differentiation. Journal of cell science *119*, 1570-1578.

Lambrechts, A., Verschelde, J.L., Jonckheere, V., Goethals, M., Vandekerckhove, J., and Ampe, C. (1997). The mammalian profilin isoforms display complementary affinities for PIP2 and proline-rich sequences. The EMBO journal *16*, 484-494.

Lanzani, C., Citterio, L., Jankaricova, M., Sciarrone, M.T., Barlassina, C., Fattori, S., Messaggio, E., Serio, C.D., Zagato, L., Cusi, D.*, et al.* (2005). Role of the adducin family genes in human essential hypertension. Journal of hypertension *23*, 543-549.

Lassing, I., and Lindberg, U. (1988). Specificity of the interaction between phosphatidylinositol 4,5-bisphosphate and the profilin:actin complex. Journal of cellular biochemistry *37*, 255-267.

Lavaur, J., Mineur, Y.S., and Picciotto, M.R. (2009). The membrane cytoskeletal protein adducin is phosphorylated by protein kinase C in D1 neurons of the nucleus accumbens and dorsal striatum following cocaine administration. Journal of neurochemistry *111*, 1129-1137.

Lee, C.W., Vitriol, E.A., Shim, S., Wise, A.L., Velayutham, R.P., and Zheng, J.Q. (2013). Dynamic localization of G-actin during membrane protrusion in neuronal motility. Current biology : CB *23*, 1046-1056.

Lee, J.K., Chan, A.F., Luu, S.M., Zhu, Y., Ho, C., Tessier-Lavigne, M., and Zheng, B. (2009). Reassessment of corticospinal tract regeneration in Nogo-deficient mice. The Journal of neuroscience : the official journal of the Society for Neuroscience *29*, 8649-8654.

Lee, J.K., Geoffroy, C.G., Chan, A.F., Tolentino, K.E., Crawford, M.J., Leal, M.A., Kang, B., and Zheng, B. (2010). Assessing spinal axon regeneration and sprouting in Nogo-, MAG-, and OMgp-deficient mice. Neuron *66*, 663-670.

Lee, S.H., and Dominguez, R. (2010). Regulation of actin cytoskeleton dynamics in cells. Molecules and cells *29*, 311-325.

Leonard, J.M., Cozens, A.L., Reid, S.M., Fahey, M.C., Ditchfield, M.R., and Reddihough, D.S. (2011). Should children with cerebral palsy and normal imaging undergo testing for inherited metabolic disorders? Developmental medicine and child neurology *53*, 226-232.

Lerer, I., Sagi, M., Meiner, V., Cohen, T., Zlotogora, J., and Abeliovich, D. (2005). Deletion of the ANKRD15 gene at 9p24.3 causes parent-of-origin-dependent inheritance of familial cerebral palsy. Human molecular genetics *14*, 3911-3920.

Letourneau, P.C. (2009). Actin in axons: stable scaffolds and dynamic filaments. Results and problems in cell differentiation *48*, 65-90.

Lewis, T.L., Jr., Courchet, J., and Polleux, F. (2013). Cell biology in neuroscience: Cellular and molecular mechanisms underlying axon formation, growth, and branching. The Journal of cell biology *202*, 837-848.

Li, X., Matsuoka, Y., and Bennett, V. (1998). Adducin preferentially recruits spectrin to the fast growing ends of actin filaments in a complex requiring the MARCKS-related domain and a newly defined oligomerization domain. The Journal of biological chemistry *273*, 19329-19338.

Lin, C.H., Espreafico, E.M., Mooseker, M.S., and Forscher, P. (1996). Myosin drives retrograde F-actin flow in neuronal growth cones. Neuron *16*, 769-782.

Lin, S., Nazif, K., Smith, A., Baas, P.W., and Smith, G.M. (2015). Histone acetylation inhibitors promote axon growth in adult dorsal root ganglia neurons. Journal of neuroscience research.

Lobato, R.D. (2008). Historical vignette of Cajal's work "Degeneration and regeneration of the nervous system" with a reflection of the author. Neurocirugia *19*, 456-468.

Lord-Fontaine, S., Yang, F., Diep, Q., Dergham, P., Munzer, S., Tremblay, P., and McKerracher, L. (2008). Local inhibition of Rho signaling by cell-permeable recombinant protein BA-210 prevents secondary damage and promotes functional recovery following acute spinal cord injury. Journal of neurotrauma *25*, 1309-1322.

Lou, H., Park, J.J., Phillips, A., and Loh, Y.P. (2013). gamma-Adducin promotes process outgrowth and secretory protein exit from the Golgi apparatus. Journal of molecular neuroscience : MN *49*, 1-10.

Lowery, L.A., and Van Vactor, D. (2009). The trip of the tip: understanding the growth cone machinery. Nature reviews Molecular cell biology *10*, 332-343.

Lukinavicius, G., Reymond, L., D'Este, E., Masharina, A., Gottfert, F., Ta, H., Guther, A., Fournier, M., Rizzo, S., Waldmann, H.*, et al.* (2014). Fluorogenic probes for live-cell imaging of the cytoskeleton. Nature methods *11*, 731-733.

Ma, X., Bao, J., and Adelstein, R.S. (2007). Loss of cell adhesion causes hydrocephalus in nonmuscle myosin II-B-ablated and mutated mice. Molecular biology of the cell *18*, 2305-2312.

Maas, C., Belgardt, D., Lee, H.K., Heisler, F.F., Lappe-Siefke, C., Magiera, M.M., van Dijk, J., Hausrat, T.J., Janke, C., and Kneussel, M. (2009). Synaptic activation modifies

microtubules underlying transport of postsynaptic cargo. Proceedings of the National Academy of Sciences of the United States of America *106*, 8731-8736.

Machesky, L.M., Cole, N.B., Moss, B., and Pollard, T.D. (1994). Vaccinia virus expresses a novel profilin with a higher affinity for polyphosphoinositides than actin. Biochemistry *33*, 10815-10824.

Maletic-Savatic, M., Malinow, R., and Svoboda, K. (1999). Rapid dendritic morphogenesis in CA1 hippocampal dendrites induced by synaptic activity. Science *283*, 1923-1927.

Manetto, V., Sternberger, N.H., Perry, G., Sternberger, L.A., and Gambetti, P. (1988). Phosphorylation of neurofilaments is altered in amyotrophic lateral sclerosis. Journal of neuropathology and experimental neurology *47*, 642-653.

Manunta, P., Barlassina, C., and Bianchi, G. (1998). Adducin in essential hypertension. FEBS letters *430*, 41-44.

Mar, F.M., Bonni, A., and Sousa, M.M. (2014). Cell intrinsic control of axon regeneration. EMBO reports *15*, 254-263.

Marro, M.L., Scremin, O.U., Jordan, M.C., Huynh, L., Porro, F., Roos, K.P., Gajovic, S., Baralle, F.E., and Muro, A.F. (2000). Hypertension in beta-adducin-deficient mice. Hypertension *36*, 449-453.

Marsick, B.M., San Miguel-Ruiz, J.E., and Letourneau, P.C. (2012). Activation of ezrin/radixin/moesin mediates attractive growth cone guidance through regulation of growth cone actin and adhesion receptors. The Journal of neuroscience : the official journal of the Society for Neuroscience *32*, 282-296.

Matsuoka, Y., Hughes, C.A., and Bennett, V. (1996). Adducin regulation. Definition of the calmodulin-binding domain and sites of phosphorylation by protein kinases A and C. The Journal of biological chemistry *271*, 25157-25166.

Matsuoka, Y., Li, X., and Bennett, V. (1998). Adducin is an in vivo substrate for protein kinase C: phosphorylation in the MARCKS-related domain inhibits activity in promoting spectrin-actin complexes and occurs in many cells, including dendritic spines of neurons. The Journal of cell biology *142*, 485-497.

Matsuoka, Y., Li, X., and Bennett, V. (2000). Adducin: structure, function and regulation. Cellular and molecular life sciences : CMLS *57*, 884-895.

Maurel, P., Rauch, U., Flad, M., Margolis, R.K., and Margolis, R.U. (1994). Phosphacan, a chondroitin sulfate proteoglycan of brain that interacts with neurons and neural cell-adhesion molecules, is an extracellular variant of a receptor-type protein tyrosine

phosphatase. Proceedings of the National Academy of Sciences of the United States of America *91*, 2512-2516.

Maxwell, M.M., Tomkinson, E.M., Nobles, J., Wizeman, J.W., Amore, A.M., Quinti, L., Chopra, V., Hersch, S.M., and Kazantsev, A.G. (2011). The Sirtuin 2 microtubule deacetylase is an abundant neuronal protein that accumulates in the aging CNS. Human molecular genetics *20*, 3986-3996.

McQuarrie, I.G., and Grafstein, B. (1973). Axon outgrowth enhanced by a previous nerve injury. Archives of neurology *29*, 53-55.

Medeiros, N.A., Burnette, D.T., and Forscher, P. (2006). Myosin II functions in actin-bundle turnover in neuronal growth cones. Nature cell biology *8*, 215-226.

Mellor, H. (2010). The role of formins in filopodia formation. Biochimica et biophysica acta *1803*, 191-200.

Michaelsen, K., Murk, K., Zagrebelsky, M., Dreznjak, A., Jockusch, B.M., Rothkegel, M., and Korte, M. (2010). Fine-tuning of neuronal architecture requires two profilin isoforms. Proceedings of the National Academy of Sciences of the United States of America *107*, 15780-15785.

Mische, S.M., Mooseker, M.S., and Morrow, J.S. (1987). Erythrocyte adducin: a calmodulin-regulated actin-bundling protein that stimulates spectrin-actin binding. The Journal of cell biology *105*, 2837-2845.

Moens, P.D. (2008). Protein Reviews. In Actin-Binding Proteins and Disease, C. dos Remedios, and D. Chhabra, eds. (Sydney: Springer), pp. 200-217.

Monaco, S., Autilio-Gambetti, L., Zabel, D., and Gambetti, P. (1985). Giant axonal neuropathy: acceleration of neurofilament transport in optic axons. Proceedings of the National Academy of Sciences of the United States of America *82*, 920-924.

Mullen, R.J., Eicher, E.M., and Sidman, R.L. (1976). Purkinje cell degeneration, a new neurological mutation in the mouse. Proceedings of the National Academy of Sciences of the United States of America *73*, 208-212.

Nakada, C., Ritchie, K., Oba, Y., Nakamura, M., Hotta, Y., Iino, R., Kasai, R.S., Yamaguchi, K., Fujiwara, T., and Kusumi, A. (2003). Accumulation of anchored proteins forms membrane diffusion barriers during neuronal polarization. Nature cell biology *5*, 626-632.

Naydenov, N.G., and Ivanov, A.I. (2010). Adducins regulate remodeling of apical junctions in human epithelial cells. Molecular biology of the cell *21*, 3506-3517.

Naydenov, N.G., and Ivanov, A.I. (2011). Spectrin-adducin membrane skeleton: A missing link between epithelial junctions and the actin cytoskeletion? Bioarchitecture *1*, 186-191.

Neukirchen, D., and Bradke, F. (2011). Neuronal polarization and the cytoskeleton. Seminars in cell & developmental biology *22*, 825-833.

Neumann, S., Bradke, F., Tessier-Lavigne, M., and Basbaum, A.I. (2002). Regeneration of sensory axons within the injured spinal cord induced by intraganglionic cAMP elevation. Neuron *34*, 885-893.

Neumann, S., and Woolf, C.J. (1999). Regeneration of dorsal column fibers into and beyond the lesion site following adult spinal cord injury. Neuron *23*, 83-91.

Nikulina, E., Tidwell, J.L., Dai, H.N., Bregman, B.S., and Filbin, M.T. (2004). The phosphodiesterase inhibitor rolipram delivered after a spinal cord lesion promotes axonal regeneration and functional recovery. Proceedings of the National Academy of Sciences of the United States of America *101*, 8786-8790.

Nolle, A., Zeug, A., van Bergeijk, J., Tonges, L., Gerhard, R., Brinkmann, H., Al Rayes, S., Hensel, N., Schill, Y., Apkhazava, D.*, et al.* (2011). The spinal muscular atrophy disease protein SMN is linked to the Rho-kinase pathway via profilin. Human molecular genetics *20*, 4865-4878.

North, B.J., Marshall, B.L., Borra, M.T., Denu, J.M., and Verdin, E. (2003). The human Sir2 ortholog, SIRT2, is an NAD+-dependent tubulin deacetylase. Molecular cell *11*, 437-444.

Ohler, S., Hakeda-Suzuki, S., and Suzuki, T. (2011). Hts, the Drosophila homologue of Adducin, physically interacts with the transmembrane receptor Golden goal to guide photoreceptor axons. Developmental dynamics : an official publication of the American Association of Anatomists *240*, 135-148.

Paturle-Lafanechere, L., Manier, M., Trigault, N., Pirollet, F., Mazarguil, H., and Job, D. (1994). Accumulation of delta 2-tubulin, a major tubulin variant that cannot be tyrosinated, in neuronal tissues and in stable microtubule assemblies. Journal of cell science *107 (Pt 6)*, 1529-1543.

Perrot, R., and Eyer, J. (2009). Neuronal intermediate filaments and neurodegenerative disorders. Brain research bulletin *80*, 282-295.

Perrot, R., Lonchampt, P., Peterson, A.C., and Eyer, J. (2007). Axonal neurofilaments control multiple fiber properties but do not influence structure or spacing of nodes of Ranvier. The Journal of neuroscience : the official journal of the Society for Neuroscience *27*, 9573-9584.

Pielage, J., Bulat, V., Zuchero, J.B., Fetter, R.D., and Davis, G.W. (2011). Hts/Adducin controls synaptic elaboration and elimination. Neuron *69*, 1114-1131.

Pilo Boyl, P., Di Nardo, A., Mulle, C., Sassoe-Pognetto, M., Panzanelli, P., Mele, A., Kneussel, M., Costantini, V., Perlas, E., Massimi, M.*, et al.* (2007). Profilin2 contributes to synaptic vesicle exocytosis, neuronal excitability, and novelty-seeking behavior. The EMBO journal *26*, 2991-3002.

Pollard, T.D., and Borisy, G.G. (2003). Cellular motility driven by assembly and disassembly of actin filaments. Cell *112*, 453-465.

Polleux, F., and Snider, W. (2010). Initiating and growing an axon. Cold Spring Harbor perspectives in biology *2*, a001925.

Porro, F., Rosato-Siri, M., Leone, E., Costessi, L., Iaconcig, A., Tongiorgi, E., and Muro, A.F. (2010). beta-adducin (Add2) KO mice show synaptic plasticity, motor coordination and behavioral deficits accompanied by changes in the expression and phosphorylation levels of the alpha- and gamma-adducin subunits. Genes, brain, and behavior *9*, 84-96.

Puttagunta, R., Tedeschi, A., Soria, M.G., Hervera, A., Lindner, R., Rathore, K.I., Gaub, P., Joshi, Y., Nguyen, T., Schmandke, A.*, et al.* (2014). PCAF-dependent epigenetic changes promote axonal regeneration in the central nervous system. Nature communications *5*, 3527.

Rabenstein, R.L., Addy, N.A., Caldarone, B.J., Asaka, Y., Gruenbaum, L.M., Peters, L.L., Gilligan, D.M., Fitzsimonds, R.M., and Picciotto, M.R. (2005). Impaired synaptic plasticity and learning in mice lacking beta-adducin, an actin-regulating protein. The Journal of neuroscience : the official journal of the Society for Neuroscience *25*, 2138-2145.

Raff, E.C., Hoyle, H.D., Popodi, E.M., and Turner, F.R. (2008). Axoneme beta-tubulin sequence determines attachment of outer dynein arms. Current biology : CB *18*, 911-914.

Ramon y Cajal, S., and May, R.M. (1928). Degeneration and regeneration of the nervous system (Oxford).

Rasband, M.N. (2010). The axon initial segment and the maintenance of neuronal polarity. Nature reviews Neuroscience *11*, 552-562.

Renthal, R., Schneider, B.G., Miller, M.M., and Luduena, R.F. (1993). Beta IV is the major beta-tubulin isotype in bovine cilia. Cell motility and the cytoskeleton *25*, 19-29.

Rivieccio, M.A., Brochier, C., Willis, D.E., Walker, B.A., D'Annibale, M.A., McLaughlin, K., Siddiq, A., Kozikowski, A.P., Jaffrey, S.R., Twiss, J.L.*, et al.* (2009). HDAC6 is a target for

protection and regeneration following injury in the nervous system. Proceedings of the National Academy of Sciences of the United States of America *106*, 19599-19604.

Robledo, R.F., Ciciotte, S.L., Gwynn, B., Sahr, K.E., Gilligan, D.M., Mohandas, N., and Peters, L.L. (2008). Targeted deletion of alpha-adducin results in absent beta- and gamma-adducin, compensated hemolytic anemia, and lethal hydrocephalus in mice. Blood *112*, 4298-4307.

Robledo, R.F., Seburn, K.L., Nicholson, A., and Peters, L.L. (2012). Strain-specific hyperkyphosis and megaesophagus in Add1 null mice. Genesis *50*, 882-891.

Rolf, B., Kutsche, M., and Bartsch, U. (2001). Severe hydrocephalus in L1-deficient mice. Brain research *891*, 247-252.

Rotshenker, S. (2011). Wallerian degeneration: the innate-immune response to traumatic nerve injury. Journal of neuroinflammation *8*, 109.

Rotzer, V., Breit, A., Waschke, J., and Spindler, V. (2014). Adducin is required for desmosomal cohesion in keratinocytes. The Journal of biological chemistry *289*, 14925-14940.

Ruediger, S., Vittori, C., Bednarek, E., Genoud, C., Strata, P., Sacchetti, B., and Caroni, P. (2011). Learning-related feedforward inhibitory connectivity growth required for memory precision. Nature *473*, 514-518.

Sagawa, H., Terasaki, H., Nakamura, M., Ichikawa, M., Yata, T., Tokita, Y., and Watanabe, M. (2007). A novel ROCK inhibitor, Y-39983, promotes regeneration of crushed axons of retinal ganglion cells into the optic nerve of adult cats. Experimental neurology *205*, 230-240.

Sahr, K.E., Lambert, A.J., Ciciotte, S.L., Mohandas, N., and Peters, L.L. (2009). Targeted deletion of the gamma-adducin gene (Add3) in mice reveals differences in alpha-adducin interactions in erythroid and nonerythroid cells. American journal of hematology *84*, 354-361.

Saunders, N.R., Kitchener, P., Knott, G.W., Nicholls, J.G., Potter, A., and Smith, T.J. (1998). Development of walking, swimming and neuronal connections after complete spinal cord transection in the neonatal opossum, Monodelphis domestica. The Journal of neuroscience : the official journal of the Society for Neuroscience *18*, 339-355.

Schutt, C.E., Myslik, J.C., Rozycki, M.D., Goonesekere, N.C., and Lindberg, U. (1993). The structure of crystalline profilin-beta-actin. Nature *365*, 810-816.

Schwer, H.D., Lecine, P., Tiwari, S., Italiano, J.E., Jr., Hartwig, J.H., and Shivdasani, R.A. (2001). A lineage-restricted and divergent beta-tubulin isoform is essential for the biogenesis, structure and function of blood platelets. Current biology : CB *11*, 579-586.

Schwoch, G., and Passow, H. (1973). Preparation and properties of human erythrocyte ghosts. Molecular and cellular biochemistry *2*, 197-218.

Seidel, B., Zuschratter, W., Wex, H., Garner, C.C., and Gundelfinger, E.D. (1995). Spatial and sub-cellular localization of the membrane cytoskeleton-associated protein alpha-adducin in the rat brain. Brain research *700*, 13-24.

Sengottuvel, V., Leibinger, M., Pfreimer, M., Andreadaki, A., and Fischer, D. (2011). Taxol facilitates axon regeneration in the mature CNS. The Journal of neuroscience : the official journal of the Society for Neuroscience *31*, 2688-2699.

Shan, X., Hu, J.H., Cayabyab, F.S., and Krieger, C. (2005). Increased phospho-adducin immunoreactivity in a murine model of amyotrophic lateral sclerosis. Neuroscience *134*, 833-846.

Shao, J., and Diamond, M.I. (2012). Protein phosphatase 1 dephosphorylates profilin-1 at Ser-137. PloS one *7*, e32802.

Shao, J., Welch, W.J., Diprospero, N.A., and Diamond, M.I. (2008). Phosphorylation of profilin by ROCK1 regulates polyglutamine aggregation. Molecular and cellular biology *28*, 5196-5208.

Shima, T., Okumura, N., Takao, T., Satomi, Y., Yagi, T., Okada, M., and Nagai, K. (2001). Interaction of the SH2 domain of Fyn with a cytoskeletal protein, beta-adducin. The Journal of biological chemistry *276*, 42233-42240.

Siebert, J.R., Conta Steencken, A., and Osterhout, D.J. (2014). Chondroitin sulfate proteoglycans in the nervous system: inhibitors to repair. BioMed research international *2014*, 845323.

Silver, J. (2009). CNS regeneration: only on one condition. Current biology : CB *19*, R444-446.

Silver, J., and Miller, J.H. (2004). Regeneration beyond the glial scar. Nature reviews Neuroscience *5*, 146-156.

Simonen, M., Pedersen, V., Weinmann, O., Schnell, L., Buss, A., Ledermann, B., Christ, F., Sansig, G., van der Putten, H., and Schwab, M.E. (2003). Systemic deletion of the myelin-associated outgrowth inhibitor Nogo-A improves regenerative and plastic responses after spinal cord injury. Neuron *38*, 201-211.

Song, A.H., Wang, D., Chen, G., Li, Y., Luo, J., Duan, S., and Poo, M.M. (2009). A selective filter for cytoplasmic transport at the axon initial segment. Cell *136*, 1148-1160.

Stevens, R.J., and Littleton, J.T. (2011). Synaptic growth: dancing with adducin. Current biology : CB *21*, R402-405.

Stiess, M., and Bradke, F. (2011). Neuronal polarization: the cytoskeleton leads the way. Developmental neurobiology *71*, 430-444.

Suriyapperuma, S.P., Lozovatsky, L., Ciciotte, S.L., Peters, L.L., and Gilligan, D.M. (2000). The mouse adducin gene family: alternative splicing and chromosomal localization. Mammalian genome : official journal of the International Mammalian Genome Society *11*, 16-23.

Tahirovic, S., and Bradke, F. (2009). Neuronal polarity. Cold Spring Harbor perspectives in biology *1*, a001644.

Tamaki, S., Iwai, N., Tsujita, Y., Nakamura, Y., and Kinoshita, M. (1998). Polymorphism of alpha-adducin in Japanese patients with essential hypertension. Hypertension research : official journal of the Japanese Society of Hypertension *21*, 29-32.

Tania, N., Condeelis, J., and Edelstein-Keshet, L. (2013). Modeling the synergy of cofilin and Arp2/3 in lamellipodial protrusive activity. Biophysical journal *105*, 1946-1955.

Toni, N., Buchs, P.A., Nikonenko, I., Bron, C.R., and Muller, D. (1999). LTP promotes formation of multiple spine synapses between a single axon terminal and a dendrite. Nature *402*, 421-425.

Torielli, L., Tivodar, S., Montella, R.C., Iacone, R., Padoani, G., Tarsini, P., Russo, O., Sarnataro, D., Strazzullo, P., Ferrari, P.*, et al.* (2008). alpha-Adducin mutations increase Na/K pump activity in renal cells by affecting constitutive endocytosis: implications for tubular Na reabsorption. American journal of physiology Renal physiology *295*, F478-487.

Tura, A., Schuettauf, F., Monnier, P.P., Bartz-Schmidt, K.U., and Henke-Fahle, S. (2009). Efficacy of Rho-kinase inhibition in promoting cell survival and reducing reactive gliosis in the rodent retina. Investigative ophthalmology & visual science *50*, 452-461.

Van Goor, D., Hyland, C., Schaefer, A.W., and Forscher, P. (2012). The role of actin turnover in retrograde actin network flow in neuronal growth cones. PloS one *7*, e30959.

Vargas, M.E., and Barres, B.A. (2007). Why is Wallerian degeneration in the CNS so slow? Annual review of neuroscience *30*, 153-179.

Verheyen, E.M., and Cooley, L. (1994). Profilin mutations disrupt multiple actin-dependent processes during Drosophila development. Development *120*, 717-728.

Vukojevic, V., Gschwind, L., Vogler, C., Demougin, P., de Quervain, D.J., Papassotiropoulos, A., and Stetak, A. (2012). A role for alpha-adducin (ADD-1) in nematode and human memory. The EMBO journal *31*, 1453-1466.

Wang, L., and Brown, A. (2010). A hereditary spastic paraplegia mutation in kinesin-1A/KIF5A disrupts neurofilament transport. Molecular neurodegeneration *5*, 52.

Watabe-Uchida, M., John, K.A., Janas, J.A., Newey, S.E., and Van Aelst, L. (2006). The Rac activator DOCK7 regulates neuronal polarity through local phosphorylation of stathmin/Op18. Neuron *51*, 727-739.

Watanabe, K., Al-Bassam, S., Miyazaki, Y., Wandless, T.J., Webster, P., and Arnold, D.B. (2012). Networks of polarized actin filaments in the axon initial segment provide a mechanism for sorting axonal and dendritic proteins. Cell reports *2*, 1546-1553.

Webber, C.A., Xu, Y., Vanneste, K.J., Martinez, J.A., Verge, V.M., and Zochodne, D.W. (2008). Guiding adult Mammalian sensory axons during regeneration. Journal of neuropathology and experimental neurology *67*, 212-222.

Winckler, B., Forscher, P., and Mellman, I. (1999). A diffusion barrier maintains distribution of membrane proteins in polarized neurons. Nature *397*, 698-701.

Winkelmann, J.C., and Forget, B.G. (1993). Erythroid and nonerythroid spectrins. Blood *81*, 3173-3185.

Witke, W., Sutherland, J.D., Sharpe, A., Arai, M., and Kwiatkowski, D.J. (2001). Profilin I is essential for cell survival and cell division in early mouse development. Proceedings of the National Academy of Sciences of the United States of America *98*, 3832-3836.

Witte, H., and Bradke, F. (2008). The role of the cytoskeleton during neuronal polarization. Current opinion in neurobiology *18*, 479-487.

Witte, H., Neukirchen, D., and Bradke, F. (2008). Microtubule stabilization specifies initial neuronal polarization. The Journal of cell biology *180*, 619-632.

Wittmann, T., Bokoch, G.M., and Waterman-Storer, C.M. (2004). Regulation of microtubule destabilizing activity of Op18/stathmin downstream of Rac1. The Journal of biological chemistry *279*, 6196-6203.

Wu, C.H., Fallini, C., Ticozzi, N., Keagle, P.J., Sapp, P.C., Piotrowska, K., Lowe, P., Koppers, M., McKenna-Yasek, D., Baron, D.M.*, et al.* (2012). Mutations in the profilin 1 gene cause familial amyotrophic lateral sclerosis. Nature *488*, 499-503.

Wu, D., Zou, Y.F., Xu, X.Y., Feng, X.L., Yang, L., Zhang, G.C., Bu, X.S., and Tang, J.L. (2011). The association of genetic polymorphisms with cerebral palsy: a meta-analysis. Developmental medicine and child neurology *53*, 217-225.

Wu, J., Masci, P.P., Chen, C., Chen, J., Lavin, M.F., and Zhao, K.N. (2015). beta-Adducin siRNA disruption of the spectrin-based cytoskeleton in differentiating keratinocytes prevented by calcium acting through calmodulin/epidermal growth factor receptor/cadherin pathway. Cellular signalling *27*, 15-25.

Xu, J., Casella, J.F., and Pollard, T.D. (1999). Effect of capping protein, CapZ, on the length of actin filaments and mechanical properties of actin filament networks. Cell motility and the cytoskeleton *42*, 73-81.

Xu, K., Zhong, G., and Zhuang, X. (2013). Actin, spectrin, and associated proteins form a periodic cytoskeletal structure in axons. Science *339*, 452-456.

Yamamoto, H., Maruo, T., Majima, T., Ishizaki, H., Tanaka-Okamoto, M., Miyoshi, J., Mandai, K., and Takai, Y. (2013). Genetic deletion of afadin causes hydrocephalus by destruction of adherens junctions in radial glial and ependymal cells in the midbrain. PloS one *8*, e80356.

Ylera, B., Erturk, A., Hellal, F., Nadrigny, F., Hurtado, A., Tahirovic, S., Oudega, M., Kirchhoff, F., and Bradke, F. (2009). Chronically CNS-injured adult sensory neurons gain regenerative competence upon a lesion of their peripheral axon. Current biology : CB *19*, 930-936.

Yoshimura, T., and Rasband, M.N. (2014). Axon initial segments: diverse and dynamic neuronal compartments. Current opinion in neurobiology *27*, 96-102.

Yu, J., Fischman, D.A., and Steck, T.L. (1973). Selective solubilization of proteins and phospholipids from red blood cell membranes by nonionic detergents. Journal of supramolecular structure *1*, 233-248.

Yu, P., Santiago, L.Y., Katagiri, Y., and Geller, H.M. (2012). Myosin II activity regulates neurite outgrowth and guidance in response to chondroitin sulfate proteoglycans. Journal of neurochemistry *120*, 1117-1128.

Yuan, A., Rao, M.V., Veeranna, and Nixon, R.A. (2012). Neurofilaments at a glance. Journal of cell science *125*, 3257-3263.

Zhang, L.N., Ji, L.D., Fei, L.J., Yuan, F., Zhang, Y.M., and Xu, J. (2013). Association between polymorphisms of alpha-adducin gene and essential hypertension in Chinese population. BioMed research international *2013*, 451094.

Zhang, M., Kalinec, G.M., Urrutia, R., Billadeau, D.D., and Kalinec, F. (2003). ROCK-dependent and ROCK-independent control of cochlear outer hair cell electromotility. The Journal of biological chemistry *278*, 35644-35650.

Zhao, K.N., Masci, P.P., Chen, J., and Lavin, M.F. (2013). Calcium prevents retinoic acid-induced disruption of the spectrin-based cytoskeleton in keratinocytes through the Src/PI3K-p85alpha/AKT/PKCdelta/beta-adducin pathways. Cell calcium *54*, 151-162.

Zhao, K.N., Masci, P.P., and Lavin, M.F. (2011). Disruption of spectrin-like cytoskeleton in differentiating keratinocytes by PKCdelta activation is associated with phosphorylated adducin. PloS one *6*, e28267.

Zheng, B., Ho, C., Li, S., Keirstead, H., Steward, O., and Tessier-Lavigne, M. (2003). Lack of enhanced spinal regeneration in Nogo-deficient mice. Neuron *38*, 213-224.

Zhong, G., He, J., Zhou, R., Lorenzo, D., Babcock, H.P., Bennett, V., and Zhuang, X. (2014). Developmental mechanism of the periodic membrane skeleton in axons. eLife *3*.

Zhu, J., Mix, E., and Winblad, B. (2001). The antidepressant and antiinflammatory effects of rolipram in the central nervous system. CNS drug reviews *7*, 387-398.

Prologue – Understanding the catalytic mechanism of the axon regeneration-enhancer Transthyretin

My interest in the field of axon growth and regeneration comes from my initial studies at Mónica Sousa's lab, where I first tried to understand the role of transthyretin as an axonal regeneration enhancer, as is described in this Prologue.

Under physiological conditions, transthyretin (TTR) is mainly known for its classical function of transporting thyroxine and retinol (through retinol binding protein), but in the 2000's several papers suggested alternative roles for this protein, namely its involvement in the biology of the nervous system (Fleming et al., 2009b; Nunes et al., 2006; Sousa et al., 2004). In this respect, our group identified transthyretin as a pro-neuritogenic protein, since TTR KO mice were shown to have impaired peripheral nerve regeneration (Fleming et al., 2007). It was later shown that the internalization of TTR by DRG neurons, through megalin receptor was fundamental for its enhancer activity in the process of axon growth (Fleming et al., 2009a). The proteolytic activity of TTR (Liz et al., 2004) was latter shown to drive this neuritogenic effect, since a TTR proteolytically-deficient mutant was not able to rescue neurite outgrowth of PC12 cells incubated in TTR KO serum, whereas a full rescue was obtained with WT TTR (Liz et al., 2009). Therefore, understanding the catalytic mechanism and regulation of the proteolytic activity of TTR was of crucial importance for the its use as a putative target in regeneration-associated therapies and in other CNS pathologies where TTR proteolytic activity was shown to be relevant, as is the case of Alzheimer's disease (Costa et al., 2008; Ribeiro et al., 2012; Stein and Johnson, 2002; Wang et al., 2014).

During my PhD, although as a side project, we characterized the catalytic activity of TTR. This work was published in Biochemichal Journal in 2012: Liz MA*, Leite SC*, Juliano L, Saraiva MJ, Damas AM, Bur D, Sousa MM. “Transthyretin is a metallopeptidase with an inducible active site” (* Equal first-authorship), where we demonstrated that:

- TTR is a metallopeptidase, and not a serine peptidase as the initial data suggested (Liz et al., 2004);
- TTR activity is mediated by a catalytic triad with an HXHXE motif, conserved in primates;
- The catalytic activity could be abolished and restored by removing / adding the metallopeptidase co-factors Zn^{2+} (as also suggested by crystallography studies- (Palmieri Lde et al., 2010)), but also by other divalent ions such Mn^{2+}, Co^{2+} and Fe^{2+}

The paper is presented below.

BJ www.biochemj.org

Biochem. J. (2012) **443**, 769–778 (Printed in Great Britain) doi:10.1042/BJ20111690

Transthyretin is a metallopeptidase with an inducible active site

Márcia A. LIZ*[1], Sérgio C. LEITE*[1], Luiz JULIANO†, Maria J. SARAIVA‡‖, Ana M. DAMAS§‖, Daniel BUR¶[2] and Mónica M. SOUSA*[2,3]

*Nerve Regeneration Group, Instituto de Biologia Molecular e Celular – IBMC, 4150-180 Porto, Portugal, †Escola Paulista de Medicina, Universidade Federal de São Paulo, 04044-020 São Paulo, Brazil, ‡Molecular Neurobiology Group, Instituto de Biologia Molecular e Celular – IBMC, 4150-180 Porto, Portugal, §Molecular Structure Group, Instituto de Biologia Molecular e Celular – IBMC, 4150-180 Porto, Portugal, ‖ICBAS, Universidade do Porto, 4099-033 Porto, Portugal, and ¶Actelion Pharmaceuticals Ltd, 4123 Allschwil, Switzerland

TTR (transthyretin) was found recently to possess proteolytic competency besides its well-known transport capabilities. It was described as a cryptic serine peptidase cleaving multiple natural substrates (including β-amyloid and apolipoprotein A-I) involved in diseases such as Alzheimer's disease and atherosclerosis. In the present study, we aimed to elucidate the catalytic machinery of TTR. All attempts to identify a catalytic serine residue were unsuccessful. However, metal chelators abolished TTR activity. Proteolytic inhibition by EDTA or 1,10-phenanthroline could be reversed with Zn^{2+} and Mn^{2+}. These observations, supported by analysis of three-dimensional structures of TTR complexed with Zn^{2+}, led to the hypothesis that TTR is a metallopeptidase. Site-directed mutagenesis of selected amino acids unambiguously confirmed this hypothesis. The TTR active site is inducible and constituted via a protein rearrangement resulting in ~7% of proteolytically active TTR at pH 7.4. The side chain of His^{88} is shifted near His^{90} and Glu^{92} establishing a Zn^{2+}-chelating pattern HXHXE not found previously in any metallopeptidase and only conserved in TTR of humans and some other primates. Point mutations of these three residues yielded proteins devoid of proteolytic activity. Glu^{72} was identified as the general base involved in activation of the catalytic water. Our results unveil TTR as a metallopeptidase and define its catalytic machinery.

Key words: apolipoprotein A-I, amyloid-β peptide, metallopeptidase, transthyretin, zinc.

INTRODUCTION

TTR (transthyretin) is a plasma protein existing mainly as a homotetramer [1]. TTR is well characterized, since point mutations can cause FAP (familial amyloid polyneuropathy) [2], a lethal neurodegenerative disorder hallmarked by deposition of TTR amyloid fibrils [3]. A myriad of crystal structures of human wtTTR (wild-type TTR) are available from the PDB [4]. Backbone hydrogen bonds between TTR monomers favour dimer formation, whereas dimers interact predominantly via amino acid side chains to form a tetramer. TTR stability depends on intact quaternary and tertiary structure, with partial unfolding initiating misassembled aggregates [5]. The presence of metal ions [6], covalent modification of Cys^{10} [7], lowered pH [8] or point mutations [9] can destabilize the tetrameric TTR structure and favour protein rearrangement.

TTR is the transporter of T_4 (thyroxine) and retinol owing to its association with RBP (retinol-binding protein) [10] in a 1:1 molar ratio *in vivo* [11], an interaction that stabilizes TTR more than 15-fold [12]. Besides interacting with T_4 and RBP, approximately 1–2% of total plasma TTR is associated with HDL (high-density lipoproteins), through binding to apoA-I (apolipoprotein A-I) [13]. In-depth analysis of the interaction of TTR with apoA-I revealed the latter to be a peptidase substrate of TTR [14]. TTR is currently described as a peptidase of unknown type (U9G.071) in the MEROPS database [15]. Initial studies suggested TTR to be a serine peptidase [14] given that it cleaves apoA-I after a phenylalanine residue at an optimal pH of 7 and that it is apparently inhibited by very high concentrations of serine peptidase inhibitors [14]. Although binding of small compounds such as T_4 has no effect on the peptidase activity of TTR, interaction with RBP completely abolishes substrate cleavage [14]. To date, a significant number of natural substrates of TTR have been identified such as apoA-I, NPY (neuropeptide Y) and Aβ (amyloid β-peptide) [14,16,17].

ApoA-I is the main protein component of HDL and is crucial for reverse cholesterol transport [18]. Limited proteolysis has demonstrated the vulnerability of the C-terminus of apoA-I in lipid-poor particles, whereas the lipid-bound protein is protected from cleavage [18]. The apoA-I N-terminus appears to be important for stabilizing the lipid-free monomeric structure, whereas the C-terminus is required for interactions with other proteins and lipids [19]. After apoA-I cleavage by TTR, HDL particles display a reduced capacity to promote cholesterol efflux, and truncated apoA-I displays increased amyloidogenicity [20], suggesting that TTR might have an impact on the development of atherosclerosis. In the case of Aβ, cleavage by TTR has only been demonstrated *in vitro* [17], and suggested to be a protective mechanism preventing Alzheimer's disease [17].

Despite the availability of a large number of wtTTR and mutated TTR X-ray structures crystallized at pH 7–8, the catalytic mechanism of TTR is still unknown. In the present study, we establish TTR as a metallopeptidase and uncover multiple catalytic residues indispensable for proteolytic activity.

Abbreviations used: Aβ, amyloid β-peptide; Abz, *o*-aminobenzoyl; ACE, angiotensin-converting enzyme; apoA-I, apolipoprotein A-I; DFP, di-isopropylfluorophosphate; EDDnp, *N*-(2,4-dinitrophenyl)-ethylenediamine; HDL, high-density lipoprotein(s); MALDI, matrix-assisted laser-desorption ionization; RBP, retinol-binding protein; T_4, thyroxine; TPCK, tosylphenylalanylchloromethane; TTR, transthyretin; wtTTR, wild-type TTR.

[1] These authors contributed equally to this work.

[2] These authors contributed equally to this work.

[3] To whom correspondence should be addressed (email msousa@ibmc.up.pt).

EXPERIMENTAL

Protein production

Recombinant wtTTR and TTR mutants were produced in BL-21 pLys *Escherichia coli* cells transformed with pETF1 carrying *TTR* cDNA [21]. Proteins were isolated and purified as described in [14]. Briefly, after bacterial lysis, protein extracts were run on DEAE-cellulose (Whatman) ion-exchange chromatography, dialysed, freeze-dried and isolated in native Prosieve® agarose (FMC) gels. After electrophoresis, the TTR band was excised and electroeluted in a Elutrap® system (Schleicher and Schuell) in 38 mM glycine and 5 mM Tris/HCl (pH 8.3) overnight at 50 V (4 °C). Finally, the protein was dialysed in 50 mM Tris/HCl (pH 7.5). Protein quantification was performed using Lowry-based DC Protein Assay (Bio-Rad Laboratories), following the manufacturer's protocol. The TTR molar concentration was always calculated assuming the exclusive presence of the tetrameric species.

Site-directed mutagenesis

The *TTR* cDNA cloned into the pETF1 vector was used to produce TTR mutants (using the QuikChange® kit; Stratagene). Mutants were constructed using two mismatched primers, introducing a base substitution in the original sequence. Minipreps of plasmid DNA were tested by sequencing at SeqLab (Göttingen, Germany). After protein production, mutations were confirmed by MALDI (matrix-assisted laser-desorption ionization)-MS of either the full-length protein or of the trypsin-digested TTR peptides (Supplementary Table S1 at http://www.BiochemJ.org/bj/443/bj4430769add.htm), at the Proteomics Unit, Institute of Molecular Pathology and Immunology at the University of Porto, Porto, Portugal.

Kinetic assays

TTR proteolytic activity was tested with the fluorigenic peptide Abz-YGGRASDQ-EDDnp [where Abz is *o*-aminobenzoyl and EDDnp is *N*-(2,4-dinitrophenyl)-ethylenediamine]. This substrate was found when screening a library of fluorigenic peptides [22]. Turnover of Abz-YGGRASDQ-EDDnp by TTR is approximately 20-fold higher ($k_{cat}/K_m = 408.8\ s^{-1} \cdot M^{-1}$) when compared with Abz-ESFKVS-EDDnp ($k_{cat}/K_m = 17.5\ s^{-1} \cdot M^{-1}$), an apoA-I sequence encompassing the TTR cleavage site. Hydrolysis of Abz-YGGRASDQ-EDDnp at 37 °C in 50 mM Tris/HCl (pH 7.5) was followed by measuring the fluorescence at λ_{em} 420 nm and λ_{ex} 320 nm in an F_{max} plate reader (Molecular Devices) for 30 min. Specificity rate constants (k_{cat}/K_m) were determined under pseudo-first-order conditions [23]. TTR (5 μM total protein) was added to the substrate (tested at 5 μM and 10 μM) in a final volume of 100 ml of reaction buffer (50 mM Tris/HCl, pH 7.5). Reactions were monitored for 30 min and pseudo-first-order rate constants were obtained from linear plots where the *y*-axis corresponds to $\ln[(F_{max} - F_{time})/F_{max}]$, where F_{max} is the fluorescence corresponding to total degradation of 5 μM or 10 μM substrate and F_{time} is the fluorescence measured at each time point, and the *x*-axis corresponds to the time of reaction. The slope of the linear plots, corresponding to the first-order rate constants, was divided by the total protein concentration to provide k_{cat}/K_m. Determination of the concentration of active enzyme in the TTR preparation was performed by titration with an irreversible phosphonate inhibitor that completely blocks TTR activity at 1 μM [16]. Active-site titration was carried out with inhibitor concentrations ranging from 0.01 to 1 μM. After enzyme/inhibitor incubation for 30 min at 37 °C, activity was monitored as described above. Concentration of active enzyme was determined from the *x*-axis intercept in the linear range of the plot of residual activity as a function of inhibitor concentration [24].

Chemical modification of TTR with serine peptidase inhibitors

TTR (5 μM) was incubated with each of the following peptidase inhibitors: Pefabloc SC (4 mM; Roche), DFP (di-isopropylfluorophosphate) (100 μM; Calbiochem), TPCK (tosylphenylalanylchloromethane) (100 μM; Roche) and PMSF (1 mM; Sigma). After 30 min of incubation at 37 °C, reaction mixtures were separated by SDS/PAGE (15 % gel) and stained with Coomassie Blue. MALDI-MS of trypsin-digested gel bands corresponding to modified TTR was performed at the Protein Core Facility, Columbia University, New York, NY, U.S.A., as described in [14]. For chemical modification of apoA-I (1.7 μM) with PMSF, the protein was incubated with 1 mM inhibitor for 30 min at 37 °C. After SDS/PAGE, MALDI-MS was performed at the Proteomics Unit, Institute of Molecular Pathology and Immunology at the University of Porto, Porto, Portugal.

Inhibition of TTR cleavage of fluorigenic peptides

For analysis of inhibition of TTR proteolytic activity using Abz-YGGRASDQ-EDDnp as substrate, TTR (5 μM) was pre-incubated for 30 min at 37 °C in reaction buffer with the following inhibitors: 1–10 mM EDTA (Merck), 10 μM E-64 [*trans*-epoxysuccinyl-L-leucylamido-(4-guanidino)butane] (Roche), 10 μM phosphoramidon (Roche), 10 μM bestatin (Sigma), 0.3 μM aprotinin (Sigma), 100 μM TPCK (Roche), 100 μM TLCK (tosyl-lysylchloromethane) (Roche), 100 μM chymostatin (Sigma), 100 μM leupeptin (Sigma), 1 mM PMSF (Sigma), 1 μM pepstatin (Sigma), 1 mM 1,10-phenanthroline (Roche) and 1 mM 1,7-phenanthroline (Alfa Aesar). After enzyme/inhibitor incubation, 5 μM Abz-YGGRASDQ-EDDnp was added and activity was monitored as described above. Relative fluorescence was converted into percentages of residual activity relative to uninhibited controls. To analyse the effect of addition of divalent metals to TTR inhibited with either 1,10-phenanthroline or EDTA, TTR was pre-incubated with the inhibitor (as described above) and then increasing concentrations of metals were added to the reaction and proteolytic activity was determined. In the experiments with $CaCl_2$ addition, reactivation of TTR with Zn^{2+} was tested in the presence of 1 mM $CaCl_2$. The apo-enzyme form of TTR was obtained by dialysis of TTR pre-incubated with 10 mM EDTA. Control measurements of the reactions where no TTR was added were performed, and the results obtained were subtracted from the results from reactions containing the peptidase.

TTR proteolysis assay using full-length apoA-I as substrate

ApoA-I digestion by TTR was performed as described previously [14]. Briefly, 2 mg of TTR was incubated with 1 mg of apoA-I in 50 mM Tris/HCl (pH 7.5) at 37 °C overnight. The inhibitory effect of EDTA was tested by the addition of 10 mM or 50 mM EDTA to TTR, before addition of apoA-I. After incubation for 30 min at 37 °C, apoA-I was added and reactions proceeded at 37 °C overnight. Reaction mixtures were subsequently separated by SDS/PAGE (15 % gel) and visualized by silver staining.

Determination of Zn^{2+} levels in TTR

The Zn^{2+} concentration in TTR samples was measured at the Chemical Speciation and Bioavailability Laboratory, Center of Marine and Environmental Research, University of Porto, Porto, Portugal, as described previously [25]. Briefly, 3.2 mg of TTR was diluted in Zn^{2+}-free double-distilled water and total Zn^{2+} content was determined by atomic absorption spectrophotometry with flame atomization (PU 9200X, Philips). For Zn^{2+} quantification, a calibration curve was created using Zn^{2+} standards. For Zn^{2+} quantification in TTR treated with EDTA, the protein was incubated with 10 mM EDTA for 30 min at 37 °C and thereafter the chelator was removed by dialysis against 50 mM Tris/HCl (pH 7.5). For measurement of Mn^{2+}, Fe^{2+} and Co^{2+} concentrations, the same protocol was followed.

Thioflavin-T-binding assay

For the thioflavin-T-binding assay, 100 μg of purified TTR was incubated in 50 mM sodium acetate (pH 4) for 72 h at room temperature (22 °C) in a final volume of 200 μl. For aggregation assays with 10 mM EDTA, 1 mM 1,10-phenanthroline or Zn^{2+}, TTR was incubated with one of these compounds for 30 min at 37 °C and subsequently thioflavin-T was added at a concentration of 30 μM in 50 mM glycine (pH 9). The excitation spectra from 400 to 500 nm were recorded on a Horiba Fluoromax-4 spectrofluorimeter at 19 °C. The intensity of fluorescence at 451 nm, which is the characteristic maximum for thioflavin-T bound to aggregated fibrils, was subtracted from the intensity of fluorescence at 451 nm of the control without TTR. Results are presented as a percentage relative to the value obtained for wtTTR. Each assay was performed in triplicate.

Size-exclusion chromatography

Size-exclusion chromatography experiments were performed with a pre-packed Superose 12 10/300 GL column (GE Healthcare). The column was equilibrated with 150 mM NaCl and 50 mM Tris/HCl (pH 7.5) and a 0.5 ml/min flow rate was used throughout the experiments. A total of 150 μg of purified TTR was used in each run. Protein elution was monitored by measuring the absorbance at 280 nm. Calibration was carried out using the following protein standards (Stokes radius, elution volume): catalase (5.22 nm, 11.03 ml), aldolase (4.81 nm, 11.26 ml), albumin (3.55 nm, 11.76 ml), ovalbumin (3.05 nm, 12.66 ml), chymotrypsinogen (2.09 nm, 14.66 ml) and ribonuclease (1.64 nm, 15.14 ml). The void volume was determined to be 7.21 ml using Blue Dextran 2000. The K_{av} parameter was determined according to the equation $K_{av} = (V_e - V_0)/(V_t - V_0)$, where V_e represents the elution volume, V_0 is the void volume of the column, and V_t is the total bed volume. The Stokes radius (R_s) for the experimental data was calculated by interpolation using: $(-\log K_{av})1/2 = f(R_s)$.

Data analysis

All assays were performed at least twice with each dataset in duplicate. Results are means ± S.D.

RESULTS

TTR is not a serine peptidase

TTR has been suggested to be a cryptic serine peptidase [14]. Serine peptidases are hallmarked by an activated nucleophilic serine [15], an oxyanion hole and a substrate-binding cleft. After an in-depth analysis of multiple X-ray structures of monomeric, dimeric and tetrameric TTR, Ser^{46}, Ser^{77} and Ser^{85} were selected as putative candidates that could act as activated nucleophiles. We mutated each of these three serine residues to glycine or alanine and confirmed the respective mutations by tryptic MS (results not shown). All three mutants retained proteolytic activity (results not shown), suggesting that TTR is not a serine-like peptidase. Ser^{8}, Ser^{23}, Ser^{50}, Ser^{52}, Ser^{100} and Ser^{117} of TTR, although they were very unlikely to be active-site candidates, were also mutated. All of these mutants retained proteolytic activity (results not shown). The only TTR serine residues that were not mutated were Ser^{112} and Ser^{115} as these are located in the hydrophobic central channel of TTR, described previously to be irrelevant for TTR activity [14].

As TTR was suggested to be a serine-like peptidase on the basis of the inhibition of apoA-I cleavage by high concentrations of serine peptidase inhibitors [14], the effect of these compounds was re-examined in detail using full-length apoA-I as substrate. MS analysis of TTR incubated with the covalent binding serine peptidase inhibitor Pefabloc SC revealed the presence of multiple modified TTR peptides (Supplementary Table S2 at http://www.BiochemJ.org/bj/443/bj4430769add.htm), indicating that highly concentrated Pefabloc SC modifies TTR unspecifically, therefore affecting peptidase activity in a non-specific manner. For TTR incubated with PMSF, DFP and TPCK, no modification of TTR was found (results not shown). However, PMSF was able to modify the substrate (apoA-I) and generate an aberrant PMSF adduct of a peptide consisting of amino acids 227–238 of apoA-I (1540.86 Da) (Supplementary Table S3 at http://www.BiochemJ.org/bj/443/bj4430769add.htm). PMSF modification of the substrate is most likely to be the reason for reduced apoA-I cleavage by TTR. Besides inhibition of TTR activity by serine peptidase inhibitors, we previously observed inhibition of TTR activity with peptide phosphonate inhibitors when using the fluorigenic apoA-I peptide substrate [16]. Phosphonate inhibitors are able to block serine peptidases, but some members of this class of compound are known to be effective inhibitors of metallopeptidases [26]. Combined, the absence of catalytic serine residues in TTR and unspecific modifications of TTR and apoA-I by peptidase inhibitors reveal that TTR is not a serine peptidase.

TTR proteolytic activity depends on metal ions and is inhibited by metal chelators

A highly reproducible assay using fluorigenic peptide substrates was set up to investigate the action of multiple prototypic peptidase inhibitors on TTR activity (Figure 1a). As we previously observed interference with proteolytic activity by post-translational modifications of Cys^{10} in TTR [16], all assays were performed with a C10A mutant which was equipotent to wtTTR (Table 1). Only two well known metallopeptidase inhibitors, EDTA and 1,10-phenanthroline, could abolish TTR proteolytic activity (Figure 1a). Interestingly, 1,7-phenanthroline, an isomeric non-chelating analogue of 1,10-phenanthroline, achieved only minor inhibition (Figure 1a). These results were corroborated with a second substrate mimicking the TTR cleavage site in apoA-I [14] (Figure 1b). Moreover, when using full-length apoA-I as substrate, when increasing amounts of EDTA are used, full inhibition is also achieved (Supplementary Figure S1 at http://www.BiochemJ.org/bj/443/bj4430769add.htm). The same inhibition profile was observed when wtTTR was used, proving that inhibition by EDTA and 1,10-phenanthroline is not

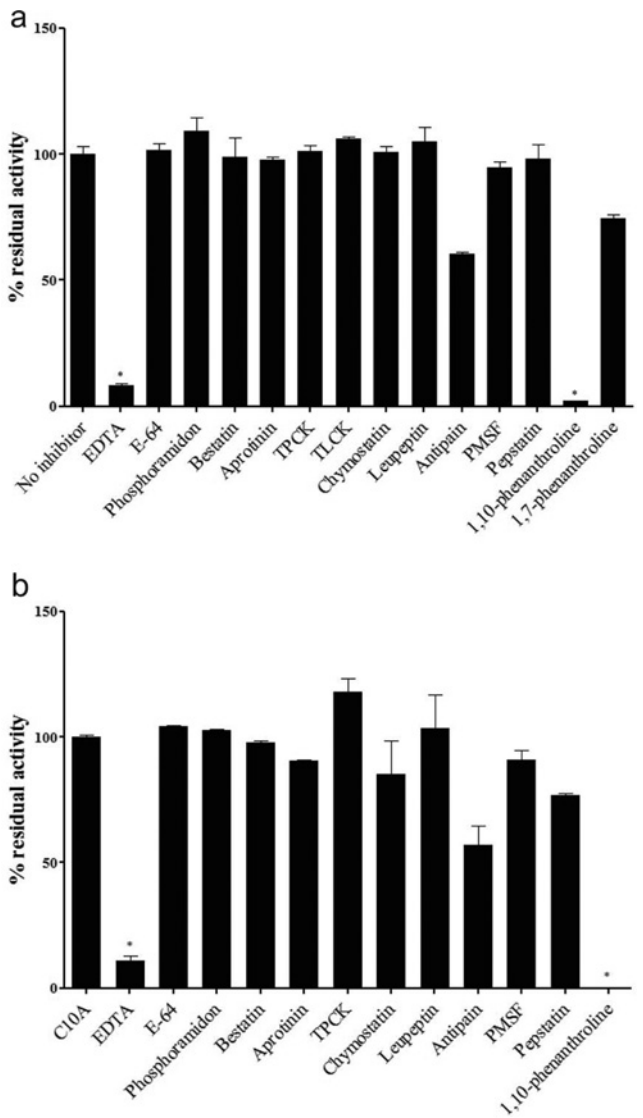

Figure 1 TTR cleavage of fluorigenic peptides is inhibited by EDTA and 1,10-phenanthroline

(**a**) TTR was pre-incubated with different peptidase inhibitors before cleavage of Abz-YGGRASDQ-EDDnp was determined. $^*P < 0.0005$. (**b**) TTR cleavage of Abz-ESFKVS-EDDnp (mimicking apoA-I cleavage site) after pre-incubation with different peptidase inhibitors. $^*P < 0.001$. Relative fluorescence values were converted into percentages of residual activity relative to uninhibited controls. Each experiment was performed twice in duplicate.

dependent on the point mutation C10A (Supplementary Figure S2 at http://www.BiochemJ.org/bj/443/bj4430769add.htm).

EDTA inhibited TTR in a dose-dependent manner (Figure 2a). Excess amounts of EDTA had to be scavenged with 1 mM Ca^{2+} ions before addition of Zn^{2+} could surmount inhibition and restore full TTR proteolytic activity (Figure 2b). Alternatively, excessive EDTA could be removed via dialysis, yielding an inactive apo-enzyme that can be reactivated by addition of Zn^{2+} (Figure 2c). This indicates that the Zn^{2+}-scavenging effect of EDTA leads to proteolytic inactivation of TTR. Similar results were obtained with wtTTR (Supplementary Figure S3 at http://www.BiochemJ.org/bj/443/bj4430769add.htm).

Complete inhibition of TTR with 1 mM 1,10-phenanthroline could be partially reversed by adding Zn^{2+} (Figure 2d). Zn^{2+} at 250 μM restored 36 % of proteolytic activity in the presence of inhibitor. This finding is similar to the results obtained

Table 1 Specificity rate constants (k_{cat}/K_m) of different TTR mutants

Each individual mutant was tested at least three times in quadruplicates. Results are means ± S.D. $^*P < 0.001$, $^{**}P < 0.0005$ compared with wtTTR.

Protein	k_{cat}/K_m ($s^{-1} \cdot M^{-1}$)
wtTTR	408.8 ± 6.3
TTR C10A	367.0 ± 20.5
TTR C10A/H88A	3.5 ± 1.8**
TTR C10A/H90A	1.5 ± 0.3**
TTR C10A/E92A	8.7 ± 4.8**
TTR C10A/E72A	3.7 ± 1.2**
TTR C10A/E89A	76.2 ± 14.8**
TTR C10A/H31G	4.8 ± 0.2**
TTR C10A/K70A	4.2 ± 2.3**
TTR C10A/D74A	168.2 ± 36.0*

with EDTA where the addition of 250 μM Zn^{2+} restored 43 % activity (Figure 2b). Zn^{2+} concentrations exceeding an optimal value (250 μM for TTR) inhibited TTR (results not shown), as described previously for other metallopeptidases [27]. Nevertheless, after inhibition of TTR with 1,10-phenanthroline, dialysis yielded an active peptidase instead of an inactive apo-enzyme (results not shown). This effect was described previously for carboxypeptidase A where inhibition of the enzyme with 1,10-phenanthroline was reversed by Zn^{2+} addition, but dialysis of the enzyme treated with the metal chelator restored the active enzyme rather than producing the apo-enzyme. In that case, it was suggested that dialysis leads to dissociation of the Zn^{2+}–1,10-phenanthroline complex permitting the re-incorporation of the Zn^{2+} ion in the enzyme [28]. Addition of 1 mM $CaCl_2$ did not sequester 1,10-phenanthroline as observed previously for EDTA, since binding of 1,10-phenanthroline to Ca^{2+} is significantly less strong [29] (Figure 2e). In summary, these results indicate that Zn^{2+} plays a crucial role in the proteolytic activity of TTR and thereby suggest that TTR is a Zn^{2+}-dependent metallopeptidase.

TTR is reactivated by other divalent metal ions

The active site necessary for proteolytic activity has never been observed in any X-ray structure of wtTTR obtained at physiologically relevant pH (pH 7–8). This triggered the question of whether this might be due to an incorrect metal being present in crystallization assays. Zn^{2+} is typically found in the active site of metallopeptidases, but Co^{2+}, Cu^{2+}, Ni^{2+}, Mn^{2+} or Fe^{2+} can also produce active metallopeptidases as described for metalloenzymes such as thermolysin [30] or peptide deformylase [31]. Interestingly, TTR complexed to Mn^{2+} was even slightly more active than its Zn^{2+} analogue (Figure 3a), indicating that TTR can be active with metals other than Zn^{2+} *in vitro*. Further metals tested (Fe^{2+} and Co^{2+}) also yielded active enzymes (Figures 3b and 3c), whereas in the presence of Ni^{2+} or Cu^{2+}, TTR displayed very little proteolytic activity (Supplementary Figures S4a and S4b respectively at http://www.BiochemJ.org/bj/443/bj4430769add.htm).

Only a fraction of TTR contains Zn^{2+} and is proteolytically competent

Metallopeptidases require a metal ion to correctly locate and activate a water molecule [15]. The metal ion is often Zn^{2+} co-ordinated by three residues of the enzyme and a water molecule. Such a structural feature could not be found in any

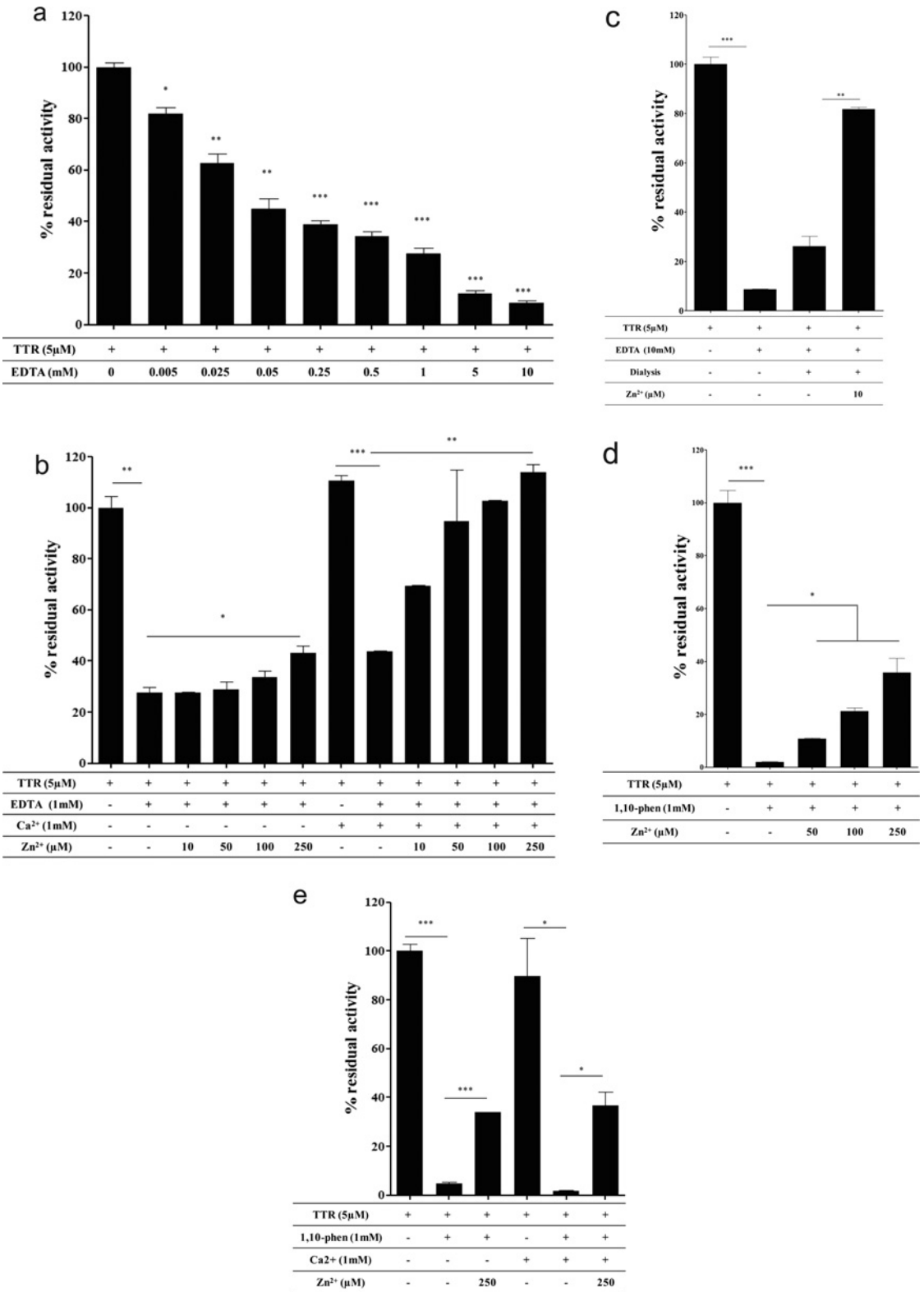

Figure 2 TTR inhibition by EDTA and 1,10-phenanthroline is reversed by addition of $ZnCl_2$

(**a**) TTR activity was assessed after pre-incubation with increasing concentrations of EDTA. (**b**) TTR proteolytic activity was blocked with 1 mM EDTA. Reactivation of TTR with Zn^{2+} was tested in either the presence or the absence of 1 mM $CaCl_2$. (**c**) After dialysis, TTR inhibited by EDTA can be reactivated by Zn^{2+}. TTR was inhibited with 10 mM EDTA, dialysed and subsequently reactivated with increasing concentrations of Zn^{2+}. (**d**) TTR was incubated with 1 mM 1,10-phenanthroline before activity was tested in the presence of increasing concentrations of Zn^{2+}. Addition of $ZnCl_2$ to TTR inhibited by 1,10-phenanthroline (1,10-phen) partially restored proteolytic activity. (**e**) $CaCl_2$ does not affect Zn^{2+} reactivation of TTR inhibited with 1,10-phenanthroline. TTR proteolytic activity was blocked with 1 mM 1,10-phenanthroline (1,10-phen). Reactivation of TTR with 250 μM Zn^{2+} was tested either in presence or absence of 1 mM $CaCl_2$. Each experiment was performed at least twice in duplicate. $^{*}P < 0.05$, $^{**}P < 0.01$, $^{***}P < 0.001$.

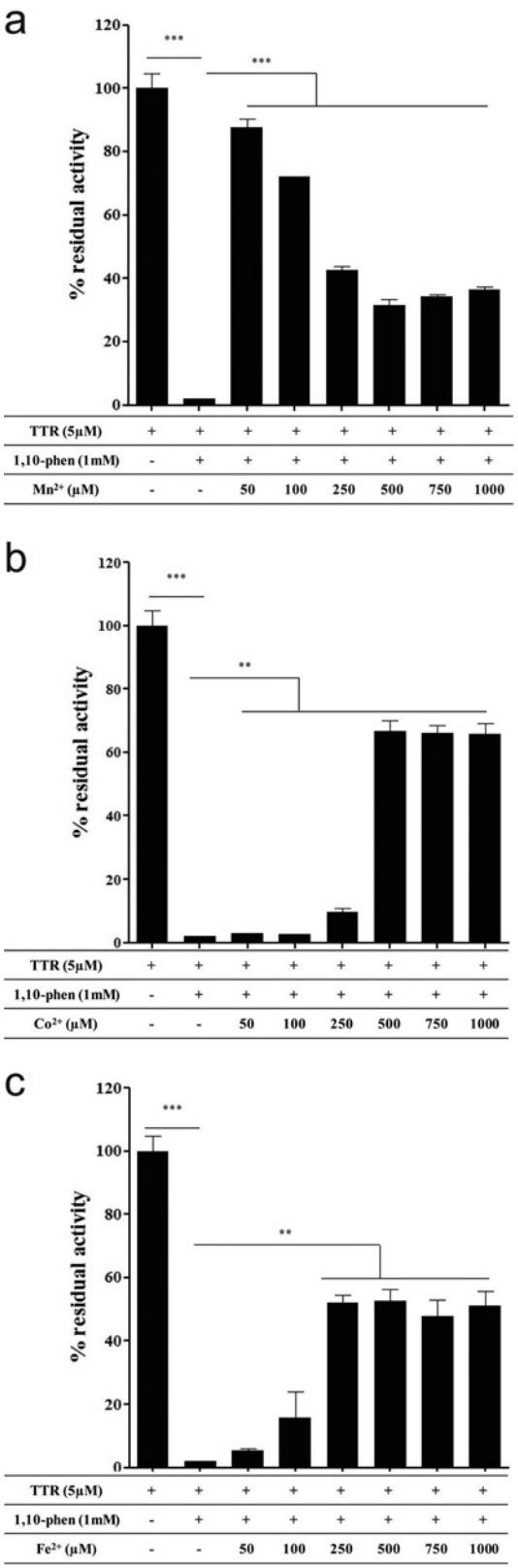

Figure 3 TTR inhibited by 1,10-phenanthroline is reactivated by divalent metal ions

TTR was incubated with 1 mM 1,10-phenanthroline (1,10-phen) before activity was tested in the presence of increasing concentrations of Mn^{2+} (**a**), Co^{2+} (**b**) or Fe^{2+} (**c**). Each experiment was performed at least twice in duplicate. $^{**}P < 0.01$, $^{***}P < 0.001$.

wtTTR X-ray structure in the PDB crystallized in the pH range 7–8. Recently, several structures of TTR double mutants (F87M/L110M) crystallized in the pH range 4.5–7.5 comprising multiple Zn^{2+}-binding sites were described [32]. In one of these structures, a large reorganization of amino acids 74–90 occurs, shifting the side chain of His^{88} by almost 9 Å (1 Å = 0.1 nm) such that this residue together with His^{90} and Glu^{92} co-ordinates a Zn^{2+} (e.g. PDB code 3GRG) [32]. These three relocated amino acids, comprising two neutral (His^{88} and His^{90}) and one negatively charged amino acid (Glu^{92}), are reminiscent of active sites in metallopeptidases.

To determine whether recombinant TTR contains Zn^{2+}, the concentration of this ion in wtTTR preparations was measured using atomic absorption spectrophotometry with flame atomization. In 5 μM wtTTR, a Zn^{2+} concentration of approximately 1 μM could be measured. Moreover, when TTR was pre-treated with EDTA before atomic absorption spectrophotometry, no Zn^{2+} was detected. As described above, metals other than Zn^{2+} were shown to interfere with TTR proteolytic activity, as is the case for Mn^{2+}, Fe^{2+} and Co^{2+}; however, these metals were not detected in the wtTTR preparations (results not shown).

We analysed the effect of adding Zn^{2+} directly to recombinant TTR. Increasing Zn^{2+} concentrations did not increase proteolytic activity further, but inhibited it (Figure 4a). Such an effect can be explained by Zn^{2+} binding near the active site, as observed previously in X-ray structures of other metallopeptidases [33]. Such a second Zn^{2+}-binding site is observed in one of the analysed TTR X-ray structures [32]. One of its residues, Asp^{74}, was mutated, but this mutation did not abolish the inhibitory effect of excessive Zn^{2+} (Figure 4a). The presence of metal ions can destabilize the TTR tetrameric structure [6]. To check whether the inhibitory effect of increasing Zn^{2+} concentrations on TTR proteolytic activity was related to an increased TTR aggregation induced by the metal, we performed thioflavin-T-binding assays of TTR in the presence of 100 and 250 μM Zn^{2+}. We observed that Zn^{2+} addition did not increase TTR aggregation (Figure 4b).

The molar ratio of TTR and Zn^{2+} determined in our preparations ($\sim$5:1 TTR/Zn^{2+}) suggested that not all recombinant TTR is in a proteolytically active state. We therefore determined the percentage of proteolytically active wtTTR by active-site titration of a 5 μM TTR solution at pH 7.5 with a strong phosphonate inhibitor identified previously [16] (Supplementary Figure S5 at http://www.BiochemJ.org/bj/443/bj4430769add.htm), which labels the enzyme active site by co-ordinating the catalytic Zn^{2+} [26]. Surprisingly, only a minor fraction of 340 nM wtTTR ($\sim$7 % of total wtTTR) was in a proteolytically active state (Figure 4c). This percentage was lower than what was expected given the TTR/Zn^{2+} molar ratio. This result indicates that only a minor amount of wtTTR has proteolytic competence at physiological pH.

TTR is a metallopeptidase with an inducible Zn^{2+}-binding site

On the basis of the above results, we hypothesized that TTR is a metallopeptidase having His^{88}, His^{90} and Glu^{92} as the three relevant residues binding the catalytic Zn^{2+}. To confirm this hypothesis, mutants of each of the above residues to alanine were generated, and their kinetic parameters were determined (Table 1). Mutating any of these three residues led to inactive TTR (Table 1), demonstrating that His^{88}, His^{90} and Glu^{92} are the active-site residues.

In metallopeptidases, a reactive hydroxyl ion is generated by transferring a proton from the catalytic water to a neighbouring

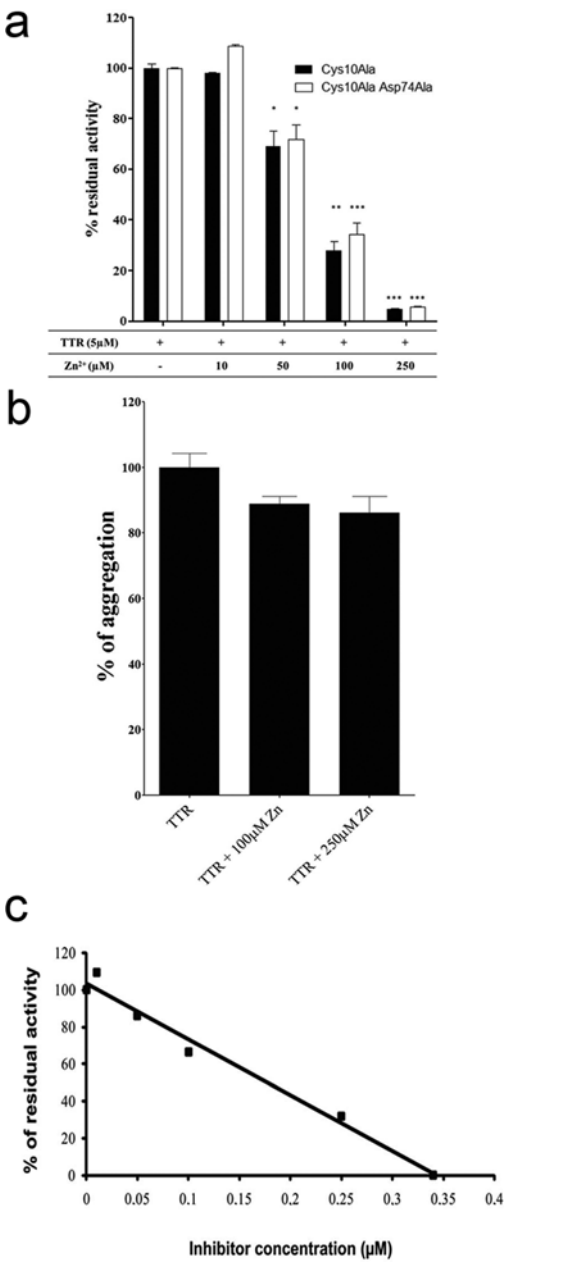

Figure 4 Only a small fraction of TTR comprises Zn^{2+} and is proteolytically competent

(**a**) Proteolytic activity of either TTR C10A or TTR C10A/D74A was tested in the presence of increasing concentrations of $ZnCl_2$. Both TTR mutants were inhibited by addition of excessive amounts of $ZnCl_2$. The statistic analysis was performed relatively to each respective mutant without $ZnCl_2$ addition. $*P < 0.05$, $**P < 0.01$, $***P < 0.001$. (**b**) Aggregation of TTR in the absence and presence of different Zn^{2+} concentrations as determined by thioflavin-T-binding assays. (**c**) Concentration of active enzyme in wtTTR preparations. The concentration of proteolytically active enzyme was determined by active-site titration with a phosphonate inhibitor. TTR activity was tested after pre-incubation with a phosphonate inhibitor. Concentration of active enzyme was determined from the *x*-axis intercept in the linear range of the plot of residual activity as a function of inhibitor concentration. Each experiment was performed twice in duplicate.

residue which acts as a general base. From structural analysis (Figure 5), Glu^{72} was favoured to be the general base and Glu^{89} was a less likely candidate. Supporting this hypothesis, mutating Glu^{72} abrogated the proteolytic activity of TTR, whereas mutating Glu^{89} resulted in a partial reduction in TTR activity. This latter residue receives two hydrogen bonds from (i) its own backbone amide, and (ii) the side chain of $Thr^{96'}$ of a neighbouring

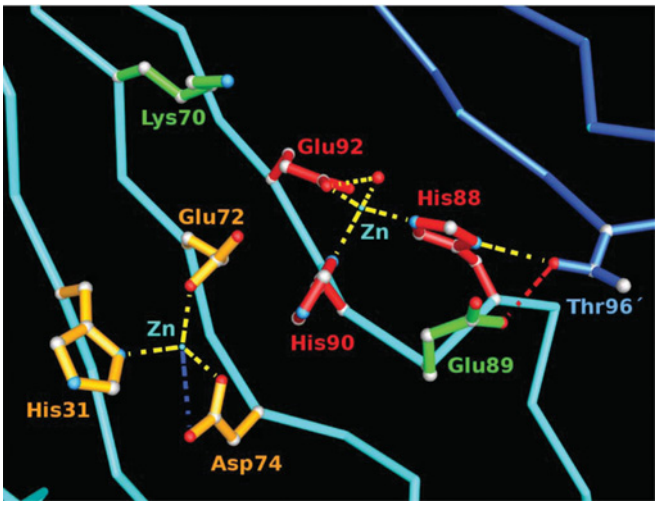

Figure 5 Structure of TTR active site (PDB code 3GRB)

A TTR monomer is represented by its C^{α} chain (cyan), and a second monomer is displayed in dark blue. A Zn^{2+} ligated by the catalytically important residues His^{88}, His^{90} and Glu^{92} (red) is contacting the catalytic water. A second Zn^{2+}-binding site consisting of general base Glu^{72}, His^{31} and Asp^{74} (orange) is located vicinal to the first site. Glu^{89} (green) is in hydrogen-bond contact with $Thr^{96'}$ (blue) of a second TTR monomer which itself also contacts His^{88}. Lys^{70} is shown in green. Attractive forces are indicated by broken lines.

second monomer which itself receives a hydrogen bond from His^{88} of the first monomer (Figure 5). As such, Glu^{89} fulfils a triple task in (i) stabilizing the new conformation of rearranged amino acids 74–90, (ii) strengthening the interaction between two monomers forming a dimer, and (iii) freezing the required conformation of $Thr^{96'}$ which keeps His^{88} in the orientation required to bind Zn^{2+} (Figure 5).

Lys^{70} is a potential hydrogen-bond partner of the general base Glu^{72} and could, as such, influence the pK_a and conformational flexibility of this residue. Modelling studies indicated that Lys^{70} is also in a position to contact a backbone carbonyl oxygen of the substrate as described previously for Arg^{203} in thermolysin and Arg^{717} in neprilysin [34]. His^{31} is a second neighbour of Glu^{72} and also a putative hydrogen-bond partner. To determine the influence of these two vicinal amino acids of Glu^{72} on catalytic activity, we mutated Lys^{70} to alanine and His^{31} to glycine. The results for both mutants confirmed their importance for catalytic activity with L70A and H31G having only 1.1 % and 1.3 % residual activity (Table 1).

A second Zn^{2+}-binding site in double mutants of TTR comprising Glu^{72}, His^{31} and Asp^{74} [32] is present in close vicinity to the TTR catalytic site. Its relevance for proteolysis in general and the role of Asp^{74} on proteolytic activity in particular were not obvious which prompted us to generate D74A. Surprisingly, this mutant suffered only a 2-fold decrease in peptidase activity (Table 1), thereby indicating that this second Zn^{2+}-binding site is not required for proteolytic activity.

In summary, TTR is a mononuclear metallopeptidase with an inducible active site with His^{88}, His^{90} and Glu^{92} serving as Zn^{2+}-complexing ligands.

TTR proteolytic activity is unrelated to protein aggregation and oligomeric state

Several factors, such as the presence of metal ions [6], covalent modification of Cys^{10} [7], lowered pH [8] or point mutations [9], can destabilize the tetrameric TTR structure. To determinate

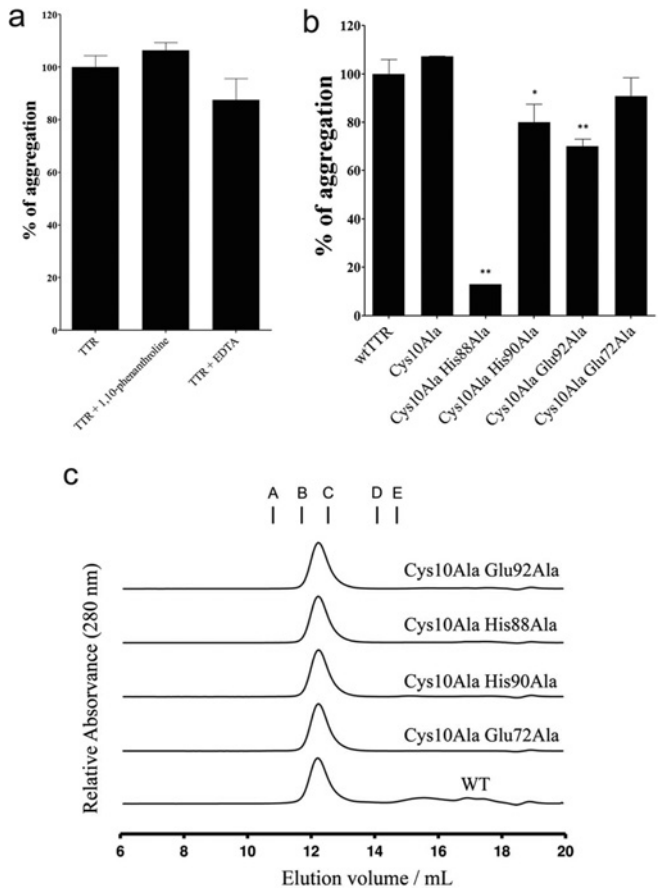

Figure 6 Correlation between TTR proteolytic activity and protein assembly and aggregation

(**a**) Thioflavin-T-binding assays of TTR incubated with the metallopeptidase inhibitors 1,10-phenanthroline and EDTA. (**b**) Thioflavin-T-binding assays of TTR mutants of the catalytically active residues. (**c**) Size-exclusion chromatography of TTR. The elution profile of wtTTR (WT) and variants C10A/E72A, C10A/H88A, C10A/H90A, C10A/E92A are shown. Size standards (Stokes radius/molecular mass] elution volumes are indicated: A, catalase (5.22 nm/232 kDa); B, albumin (3.55 nm/67 kDa); C, ovalbumin (3.05 nm/43 kDa); D, chymotrypsinogen (2.09 nm/25 kDa); E, ribonuclease (1.64 nm/13.7 kDa). Experiments were performed in triplicate. $^{*}P < 0.05$, $^{**}P < 0.01$.

whether TTR aggregation propensity is increased in the presence of 1,10-phenanthroline and EDTA or by the TTR mutants of the active-site residues His^{88}, His^{90}, Glu^{92} and Glu^{72}, we performed thioflavin-T-binding assays after protein acidification. In the case of 1,10-phenanthroline and EDTA, no major effects on wtTTR aggregation potential were observed (Figure 6a). Regarding the TTR mutants, no increased aggregation was detected after the thioflavin-T-binding assay in any of the mutants tested, if compared with wtTTR (Figure 6b). In accordance with the similar catalytic efficiency and inhibition profile, TTR C10A presented an aggregation potential similar to that of wtTTR (Figure 6b). Interestingly, TTR C10A/H88A, TTR C10A/H90A and TTR C10A/E92A had a decreased aggregation profile if compared with either wtTTR or TTR C10A. For TTR C10A/E72A, no differences in aggregation were detected (Figure 6b). Previous studies with wtTTR in an acidic environment revealed the importance of the EF helix–loop region of residues 75–90 in conformational changes leading to disassembly and subsequent aggregation of TTR monomers [8]. Interestingly, mutation of these residues may lead to a decrease in the protein aggregation potential under acidic conditions. These findings demonstrate that TTR catalytic activity and protein aggregation are independent protein properties.

To further investigate possible alterations in the protein oligomerization state introduced by the mutants described in the present paper, we subjected wtTTR and all TTR variants used in the present study to size-exclusion chromatography. All TTR species eluted in a single highly symmetrical peak (Figure 6c) with an elution volume of 12.25 ml, corresponding to an estimated Stokes radius of 3.75 nm. This size is in agreement with the size (3.20–3.40 nm) reported in the literature for the wtTTR tetramer [35,36]. No species of greater size were detected in any of the TTR variants elution profiles.

DISCUSSION

TTR is well known as a transporter of T_4 and retinol. In the present study, we have shown that a change in the secondary structure of TTR can provide this protein with a complete new functionality. If it undergoes a partial conformational change, it acquires the ability to bind Zn^{2+} and to obtain proteolytic competence. Despite decades of research on TTR, its proteolytic activity remained elusive, a fact only explained by (i) the low activity of TTR, and (ii) the unfavourable equilibrium between proteolytic inactive and active conformation of wtTTR present at neutral pH. The structural lability of TTR in the region of amino acids 74–90 is clearly observable in wtTTR X-ray structures obtained at low pH (4.0 and 3.5) (PDB codes 3D7P and 3CBR) [8]. These structures revealed significant changes in this region, proving the existence of multiple conformations in wtTTR. Recent NMR measurements [32] performed on wtTTR at pH 7.5 and increasing amounts of Zn^{2+} left the vast majority of the protein unaffected in the region 74–90 with only a small part assuming a modified conformation. The authors concluded that multiple conformations of wtTTR exist in a dynamic equilibrium with only a rather small fraction being able to complex Zn^{2+}. These observations coincide well with our finding that only about 7 % of total tetrameric wtTTR is in a proteolytic competent conformation at neutral pH.

Interestingly, the very short HXHXE Zn^{2+}-binding pattern is novel and was not found in any metallopeptidase known to date. Since there was no perfect match detected in the MEROPS database [15], we looked for close analogues and found a permutated analogue HXEXH in family M22 (*O*-sialoglycoprotein peptidase) [37]. Coincidentally, both enzymes are inhibited by EDTA and 1,10-phenanthroline, but are insensitive towards phosphoramidon, a well-known inhibitor of metallopeptidases.

A search of Pfam [38] through 597 TTR sequences revealed that only in humans and in some non-human primates are all three amino acids (His^{88}, His^{90} and Glu^{92}) conserved, whereas most other organisms lack His^{90}. These findings imply that the proteolytic activity in TTR was introduced only very late in evolution possibly to modulate and fine-tune concentrations of specific substrates.

Interestingly, inhibition of proteolytic activity of TTR by metal chelators *in vitro* can be reversed by addition of various divalent metal ions as already observed for thermolysin [30]. In TTR, Zn^{2+} and Mn^{2+} restored full proteolytic activity, whereas other metals such as Fe^{2+} and Co^{2+} only partially reactivated the enzyme. *In vivo*, the plasma concentration of a given metal and the stability of a metal–TTR complex will define which metal is preferentially bound to the TTR active site. The apparent dissociation constant [K_d (app)] of Zn^{2+}–TTR is 1 μM [6], which suggests that plasma TTR may circulate as a complex with Zn^{2+}. However, we cannot fully exclude that Mn^{2+} plays a (structural) role different from

the one assumed for Zn^{2+} (catalytic), but other metallopeptidases such as thermolysin [30] or peptide deformylase [31] also tolerate multiple metal ions in their active site. Nevertheless, Mn^{2+}, Fe^{2+} or Co^{2+} could not be detected in our TTR preparations.

We determined a k_{cat}/K_m value of 408.8 $s^{-1} \cdot M^{-1}$ for the active fraction of TTR (7%), which translates to an effective k_{cat}/K_m value of 6.0×10^3 $s^{-1} \cdot M^{-1}$. In comparison with other metallopeptidases, TTR has a lower (although comparable in some cases) activity than thermolysin (3×10^4 $s^{-1} \cdot M^{-1}$) [39], ACE (angiotensin-converting enzyme) (2.9×10^5 $s^{-1} \cdot M^{-1}$) [40] and neprilysin (3.5×10^6 $s^{-1} \cdot M^{-1}$) [41]. Nevertheless, taking into account the higher plasma concentration of TTR (approximately 5 μM, which corresponds to 350 nM of proteolytically active TTR) if compared with other typical plasma metallopeptidases such as ACE (205 pM) [42], one can conclude that TTR proteolytic activity and its physiological impact should not be neglected. Moreover, cleavage of prominent substrates such as apoA-I and Aβ, which are both involved in late-onset diseases of prime interest such as atherosclerosis and Alzheimer's disease, drastically increase the significance of TTR proteolysis. In fact, we have shown previously that cleavage of apoA-I by TTR might affect the development of atherosclerosis [20]. In addition, TTR cleavage of Aβ peptide, identified *in vitro*, might influence Aβ deposition [17].

In summary, we have determined that TTR is a metallopeptidase and identified the residues important for catalytic activity. The identification of TTR catalytic residues enables the assessment of the physiological relevance of TTR proteolysis by the generation of transgenic mice carrying either human wtTTR or proteolytically inactive human TTR. Furthermore, knowing the TTR catalytic machinery may be useful for the design and screening of compounds modulating diseases that are dependent on TTR-mediated proteolysis such as Alzheimer's disease and atherosclerosis.

AUTHOR CONTRIBUTION

Ana Damas, Daniel Bur and Mónica Sousa designed the study. Márcia Liz and Sérgio Leite carried out research. Maria Saraiva and Luiz Juliano contributed new reagents and analytical tools. Márcia Liz, Sérgio Leite, Maria Saraiva, Daniel Bur and Mónica Sousa analysed data. Márcia Liz, Daniel Bur and Mónica Sousa wrote the paper.

ACKNOWLEDGEMENTS

We thank Dr Matthew Bogyo (Stanford University, Palo Alto, CA, U.S.A.) for the phosphonate compound, Dr Marisa Almeida (Chemical Speciation and Bioavailability Laboratory, Center of Marine and Environmental Research, University of Porto) for the determination of metal levels in TTR, Dr Rita Costa (Instituto de Biologia Molecular e Celular, University of Porto) for the help with the thioflavin-T-binding assays and Dr Frederico Silva (Instituto de Biologia Molecular e Celular, University of Porto) for the analytical gel-filtration assays.

FUNDING

This project was supported by the Fundação para a Ciência e Tecnologia (FCT) [grant numbers PTDC/SAU-GMG/111761/2009 and PTDC/SAU-ORG/118863/2010] under the programs FEDER and COMPETE, and Association Française contre les Myopathies, France. In Brazil, the support was from Fundação de Amparo Pesquisa do Estado de São Paulo (FAPESP) and Conselho Nacional de Desenvolvimento Científico e Tecnológico (CNPq). M.A.L. and S.C.L. are Fundação para a Ciência e a Tecnologia (FCT) fellows [grant numbers SFRH/BPD/34811/2007 and SFRH/BD/72240/2010].

REFERENCES

1 Kanda, Y., Goodman, D. S., Canfield, R. E. and Morgan, F. J. (1974) The amino acid sequence of human plasma prealbumin. J. Biol. Chem. **249**, 6796–6805
2 Saraiva, M. J. (2001) Transthyretin mutations in hyperthyroxinemia and amyloid diseases. Hum. Mutat. **17**, 493–503
3 Andrade, C. (1952) A peculiar form of peripheral neuropathy; familiar atypical generalized amyloidosis with special involvement of the peripheral nerves. Brain **75**, 408–427
4 Blake, C. C., Geisow, M. J., Oatley, S. J., Rerat, B. and Rerat, C. (1978) Structure of prealbumin: secondary, tertiary and quaternary interactions determined by Fourier refinement at 1.8 Å. J. Mol. Biol. **121**, 339–356
5 Hurshman Babbes, A. R., Powers, E. T. and Kelly, J. W. (2008) Quantification of the thermodynamically linked quaternary and tertiary structural stabilities of transthyretin and its disease-associated variants: the relationship between stability and amyloidosis. Biochemistry **47**, 6969–6984
6 Wilkinson-White, L. E. and Easterbrook-Smith, S. B. (2007) Characterization of the binding of Cu(II) and Zn(II) to transthyretin: effects on amyloid formation. Biochemistry **46**, 9123–9132
7 Zhang, Q. and Kelly, J. W. (2005) Cys-10 mixed disulfide modifications exacerbate transthyretin familial variant amyloidogenicity: a likely explanation for variable clinical expression of amyloidosis and the lack of pathology in C10S/V30M transgenic mice? Biochemistry **44**, 9079–9085
8 Palaninathan, S. K., Mohamedmohaideen, N. N., Snee, W. C., Kelly, J. W. and Sacchettini, J. C. (2008) Structural insight into pH-induced conformational changes within the native human transthyretin tetramer. J. Mol. Biol. **382**, 1157–1167
9 Cendron, L., Trovato, A., Seno, F., Folli, C., Alfieri, B., Zanotti, G. and Berni, R. (2009) Amyloidogenic potential of transthyretin variants: insights from structural and computational analyses. J. Biol. Chem. **284**, 25832–25841
10 Raz, A. and Goodman, D. S. (1969) The interaction of thyroxine with human plasma prealbumin and with the prealbumin-retinol-binding protein complex. J. Biol. Chem. **244**, 3230–3237
11 Monaco, H. L., Rizzi, M. and Coda, A. (1995) Structure of a complex of two plasma proteins: transthyretin and retinol-binding protein. Science **268**, 1039–1041
12 Hyung, S. J., Deroo, S. and Robinson, C. V. (2010) Retinol and retinol-binding protein stabilize transthyretin via formation of retinol transport complex. ACS Chem. Biol. **5**, 1137–1146
13 Sousa, M. M., Berglund, L. and Saraiva, M. J. (2000) Transthyretin in high density lipoproteins: association with apolipoprotein A-I. J. Lipid Res. **41**, 58–65
14 Liz, M. A., Faro, C. J., Saraiva, M. J. and Sousa, M. M. (2004) Transthyretin, a new cryptic protease. J. Biol. Chem. **279**, 21431–21438
15 Rawlings, N. D., Barrett, A. J. and Bateman, A. (2010) MEROPS: the peptidase database. Nucleic Acids Res. **38**, D227–D233
16 Liz, M. A., Fleming, C. E., Nunes, A. F., Almeida, M. R., Mar, F. M., Choe, Y., Craik, C. S., Powers, J. C., Bogyo, M. and Sousa, M. M. (2009) Substrate specificity of transthyretin: identification of natural substrates in the nervous system. Biochem. J. **419**, 467–474
17 Costa, R., Ferreira-da-Silva, F., Saraiva, M. J. and Cardoso, I. (2008) Transthyretin protects against A-β peptide toxicity by proteolytic cleavage of the peptide: a mechanism sensitive to the Kunitz protease inhibitor. PLoS ONE **3**, e2899
18 Fielding, C. J. and Fielding, P. E. (1995) Molecular physiology of reverse cholesterol transport. J. Lipid Res. **36**, 211–228
19 Tanaka, M., Dhanasekaran, P., Nguyen, D., Ohta, S., Lund-Katz, S., Phillips, M. C. and Saito, H. (2006) Contributions of the N- and C-terminal helical segments to the lipid-free structure and lipid interaction of apolipoprotein A-I. Biochemistry **45**, 10351–10358
20 Liz, M. A., Gomes, C. M., Saraiva, M. J. and Sousa, M. M. (2007) ApoA-I cleaved by transthyretin has reduced ability to promote cholesterol efflux and increased amyloidogenicity. J. Lipid Res. **48**, 2385–2395
21 Goldsteins, G., Andersson, K., Olofsson, A., Dacklin, I., Edvinsson, A., Baranov, V., Sandgren, O., Thylen, C., Hammarstrom, S. and Lundgren, E. (1997) Characterization of two highly amyloidogenic mutants of transthyretin. Biochemistry **36**, 5346–5352
22 Angelo, P. F., Lima, A. R., Alves, F. M., Blaber, S. I., Scarisbrick, I. A., Blaber, M., Juliano, L. and Juliano, M. A. (2006) Substrate specificity of human kallikrein 6: salt and glycosaminoglycan activation effects. J. Biol. Chem. **281**, 3116–3126
23 Le Bonniec, B. F., Myles, T., Johnson, T., Knight, C. G., Tapparelli, C. and Stone, S. R. (1996) Characterization of the P2′ and P3′ specificities of thrombin using fluorescence-quenched substrates and mapping of the subsites by mutagenesis. Biochemistry **35**, 7114–7122
24 Barrett, A. J. and Kirschke, H. (1981) Cathepsin B, Cathepsin H, and cathepsin L. Methods Enzymol. **80**, 535–561
25 Almeida, C. M., Mucha, A. P. and Vasconcelos, M. T. (2004) Influence of the sea rush *Juncus maritimus* on metal concentration and speciation in estuarine sediment colonized by the plant. Environ. Sci. Technol. **38**, 3112–3118
26 Agamennone, M., Campestre, C., Preziuso, S., Consalvi, V., Crucianelli, M., Mazza, F., Politi, V., Ragno, R., Tortorella, P. and Gallina, C. (2005) Synthesis and evaluation of new tripeptide phosphonate inhibitors of MMP-8 and MMP-2. Eur. J. Med. Chem. **40**, 271–279

27 Swann, J. C., Reynolds, J. J. and Galloway, W. A. (1981) Zinc metalloenzyme properties of active and latent collagenase from rabbit bone. Biochem. J. **195**, 41–49
28 Felber, J. P., Coombs, T. L. and Vallee, B. L. (1962) The mechanism of inhibition of carboxypeptidase A by 1,10-phenanthroline. Biochemistry **1**, 231–238
29 Salvesen, G. S. and Nagase, H. (1989) Inhibition of proteolytic enzymes. In Proteolytic Enzymes: a Practical Approach (Beynon, R. J. and Bond, J. S., eds), pp. 105–130, IRL Press, Oxford
30 Holmquist, B. and Vallee, B. L. (1974) Metal substitutions and inhibition of thermolysin: spectra of the cobalt enzyme. J. Biol. Chem. **249**, 4601–4607
31 Rajagopalan, P. T., Datta, A. and Pei, D. (1997) Purification, characterization, and inhibition of peptide deformylase from *Escherichia coli*. Biochemistry **36**, 13910–13918
32 Palmieri, L. de C., Lima, L. M., Freire, J. B., Bleicher, L., Polikarpov, I., Almeida, F. C. and Foguel, D. (2010) Novel Zn^{2+}-binding sites in human transthyretin: implications for amyloidogenesis and retinol-binding protein recognition. J. Biol. Chem. **285**, 31731–31741
33 Holland, D. R., Hausrath, A. C., Juers, D. and Matthews, B. W. (1995) Structural analysis of zinc substitutions in the active site of thermolysin. Protein Sci. **4**, 1955–1965
34 Marie-Claire, C., Ruffet, E., Antonczak, S., Beaumont, A., O'Donohue, M., Roques, B. P. and Fournie-Zaluski, M. C. (1997) Evidence by site-directed mutagenesis that arginine 203 of thermolysin and arginine 717 of neprilysin (neutral endopeptidase) play equivalent critical roles in substrate hydrolysis and inhibitor binding. Biochemistry **36**, 13938–13945
35 Jiang, X., Smith, C. S., Petrassi, H. M., Hammarstrom, P., White, J. T., Sacchettini, J. C. and Kelly, J. W. (2001) An engineered transthyretin monomer that is nonamyloidogenic, unless it is partially denatured. Biochemistry **40**, 11442–11452
36 Pires, R. H., Saraiva, M. J., Damas, A. M. and Kellermayer, M. S. (2010) Structure and assembly–disassembly properties of wild-type transthyretin amyloid protofibrils observed with atomic force microscopy. J. Mol. Recognit. **24**, 467–476
37 Jiang, P. and Mellors, A. (2004) O-Sialoglycoprotein endopeptidase. In Handbook of Proteolytic Enzymes, (2nd edn) (Barrett, A. J., Rawlings, N. D. and Woessner, J. F., eds), pp. 977–980, Elsevier, Amsterdam
38 Finn, R. D., Mistry, J., Tate, J., Coggill, P., Heger, A., Pollington, J. E., Gavin, O. L., Gunasekaran, P., Ceric, G., Forslund, K. et al. (2010) The Pfam protein families database. Nucleic Acids Res. **38**, D211–D222
39 Inouye, K. (2002) Thermolysin. In Handbook of Food Enzymology (Whitaker, J. R., Voragen, A. G. J. and Wong, D. W. S., eds), pp. 1019–1028, CRC Press, Boca Raton
40 Rice, G. I., Thomas, D. A., Grant, P. J., Turner, A. J. and Hooper, N. M. (2004) Evaluation of angiotensin-converting enzyme (ACE), its homologue ACE2 and neprilysin in angiotensin peptide metabolism. Biochem. J. **383**, 45–51
41 Barros, N. M., Campos, M., Bersanetti, P. A., Oliveira, V., Juliano, M. A., Boileau, G., Juliano, L. and Carmona, A. K. (2007) Neprilysin carboxydipeptidase specificity studies and improvement in its detection with fluorescence energy transfer peptides. Biol. Chem. **388**, 447–455
42 McPherson, R. A., Pincus, M. R. and Henry, J. B. (eds) (2007) Henry's Clinical Diagnosis and Management by Laboratory Methods (21st edn), Saunders Elsevier, Amsterdam

Received 20 September 2011/3 February 2012; accepted 15 February 2012
Published as BJ Immediate Publication 15 February 2012, doi:10.1042/BJ20111690

Biochem. J. (2012) **443**, 769–778 (Printed in Great Britain) doi:10.1042/BJ20111690

SUPPLEMENTARY ONLINE DATA

Transthyretin is a metallopeptidase with an inducible active site

Márcia A. LIZ*[1], Sérgio C. LEITE*[1], Luiz JULIANO†, Maria J. SARAIVA‡‖, Ana M. DAMAS§‖, Daniel BUR¶[2] and Mónica M. SOUSA*[2,3]

*Nerve Regeneration Group, Instituto de Biologia Molecular e Celular – IBMC, 4150-180 Porto, Portugal, †Escola Paulista de Medicina, Universidade Federal de São Paulo, 04044-020 São Paulo, Brazil, ‡Molecular Neurobiology Group, Instituto de Biologia Molecular e Celular – IBMC, 4150-180 Porto, Portugal, §Molecular Structure Group, Instituto de Biologia Molecular e Celular – IBMC, 4150-180 Porto, Portugal, ‖ICBAS, Universidade do Porto, 4099-033 Porto, Portugal, and ¶Actelion Pharmaceuticals Ltd, 4123 Allschwil, Switzerland

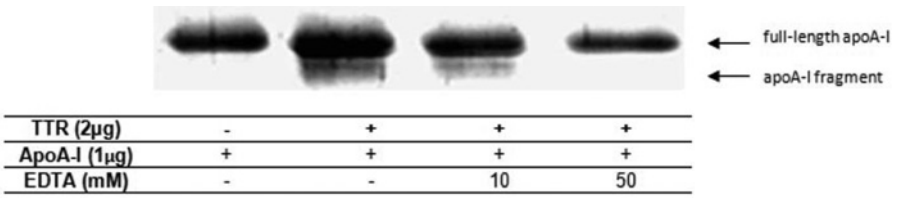

Figure S1 ApoA-I cleavage by TTR is blocked by increasing concentrations of EDTA

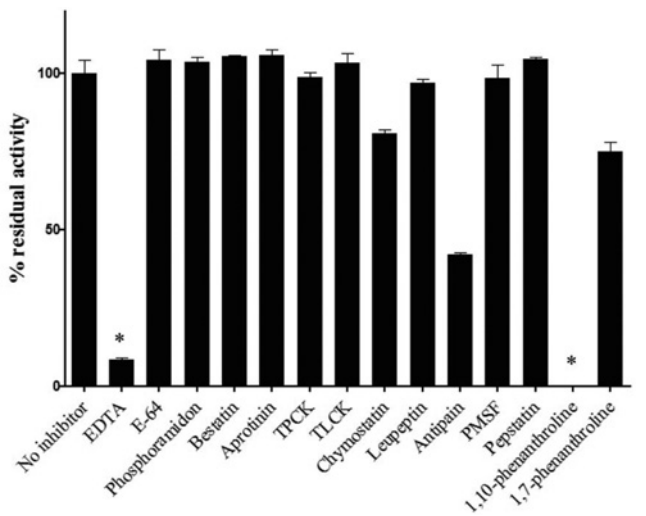

Figure S2 Cleavage of fluorigenic peptides by wtTTR is inhibited by EDTA and 1,10-phenanthroline

wtTTR was pre-incubated with different peptidase inhibitors before cleavage of Abz-YGGRASDQ-EDDnp was determined. $*P < 0.0001$. Relative fluorescence values were converted into percentages of residual activity relative to uninhibited controls. Two independent experiments, each with datasets in duplicate, were performed.

[1] These authors contributed equally to this work.
[2] These authors contributed equally to this work.
[3] To whom correspondence should be addressed (email msousa@ibmc.up.pt).

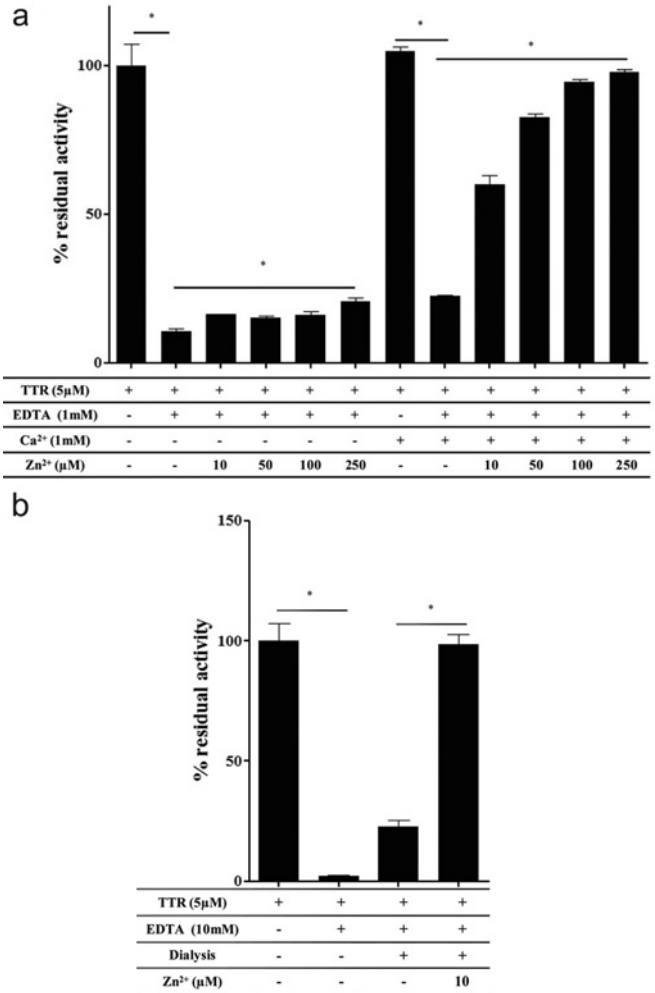

Figure S3 wtTTR inhibition by EDTA is reversed by addition of $ZnCl_2$

(**a**) TTR proteolytic activity was blocked with 1 mM EDTA. Reactivation of TTR with Zn^{2+} was tested in either the presence or absence of 1 mM $CaCl_2$. (**b**) After dialysis, TTR inhibited by EDTA can be reactivated by Zn^{2+}. TTR was inhibited with 10 mM EDTA, dialysed and subsequently reactivated with increasing concentrations of Zn^{2+}. Representative results are shown and the experiment was performed at least twice in duplicate. $^{*}P < 0.001$.

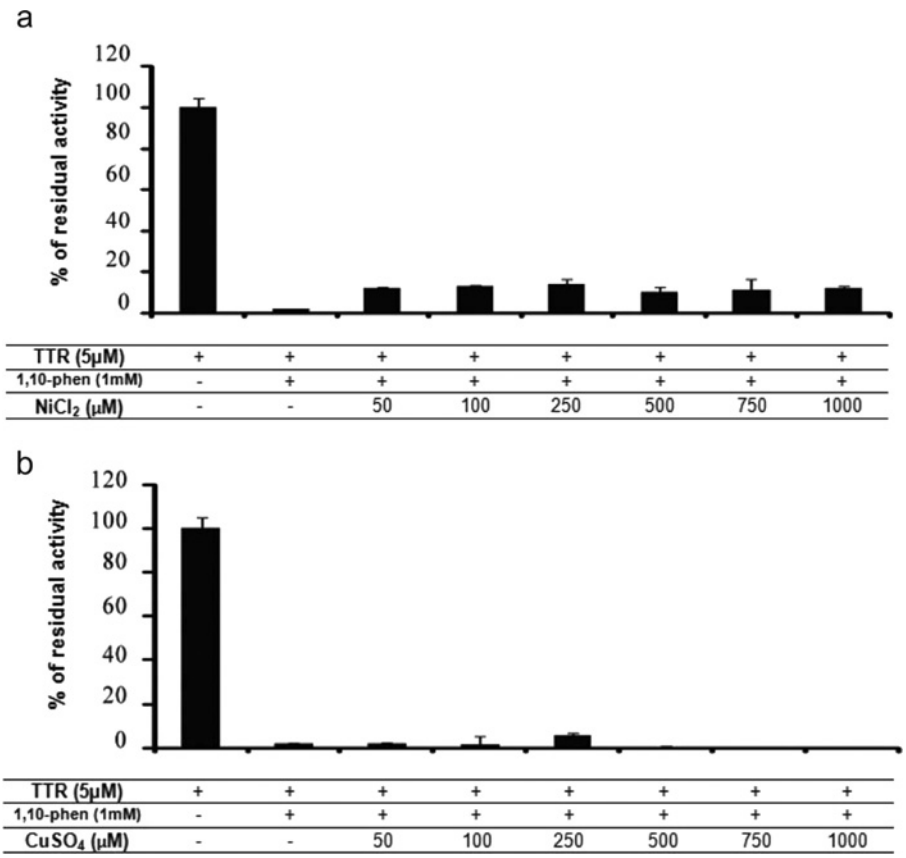

Figure S4 TTR inhibited by 1,10-phenanthroline can be reactivated by divalent metal ions

TTR was inhibited with 1 mM 1,10-phenanthroline (1,10-phen) and subsequently reactivation was tested with increasing concentrations of Ni^{2+} (**a**) and Cu^{2+} (**b**).

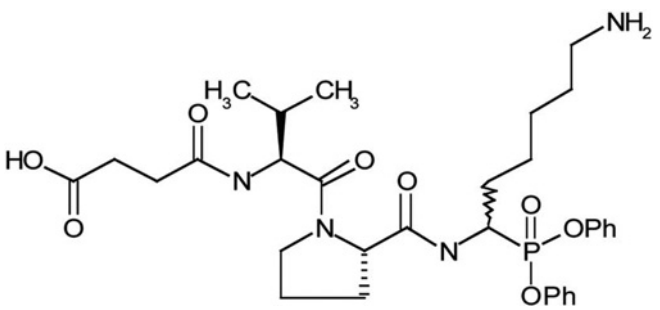

Figure S5 Structure of the phosphonate inhibitor used for active-site titration of TTR

Table S1 MS analysis of full-length TTR or tryptic TTR peptides

For each mutant, both the predicted and the observed mass of the full-length protein or of the tryptic peptide containing the mutated amino acid are shown.

Mutation	Peptide	Predicted mass (Da)	Observed mass (Da)
C10A	1–15 (including initiator methionine)	1603.82	1604.95
H31G	22-35	1414.82	1414.83
K70A	49–76	3083.46	3083.45
C10A/E72A	Full-length	13802.50	13804.31
D74A	49–76	3096.53	3096.55
H88A	81–104	2541.28	2541.33
E89A	81–103	2435.25	2435.23
H90A	81–104	2541.28	2541.28
C10A/E92A	Full-length	13802.50	13798.51

Table S2 MS analysis of tryptic peptides derived from TTR modified with Pefabloc SC

Tryptic TTR peptides modified with pefabloc are highlighted in bold. Pefabloc SC modification corresponds to an increase in mass of 183 Da.

Peptide	Predicted mass (Da)	Observed mass (Da)	Variation
16-34	2021.37	2021.13	− 0.24
16–35	2149.55	2149.29	− 0.26
22–34	1367.59	1367.92	0.33
22–35	1495.77	1495.78	0.01
22–48	2798.13	2797.7	− 0.43
35–48	1449.56	1449.67	0.11
	1449.56	**1632.95**	**183.39**
36–48	1321.39	1321.51	0.12
49–76	3142.40	3142.46	0.06
	3142.40	**3325.69**	**183.29**
49–80	3707.04	3706.36	− 0.65
71–80	1269.44	1268.55	− 0.89
77–103	**3017.33**	**3200.24**	**182.91**
81–103	2452.69	2453.05	0.36
104–126	2517.88	2517.81	− 0.07
104–127	2647.00	2646.98	− 0.02
105–126	2361.70	2361.85	0.15

Table S3 MS analysis of tryptic peptides derived from apoA-I modified with PMSF

The apoA-I tryptic peptide modified with PMSF is highlighted in bold. PMSF modification corresponds to an increase in mass of 154 Da.

Peptide	Predicted mass (Da)	Observed mass (Da)	Variation
1–10	1226.54	1226.55	0.01
1–12	1453.71	1453.71	0.00
11–27	1878.03	1878.03	0.00
13–27	1650.87	1650.87	0.00
13–40	3032.52	3032.50	− 0.02
24-40	1815.85	1815.85	0.00
46–59	1612.79	1612.78	− 0.01
60–77	2202.12	2202.12	0.00
62–77	1932.93	1932.97	0.04
78–94	2020.99	2021.00	0.01
95–107	1579.85	1579.85	0.00
97–107	1380.72	1380.71	− 0.01
108–116	1283.57	1283.57	0.00
117–131; 119–133	1723.94	1723.94	0.00
119–131	1467.79	1467.78	− 0.01
141–149	1031.52	1031.53	0.01
154–160	781.43	781.43	0.00
161–173	1585.81	1585.82	0.01
189–195	831.44	831.44	0.00
207–215	1012.58	1012.58	0.00
207–226	2224.27	2224.27	0.00
227–238	1386.72	1380.70	− 0.02
	1386.72	**1540.81**	**154.09**

Received 20 September 2011/3 February 2012; accepted 15 February 2012
Published as BJ Immediate Publication 15 February 2012, doi:10.1042/BJ20111690

References

Costa, R., Ferreira-da-Silva, F., Saraiva, M.J., and Cardoso, I. (2008). Transthyretin protects against A-beta peptide toxicity by proteolytic cleavage of the peptide: a mechanism sensitive to the Kunitz protease inhibitor. PLoS One 3, e2899.

Fleming, C.E., Mar, F.M., Franquinho, F., Saraiva, M.J., and Sousa, M.M. (2009a). Transthyretin internalization by sensory neurons is megalin mediated and necessary for its neuritogenic activity. J Neurosci 29, 3220-3232.

Fleming, C.E., Nunes, A.F., and Sousa, M.M. (2009b). Transthyretin: more than meets the eye. Prog Neurobiol 89, 266-276.

Fleming, C.E., Saraiva, M.J., and Sousa, M.M. (2007). Transthyretin enhances nerve regeneration. J Neurochem 103, 831-839.

Liz, M.A., Faro, C.J., Saraiva, M.J., and Sousa, M.M. (2004). Transthyretin, a new cryptic protease. J Biol Chem 279, 21431-21438.

Liz, M.A., Fleming, C.E., Nunes, A.F., Almeida, M.R., Mar, F.M., Choe, Y., Craik, C.S., Powers, J.C., Bogyo, M., and Sousa, M.M. (2009). Substrate specificity of transthyretin: identification of natural substrates in the nervous system. Biochem J 419, 467-474.

Nunes, A.F., Saraiva, M.J., and Sousa, M.M. (2006). Transthyretin knockouts are a new mouse model for increased neuropeptide Y. FASEB J 20, 166-168.

Palmieri Lde, C., Lima, L.M., Freire, J.B., Bleicher, L., Polikarpov, I., Almeida, F.C., and Foguel, D. (2010). Novel Zn2+-binding sites in human transthyretin: implications for amyloidogenesis and retinol-binding protein recognition. J Biol Chem 285, 31731-31741.

Ribeiro, C.A., Saraiva, M.J., and Cardoso, I. (2012). Stability of the transthyretin molecule as a key factor in the interaction with a-beta peptide--relevance in Alzheimer's disease. PLoS One 7, e45368.

Sousa, J.C., Grandela, C., Fernandez-Ruiz, J., de Miguel, R., de Sousa, L., Magalhaes, A.I., Saraiva, M.J., Sousa, N., and Palha, J.A. (2004). Transthyretin is involved in depression-like behaviour and exploratory activity. J Neurochem 88, 1052-1058.

Stein, T.D., and Johnson, J.A. (2002). Lack of neurodegeneration in transgenic mice overexpressing mutant amyloid precursor protein is associated with increased levels of transthyretin and the activation of cell survival pathways. J Neurosci 22, 7380-7388.

Wang, X., Cattaneo, F., Ryno, L., Hulleman, J., Reixach, N., and Buxbaum, J.N. (2014). The systemic amyloid precursor transthyretin (TTR) behaves as a neuronal stress protein regulated by HSF1 in SH-SY5Y human neuroblastoma cells and APP23 Alzheimer's disease model mice. J Neurosci 34, 7253-7265.

Research goals

The main focus of this Thesis was to understand the role of the actin cytoskeleton and of its dynamics in axon growth and regeneration. For that, we proposed the following objectives:

- Understand the role of the actin binding protein adducin in neurons and understand how its absence impacts the organization of the neuronal cytoskeleton. For that we used α-adducin KO mice, the truly full adducin KO, to study the role of adducin in the development and maintenance of the nervous system (Chapter 1)

- Explore the role of adducins during the course of axon growth and regeneration. Phosphorylated adducins were found to be increased – i.e. inhibited – in the growth cones of regenerating axons, in the conditioning lesion model. We used the α-adducin KO mice to mimic the conditioning effect, both *in vitro* and *in vivo* to understand the role of this actin-binding protein in axon extension (Chapter 2)

- Dissect the function of profilin-1 in axon growth and regeneration Profilin-1 was also suggested to be an important component in the regulation of axon regeneration, as supported by proteomic analysis of regenerating axons. Therefore we evaluated its role in neuritogenesis and axon extension (Chapter 3)

Chapter 1

The actin-binding protein α-adducin is required for maintaining axon diameter

Sérgio Carvalho Leite,[1,3,4] Paula Sampaio,[2,3] Vera Filipe Sousa,[1,3,4] Joana Nogueira-Rodrigues,[1,3] Rita Pinto-Costa,[1,3] Luanne L. Peters,[5] Pedro Brites,[1,3] and Mónica Mendes Sousa[1,3]

[1]Nerve Regeneration group and [2]Advanced Light Microscopy unit, IBMC-Instituto de Biologia Molecular e Celular, Universidade do Porto, 4150-180 Porto, Portugal

[3]Instituto de Investigação e Inovação em Saúde, Universidade do Porto, 4200 Porto, Portugal

[4]ICBAS, Universidade do Porto, 4050-313 Porto, Portugal

[5]The Jackson Laboratory, Bar Harbor, Maine 04609, USA

Correspondence: msousa@ibmc.up.pt (M.M.S.)

Summary

The actin-binding protein adducin was recently shown to be part of actin rings in the axon subcortical cytoskeleton. Here we analyzed α-adducin knockout mice to uncover adducin's function in actin rings. *In vitro*, lack of adducin impaired axonal transport and cytoskeleton dynamics. *In vivo*, α-adducin knockout mice presented progressive axon enlargement that preceded axon degeneration. Using stimulated emission depletion super-resolution *microscopy*, *we observed that* in the absence of adducin, the periodicity of actin rings was maintained, whereas their diameter was increased. Our data supports that adducin's actin-spectrin crosslinking activity is not essential for generating the periodic ring pattern, whereas its capping activity is necessary to control actin filament growth within rings. Moreover, we further establish the ubiquitous nature of the periodic neuronal actin rings by observing their presence in dorsal root ganglia and retinal ganglion cells. Finally, our work raises the possibility that changes in neuronal actin rings trigger degeneration.

Introduction

In neurons, the tight regulation of cytoskeleton organization and dynamics has emerged as a key factor in polarization, synaptogenesis, axon growth and degeneration. Recently, using stochastic optical reconstruction microscopy (STORM) a new view on the structure of the actin cytoskeleton in neurons was proposed (Xu et al., 2013). Initially observed in axons of cultured hippocampal neurons, actin was shown to form ring-like structures wrapping around the axonal circumference with an even periodic spacing of 180–190 nm (Lukinavicius et al., 2014; Xu et al., 2013). Periodic actin rings were then shown to be also present in dendrites and in other neuron types, including the nodes of Ranvier in the peripheral nervous system (D'Este et al., 2015). Neuronal actin rings contained adducin, an actin-capping protein, and were crosslinked by βII/αII spectrin tetramers (Xu et al., 2013). In hippocampal neuron cultures, the actin rings emerged early during axon development, after axon specification, had a proximal to distal assembly fashion along the length of the axon, and were maintained in mature neurons. (Xu et al., 2013; Zhong et al., 2014). Once assembled, the structure was suggested to be highly stable, with slow turnover of its components (Zhong et al., 2014). Although the function of neuronal actin rings remains largely elusive, this submembraneous cytoskeleton may provide mechanical support for the thin structure of axons and dendrites. Supporting this notion, deletion of β spectrin in C.elegans leads to axon breakage upon movement of the worm (Hammarlund et al., 2007).

So far, adducin is the only actin-binding protein identified as part of neuronal actin rings. Adducin has three main functions as a regulator of the actin cytoskeleton: i) it promotes the bundling of actin filaments, ii) it caps the actin filament barbed ends inhibiting the incorporation of new actin monomers, and iii) it is involved in the recruitment and crosslinking of spectrin to the ends of actin filaments (Li et al., 1998). In accordance with its function as an actin-binding protein, adducin is found in actin-enriched sites in the nervous system, primarily in growth cones and synaptic structures such as dendritic spines. In this context, adducin is an important molecule in synapse formation, as mouse and fly adducin mutants have decreased synaptic stability (Bednarek and Caroni, 2011; Pielage et al., 2011). Adducin has been associated with neurodegenerative conditions including amyotrophic lateral sclerosis (Gallardo et al., 2014) and cerebral palsy (Kruer et al., 2013), further supporting its important role in the homeostasis of the actin cytoskeleton in the nervous system.

Mammalian adducins comprise 3 closely related genes (α, β and γ), with α and γ being ubiquitously expressed and β being abundant in the brain and in erythrocytes (Matsuoka et al., 2000). Functional tetrameric adducin is composed of two heterodimers, in which the presence of the α monomer is an absolute requirement. To further understand the participation of adducin in the biology of the nervous system, we characterized α-adducin knockout (KO) mice (Robledo et al., 2008; Robledo et al., 2012). Here we show that loss of α-adducin in vivo causes progressive axon enlargement and degeneration and that, in vitro, adducin-deficient hippocampal neurons have axon actin rings with increased diameters. Our data propose a model in which alterations in the composition of actin rings may be involved in regulating axon diameter.

Results

α-adducin KO mice develop progressive axon enlargement and degeneration

Functional adducin consists of a tetrameric complex of two heterodimers where the α monomer is essential. Nervous tissue from α-adducin KO mice had severely decreased levels of β- and γ-adducin (Figure 1A), similar to what is observed in erythrocytes from α-adducin KO mice (Robledo et al., 2008). Consistently, in α-adducin KO mouse brains no dimer/tetramer formation was visualized by western blot after native PAGE (Figure 1B). In the absence of α-adducin, capping protein (EcapZ) levels were similar to those found in WT animals (Figure 1C). Immunofluorescence of hippocampal neurons further confirmed the absence of adducin in α-adducin KO neurons (Figure 1D). After having confirmed that α-adducin KO mice lack functional adducin, we examined this model to uncover adducin's function in the development and homeostasis of the nervous system.

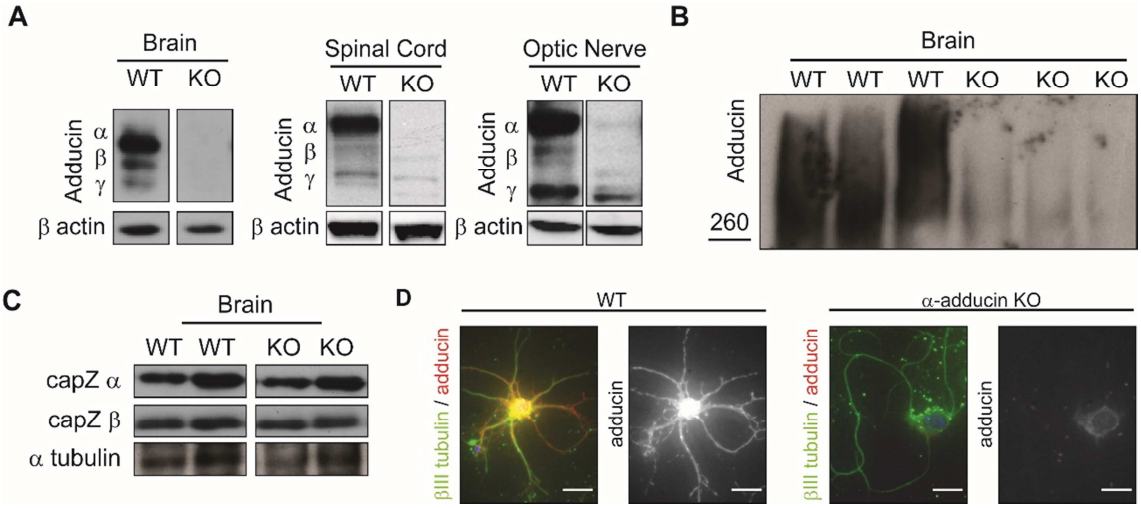

Figure 1. α-adducin KO mice have severely decreased levels of β- and γ-adducin and lack functional adducin tetramers. (A) Western blot analysis of brain, spinal cord and optic nerve of WT and α-adducin KO mice using a pan-specific antibody that recognizes the in α-, β- and γ-adducin forms (Xu et al., 2013). (B) Anti-adducin western blot analysis of brain extracts of WT and α-adducin KO brain extracts run on native gels. The 260kDa standard is indicated (note that under reducing conditions the observed MW of an adducin dimer is of approximately 210-260 kDa (Gardner and Bennett, 1986). (C) Western blot analysis of capping protein (CapZ) in brain extracts of WT and α-adducin KO mice. (D) Anti-adducin immunofluorescence in E16 hippocampal neurons isolated from WT and α-adducin KO mice. Left panels: DAPI (blue), βIII-tubulin (green) and pan-adducin (red); right panels: pan-adducin (white). Scale bar: 10µm

To understand the relevance of adducin's loss in neuron biology, we analyzed the central and peripheral nervous system of α-adducin KO mice. In the central nervous system, the absence of α-adducin led to axon loss in both the optic nerve (Figure 2A and 2B) and the spinal cord (Figure 2D and 2E). In the optic nerve, axon loss was progressive since normal axon density was observed at postnatal day 20 (P20), but by P100 α-adducin KO optic nerves had a 40% reduction of axon density (WT: 731044 axons/mm^2 ±22718; α-adducin KO: 444215 axons/mm^2 ±63918; $p<0.01$) (Figure 2B). At this age, we also observed severe atrophy (Figure 2C) with a 33% decreased optic nerve area in mutant nerves (WT: 0.088mm^2 ±0.002; α-adducin KO: 0.058mm^2 ±0.005; $p<0.001$). Overall, the decreased axon density and nerve cross-sectional area resulted in an estimated loss of 60% of the total number of axons in α-adducin KO optic nerves. A decreased axon density was also visible in α-adducin KO spinal cords. Analysis of the corticospinal tract (CST) revealed a 25% decreased axonal density in the absence of α-adducin (WT: 462197 axons/mm^2 ±35667; α-adducin KO: 305513 axons/mm^2 ±13447; $p<0.05$) (Figures 2D and 2E). In the peripheral nervous system, we also observed a decreased density of myelinated axons in sciatic nerves from α-adducin KO mice (data not shown). Combined, these results support previous analyses in the PNS (Robledo et

al., 2012), and highlight that loss of adducin has a major impact in central and peripheral nervous system axons.

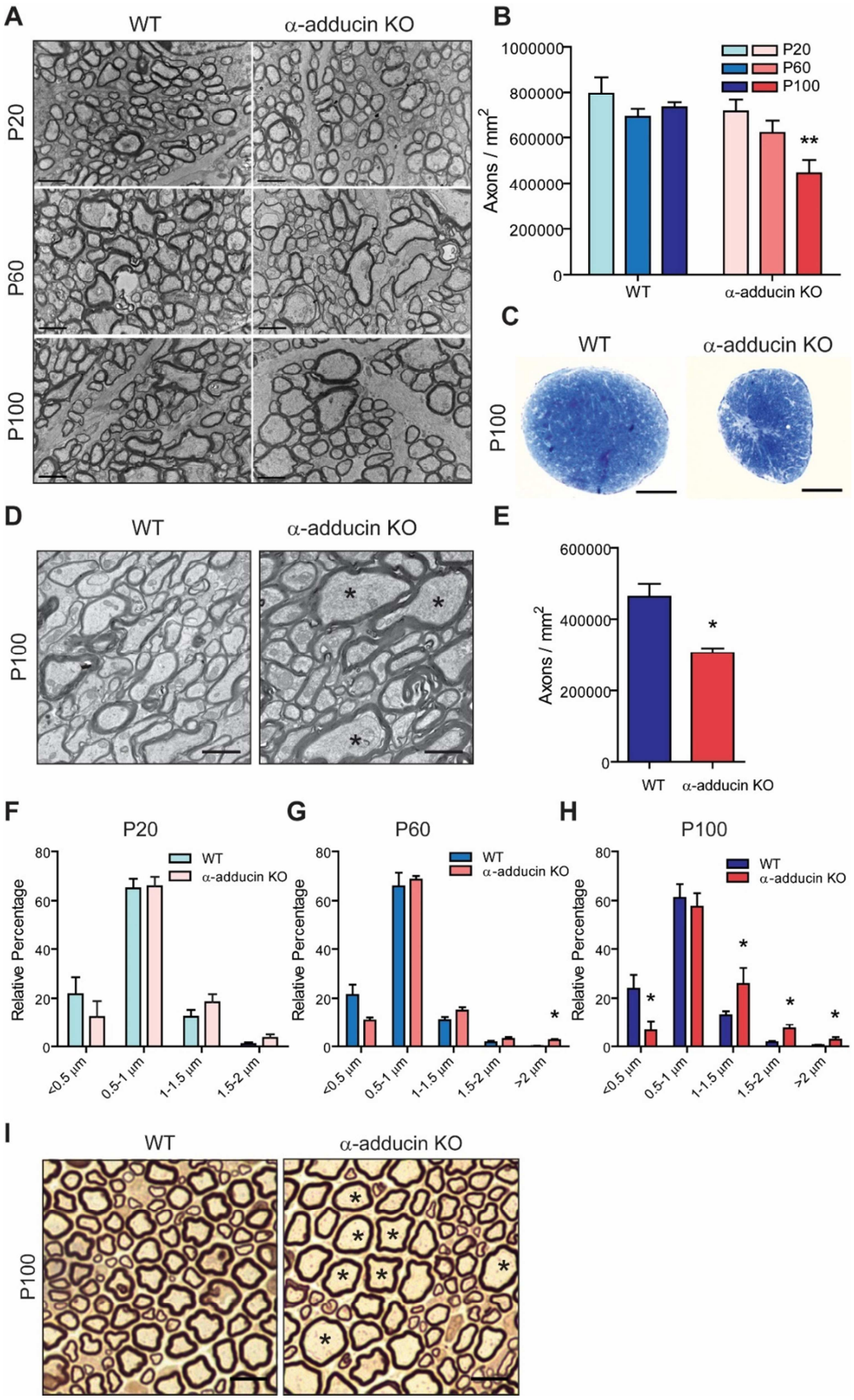

Figure 2. α-adducin KO mice show progressive axon enlargement and axonopathy. (A) Representative 12000x microphotographs of ultra-thin sections of optic nerves from WT and α-adducin KO mice at P20, P60 and P100; Scale bar: 2µm. (B) Axon density in the optic nerve of WT (P20 n=4; P60 n=5; P100 n=5) and α-

adducin KO mice (P20 n=4; P60 n=5; P100 n=4) at P20, P60 and P100. (C) Representative semi-thin cross sections of WT and α-adducin KO optic nerves stained with toluidine blue; Scale bar: 100µm. (D) Representative 6000x microphotographs of ultra-thin sections of WT and α-adducin KO corticospinal tracts; asterisks highlight axons with enlarged diameter; Scale bar: 1µm. (E) Axon density in the corticospinal tract of WT (n=4) and α-adducin KO mice (n=4) at P100. (F-G) Axon distribution according to diameter in P20 (F), P60 (G) and P100 (H) WT (P20 n=5; P60 n=4; P100 n=6) and α-adducin KO (P20 n=4; P60 n=4; P100 n=5) optic nerves. (I) Representative semi-thin sections of WT and α-adducin KO sciatic nerves; asterisks highlight axons with enlarged diameter; Scale bar: 10µm. Graphs show mean ± SEM; p-value *<0.05, **<0.01.

Interestingly, progressive axonal enlargement preceded axon loss in α-adducin KO mice. The distribution of axons of different diameters was normal in the P20 optic nerve, but by P60 an increase in high diameter (> 2µm) axons was observed and was exacerbated at P100 where an overall decrease in small diameter axons was accompanied by an increase in large diameter axons (Figures 2F, 2G and 2H). Interestingly, myelin thickness as determined by the g-ratio was similar in the optic nerve of P100 WT and α-adducin KO mice (data not shown) suggesting that enlarged axons are normally myelinated. Abnormally large axons were also found in the spinal cord (Figure 2D, asterisks) and sciatic nerve (Figure 2I, asterisks). In summary, our results show that in the absence of adducin, there is an enlargement of axon diameter and axonal loss in both the CNS and PNS.

Loss of adducin impairs cytoskeleton dynamics in the growth cone and axonal transport

Cytoskeleton deregulation is generally related to axon enlargement and axonopathy. Therefore, we examined the effects of α-adducin depletion on the axonal cytoskeleton. P100 α-adducin KO optic nerve axons had a constant axon diameter as observed in longitudinal sections, without focal enlargements or visible accumulation of organelles (Figure 3A) and with normal microtubule and neurofilament density (Figure 3B and 3C). *In vitro*, the growth cones of α-adducin KO hippocampal (Figure 3D and 3E) and DRG neurons (Figure 4A-B) had increased actin retrograde flow as determined after transfection with LifeAct-GFP (Riedl et al., 2008), probably resulting from the loss of the actin-capping activity of adducin. Moreover, the growth speed of protruding microtubules, as assessed after transfection with the microtubule *plus*-end tracking protein, end-binding protein 3 (EB3)-GFP (Stepanova et al., 2003), was also increased in α-adducin KO growth cones (Figure 3F and 3G), suggesting a synergistic effect of increased actin dynamics and microtubule invasion and growth. Subsequent analysis of microtubule modifications by immunofluorescence in hippocampal neuron growth cones suggested that increased

microtubule growth speed is probably independent of the dynamic state of tubulin as the acetylated/tyrosinated microtubule ratio was normal in α-adducin KO neurons (Figure 3H and 3I). This data supports the notion that increased microtubule growth speed in α-adducin KO growth cones is likely a consequence of actin destabilization.

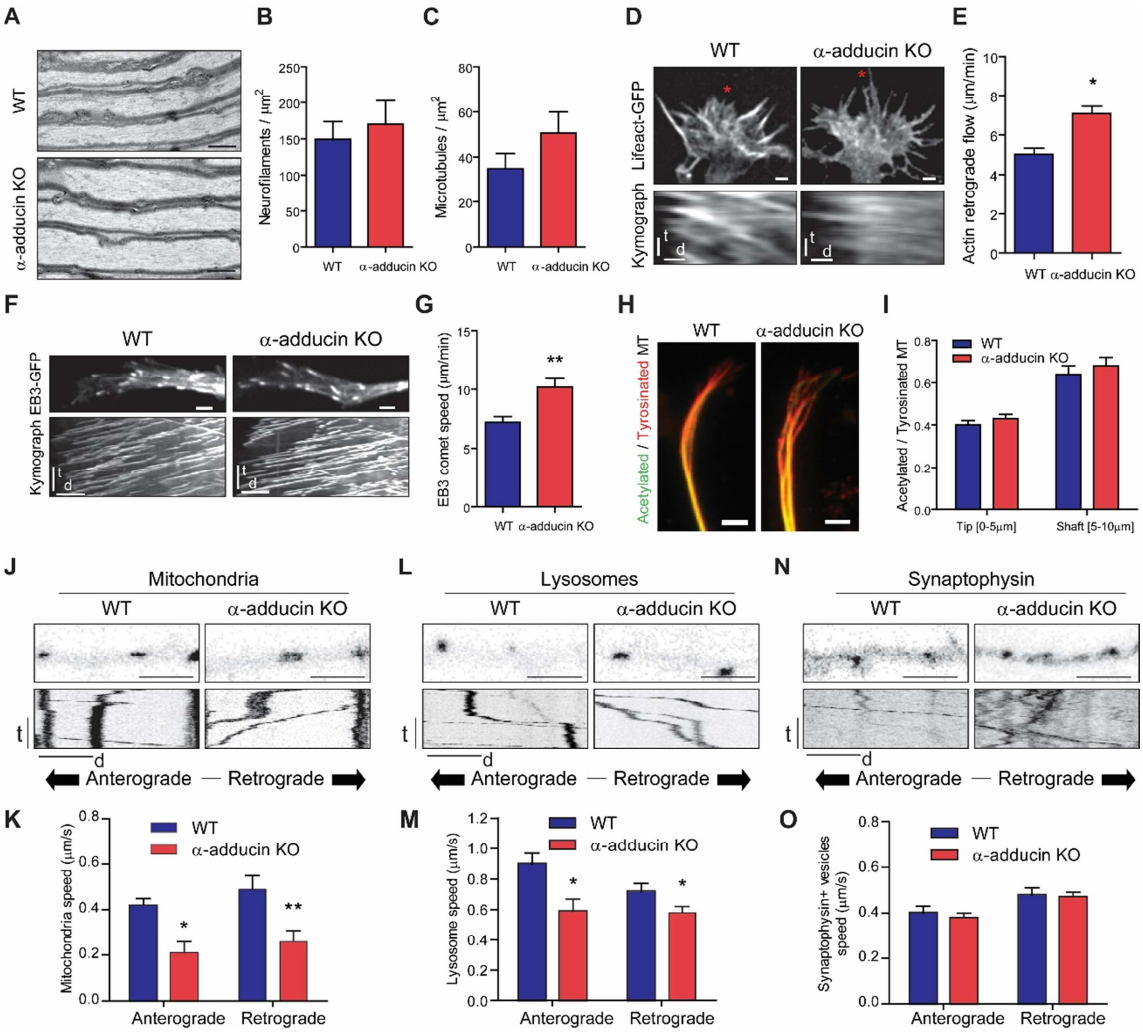

Figure 2. Loss of adducin impairs cytoskeleton dynamics in the growth cone and axonal transport. (A) Longitudinal sections of WT and α-adducin KO optic nerves; Scale bar 1µm. (B-C) Analysis of neurofilament (B) and microtubule (C) densities were measured in WT (n=6) and α-adducin KO (n=5) optic nerves. (D) Representative growth cones of lifeAct-GFP transfected hippocampal neurons (upper) and respective kymographs (lower). Red asterisks highlight the region where kymographs were performed. (E) Quantification of actin retrograde flow in hippocampal neurons from WT and α-adducin KO mice. (F) Representative growth cones of EB3-GFP transfected DRG neurons (upper) and respective kymographs (lower). (G) Quantification of microtubule growth speed in DRG neurons from WT and α-adducin KO mice. (D and F) Upper panel: scale bar: 2µm; Bottom panel: vertical scale bar- time (t): 50 seconds, horizontal scale bar- distance (d): 1µm. (H) Immunofluorescence of acetylated and tyrosinated microtubules (MT) in hippocampal neuron growth cones from WT and α-adducin KO mice. Scale bar: 2µm. (I) Quantification of acetylated and tyrosinated microtubules in the tip and shaft of growth cones represented in H. (J-O) Analysis in WT and α-adducin KO hippocampal neurons of the axonal transport of mitochondria (J, K), lysosomes (L, M) and synaptophysin (N, O); (J, L and

N) Upper-still images at t=0 and lower- kymographs; (K, M and O) Quantification of the speed of axonal transport. Scale bar: time (t): 100 seconds; distance (d): 5µm. Graphs show mean ± SEM; p-value *<0.05, **<0.01.

As changes in cytoskeleton dynamics and axon enlargement are largely related to impaired axonal transport, we compared the movement of organelles and synaptic vesicles in WT and α-adducin KO hippocampal and DRG neurons. In hippocampal neurons, the absence of adducin affected the speed of axonal transport of mitochondria (Figure 3J and 3K) and lysosomes (Figure 3L and 3M). Despite the decreased speed of axonal transport in both the anterograde and retrograde directions, we did not observe a consistent impact in the percentage of moving cargos (data not shown). Interestingly, no difference in the speed of transport of synaptic vesicles was observed (Figure 3N and 3O). In DRG neurons, similar findings were made, i.e., in the absence of adducin decreased speed of transport of organelles and unchanged speed of transport of synaptic vesicles were detected (Figure 4C-H). Of note, the levels of motor proteins in WT and α-adducin KO mice were comparable (data not shown).

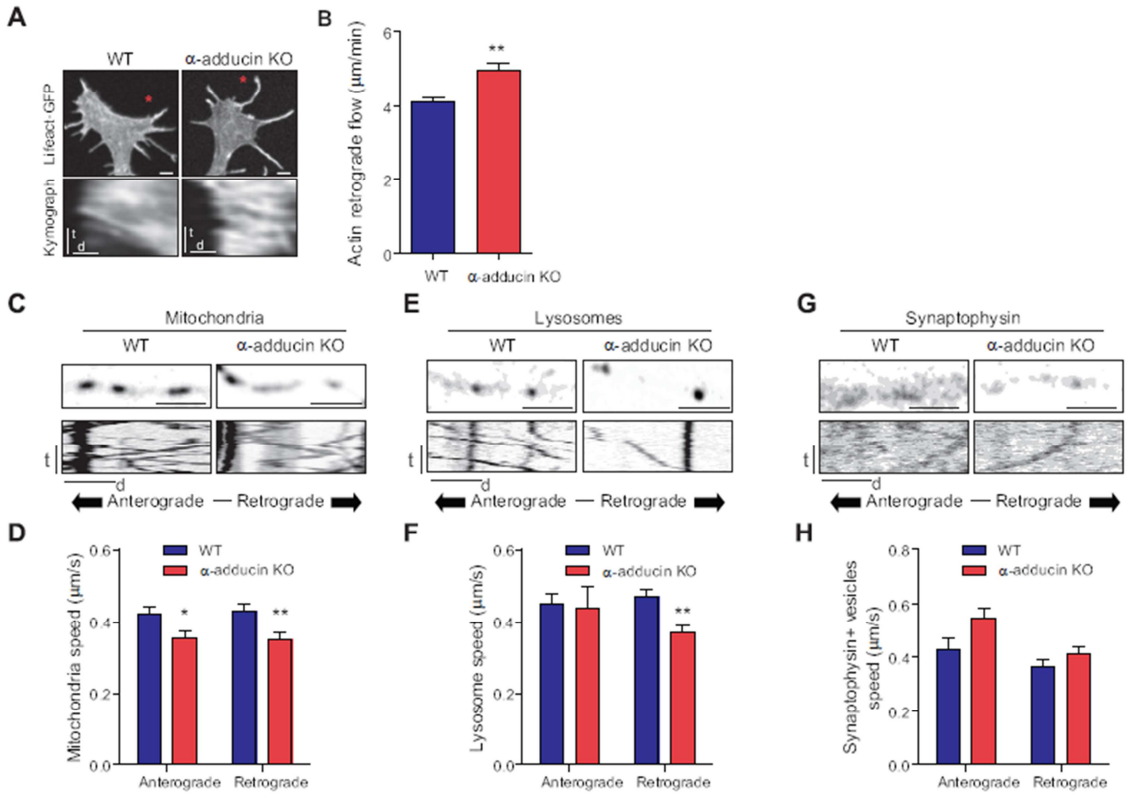

Figure 4. α-adducin KO impairs actin cytoskeleton and axonal transport in DRG neurons. (A) Representative growth cones of lifeAct-GFP transfected DRG neurons (upper) and respective kymographs (lower). Red asterisks highlight the region where kymographs were performed. Upper panel: scale bar: 2µm; Bottom panel: vertical scale bar (time (t)): 50 seconds, horizontal scale bar (distance (d)): 1µm. (B) Quantification of actin retrograde flow in DRG neurons from WT and α-adducin KO mice. (C-H) Analysis in WT and α-adducin KO

DRG neurons of the axonal transport of mitochondria (C, D), lysosomes (E, F) and synaptophysin (G, H); (C, E and G) Upper-still images at t=0 and lower- kymographs; (D, F and H) Quantification of the speed of axonal transport. Scale bar: time (t): 100 seconds; distance (d): 5µm. Graphs show mean ± SEM; p-value *<0.05, **<0.01.

The periodic nature of the actin-spectrin submembraneous cytoskeleton is conserved in retinal ganglion cells and DRG neurons

Recently, adducin was shown to be a component of actin rings in hippocampal neurons (Xu et al., 2013). The development of silicon rhodamine actin (SiR-actin), and the usage of stimulated emission depletion (STED) microscopy, allowed the detection of actin rings in axons, dendrites and, at the nodes of Ranvier (D'Este et al., 2015). The function of this novel organization of the neuronal actin cytoskeleton remains elusive, and it is not known if these structures are present in other neurons. Using SiR-actin and STED microscopy, we show that DRG neurons (Figure 5A) and retinal ganglion cell neurons (Figure 5B) also assemble actin rings. In these neuron types, the spacing of approximately 190 nm between rings was maintained. In DRG neurons the ring periodicity was of 194.4±0.5 nm (442 measurements) (Figure 5C) and in retinal ganglion cells 190.2±4.1 nm (62 measurements) (Figure 5D). Interestingly, in both DIV2 DRG neurons and DIV5 retinal ganglion cells, the actin-spectrin lattice was not visible in all of the cells (data not shown). In rat DRG neurons, either the rings were visible in all the neurites of a given cell or alternatively, they were not detected in any of the neurites (data not shown). Throughout the axon shaft, parallel long actin fibers were visible in axons from DRG neurons (Figure 5E) and retinal ganglion cells (not shown), similar to what has been reported in hippocampal neurons (D'Este et al., 2015). In summary, our data further establishes the ubiquitous nature of the subcortical cytoskeleton periodicity.

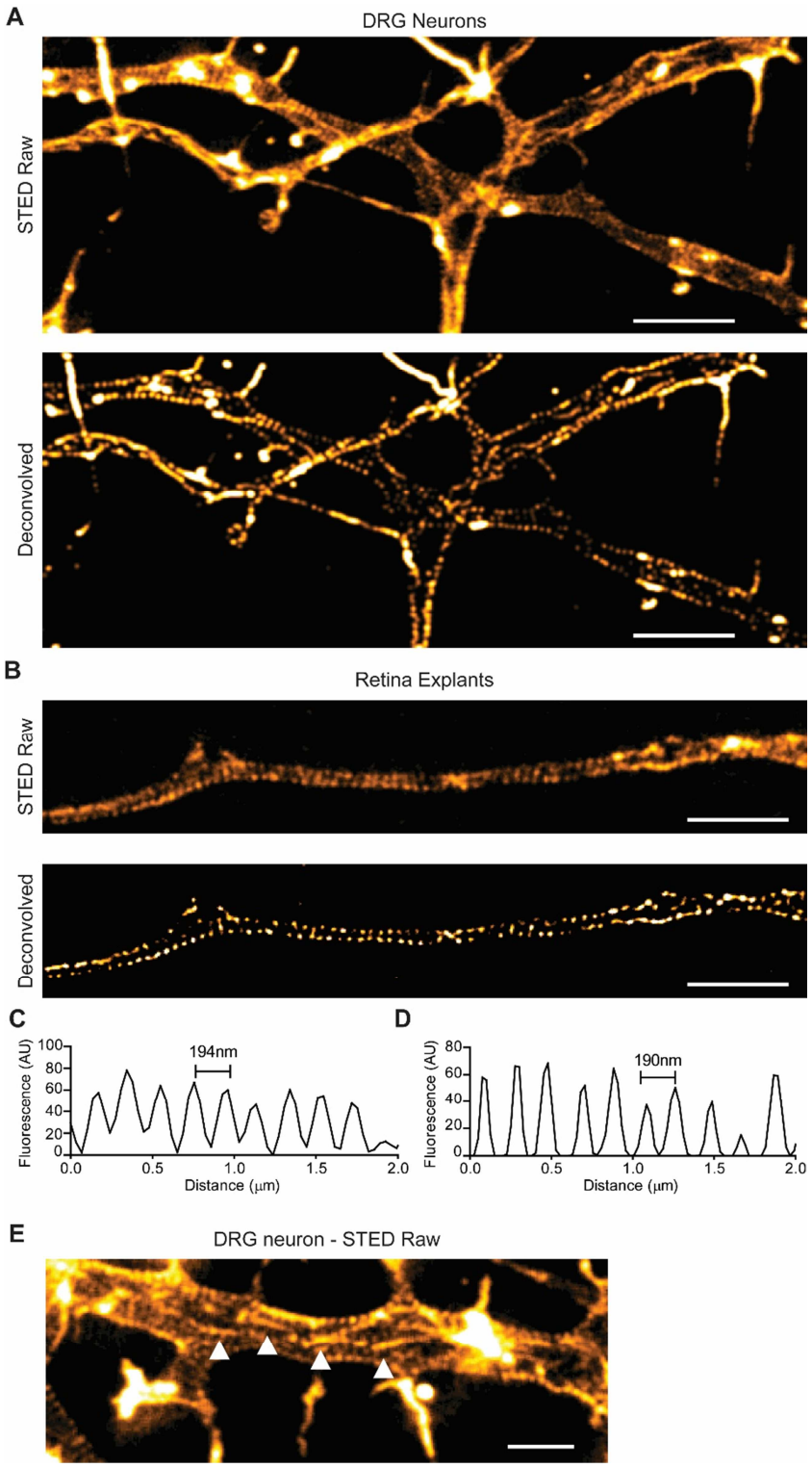

Figure 5. The periodicity of actin rings is maintained in retinal ganglion cells and DRG neurons. (A-B) STED super resolution microscopy was performed in DIV2 rat DRG (A) and DIV5 mouse retina explants (B). STED images were obtained (upper) and deconvolved (lower) using Huygens Essential software. Scale bars: 2µm. (C-D) Analysis of the distribution of the axonal actin rings in (A) and (B), respectively. Measurements were performed in deconvolved images (DRG neurons: n=16 axons, 442 measurements; retinal ganglion cells: n=2 axons, 62 measurements). (E) DIV2 DRG neurons present longitudinal actin filaments, highlighted with white arrowheads. Scale bar: 1µm.

Adducin is not essential for generating the periodic pattern of neuronal actin rings but is necessary for the maintenance of axonal diameter

The role of adducin in actin ring formation and organization is still unknown. Given the different roles of adducin in the regulation of the actin-spectrin cytoskeleton, we hypothesized that in the absence of this protein the periodic pattern of rings would be disrupted due to decreased crosslinking of actin-spectrin junctions, and/or the lack of adducin's capping activity would give rise to aberrant F-actin sized filaments, resulting in enlarged ring diameter. To analyze actin rings in α-adducin KO mice, DIV16 hippocampal neurons were stained with SiR-actin. Dendrites were enriched in longitudinal actin fibers and actin-enriched dendritic spines laterally. At this stage, as previously described (D'Este et al., 2015), the presence of spines highly enriched in actin precluded the identification of the periodic actin pattern in dendrites. Axons were clearly distinguished by the low abundance of longitudinal actin fibers and absence of dendritic spines (Figure 6A). At DIV16, both WT and α-adducin KO axons had actin rings throughout the entire axon shaft. The periodic pattern of these structures was independent of the presence of adducin in F-actin filaments (Figures 6B, 6C). Similar periodicities were seen in WT and α-adducin KO axons (WT=194.5±1.0 nm, n=60 axons; α-adducin KO=194.7±2.0 nm, n=38 axons; p=0.89) (Figures 6D-F). These data suggest that the N-terminus actin-binding domain of spectrin is probably sufficient for actin ring binding to the spectrin lattice.

In the model proposed for actin ring organization in neurons (Xu et al., 2013), each ring is composed by several short and stable actin filaments capped at their barbed ends by adducin. Removal of the capping protein is predicted to lead to dysregulation of actin filament length, resulting in increased filament size and concomitantly increased diameter of the neuronal actin rings. In α-adducin KO axons actin rings had a 1.3-fold enlarged diameter (WT: 409.2±21.8 nm, n=50 axons; α-adducin KO: 521.7±29.2nm, n=33 axons; p=0.002) (Figure 6G). These findings suggest that the capping activity of adducin, rather than its spectrin recruiting activity, is required to maintain axonal actin ring diameter and when absent, the rings become enlarged. Together, our findings open the exciting possibility that the dysregulation of axonal diameter, such as observed in α-adducin KO mice, occurs as a consequence of altered axon actin rings, which ultimately leads to axonal degeneration.

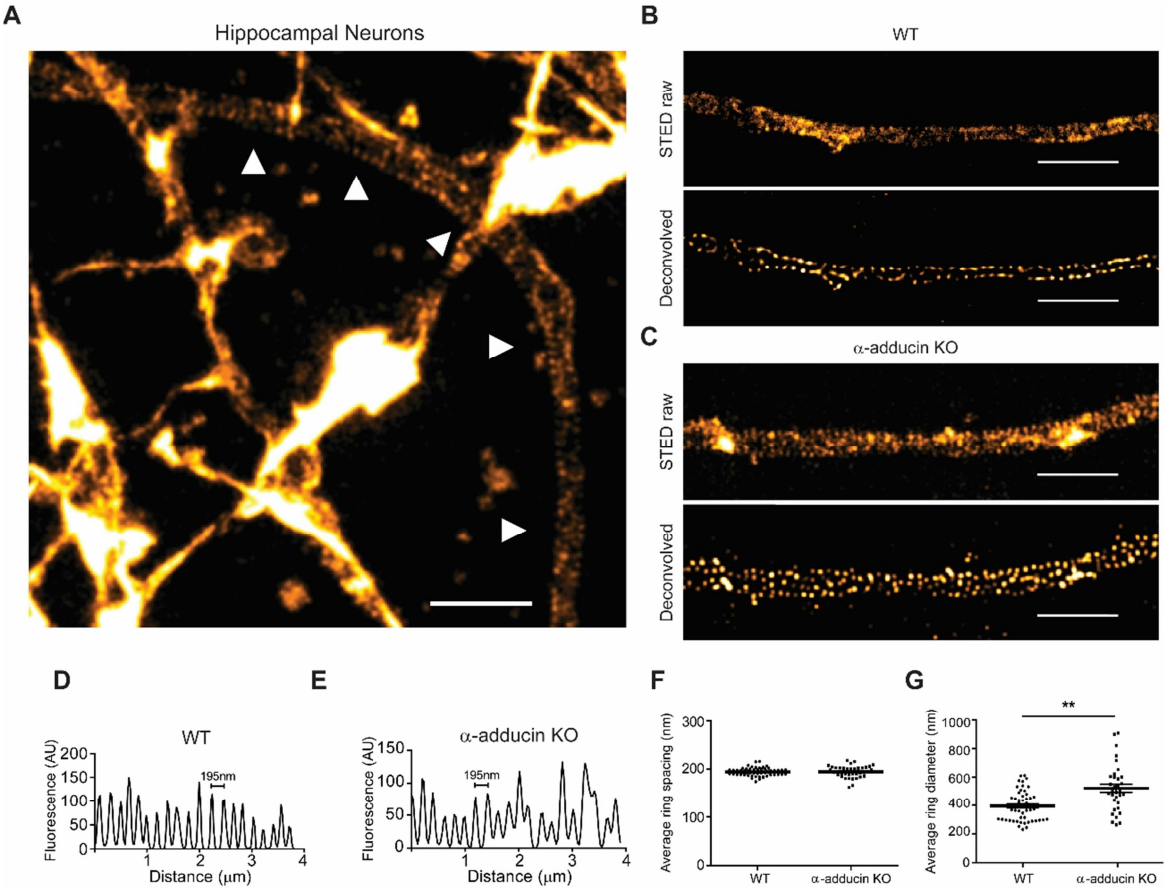

Figure 4. Analysis of axonal actin rings in WT and α-adducin KO DIV16 hippocampal neurons. (A) STED super resolution microscopy of DIV16 hippocampal neurons. One axon is highlighted with white arrowheads. Scale bar: 2µm. (B-C) WT (B) and α-adducin KO (C) hippocampal neurons were imaged by STED microscopy (upper) and deconvolved (lower). Scale bars: 2µm. (D-E) Analysis of the distribution of axonal actin rings in WT (D) and α-adducin KO (E) hippocampal neurons. (F) Quantification of the average ring spacing in WT (n=1450 inter-ring spacings, n=60 axons) and α-adducin KO hippocampal neurons (n=1140 inter-ring spacings, n=38 axons). (G) Quantification of the average ring diameter in WT (n=1533 measurements, n=50 axons) and α-adducin KO (n=1164 inter-ring spacings, n=33 axons) hippocampal neurons. All measurements were done in deconvolved images. Graphs show mean ± SEM; each dot is the average measurement for a given individual axon; p-value **<0.01.

Discussion

The neuronal cytoskeleton is a tightly regulated structure where the interplay of its three main components, actin, microtubules and neurofilaments is crucial. Up to the discovery of axon actin rings, the neuronal actin cytoskeleton had its relevance mainly restricted to growth cones, synaptic structures and the axon initial segment. The identification of these novel ring structures certainly opened new exciting prospects on our understanding of neurobiology. Still, the molecular details of ring composition, assembly, maintenance,

behavior and function (both under physiological conditions and upon dysfunction) are largely unknown. Although molecular detail is still lacking, three components have been identified in axonal rings namely, actin, spectrin and adducin (Xu et al., 2013). Here we show that the absence of adducin *in vivo* leads to a time-dependent axon enlargement and loss, and *in vitro* to increased actin ring diameter. Previous evidence suggested that adducin is an important player in brain homeostasis and disease: some α-adducin KO mice develop hydrocephaly in a background dependent manner (Robledo et al., 2008; Robledo et al., 2012); β-adducin KO mice have impaired dendritic spine assembly and maintenance in conditions of high synaptic turnover (Bednarek and Caroni, 2011); and γ-adducin mutations are associated with cerebral palsy, possibly resulting from defects in neuronal migration (Kruer et al., 2013). Here we showed that the absence of adducin leads to axon enlargement and axonal loss. These defects were independent of hydrocephaly, as they occurred irrespectively of the presence of ventricle enlargement.

Axonal actin rings, axon diameter and axon degeneration

The progressive enlargement of axons in α-adducin KO mice was found to be related to an early increase in axon actin ring diameter *in vitro*. This raises new views on the regulation of axon diameter, and its relationship with axon degeneration. As previously suggested (Xu et al., 2013; Zhong et al., 2014) and given the actin-capping activity of adducin, actin rings are unlikely to be made of continuous F-actin filaments spanning the entire ring, but should be made of short adducin-capped filaments. In this context, adducin would control the length of F-actin filaments within the ring and thereby function as a regulator of ring and axonal diameter. In axonal actin rings, adducin could serve the additional function of crosslinking actin to the spectrin lattice. However, our data supports that the adducin crosslinking activity is not necessary for the periodicity of the actin-spectrin lattice, although the possibility that this activity is necessary for the stability of the submembraneous actin cytoskeleton remains to be determined. In this respect, adducin was suggested to stabilize the actin cytoskeleton during neuronal maturation (Xu et al., 2013; Zhong et al., 2014). The periodic distribution of spectrin and actin is visualized at DIV2-3, whereas adducin's presence in the rings is only visible at DIV6 (Zhong et al., 2014). Early adducin-deficient actin rings are probably more sensitive to membrane extraction (as needed for phalloidin staining) and this may be the reason why under these conditions, actin rings are not detected before DIV5. In contrast, the use of cell-permeable probes (such as SiR-actin) allows the observation of actin rings as early as DIV2 (D'Este et al., 2015). This increased stability of actin rings may be conferred by adducin

recruitment to the lattice that would allow the subcortical cytoskeleton to become more stable as axons mature.

There are several similarities between the spectrin-actin lattice in neurons and erythrocytes. In erythrocytes, spectrin, actin and associated proteins are organized into a stable cortical cytoskeleton, often referred to as the membrane skeleton, that confers strength and elasticity to the red cell (Mohandas and Gallagher, 2008). The absence of adducin results in misshaped erythrocytes that are less resistant to mechanic stresses such as osmotic pressure (Gilligan et al., 1999; Robledo et al., 2008). However, when erythrocytes need to squeeze through small capillaries, the erythrocyte cortical cytoskeleton becomes dynamic and deformable. In neurons, it would be interesting to assess whether the actin-spectrin lattice is also able to become dynamic in specific contexts such as during axon degeneration and plasticity events where actin rings may be rearranged/disassembled to promote either constriction of the axonal membrane, axon branching, among others.

Axon actin rings, microtubules and axonal transport

The reason underlying the decreased velocity of axonal transport of mitochondria and lysosomes in α-adducin KO neurons remains elusive. The fact that only the transport of organelles is impaired, and not that of synaptic vesicles, might be related to the different sizes of these cargos or to their different binding partners. Could there be a link between the increased axonal diameter in α-adducin KO neurons and the decreased speed of axonal transport? This correlation is not straightforward as the rate of fast axonal transport is thought to be independent of axon caliber variations, at least within the range of those here reported for α-adducin KO axons (Ochs, 1972; Wortman et al., 2014). Decreased microtubule density could lead to decreased speed of axonal transport (Wortman et al., 2014). However, microtubule density was unaffected in α-adducin KO mice. Of possible interest, at least in the context of cell cycle, α-adducin was shown to interact with microtubules via myosin X (Myo10) (Chan et al., 2014), establishing a link between adducin and the microtubule cytoskeleton. Could there be a link between axonal actin rings, microtubules and axonal transport? In fact, axonal actin rings are dependent on microtubule integrity; microtubule destabilization with nocodazole leads to loss of actin rings in axons (Zhong et al., 2014). How these different components of the axonal cytoskeleton crosstalk, however, is unknown. A possible relation between actin rings and axonal transport has already been raised (Gallo, 2013). According to this hypothesis, actin rings could serve as docking sites for axonal cargos associated with myosins, which

would allow an approximately 200nm resolution for the control of axonal transport (Gallo, 2013). Supporting this notion, in neurons, mitochondria dock along axons through myosinV, and depletion of myosins results in increased speed and length of microtubule-based runs (Pathak et al., 2010). Would actin rings with an increased diameter have an increased capacity to 'sequester' myosin motors, decreasing the average speed of axonal transport? The answer to this question, together with several others raised by the identification of these novel ring structures, relies intimately on the identification of the actin-binding proteins that shape actin rings, on their mechanistic assembly, on determining their relevance to the mechanical properties of axons and dendrites, and on the characterization of their organization in the course of axon degeneration.

EXPERIMENTAL PROCEDURES

Animals

α-adducin KO mice and WT littermates were obtained from heterozygous breeding pairs and genotyped as described (Robledo et al., 2008). Mice were handled according to European Union and National legislation.

Western blotting

For analyses under denaturing conditions, 10% SDS-PAGE gels or Criterion XT 3-8% gradient gels (Bio-rad), were run with brain, spinal cord or optic nerve extracts from at least n=3 WT and n=3 α-adducin KO P30 mice. Gels were transferred to nitrocellulose membranes for 2 hours using a semi-dry system. For analyses under native conditions, 4% PAGE gels were used with 50µg of brain extracts from WT (n=3) and α-adducin KO mice (n=3). Native gels were run and transferred to a PVDF membrane for 2 hours using a semi-dry system. Membranes were washed in Tris buffered saline (TBS) with 0.1% Tween-20, blocked in 5% non-fat dried milk in TBS for 1 hour at room temperature, and incubated with primary antibodies (in 5% BSA in TBS with 0.1% Tween-20) for 1 hour at room temperature or overnight at 4ºC. The following primary antibodies were used: rabbit anti-adducin, 1:1000 (Abcam, ab51130); mouse anti-β-actin, 1:5000 (Sigma, A5441); mouse anti-capping protein α1/2, 1:50 (Developmental Studies Hybridoma Bank, MAB 5B12.3) and mouse anti-capping protein β2, 1:150 (Developmental Studies Hybridoma Bank, MAB 3F2.3). Membranes were washed and incubated with secondary antibodies in 5% non-fat dried milk in TBS for 1 hour, at room temperature. The secondary antibodies

used were: donkey anti-mouse IgG, donkey anti-rat IgG or donkey anti-rabbit IgG conjugated with HRP, 1:5000 (all from Jackson Immunoresearch Europe). Membranes were then incubated for 5 minutes at room temperature with Luminata Crescendo Western HRP substrate (Millipore) and chemiluminescence was analyzed by either exposure to Amersham Hyperfilm ECL (GE healthcare) or detection in ChemiDoc XRS System (Bio-Rad).

Hippocampal neuron cultures

Hippocampal neuron cultures were performed as described (Kaech and Banker, 2006). Briefly, E16.5 embryos were individually dissected and genotyped. The hippocampus of each individual pup was digested 15 minutes in 0.06% porcine trypsin solution (Sigma, T4799), triturated, and plated either at 16000 cells/well in 24-well plates containing pre-coated glass cover slips treated with 20µg/mL poly-L-lysine (Sigma, P2636), or at 12200 cells/well in 8-well µ-dishes (IBIDI, 80827) coated with 20µg/mL poly-L-lysine for STED microscopy and axonal transport assays. Neurons were cultured in Neurobasal medium (Invitrogen) supplemented with 1x B27 (Gibco), 1% penicillin/streptomycin (Gibco) and 2mM L-glutamine (Gibco).

DRG neuron cultures

DRG neuron cultures were performed following the protocol detailed in (Fleming et al., 2009). Briefly, DRG from 8 weeks old Wistar rats were collected, digested for 90 minutes with 0.125% collagenase IV-S (Sigma, C1189), triturated and centrifuged in a 15% BSA gradient. For STED microscopy, 3750 cells/well were plated in 8-well µ-dishes coated with 20µg/mL poly-L-lysine (Sigma, P2636) and 5µg/mL laminin (Sigma, L2020) and grown in DMEM:F12 (Sigma, D8437) supplemented with 1x B27 (Gibco), 1% penicillin/streptomycin (Gibco), 2mM L-glutamine (Gibco) and 50ng/mL NGF (Millipore, 01-125).

Retina explants cultures

For retina explants, retinas from P5 Sv129/b6 mice were dissected in neurobasal medium and gently titrated with a P1000 tip. For STED microscopy, retina fragments were washed 3x with neurobasal medium and plated in 8-well µ-dishes (IBIDI, 80827) coated with 20µg/mL poly-L-lysine (Sigma, P2636) and 2µg/mL laminin (L2020, Sigma). Explants were incubated with complete retina explant growth media- Neurobasal (Invitrogen,)

supplemented with 1x B27 (Gibco), 1% penicillin/streptomycin (Gibco), 0.2% fungizone (Gibco), 1mM L-glutamine (Gibco), 5ng/mL human recombinant BDNF (PeproTech) and 1ng/mL CNTF (PrepoTech).

Morphometric analysis

For morphometric analyses, WT and α-adducin KO littermates were sacrificed at 3 different time points, P20 (n=4 WT; n=4 α-adducin KO), P60 (n=5 WT; n=5 α-adducin KO) and P100 (n=5 WT; n=4 α-adducin KO). Spinal cords, optic nerves and sciatic nerves were fixed for two weeks in 4% glutaraldehyde (Merck) in 0.1M sodium cacodylate buffer (pH 7.4). After post-fixation with 1% OsO4 in 0.1M sodium cacodylate buffer (pH 7.4) for 2 hours, tissues were dehydrated and embedded in Epon (Electron Microscopy Sciences).

To determine axon caliber and density in the optic nerve and spinal cord, and unmyelinated axon density in sciatic nerve samples, ultrathin sections (60nm) prepared in a Leica ultramicrotome were placed on 200-mesh copper grids (Electron Microscopy Sciences) and counterstained with alcoholic uranyl acetate solution (2% w/v; 10 minutes), uranyl acetate solution (2% w/v; 10 minutes) and lead citrate (4% w/v; 10 minutes). Grids were observed in a JEOL JEM-1400 transmission electron microscope equipped with an Orious Sc1000 digital camera. Ten to 15 non-overlapping photomicrographs were obtained at 12000x (area of each microphotograph was 165µm2) for optic nerve samples, and 5 non-overlapping images were obtained at 6000x (area of each microphotograph was 635µm2) for spinal cord samples, and used for determinations of axon density. For the analysis of axon diameter in the optic nerve, two 165µm2 photomicrographs were used, with a minimum of 112 axons measured.

In sciatic nerves, to determine axon caliber and the density of myelinated axons, 1µm-thick nerve sections were stained for 10 minutes with 1% p-phenylenediamine (PPD) in absolute methanol, dried, and mounted on a drop of DPX (Merck). The entire area of the nerve was photographed using an Olympus optical microscope equipped with an Olympus DP 25 camera and Cell B software, and images were imported into Photoshop (Adobe).

Actin retrograde flow and microtubule dynamics

DRG from WT and α-adducin KO P30 mice were nucleofected with either 0.75µg Lifeact-GFP (Riedl et al., 2008) or 0.5µg EB3-GFP (Stepanova et al., 2003), using the 4D Nucleofector Amaxa system (Lonza, CM#137 program), left in suspension in complete medium for 24h, and then plated 5700 cells/cm2 in 20µg/mL poly-L-lysine (Sigma) and

5µg/mL laminin (Sigma) coated 35mm µ-Dish (IBIDI, 81158). Hippocampal neurons were nucleofected with 0.75µg Lifeact-GFP, using the 4D Nucleofector Amaxa system (Lonza, CU#133 program) and plated 70000 cells/cm2 in 20µg/mL poly-L-lysine (Sigma) coated 35mm µ-Dish (Ibidi, 81158). Time-lapse recordings were performed in an Andor Revolution XD spinning disk (Andor Technologies) at 37ºC, at DIV2 for DRG neurons and DIV3 in hippocampal neurons. For the analysis of actin retrograde flow, neurons were imaged for 200 seconds (40 frames, captured each 5 seconds) and kymographs were generated with the Kymograph plug-in for ImageJ (DRG neurons: n=217 measurements from 40 WT growth cones; n=135 measurements from 27 α-adducin KO growth cones; hippocampal neurons: n=103 measurements from 14 WT growth cones; n=123 measurements from 15 α-adducin KO growth cones). For the analysis of microtubule dynamics, neurons were imaged for 200 seconds (100 frames, captured each 2 seconds) and kymographs were generated using a Matlab script (LAPSO) (Pereira and Maiato, 2010) (n=324 measurements from 13 WT growth cones; n=240 measurements from 14 α-adducin KO growth cones).

Axonal transport

Hippocampal and DRG neuron cultures were performed as detailed above. For the live imaging of axonal transport, DIV4 (DIV5 for synaptophysin) hippocampal neurons (a timepoint at which their polarized morphology allows the clear identification of the axon as the longest neurite) or DIV2 DRG neurons were used. Briefly neurons were incubated for 45 minutes with 100nM of either Lysotracker (Life Technologies) or Mitotracker (Life Technologies) in complete medium. For synaptic vesicles analysis, DIV4 neurons were infected 24 hours with baculovirus expressing synaptophysin-GFP (Life Technologies). Transport of axonal mitochondria, lysosomes or synaptic vesicles was analyzed in a Leica SP5II confocal microscope (Leica Microsystems) with acquisition at 0.8 Hz for 2 min. Only vesicles and organelles moving for 10 consecutive frames were considered. In each case, at least 48 vesicles or organelles were measured per condition, from 15 axons; for DRG neurons, at least 114 vesicles or organelles were measured per condition from a minimum of 14 DRG neurons.

Acetylated/tyrosinated α-tubulin

The assessment of acetylated/tyrosinated α-tubulin was performed using WT and α-adducin KO DIV3 hippocampal neurons extracted in PEM buffer (100mM PIPES, 5mM EGTA, 1MgCl2, pH6.9) containing 1% Triton X-100, 2% PEG, 2µM phalloidin and 2µM

Taxol, and fixed in 2% GTA in 0.1M cacodylate. Immunofluorescence was performed using mouse anti-acetylated tubulin (1:20000, # T7451, Sigma) and rat anti-tyrosinated tubulin (1:15000, MCA77G, Serotech). The ratio of acetylated versus tyrosinated α-tubulin was determined by measuring the fluorescence intensities of acetylated α-tubulin and of tyrosinated α-tubulin with ImageJ. Measurements were done in the distal 0-5µm and 5-10µm of the growth cone tip, considering the labeling in the tyrosinated α-tubulin channel, after background subtraction for each channel. At least 150 growth cones were measured per condition.

Adducin immunofluorescence

DIV16 hippocampal neurons were treated with 0.1% Triton-X, blocked and incubated with the primary antibodies rabbit anti-adducin, 1:200 (Abcam, ab51130) and mouse anti βIII-tubulin, 1:1000 (Promega, G7121). Secondary antibodies used were donkey-anti-mouse Alexa Fluor 488 and donkey-anti rabbit Alexa Fluor 568, both diluted 1:1000 (Invitrogen, A-21202 and A10042 respectively). Coverslips were mounted in fluoroshield (Sigma). Images were acquired in a Leica DMI 6000B inverted microscope at 40x.

STED imaging of axonal actin rings

Actin ring analysis was done using the silicon-rhodamine (SiR)-actin probe (Lukinavicius et al., 2014) and stimulated emission depletion microscopy (Lukinavicius et al., 2014), in a Leica TCS SP8 STED 3X (Leica Microsystems). DIV16 hippocampal neurons, DIV2 rat DRG neurons and DIV5 mouse retina explants were incubated for 1 hour with 2µM SiR-actin (kindly provided by Prof Kai Johnsson, École Polytechnique Fédérale de Lausanne, Switzerland), fixed 20 minutes in 4% PFA and post-fixed in PBS. Samples were initially visualized by confocal and then STED microscopy was performed. Axons were fine-tuned focused in their lateral outmost points and the focus point was confirmed by STED image sharpness. Raw STED images were deconvolved using Huygens Essential software (Scientific Volume Imaging B.V), using the adjusted GMLE algorithm. To analyze ring distribution, deconvolved images were plotted longitudinally in n=1450 WT inter-ring spacings (from 60 axons) and n=1140 α-adducin KO inter-ring spacings (from 38 axons) in hippocampal neurons; n=442 inter-ring spacings in rat DRG neurons (from 16 axons); and n=62 inter-ring spacings in retina explants (from 2 axons). All measurements were performed using Huygens Software. To determine axon diameter, the distance between the outer points (brighter, in the focus plane) that formed the actin ring was determined.

Only actin rings unequivocally focused in the maximum wide plan were considered (n=1533 WT actin rings, from 50 axons and n=1164 α-adducin KO rings, from 33 axons).

Statistics

Data are shown as mean ± SEM. Statistical significance was determined by Student's t test using Prism (GraphPad Software).

ACKNOWLEDGEMENTS

This work was funded by the International Foundation for Research in Paraplegia (IRP). Leite SC was supported by Fundação para a Ciência e Tecnologia (FCT) (SFRH/BD/72240/2010) and Brites P is an Investigator FCT. Generation of α-adducin KO mice was supported by National Institutes of Health grant HL075714 (L.L.P.). We thank the excellent technical support of the IBMC Animal Facility. We are indebted to Leica Microsystems (Mannheim, Germany), especially to Dr Ulf Schwarz, for making a STED microscope available for this study. We thank Dr Ana Carvalho (IBMC) for fruitful discussions, Dr Casper Hoogenraad (Utrecht University, The Netherlands) for critical reading of the manuscript and Marlene Morgado (IBMC) for quantification of acetylated/tyrosinated microtubules. The authors have no conflicts of interest to declare.

References

Bednarek, E., and Caroni, P. (2011). beta-Adducin is required for stable assembly of new synapses and improved memory upon environmental enrichment. Neuron 69, 1132-1146.

Chan, P.C., Hsu, R.Y., Liu, C.W., Lai, C.C., and Chen, H.C. (2014). Adducin-1 is essential for mitotic spindle assembly through its interaction with myosin-X. J Cell Biol 204, 19-28.

D'Este, E., Kamin, D., Göttfert, F., El-Hady, A., and Hell, S.W. (2015). STED Nanoscopy Reveals the Ubiquity of Subcortical Cytoskeleton Periodicity in Living Neurons. Cell Rep 10.

Gallardo, G., Barowski, J., Ravits, J., Siddique, T., Lingrel, J.B., Robertson, J., Steen, H., and Bonni, A. (2014). An alpha2-Na/K ATPase/alpha-adducin complex in astrocytes triggers non-cell autonomous neurodegeneration. Nat Neurosci 17, 1710-1719.

Gallo, G. (2013). More than one ring to bind them all: recent insights into the structure of the axon. Dev Neurobiol 73, 799-805.

Gardner, K., and Bennett, V. (1986). A new erythrocyte membrane-associated protein with calmodulin binding activity. Identification and purification. J Biol Chem 261, 1339-1348.

Gilligan, D.M., Lozovatsky, L., Gwynn, B., Brugnara, C., Mohandas, N., and Peters, L.L. (1999). Targeted disruption of the beta adducin gene (Add2) causes red blood cell spherocytosis in mice. Proc Natl Acad Sci U S A 96, 10717-10722.

Hammarlund, M., Jorgensen, E.M., and Bastiani, M.J. (2007). Axons break in animals lacking beta-spectrin. J Cell Biol 176, 269-275.

Kaech, S., and Banker, G. (2006). Culturing hippocampal neurons. Nat Protoc 1, 2406-2415.

Kruer, M.C., Jepperson, T., Dutta, S., Steiner, R.D., Cottenie, E., Sanford, L., Merkens, M., Russman, B.S., Blasco, P.A., Fan, G.*, et al.* (2013). Mutations in gamma adducin are associated with inherited cerebral palsy. Ann Neurol 74, 805-814.

Li, X., Matsuoka, Y., and Bennett, V. (1998). Adducin preferentially recruits spectrin to the fast growing ends of actin filaments in a complex requiring the MARCKS-related domain and a newly defined oligomerization domain. J Biol Chem 273, 19329-19338.

Lukinavicius, G., Reymond, L., D'Este, E., Masharina, A., Gottfert, F., Ta, H., Guther, A., Fournier, M., Rizzo, S., Waldmann, H.*, et al.* (2014). Fluorogenic probes for live-cell imaging of the cytoskeleton. Nat Methods 11, 731-733.

Matsuoka, Y., Li, X., and Bennett, V. (2000). Adducin: structure, function and regulation. Cell Mol Life Sci 57, 884-895.

Mohandas, N., and Gallagher, P.G. (2008). Red cell membrane: past, present, and future. Blood 112, 3939-3948.

Ochs, S. (1972). Rate of fast axoplasmic transport in mammalian nerve fibres. J Physiol 227, 627-645.

Pathak, D., Sepp, K.J., and Hollenbeck, P.J. (2010). Evidence that myosin activity opposes microtubule-based axonal transport of mitochondria. J Neurosci 30, 8984-8992.

Pereira, A.J., and Maiato, H. (2010). Improved kymography tools and its applications to mitosis. Methods 51, 214-219.

Pielage, J., Bulat, V., Zuchero, J.B., Fetter, R.D., and Davis, G.W. (2011). Hts/Adducin controls synaptic elaboration and elimination. Neuron 69, 1114-1131.

Riedl, J., Crevenna, A.H., Kessenbrock, K., Yu, J.H., Neukirchen, D., Bista, M., Bradke, F., Jenne, D., Holak, T.A., Werb, Z.*, et al.* (2008). Lifeact: a versatile marker to visualize F-actin. Nat Methods 5, 605-607.

Robledo, R.F., Ciciotte, S.L., Gwynn, B., Sahr, K.E., Gilligan, D.M., Mohandas, N., and Peters, L.L. (2008). Targeted deletion of alpha-adducin results in absent beta- and

gamma-adducin, compensated hemolytic anemia, and lethal hydrocephalus in mice. Blood 112, 4298-4307.

Robledo, R.F., Seburn, K.L., Nicholson, A., and Peters, L.L. (2012). Strain-specific hyperkyphosis and megaesophagus in Add1 null mice. Genesis 50, 882-891.

Stepanova, T., Slemmer, J., Hoogenraad, C.C., Lansbergen, G., Dortland, B., De Zeeuw, C.I., Grosveld, F., van Cappellen, G., Akhmanova, A., and Galjart, N. (2003). Visualization of microtubule growth in cultured neurons via the use of EB3-GFP (end-binding protein 3-green fluorescent protein). J Neurosci 23, 2655-2664.

Wortman, J.C., Shrestha, U.M., Barry, D.M., Garcia, M.L., Gross, S.P., and Yu, C.C. (2014). Axonal transport: how high microtubule density can compensate for boundary effects in small-caliber axons. Biophys J 106, 813-823.

Xu, K., Zhong, G., and Zhuang, X. (2013). Actin, spectrin, and associated proteins form a periodic cytoskeletal structure in axons. Science 339, 452-456.

Zhong, G., He, J., Zhou, R., Lorenzo, D., Babcock, H.P., Bennett, V., and Zhuang, X. (2014). Developmental mechanism of the periodic membrane skeleton in axons. Elife 3.

Chapter 2

Regulation of the activity of adducin in the growth cone is required for optimal axon growth and regeneration

Sérgio Carvalho Leite[1,2], Márcia Almeida Liz[1], Marlene Marques Morgado[1], Carla Tavares[1], Fernando Milhazes Mar[1] and Mónica Mendes Sousa[1]

[1]Nerve Regeneration Group, IBMC-Instituto de Biologia Molecular e Celular, Universidade do Porto, 4150-180 Porto, Portugal

[2] ICBAS, Universidade do Porto, 4050-313 Porto, Portugal

Correspondence: msousa@ibmc.up.pt (M.M.S.)

Summary

The conditioning lesion model is a well-established paradigm where gain of regenerative capacity of dorsal column tract axons occurs. Here we show, by comparative proteomic analysis of conditioned and naive DRG neurons, that the α and the γ forms of the actin-capping protein adducin are inactivated after conditioning lesion both in cell bodies and in growth cones of fast-regenerating axons. α-adducin KO DRG neurons, that lack all adducin isoforms, have increased neurite outgrowth capacity *in vitro,* even when grown in the presence of an inhibitory environment, and *in vivo*, after spinal cord injury. These data suggest that adducin is a negative regulator of cytoskeleton dynamics and that its inactivation is an important event such that an enhanced regenerative capacity is acquired by DRG neurons after a priming peripheral injury.

Introduction

The process of axon extension is greatly dependent on the actin cytoskeleton. The growth one, i.e. the structure responsible for the guidance and the growth rate of the axons, is enriched not only in actin, but also in different actin binding proteins (ABPs). The proper concentration and activity of these ABPs is crucial for the correct regulation of the actin cytoskeleton. For that reason, the growth cone is able to 'interpret' the external cues and therefore accelerate or abolish the actin turnover in a specific direction depending on the cue being attractive or inhibitory, respectively (Gomez and Letourneau, 2014; Lowery and Van Vactor, 2009). The increase of actin turnover in a specific growth cone site leads to increased polymerization of microtubules in that region – the axon will consequently turn and extend in that direction. Conversely, an inhibitory cue will abolish the actin turnover and microtubules will not protrude in that direction. Therefore, if the inhibitory cue is present all over the growth cone, a retraction bulb will be generated due to the collapse of actin dynamics, whereas neurons growing freely in culture extend their neurites without a particular direction, but often straight due to the momentum of extension (Dent and Gertler, 2003; Dent et al., 2011; Lowery and Van Vactor, 2009).

ABPs are crucial in the translation of the axon's external environment to an effect in axon growth. In this context and given our previous data showing that in the absence of adducin both actin dynamics and microtubule growth speed in the growth cone are increased, adducin emerged as a possible candidate to be involved in actin cytoskeleton regulation in the growth cone. Adducins are capping proteins that control the addition of actin monomers and consequent extension of actin filaments. Adducin is present in growth cones (Estrada-Bernal et al., 2012), and is regulated by pathways that are well-established in the context of axon regeneration. Calmodulin (Mische et al., 1987), PKC and PKA (Matsuoka et al., 1996; Matsuoka et al., 1998) are inhibitors of adducin's affinity to actin. Of note, PKA is activated by cAMP signaling, which is an important enhancer of axon regeneration (Nikulina et al., 2004). Besides, calmodulin is activated by increased intracellular calcium levels, which also occur (transiently) after injury and are fundamental for axon regeneration to occur (Bradke et al., 2012). In contrast, adducin's affinity to actin is increased by phosphorylation by Rho A signaling (Fukata et al., 1999), which is a key molecule in axon regeneration inhibition (Fujita and Yamashita, 2014). Therefore, adducin is a very interesting candidate molecule to play a role in axon growth – and consequently in axon regeneration.

The conditioning lesion is a very advantageous model to study neuronal intrinsic factors that impact axon extension – both positive and negative regulators. In this

paradigm, the growth capacity of DRG axons through the inhibitory lesion site formed upon a spinal cord injury is increased after a priming lesion to their peripheral branch (Neumann and Woolf, 1999; Silver, 2009). The conditioning effect results on the reprograming of gene expression (Cho et al., 2013; Hoffman, 2010; Kiryu-Seo and Kiyama, 2011; Mar et al., 2014; Puttagunta et al., 2014) that culminates in the expression of regeneration associated transcription factors such as CREB and ATF3, and growth related genes such as actin, GAP-43 and growth associated tubulin isotypes (Fagoe et al., 2014; Mar et al., 2014). Here we explored through a proteomic approach proteins differentially expressed/regulated after conditioning lesion. Our results support the notion that adducin is an important regulator of actin dynamics in the growth cone and that its activity needs to be tightly regulated such that increased axon growth is obtained.

Results

C-terminally phosphorylated adducin is upregulated in conditioned axons

Although the expression profile of DRG neurons in the conditioning lesion model is known to be different from that of non-conditioned neurons, at the post-transcriptional level the information available is limited. Here we compared the L4-L6 DRG proteome from Wistar rats where a sciatic nerve injury was followed 1 week later by a spinal cord injury (thereafter referred to as conditioning lesion - CL group) with that of Wistar rats where only spinal cord injury (SCI) was performed. For that we used a phospho-site antibody array (Kinexus www.kinexus.ca), to identify phosphorylated forms of key signaling proteins. This screen examines 37 phosphorylation sites in 32 proteins with antibodies that recognize specific phosphorylated epitopes (the identity of the proteins that are present in this array is in Table 1). From the 54 epitopes present in the array, 30 were not detected in our samples (ND) and 12 did not reach significant differences amongst samples (NS). The proteins with a fold change CL/SCI lower than 0.75 or higher than 1.25 were selected and are highlighted in grey in table 1. Of note, the AKT/GSK3β pathway (highlighted in light grey), that was found to be differentially regulated following CL, has already been characterized in the context of axon regeneration in a previous study of our group (Liz et al., 2014). In our screening, α- and γ-adducins emerged as key regulatory proteins with increased phosphorylation levels after conditioning lesion.

Table 1: List of proteins assessed using the Kinexus phospho-site antibody array. The ratio of modified protein levels in DRG from animals with conditioning lesion (CL)/spinal cord injury (SCI) is shown; ND: not detected; NS: without significant differences amongst samples.

Full name of the protein (abbreviated protein name) [phosphorylated epitope]	CL/SC
Adducin gamma (ADD3) [S693]	**4,30**
Adducin alpha (ADD1) [S726]	**2,50**
Mitogen & stress-activated protein-serine kinase 1 (MAPK1) [S376]	1,95
Raf1 proto-oncogene-encoded protein-serine kinase (c-Raf) [S259]	1,83
Src proto-oncogene-encoded protein-tyrosine kinase (c-Src) [Y529]	1,57
Glycogen synthase-serine kinase 3 beta (GSK3β) [S9]	1,55
Protein-serine kinase B alpha (AKT) [S473]	1,53
Protein-serine kinase C alpha/beta 2 (PKC α/β2) [T638/T641]	0,73
p85 ribosomal protein-serine S6 kinase alpha (RPS6KB1) [T389]	0,60
Glycogen synthase-serine kinase 3 beta (GSK3β) [Y216] (39)	0,59
Extracellular regulated protein-serine kinase 2 (p42 MAP kinase) (ERK2) [T185+Y187]	0,56
Glycogen synthase-serine kinase 3 beta (GSK3β) [Y216]	0,52
MAPK/ERK protein-serine kinase 1/2 (MKK1/2) [S218+S222]	NS
Glycogen synthase-serine kinase 3 alpha (GSK3β) [Y279]	NS
Jun N-terminus protein-serine kinase (stress-activated protein kinase (SAPK)) [T183+Y185]	NS
Extracellular regulated protein-serine kinase 1 (p44 MAP kinase) (ERK1) [T202+Y204]	NS
Signal transducer and activator of transcription 1 (STAT1) [Y701]	NS
Glycogen synthase-serine kinase 3 alpha (GSK3α) [S21]	NS
Retinoblastoma-associated protein 1 (RB1) [S807+S811]	NS
Jun N-terminus protein-serine kinase (stress-activated protein kinase (SAPK)) [T183+Y185]	NS
Raf1 proto-oncogene-encoded protein-serine kinase (c-Raf) [S259]	NS
Protein-serine kinase C alpha (PKCα) [S657]	NS
Mitogen-activated protein-serine kinase p38 alpha [T180+Y182]	NS
cAMP response element binding protein 1 (CREB1) [S133]	NS
B23 (nucleophosmin, numatrin, nucleolar protein NO38) [S4]	ND
Cyclin-dependent protein-serine kinase 1/2 (CDK1/2) [Y15]	ND
Cyclin-dependent protein-serine kinase 1/2 (CDK1/2) [Y15]	ND
Double-stranded RNA-dependent protein-serine kinase (PKR) [T451]	ND
Double-stranded RNA-dependent protein-serine kinase (PKR) [T451]	ND
Glycogen synthase-serine kinase 3 alpha (GSK3α) [Y279]	ND
Jun N-terminus protein-serine kinase (stress-activated protein kinase (SAPK)) [T183+Y185]	ND
Jun N-terminus protein-serine kinase (stress-activated protein kinase (SAPK)) [T183+Y185]	ND
Jun proto-oncogene-encoded AP1 transcription factor (c-jun) [S73]	ND
Jun proto-oncogene-encoded AP1 transcription factor (c-jun) [S73]	ND
Jun proto-oncogene-encoded AP1 transcription factor (c-jun) [S73]	ND
Jun proto-oncogene-encoded AP1 transcription factor (c-jun) [S73]	ND
MAPK/ERK protein-serine kinase 3/6 (MKK3/6) [S189/S207]	ND
Mitogen & stress-activated protein-serine kinase 1 (MAPK1) [S376]	ND
Mitogen-activated protein-serine kinase p38 alpha [T180+Y182]	ND
N-methyl-D-aspartate (NMDA) glutamate receptor 1 subunit zeta (GRIN1) [S896]	ND
p70 ribosomal protein-serine S6 kinase alpha (PS6K) [T389]	ND
Protein-serine kinase B alpha (PKBα) [T308]	ND

Protein-serine kinase C delta (PKCδ) [T507]	ND
Protein-serine kinase C epsilon (PKCε) [S729]	ND
Retinoblastoma-associated protein 1 (RP1) [S780]	ND
Ribosomal S6 protein-serine kinase 1/3 (RSK1/3) [T359+S363/T356+S360]	ND
Ribosomal S6 protein-serine kinase 1/3 (RSK1/3) [T359+S363/T356+S360]	ND
Signal transducer and activator of transcription 1 (STAT1) [Y701]	ND
Signal transducer and activator of transcription 3 (STAT3) [S727]	ND
Signal transducer and activator of transcription 5A (STAT5A) [Y694]	ND
SMA- and mothers against decapentaplegic homologs 1/5/9 [S463+S465/S463+S465/S465+S467]	ND
Src proto-oncogene-encoded protein-tyrosine kinase (c-Src) [Y418]	ND
Src proto-oncogene-encoded protein-tyrosine kinase (c-Src) [Y418]	ND
Src proto-oncogene-encoded protein-tyrosine kinase (c-Src) [Y529]	ND

Adducin participates in the regulation of the spectrin-actin cytoskeleton by enhancing the interaction of spectrin with actin (Li et al., 1998). In the proteomic analysis, both phosphorylated α- and γ-adducin (S726 and S673, respectively) were increased in the DRG of conditioned animals. Validation of the array data by western blot in the spinal cord lesion site, where the regenerating growth cones are present, confirmed the augmented phosphorylation of both α (110kDa) and γ adducin (80kDa), 2.5 and 4.3 fold, respectively in conditioned animals (figure 1). Interestingly, we did not detect β-adducin (100kDa) in spinal cord samples as although this isoform is known to be nervous system (brain)-restricted it is not enriched in the spinal cord (Chapter 1, Figure 1).

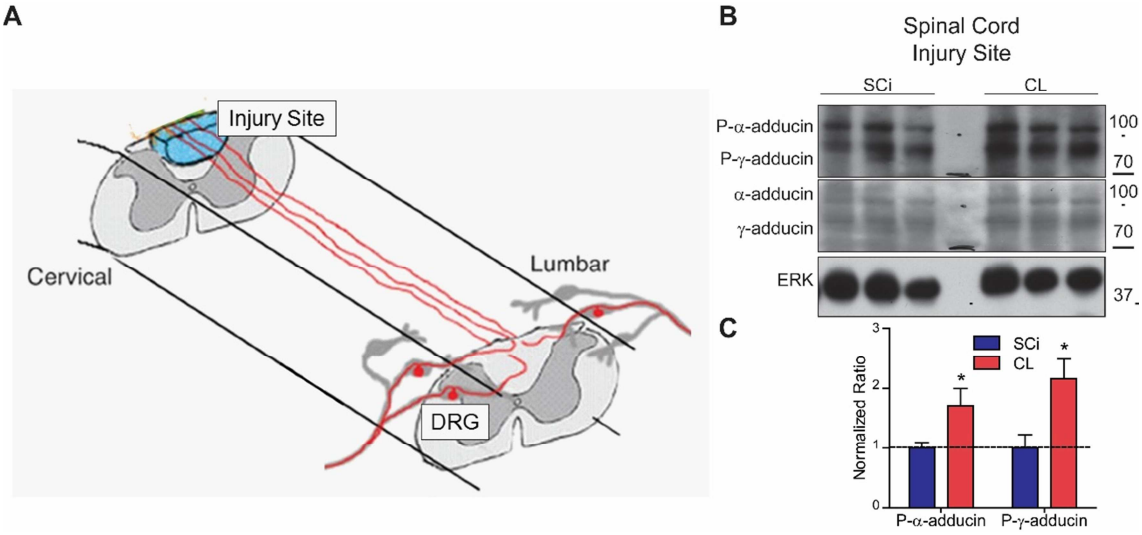

Figure 1 – Phosphorylated α- and γ-adducin are increased upon conditioning injury. (A) Schematic representation of the spinal cord. The injury site is highlighted in blue; the central (dorsal colum tract) and peripheral DRG axons are highlighted in red. Spinal cord injury site samples correspond to the region 2.5mm caudal and 2.5mm rostral from the lesion site. Adapted from (Gilligan et al., 1999). (B) Representative western blots of phospho-adducin, total adducin and total ERK1/2 in spinal cord injury

samples from rats with either SCI or CL. (C) Quantification of (B). p-value: *<0.05. (A) Adapted from (Alto et al., 2009).

To further confirm the increase of adducin in regenerating growth cones immunofluorescence of phosphorylated and total adducin was performed in cultures of DRG neurons collected from either naïve animals or conditioned animals (i.e., where a sciatic nerve lesion was performed 1 week before establishing the culture) (figure 2A and 2B). The validation by ICC confirmed that adducin was indeed modulated in the conditioning lesion model, being increased in the growth cones of neurons with enhanced growth capacity.

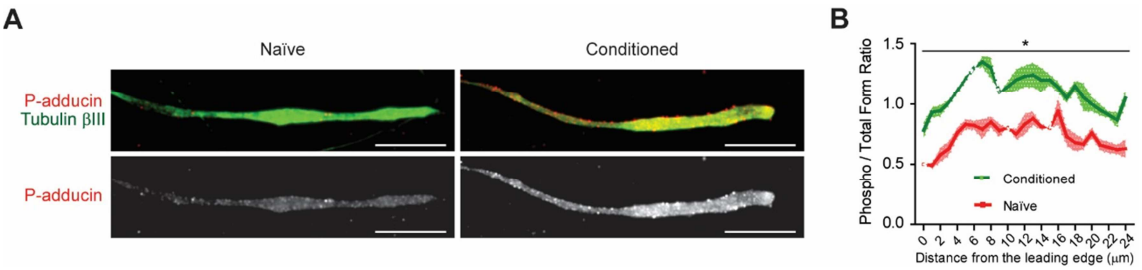

Figure 2 – Phosphorylated adducin is increased in fast-growing axons. (A) Immunofluorescence of the phosphorylated form of adducin (red) and βIII-tubulin (green) in naïve and conditioned rat DRG neurons. (B) Quantification of the ratio of phosphorylated/total adducin in relation to the distance from the leading edge of the growth cone. Scale bar: 10μm. p-value *<0.05

Neurite extension and axon regeneration are increased in α-adducin KO neurons

Adducin is an ABP that binds F-actin in the barbed ends and also interacts with spectrin-actin junctions, increasing their stability (Matsuoka et al., 1998). For this interaction, Serine phosphorylation in the C-terminus MARCKS domain plays a fundamental role (Matsuoka et al., 1998). Interestingly, increased phosphorylation of adducin leads to loss of affinity towards actin and spectrin, allowing the incorporation of new monomers into the F-actin barbed ends and also promoting the disassembly of the spectrin-actin junctions (Matsuoka et al., 1996; Matsuoka et al., 1998). As our data shows that adducin inactivation is promoted in the conditioned neurons – that grow more and with increased speed (Martin et al., 2013), we hypothesized that upon injury, the absence of adducin might mimic the conditioning effect. Of note, as described in the previous chapter of this thesis, α-adducin KO neurons have increased actin retrograde flow and microtubule growth speed, which are parameters positively related with the neuritogenic process and axon growth (Bradke and Dotti, 1999; Flynn et al., 2012). For that reason we analyzed neurite outgrowth in α-adducin KO neurons. α-

adducin KO hippocampal neurons (DIV3) had an increased growth capacity (figure 3B). In DRG neurons of α-adducin KO mice neurite outgrowth was also increased (figure 3A-B). As adducin was found to be differentially activated in a screening where DRG axons need to regenerate in the presence of inhibitory molecules, we assessed whether the absence of adducin would mimic the enhanced growth capacity of conditioned DRG neurons. For that, we plated WT and α-adducin KO DRG neurons in the presence of inhibitory molecules such as the myelin protein fraction and aggrecan, a chondroitin sulfate proteoglycan (CSPG) found in the glial scar (Galtrey and Fawcett, 2007; Siebert et al., 2014). Interestingly, α-adducin KO neurons presented enhanced growth ability under both inhibitory conditions (figure 3A-C). This data suggest a decreased sensitivity of α-adducin KO neurons to the inhibitory molecules of the glial scar.

Does the absence of α-adducin increase axon regeneration *in vivo*? To test this possibility, regeneration of dorsal column tract axons was assessed in WT and α-adducin KO mice following spinal cord injury (dorsal hemisection). The analysis of regeneration of the dorsal column fibers of WT and α-adducin KO mice revealed that the absence of adducin results in a lower degree of inhibition of the regenerating axons when entering the glial scar (figure 3D-E), supporting our *in vitro* data. Although the maximal axon extension was not significantly different, only 4 out of 10 WT animals extended axons within the glial scar whereas 7 out 8 of α-adducin KO animals were able to extend axons within the glial scar. Moreover, the α-adducin KO mice had an increased number of axons extending into the glial scar (WT: 1 axon/animal; α-adducin KO mice: 6 axons/animal).

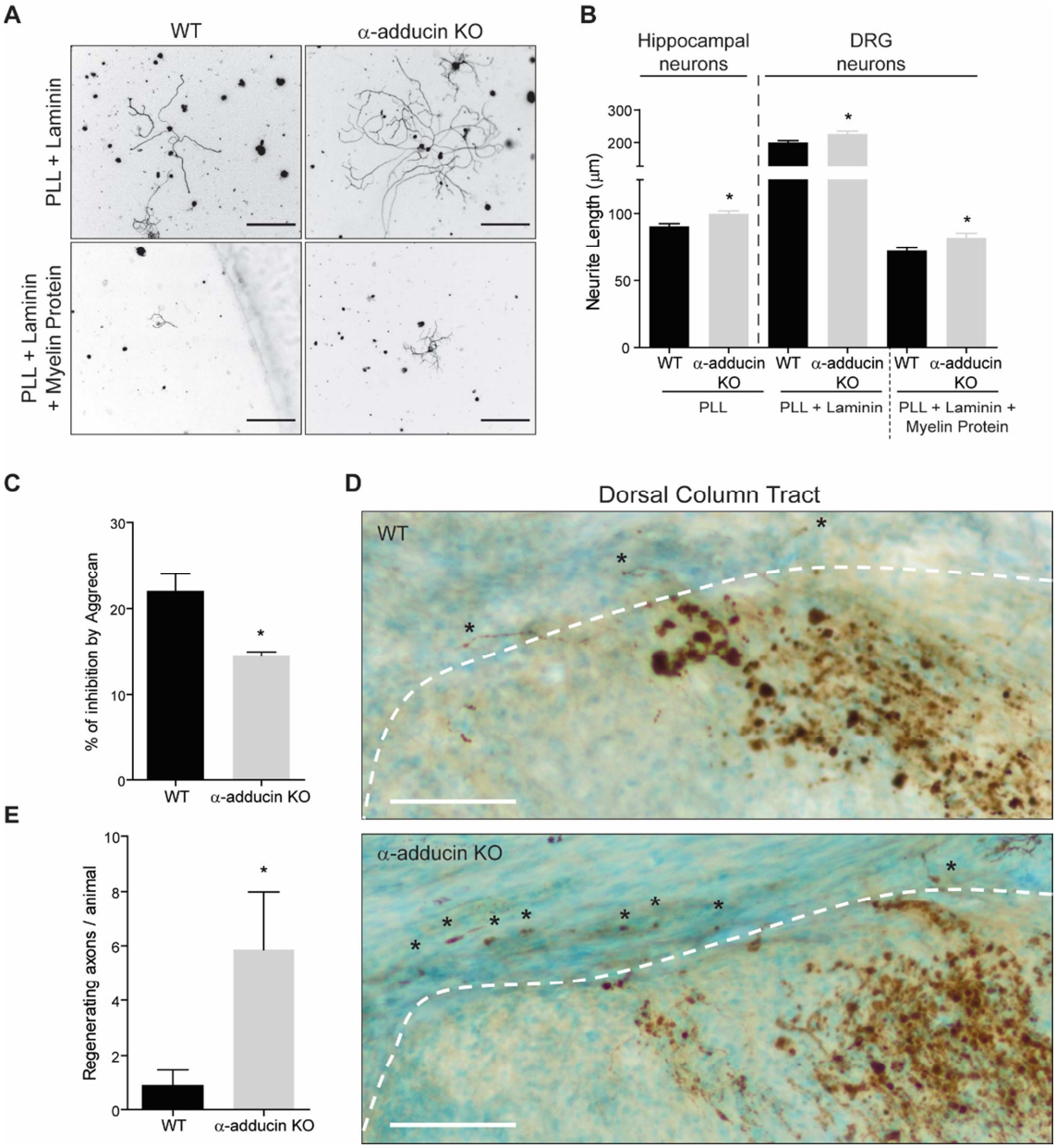

Figure 3 – The absence of adducin decreases neurite outgrowth *in vitro* and axon regeneration *in vivo*. (A) Representative photomicrographs of WT and α-adducin KO DRG neurons grown either in a permissive substrate (PLL + laminin) or in an inhibitory substrate (PLL + laminin + myelin protein). (B) Neurite length of WT and α-adducin KO hippocampal neurons grown in PLL and DRG neurons grown in either PLL + laminin or PLL + laminin + myelin protein. (C) Percentage of inhibition of the length of longest neurite in WT and α-adducin KO DRG neurons grown in the presence of the CSPG aggrecan. (D) Anti-cholera toxin B subunit (CT-B) n immunohistochemistry (brown) of representative longitudinal spinal cord sections of WT and α-adducin KO mice with dorsal column hemisection and CT-B injection in the sciatic nerve. Counterstaining was done with hematoxilin (blue). The dashed white line represents the boarder of the glial scar. Asterisks highlight regenerating axons. (E) Total number of regenerating axons present in the glial scar of WT and α-adducin KO mice. Scale bar: 250 μm for DRG neuron cultures (A) and 100μm for spinal cord sections (D). *p<0.05

Discussion

The conditioning lesion is a very interesting model to study the neuronal intrinsic factors that impact axonal extension – both positive and negative regulators. Our analysis to understand which proteins, namely which ABPs, are differently regulated in conditioned neurons revealed that adducin has increased S726 phosphorylation levels after a priming injury i.e., that it's capping activity towards F-actin is decreased. Our data also revealed that this increased phosphorylation occurs not only in the cell body but also in the spinal cord lesion site, where regenerating growth cones are present. This suggests that accumulation of phosphorylated inactive adducin species in growth cones is part of the post-translational events required for enhancement of axon (re)growth. In this context, we hypothesized that adducin depletion in α-adducin KO mice neurons could mimic the decreased adducin activity found in conditioned neurons.

In α-adducin KO mice, as shown in Chapter 1, all adducin forms are almost completely depleted, due to the requirement of α-adducin to generate functional adducin heterodimers/heterotetramers. Therefore we proceeded to the analysis of the consequences of adducin's absence in neurons. Dynamic analysis of the growth cones of WT and α-adducin KO neurons *in vitro* by live cell imaging demonstrated increased cytoskeleton dynamics – increased actin retrograde flow, due to the putative increase in actin polymerization; and increased microtubule growth speed (Chapter 1). Given the increased cytoskeleton dynamics in α-adducin KO neurons, we decided to assess whether this would be translated in increased growth capacity. Indeed, neurite outgrowth assays revealed an increased growth ability, both in hippocampal and DRG neurons. Interestingly, a similar phenotype was observed when tropomodulins, the capping proteins of the growth cone pointed ends, were abolished (Fath et al., 2011). Besides the increased outgrowth under permissive conditions, we also assessed if adducin's absence would be beneficial under non-permissive conditions *in vitro*. Using the myelin protein fraction and the chondroitin sulphate proteoglycan aggrecan as inhibitory substrates, we found that α-adducin KO neurons were less inhibited by these molecules. Both myelin protein and CSPGs exert their inhibitory effect through activation of RhoA signaling (Fujita and Yamashita, 2014), which interestingly is a positive regulator of adducin's capping activity (Kimura et al., 1998). Given our *in vitro* data and the fact that α and γ adducin were inhibited in conditioned regenerating axons, we assessed axon regeneration of α-adducin KO mice following spinal cord injury. Our analysis of the dorsal column tract (the tract used in our initial screening)

showed that the loss of adducin results in increased regeneration capacity, with α-adducin KO mice presenting an increased number of axons regenerating into the inhibitory glial scar. No effect was however observed in the length of the regenerating axons when comparing genotypes. In this respect, one should note that the straight α-adducin knockout model is not a clean model for the assessment of the importance of adducin in axon regeneration, given the primary defects of α-adducin KO axons illustrated in Chapter 1 that include axonal transport impairment, axonopathy, and axon degeneration. It is therefore possible that these primary impairments mask the beneficial effect of adducin inactivation in axon outgrowth and regeneration. In order to surpass the limitations of this animal model, one possibility would be to have a model of inducible tissue specific depletion of adducin to allow a normal nervous system development and maturation and the subsequent depletion of adducin immediately prior to regeneration studies.

Other possible alternatives to further consolidate the importance of the regulation of adducin in the process of axon regeneration include modulation of PKC (that inactivates adducin) and overexpression of PKC phospho-site adducin mutants. The PKC family is the better characterized kinase that regulates adducin's function (Matsuoka et al., 1998, 2000). However modulating PKC activity is a complex biological event in one hand and on the other PKC has numerous downstream targets (Larsson, 2006). PKC is a large family of 16 kinases with specific effects – even contradictory – in neuritogenesis and neurite extension (Larsson, 2006; Teng and Tang, 2006). The specific PKC isoform that phosphorylates adducin is not yet known – the literature suggests that PKCδ is the adducin-specific isoform but most of the supporting data is based in the usage of rottlerin, a non-specific PKCδ inhibitor (Soltoff, 2007). One should also consider that the role of *phorbol-12-myristate-13-acetate* (PMA), or other phorbol esters, as stimulators of PKC activation in assays of axon growth have contradictory results in the literature. In some experiments these compounds are suggested to have a pro-neuritogenic effect (Brodie et al., 1999; Mehta et al., 1993) whereas in other approaches the effect observed was the opposite (Sivasankaran et al., 2004; Xu et al., 2011). Overexpression of adducin mutants that interfere with its activity, namely S726A (phospho-resistant) and S726D (phospho-mimetic), could provide further insight on the importance of the regulation of the activity of this protein during axon growth and regeneration. However, it is also possible that confounding effects are observed as a result of adducin overexpression. To start with, which would be the best adducin form to overexpress? Adducins are organized as heterotetramers, composed by two heterodimers (Matsuoka et al., 2000). Overexpression of α-adducin

could lead to dysregulated levels of hetero and α/α-homodimers that might impact the different adducin activities including the capping activity. There are reports supporting that β-adducin overexpression leads to increased outgrowth ability of cortical neurons (Farghaian et al., 2011), and that γ-adducin overexpression in COS7 fibroblasts increases neuritogenesis (Lou et al., 2013). One would expect that increased adducin levels generate a less dynamic actin turnover in the growth cone, and consequently a decreased ability to grow, but this should be measured with the appropriate assays.

Conclusion

How different ABP affect neuritogenesis and neurite extension is still an open field in neuroscience. Several studies have established some ABPs as promoters of neurite extension and regeneration, whereas others act in a negative fashion, such that their inactivity is beneficial to axon regeneration. This work suggests that adducin regulation is part of a major regulatory system that enhances axon regeneration, at least following a priming (conditioning) lesion. This is a step towards to better understand axon regeneration in the CNS, and to develop more effective and elegant strategies to promote it.

Material and methods

Animals

Mice were handled according to European Union and National rules, maintained under a 12-h light/dark cycle and fed with regular rodent's chow and tap water *ad libitum*. α-adducin KO mice (kindly provided by Dr Luanne Peters, Jackson Laboratories) were generated and genotyped as described (Robledo et al., 2008). Analyses were performed using WT and α-adducin KO littermates obtained from heterozygous progenitors.

Sciatic nerve and spinal cord lesions

Sciatic nerve transection: 8-10 weeks old Wistar rats were used. Animals were anesthetized with ketamine (75mg/Kg)/medetomidine (0.6mg/Kg). The skin was shaved and the sciatic nerve was exposed at the mid-tight. Transections were

performed using a scissor. Animals received analgesia (butorphanol) twice a day, for 48 hours.

Spinal cord injury (SCI): 10-12 weeks old Wistar rats, or 8 weeks old mice, were used. Animals were anesthetized with ketamine/medetomidine, as above. The skin was shaved and the spinal cord was exposed at the thoracic level. Laminectomy was performed at the T6-T8 level (in rats), or at the T7-T9 level in mice. Dorsal hemisection was donewith a microscissor (in rats) or using a micro-scalpel (in mice) for proteomic analysis and for dorsal column tract analysis. Animals received analgesia (butorphanol) twice a day, for 72 hours and fluid therapy once a day (Duphalyte), for 72 hours. Animals also required manual voiding of the bladder twice a day for the rest of the experimental period. Wet food was placed in the cage floor and water with antibiotic (0.016% Baytril) was supplied in long nipple bottles.

Conditioning lesion: sciatic nerve injury was performed as described above and one week later dorsal hemisection was conducted, also as described above.

The recovery period after spinal cord injury was: i) 1 week for validation of phospho-site broad signaling pathway screen, ii) 4 weeks for dorsal column tract analysis and iii) 5 weeks for the analysis of raphespinal serotonergic axon regeneration.

Phospho-site broad signaling pathway screen

DRGs (L4-L6) from a pool of six rats (8 to 10 weeks-old) subjected to either SCI or conditioning lesion were sacrificed one week after SCI. DRG were homogenized in lysis buffer (20mM 4-morpholinepropanesulfonic acid (MOPS), 2mM ethylene glycol tetraacetic acid (EGTA), 5mM ethylenediaminetetraacetic acid (EDTA), 30mM sodium fluoride, 60mM β-glycerophosphate, 20mM sodium pyrophosphate, 1mM sodium orthovanadate, 1% Triton X-100, 1% dithiothreitol (DTT), 1mM phenylmethylsulfonyl fluoride (PMSF) and protease inhibitor cocktail (GE Healthcare, Carnaxide, Portugal)). Protein extracts (500µg) were analyzed using the Kinexus phospho-site broad signaling pathway screen version 1.3 (KPSS-1.3, Kinexus Bioinformatics Corp, Vancouver, Canada). This screen examines 37 phosphorylation sites in 32 proteins with antibodies that recognize specific phosphorylated epitopes. The intensities of signals for target protein bands on the Kinetworks immunoblots were quantified as described (Pelech et al., 2003). Proteins with a fold change CL/SCI lower than 0.75 or higher than 1.25 were selected for further validation by Western blot.

Western blotting

For western blotting, the following primary antibodies were used: rabbit anti-phosphorylated α (S726), β (S713) and γ (S693) adducin, 1:1000 (Santa Cruz, SC-16736R); rabbit anti-adducin, 1:1000 (Abcam, ab51130); and mouse anti-β-actin, 1:5000 (Sigma, A5441). The secondary antibodies were: donkey anti-mouse or donkey anti-rabbit conjugated with HRP, 1:5000 (Jackson). Samples were homogenized in PBS with 0.3%Triton-X100 (Sigma), 1mM sodium orthovanadate (Sigma) and protease inhibitor cocktail (Roche). For the western blot of the spinal cord injury site (encompassing the region 2.5mm caudal and 2.5mm rostral from the lesion site), 10-15% SDS-PAGE gels with 50 µg of sample were run and transferred for 2 hours in a semi-dry system to a nitrocellulose membrane. Membranes were washed in TBS with 0.1% of Tween-20, blocked in 5% non-fat dried milk (Sigma) in TBS for 1 hour at room temperature, incubated with primary antibody (in either 5% BSA or 5% non-fat dried milk, in TBS) 1 hour at room temperature or overnight at 4ºC. Membranes were then washed and incubated with secondary antibody in 5% non-fat dried milk in TBS for 1 hour at room temperature and then incubated 5 minutes at room temperature with Pierce ECL (Pierce) for development. Chemiluminescence was analysed by either exposure to Amersham Hyperfilm ECL (GE Healthcare) or detection in ChemiDoc (Bio-rad). The quantification of the western blots was performed by normalizing the ratios of phosphorylated adducin/total adducin relatively to those obtained in the spinal cord injury samples.

DRG neuron cultures

DRG neuron cultures were performed as detailed (Miranda et al., 2011). Briefly, WT and α-adducin KO mice at either P7-9 (for neurite outgrowth experiments) or 8 weeks-old Wistar rats either uninjured (naïve) or with sciatic nerve injury (for the analysis of phospho/total adducin ratio in growth cones) were sacrificed and DRG were collected (in the case of rats, only L4-6 DRG) and digested for 90 minutes with 0.125% collagenase IV-S (C1189, Sigma). DRG were then triturated and passed through a 15% BSA gradient. Cells were counted and plated at a density of 40 cells/mm2 in previously treated 24-well plate coverslips, coated with 20µg/mL poly-L-lysine (P2636, Sigma) and 5µg/mL laminin (L2020, Sigma). Neurons were grown in DMEM:F12 (D8437, Sigma) supplemented with 1x B27 (Gibco), 1% penicillin/streptomycin (Gibco), 2mM L-glutamine (Gibco) and 50ng/mL NGF (01-125, Millipore). For the assessment of the ratio of phosphorylated/total adducin, Wistar rat L4-6 DRG collected from either

naïve animals or animals with sciatic nerve injury were grown for 12 hours and then fixed in 4% PFA for 20 minutes. For immunofluorescence DRG neurons were stained with either anti phospho-adducin S726 (SC-16736R, Santa Cruz) or anti total-adducin (Ab51130, Abcam) and anti βIII-tubulin (G7121, Promega) and then incubated with secondary antibodies. Image acquisition was performed with equal exposure time for all the conditions. Measurements were done by drawing a 0.5µm wide and 25µm long line from the tip of the growth cone to the cell body. The ratios were calculated using Fiji software and plotted with a 1µm resolution. At least 24 growth cones were measured in each condition.

Hippocampal neuron cultures

Hippocampal neuron cultures were performed following the general protocol detailed in the Kaech and Banker protocol (2007). Briefly, pregnant α-adducin heterozygous or NMRI WT mice at E16.5 were sacrificed and pups were individually dissected and genotyped. The hippocampus of each pup was digested 15 minutes in 0.06% porcine tryspin solution (T4799, Sigma), triturated and plated at a density of 125 cells/mm^2 in 24 well plates containing glass cover slips previously treated with 20µg/mL poly-L-lysine (P2636, Sigma). Neurons were plated in Neurobasal (21103-049, Invitrogen) supplemented with 1x B27 (Gibco), 1% penicillin/streptomycin (Gibco) and 2mM L-glutamine (Gibco).

Myelin and Aggrecan inhibition

Myelin protein fraction was obtained from P3-4 mice. Briefly, crude myelin extracts (Mar et al., 2015) were incubated with 3.6% CHAPS in PBS for 1h at 4ºC. After centrifugation, the supernatant was dialyzed for 16h with 2 buffer exchanges and protein levels were determined using DC Protein Assay (Bio-rad). DRG neurons (from P5 mice) were plated either in PLL (20µg/mL) / laminin (1µg/mL) or PLL (20µg/mL) / laminin (1µg/mL) / myelin protein fraction (4.3µg/cm^2). Eighteen hours later, cells were fixed, immunofluorescence for β-III tubulin was performed and the length of the longest neurite was determined using NeuronJ plug-in for ImageJ. For experiments using aggrecan, DRG neurons (from P5 mice) were plated in either PLL (20µg/mL) / laminin (5µg/mL) or PLL (20µg/mL) / laminin (5µg/mL) / aggrecan (25µg/mL) (Sigma). DRG neurons were grown for 12h fixed with 4% PFA for 20 minutes and, immunofluorescence for β-III tubulin was performed. The length of the longest neurite

was determined using NeuronJ plug-in for ImageJ. Inhibition of neurite outgrowth was determined based on the following formula:

$$\%\ of\ inhibition = (1 - \frac{Control\ Length - Aggrecan\ Length}{Control\ Length})) * 100$$

Where length= average length of the longest neurite.

Analysis of regeneration of dorsal column fibers

Eight weeks-old WT and α-adducin KO mice were subjected to spinal cord dorsal hemisection and allowed to recover for 4 weeks. Four days prior euthanasia, 2μL of 1% cholera toxin B (CT-B) (List Biologicals, Campbell, CA, USA) was injected in both sciatic nerves. Animals were perfused with formalin, tissues were cryopreserved in sucrose and sectioned at 50μm. Consecutive spinal cord sagittal sections were collected for free floating immunohistochemistry with anti-CT-B (1:30000; List Biologicals, #703). Image analysis was done with Photoshop CS5. Dorsal column fibers were quantified by counting the total number of axons within the glial scar, in the CT-B positive sections (2-4 sections per animal). The length of the longest CT-B labeled axon found rostrally to the injury site, was measured using as the origin a vertical line placed at the rostral end of the dorsal column tract (that is, where CT-B labeling accumulates). Lesion margins were evident under phase-contrast optics as a distinct change in the appearance of the structure of the white and grey matter was observed.

Acknowledgements

This work was funded by the International Foundation for Research in Paraplegia (IRP). Leite SC was supported by Fundação para a Ciência e Tecnologia (FCT) (SFRH/BD/72240/2010). We thank the excellent technical support of the IBMC Animal Facility. The authors have no conflicts of interest to declare.

References

Alto, L.T., Havton, L.A., Conner, J.M., Hollis, E.R., 2nd, Blesch, A., and Tuszynski, M.H. (2009). Chemotropic guidance facilitates axonal regeneration and synapse formation after spinal cord injury. Nat Neurosci 12, 1106-1113.

Bradke, F., and Dotti, C.G. (1999). The role of local actin instability in axon formation. Science 283, 1931-1934.

Bradke, F., Fawcett, J.W., and Spira, M.E. (2012). Assembly of a new growth cone after axotomy: the precursor to axon regeneration. Nat Rev Neurosci 13, 183-193.

Brodie, C., Bogi, K., Acs, P., Lazarovici, P., Petrovics, G., Anderson, W.B., and Blumberg, P.M. (1999). Protein kinase C-epsilon plays a role in neurite outgrowth in response to epidermal growth factor and nerve growth factor in PC12 cells. Cell Growth Differ 10, 183-191.

Cho, Y., Sloutsky, R., Naegle, K.M., and Cavalli, V. (2013). Injury-induced HDAC5 nuclear export is essential for axon regeneration. Cell 155, 894-908.

Dent, E.W., and Gertler, F.B. (2003). Cytoskeletal dynamics and transport in growth cone motility and axon guidance. Neuron 40, 209-227.

Dent, E.W., Gupton, S.L., and Gertler, F.B. (2011). The growth cone cytoskeleton in axon outgrowth and guidance. Cold Spring Harb Perspect Biol 3.

Estrada-Bernal, A., Sanford, S.D., Sosa, L.J., Simon, G.C., Hansen, K.C., and Pfenninger, K.H. (2012). Functional complexity of the axonal growth cone: a proteomic analysis. PLoS One 7, e31858.

Fagoe, N.D., van Heest, J., and Verhaagen, J. (2014). Spinal cord injury and the neuron-intrinsic regeneration-associated gene program. Neuromolecular Med 16, 799-813.

Farghaian, H., Turnley, A.M., Sutherland, C., and Cole, A.R. (2011). Bioinformatic prediction and confirmation of beta-adducin as a novel substrate of glycogen synthase kinase 3. J Biol Chem 286, 25274-25283.

Fath, T., Fischer, R.S., Dehmelt, L., Halpain, S., and Fowler, V.M. (2011). Tropomodulins are negative regulators of neurite outgrowth. Eur J Cell Biol 90, 291-300.

Flynn, K.C., Hellal, F., Neukirchen, D., Jacob, S., Tahirovic, S., Dupraz, S., Stern, S., Garvalov, B.K., Gurniak, C., Shaw, A.E.*, et al.* (2012). ADF/cofilin-mediated actin

retrograde flow directs neurite formation in the developing brain. Neuron 76, 1091-1107.

Fujita, Y., and Yamashita, T. (2014). Axon growth inhibition by RhoA/ROCK in the central nervous system. Front Neurosci 8, 338.

Fukata, Y., Oshiro, N., Kinoshita, N., Kawano, Y., Matsuoka, Y., Bennett, V., Matsuura, Y., and Kaibuchi, K. (1999). Phosphorylation of adducin by Rho-kinase plays a crucial role in cell motility. J Cell Biol 145, 347-361.

Galtrey, C.M., and Fawcett, J.W. (2007). The role of chondroitin sulfate proteoglycans in regeneration and plasticity in the central nervous system. Brain Res Rev 54, 1-18.

Gilligan, D.M., Lozovatsky, L., Gwynn, B., Brugnara, C., Mohandas, N., and Peters, L.L. (1999). Targeted disruption of the beta adducin gene (Add2) causes red blood cell spherocytosis in mice. Proc Natl Acad Sci U S A 96, 10717-10722.

Gomez, T.M., and Letourneau, P.C. (2014). Actin dynamics in growth cone motility and navigation. J Neurochem 129, 221-234.

Hoffman, P.N. (2010). A conditioning lesion induces changes in gene expression and axonal transport that enhance regeneration by increasing the intrinsic growth state of axons. Exp Neurol 223, 11-18.

Kimura, K., Fukata, Y., Matsuoka, Y., Bennett, V., Matsuura, Y., Okawa, K., Iwamatsu, A., and Kaibuchi, K. (1998). Regulation of the association of adducin with actin filaments by Rho-associated kinase (Rho-kinase) and myosin phosphatase. J Biol Chem 273, 5542-5548.

Kiryu-Seo, S., and Kiyama, H. (2011). The nuclear events guiding successful nerve regeneration. Front Mol Neurosci 4, 53.

Larsson, C. (2006). Protein kinase C and the regulation of the actin cytoskeleton. Cell Signal 18, 276-284.

Li, X., Matsuoka, Y., and Bennett, V. (1998). Adducin preferentially recruits spectrin to the fast growing ends of actin filaments in a complex requiring the MARCKS-related domain and a newly defined oligomerization domain. J Biol Chem 273, 19329-19338.

Liz, M.A., Mar, F.M., Santos, T.E., Pimentel, H.I., Marques, A.M., Morgado, M.M., Vieira, S., Sousa, V.F., Pemble, H., Wittmann, T.*, et al.* (2014). Neuronal deletion of GSK3beta increases microtubule speed in the growth cone and enhances axon regeneration via CRMP-2 and independently of MAP1B and CLASP2. BMC Biol 12, 47.

Lou, H., Park, J.J., Phillips, A., and Loh, Y.P. (2013). gamma-Adducin promotes process outgrowth and secretory protein exit from the Golgi apparatus. J Mol Neurosci 49, 1-10.

Lowery, L.A., and Van Vactor, D. (2009). The trip of the tip: understanding the growth cone machinery. Nat Rev Mol Cell Biol 10, 332-343.

Mar, F.M., Bonni, A., and Sousa, M.M. (2014). Cell intrinsic control of axon regeneration. EMBO Rep 15, 254-263.

Mar, F.M., da Silva, T.F., Morgado, M.M., Rodrigues, L.G., Rodrigues, D., Pereira, M.I., Marques, A., Sousa, V.F., Coentro, J., Sa-Miranda, C.*, et al.* (2015). Myelin Lipids Inhibit Axon Regeneration Following Spinal Cord Injury: a Novel Perspective for Therapy. Mol Neurobiol.

Martin, M., Benzina, O., Szabo, V., Vegh, A.G., Lucas, O., Cloitre, T., Scamps, F., and Gergely, C. (2013). Morphology and nanomechanics of sensory neurons growth cones following peripheral nerve injury. PLoS One 8, e56286.

Matsuoka, Y., Hughes, C.A., and Bennett, V. (1996). Adducin regulation. Definition of the calmodulin-binding domain and sites of phosphorylation by protein kinases A and C. J Biol Chem 271, 25157-25166.

Matsuoka, Y., Li, X., and Bennett, V. (1998). Adducin is an in vivo substrate for protein kinase C: phosphorylation in the MARCKS-related domain inhibits activity in promoting spectrin-actin complexes and occurs in many cells, including dendritic spines of neurons. J Cell Biol 142, 485-497.

Matsuoka, Y., Li, X., and Bennett, V. (2000). Adducin: structure, function and regulation. Cell Mol Life Sci 57, 884-895.

Mehta, S., Hsu, L., Jeng, A.Y., and Chen, K.Y. (1993). Neurite outgrowth and protein phosphorylation in chick embryonic sensory ganglia induced by a brief exposure to 12-O-tetradecanoylphorbol 13-acetate. J Neurochem 60, 972-981.

Miranda, C.O., Teixeira, C.A., Liz, M.A., Sousa, V.F., Franquinho, F., Forte, G., Di Nardo, P., Pinto-Do, O.P., and Sousa, M.M. (2011). Systemic delivery of bone marrow-derived mesenchymal stromal cells diminishes neuropathology in a mouse model of Krabbe's disease. Stem Cells 29, 1738-1751.

Mische, S.M., Mooseker, M.S., and Morrow, J.S. (1987). Erythrocyte adducin: a calmodulin-regulated actin-bundling protein that stimulates spectrin-actin binding. J Cell Biol 105, 2837-2845.

Neumann, S., and Woolf, C.J. (1999). Regeneration of dorsal column fibers into and beyond the lesion site following adult spinal cord injury. Neuron 23, 83-91.

Nikulina, E., Tidwell, J.L., Dai, H.N., Bregman, B.S., and Filbin, M.T. (2004). The phosphodiesterase inhibitor rolipram delivered after a spinal cord lesion promotes axonal regeneration and functional recovery. Proc Natl Acad Sci U S A 101, 8786-8790.

Pelech, S., Sutter, C., and Zhang, H. (2003). Kinetworks protein kinase multiblot analysis. Methods Mol Biol 218, 99-111.

Puttagunta, R., Tedeschi, A., Soria, M.G., Hervera, A., Lindner, R., Rathore, K.I., Gaub, P., Joshi, Y., Nguyen, T., Schmandke, A.*, et al.* (2014). PCAF-dependent epigenetic changes promote axonal regeneration in the central nervous system. Nat Commun 5, 3527.

Robledo, R.F., Ciciotte, S.L., Gwynn, B., Sahr, K.E., Gilligan, D.M., Mohandas, N., and Peters, L.L. (2008). Targeted deletion of alpha-adducin results in absent beta- and gamma-adducin, compensated hemolytic anemia, and lethal hydrocephalus in mice. Blood 112, 4298-4307.

Siebert, J.R., Conta Steencken, A., and Osterhout, D.J. (2014). Chondroitin sulfate proteoglycans in the nervous system: inhibitors to repair. Biomed Res Int 2014, 845323.

Silver, J. (2009). CNS regeneration: only on one condition. Curr Biol 19, R444-446.

Sivasankaran, R., Pei, J., Wang, K.C., Zhang, Y.P., Shields, C.B., Xu, X.M., and He, Z. (2004). PKC mediates inhibitory effects of myelin and chondroitin sulfate proteoglycans on axonal regeneration. Nat Neurosci 7, 261-268.

Soltoff, S.P. (2007). Rottlerin: an inappropriate and ineffective inhibitor of PKCdelta. Trends Pharmacol Sci 28, 453-458.

Teng, F.Y., and Tang, B.L. (2006). Axonal regeneration in adult CNS neurons--signaling molecules and pathways. J Neurochem 96, 1501-1508.

Xu, Z.X., Qin, S.Z., Xu, G.Z., Hu, J.M., and Ma, L.T. (2011). Enhancement of axonal regeneration of retinal ganglion cells in adult rats by etomidate: involvement of protein kinase C. Invest Ophthalmol Vis Sci 52, 8117-8122.

Chapter 3

Profilin is a key mediator in regulating actin dynamics and axon growth

Sérgio Carvalho Leite*, Rita Costa*, Raquel Mendes, Márcia Almeida Liz, Fernando Milhazes Mar and Mónica Mendes Sousa

[1]Nerve Regeneration Group, IBMC-Instituto de Biologia Molecular e Celular, Universidade do Porto, 4150-180 Porto, Portugal

Correspondence: msousa@ibmc.up.pt (M.M.S.)

* Authors contributed equally

Summary

Although actin is well recognized as a key player in axon growth, how different actin-binding proteins control its dynamics is still not fully understood. Using the conditioning lesion, a model in which the axon regeneration capacity of spinal dorsal column axons is increased following a priming lesion to the sciatic nerve, we determined that profilin-1 (Pfn1) is increased in regenerating axons whereas the inactive form of the protein (Phospho-S137) is severely decreased. Profilins provide the pool of competent ATP-actin monomers that can be added to free filamentous actin ends to support their polymerization and growth. Here we show that acute *in vitro* ablation of Pfn1 precludes axon formation in hippocampal neurons and significantly decreases neurite outgrowth in DRG neurons, suggesting a critical role of Pfn1 during early neuritogenesis and axon growth. To unravel the importance of Pfn1 during axon regeneration, we generated mice with an inducible neuronal deletion of Pfn1 using cre-lox technology. $Cre^{+/-}Pfn1^{fl/fl}$ neurons, displayed impaired actin dynamics and defective neurite outgrowth which was exacerbated after co-ablation of Pfn2. Moreover, *in vivo* in $cre^{+/-}Pfn1^{fl/fl}$ mice, regeneration of both peripheral and central DRG axons was diminished in the absence of Pfn1. Interestingly, overexpression of constitutively active profilin-1 (S137A) enhanced neurite outgrowth. In summary, our work provides evidence that Pfn1 is a determinant of axon regeneration capacity, acting as a key regulator mediating actin dynamics after injury. In the future, exploring the mechanisms by which Pfn1 acts in neurons would enable to set the foundations for drug screens unveiling modulators of its activity with therapeutic potential for spinal cord injury treatment.

Introduction

Emerging evidence suggests that regulators of cytoskeleton dynamics might be attractive targets to control axon formation, growth and regeneration. Specifically, actin dynamics in the growth cone is thought to play a major role in regulating the rate and direction of axon extension. As such, interventions aimed at promoting axonal regeneration may converge on the manipulation of this mechanism. Although actin is well recognized as a key player in axon growth, how different actin-binding proteins control its dynamics is still not fully understood. A correctly assembled growth cone is fundamental for the regeneration process to occur (Bradke et al., 2012). Actin, as a major component of the growth cone peripheral domain is required to generate its dynamism and organization (Lewis et al., 2013; Stiess and Bradke, 2011).

Both cofilin and profilin are two ABPs known to be fundamental for actin dynamics (Didry et al., 1998), acting synergistically, increasing the treadmilling rate of actin by 400 fold (Didry et al., 1998). The continuous incorporation of ATP bound G-actin is fundamental for maintaining actin dynamism, and in growth cones this task is undertaken by profilin (Lee et al., 2013). Profilins provide the pool of competent ATP-actin monomers that can be added to free filamentous actin ends to support their polymerization and growth. Interestingly, negative regulators of actin dynamism such as the Rho kinases operate via profilin (and cofilin) phosphorylation, inhibiting their activity (Da Silva et al., 2003). The role of ADF/cofilin in axon formation and growth is well established (Flynn et al., 2012; Garvalov et al., 2007). Besides, unpublished work from the Bradke lab shows that a conditioning lesion, a model in which an increased regenerative capacity of dorsal column axons is induced (Silver, 2009), drives axon regeneration through increased cofilin-mediated actin turnover (personal communication).

In humans, profilins comprise a family of small ABPs, in a total of 4 different forms (Moens, 2008). Profilin-1 (Pfn1) is ubiquitously expressed, whereas the other three forms are tissue specific. Profilin-2 (Pfn2) is neuronal, mostly CNS-restricted and Profilin-3 (Pfn3) and Profilin-4 (Pfn4) are expressed in germ cells. In the nervous system, profilins have been mainly associated with synapse formation (Michaelsen et al., 2010; Neuhoff et al., 2005), axon extension and degeneration (Da Silva et al., 2003; Wu et al., 2012) and Purkinje cell survival (Kullmann et al., 2012b). Pfn1 has been suggested to have an important function in mediating the turnover of the G-actin pool at the leading edge of growth cones (Lee et al., 2013). However, Pfn1 is probably not

fundamental for axon extension since Nestin Cre mediated depletion of Pfn1 at the early stages of neuronal differentiation, resulted in normal brain formation, with only a visible phenotype in neuron migration in the cerebellum (Kullmann et al., 2012b). Nevertheless, Pfn1 mutations in the actin-binding site were associated with amyotrophic lateral sclerosis (ALS) and mutant motor neurons displayed neurite outgrowth impairment that was suggested to result from the loss of actin-related function (Wu et al., 2012). In the case of Pfn2, its overexpression in hippocampal neurons leads to decreased neurite outgrowth, whereas knockdown leads to increased outgrowth (Da Silva et al., 2003). Here we further explored the role of profilins in axon growth and regeneration following injury.

Results

A conditioning injury drives an increased Pfn1 activity in the growth cone.

Both cofilin and profilin are two ABPs known to be fundamental for actin dynamics (Didry et al., 1998), acting synergistically and increasing the treadmilling rate of actin by 400 fold (Didry et al., 1998). Given the crucial role of cofilin and profilin in actin treadmilling in the growth cone, and to further evaluate their importance during axon regeneration, we analyzed their levels in the spinal cord injury site of rats with and without a previous sciatic nerve injury (condition lesion – CL). Of note, a conditioning lesion (Figure 1A) is a well-established paradigm to induce axon growth *in vitro* (Ylera et al., 2009) and regeneration *in vivo* (Neumann and Woolf, 1999). Interestingly, the spinal cord injury site of animals with conditioning lesion (CL) had increased levels of cofilin-1 (Cfl-1), in accordance with data from the Bradke lab, and in the levels of profilin-1 (Pfn1), when compared to animals that were just submitted to spinal cord injury (SCI) (Figure 1B-C). Moreover, the levels of phosphorylated S137 Pfn1, a phosphorylation that inhibits its activity (Shao et al., 2008), were 10-fold decreased in spinal cord samples from conditioned rats (Figure 1B-C). These results suggest a differential regulation of these two ABPs in the regenerating axons.

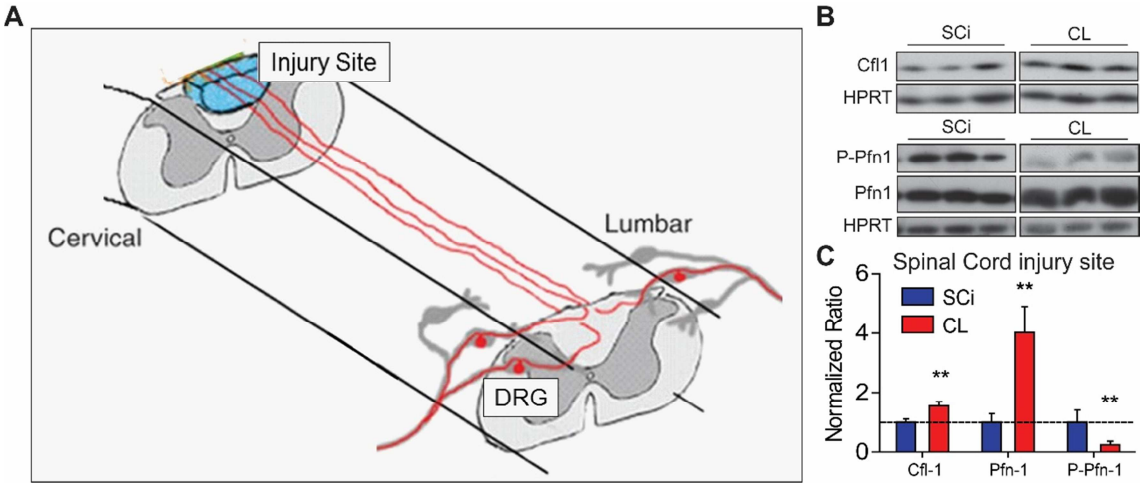

Figure 1. The levels of the ABPs Pfn1 and Cfl1 are increase following conditioning effect. (A) Schematic representation of the spinal cord. The injury site is highlighted in blue; the central (dorsal column tract) and peripheral DRG axons are highlighted in red. Spinal cord injury site samples correspond to the region 2.5mm caudal and 2.5mm rostral from the lesion site. Adapted from (Alto et al., 2009). (B) Western blot analysis of Cfl1, Pfn1 and p-Pfn1 in spinal cord injury samples of rats with either spinal cord injury (SCI) or conditioning lesion (CL). (C) Quantification of (B); normalized ratios of protein of interest/HPRT are shown. p-value: **<0.01.

The acute deletion of Pfn1 impairs neuritogenesis and neurite outgrowth

The continuous incorporation of ATP bound G-actin is essential for maintaining the dynamism of a growing axon. In growth cones, this is undertaken by profilin (Lee et al., 2013). Here we assessed the role of Pfn1 in neuritogenesis and axon growth. For that, our initial approach was to perform the acute ShRNA-mediated depletion of Pfn1 in both hippocampal and DRG neurons. In both neuron types the knockdown of Pfn1 was efficient (83% ±0.02 decreased expression for hippocampal neurons (Figure 2A) and 86% ±0.05 for DRG neurons) (Figure 2C) and was not accompanied by an increased expression of Pfn2. Pfn1 depletion precluded the ability of hippocampal neurons to form axons and cells were not able to extend filopodia or exit stage 1 (Figure 2B), suggesting a fundamental role of Pfn1 during early neuritogenesis. In DRG neurons, although the knockdown of Pfn1 was also efficient and did not lead to increased Pfn2 levels (Figure 2C), neurons were able to form neurites but these had a decreased length (Figure 2D, E).

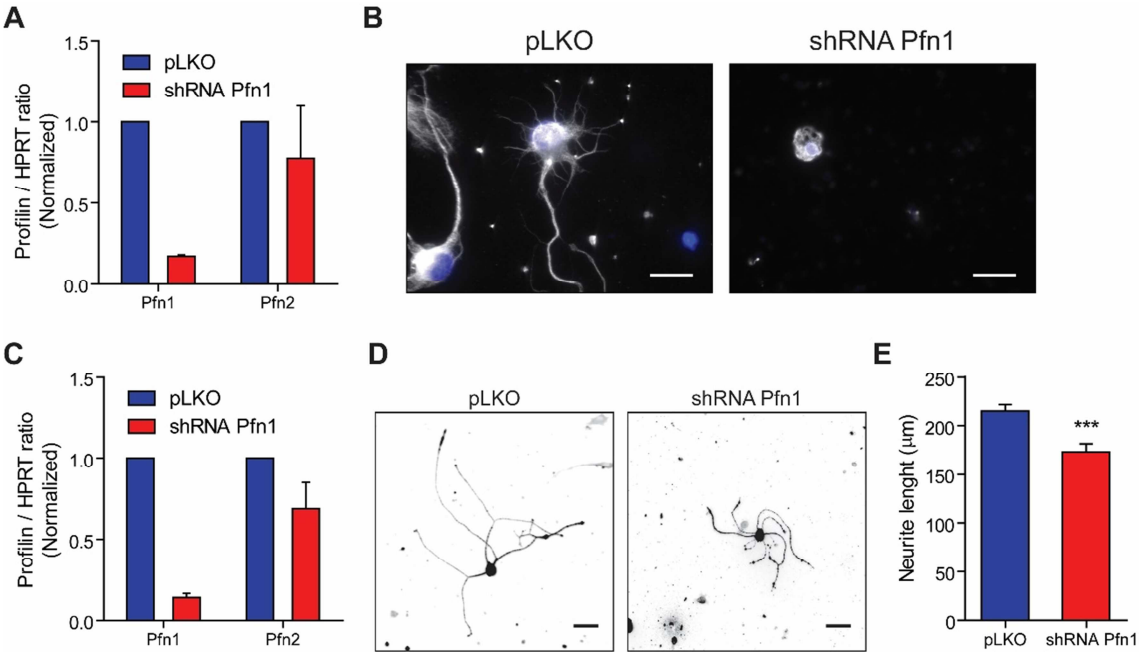

Figure 2. Pfn1 is a regulator of neuritogenesis and axon growth. (A) qPCR of Pfn1 and Pfn2 in DIV5 hippocampal neurons transduced with either a control lentivirus (pLKO) or a lentivirus targeting Pfn1 (ShRNA Pfn1). The ratio is normalized in relation to the control (pLKO). (B) Representative βIII-tubulin immunofluorescence (in grey) in DIV2 (post replating) hippocampal neurons transduced with either an empty lentivirus (pLKO) or a lentivirus targeting Pfn1 (ShRNA Pfn1). DAPI - blue; scale bar- 200µm. (C) qPCR of Pfn1 and Pfn2 in DIV5 rat DRG neurons treated with either a control lentivirus (pLKO) or a lentivirus targeting Pfn1 (ShRNA Pfn1). The ratio is normalized in relation to the control (pLKO). (D) Representative βIII-tubulin immunofluorescence in DRG neurons grown for 12 hour post replating treated with either an empty lentivirus (pLKO) or a lentivirus targeting Pfn1 (ShRNA Pfn1). Scale bar - 100µm. (E) Quantification of length of the longest neurite in DRG neurons shown in (D), treated with either an empty lentivirus (pLKO) or a lentivirus targeting Pfn1 (ShRNA Pfn1). p-value ***<0.001.

The absence of Pfn1 leads to reversion of the conditioning effect and to decreased actin retrograde flow in the growth cone

To further evaluate the role of profilin in axon formation and growth, we crossed the $Pfn1^{fl/fl}$ mice, where the first exon of the Pfn1 gene is flanked by loxP sites (Bottcher et al., 2009) with the Slick-H mice, that express inducible $CreER^{T2}$ and YFP under the control of the neuronal Thy1 promoter (Young et al., 2008). The deletion of Pfn1 was confirmed by western blot in the brain and spinal cord of $cre^{+}Pfn1^{f/f}$ mice (Figure 3A-C) and in the DRG, 41% of the neurons were YFP-positive (Liz et al., 2014). We used DRG neuron cultures from $cre^{+}Pfn1^{f/f}$ mice as a model of chronic Pfn1 depletion. The conditioning lesion effect was clearly visible *in vitro*, with DRG neurons collected from animals with a priming peripheral branch injury displaying a different growth type, with decreased branching and increased elongation, resembling embryonic and early post-natal DRG neurons (Martin et al., 2013). Conditioned neurons from $cre^{+}Pfn1^{fl/fl}$ mice

presented a decreased growth ability, when compared to the cre^{-}Pfn1$^{fl/fl}$ controls (cre^{-} Pfn1$^{fl/fl}$: 432.1±117.9µm, n=48 cells; cre^{+}Pfn1$^{fl/fl}$: 371.6±118.6µm, n=39 cells) (Figure 3D-E). Of note, in cre^{+}Pfn1$^{f/f}$ DRG neurons, depletion of Pfn2 by specific ShRNA lentiviral mediated knockdown, resulted in a severe decrease in neurite outgrowth (cre^{+}Pfn1$^{f/f}$ + control lentivirus (pLKO): 404±188µm, n=41 cells; cre^{+}Pfn1$^{f/f}$ + Pfn2 ShRNA directed lentivirus (ShRNA Pfn2): 246±193µm, n=32cells) (Figure 3F-G), suggesting that at least in the absence of Pfn1, Pfn2 can regulate neurite outgrowth.

To evaluate whether the chronic depletion of Pfn1 resulted in an abnormal actin dynamics in the growth cone, DRG neuronal cultures of cre^{+}Pfn1$^{wt/wt}$ and cre^{+}Pfn1$^{fl/fl}$ were transfected with lifeAct-RFP and actin retrograde flow was measured (Figure 3H-I). In cre^{+}Pfn1$^{fl/fl}$ DRG neurons, actin retrograde flow was decreased, highlighting the role of profilin in mediating the transition of ADP to ATP bound actin, required for the dynamism that the growth cones present during axon extension

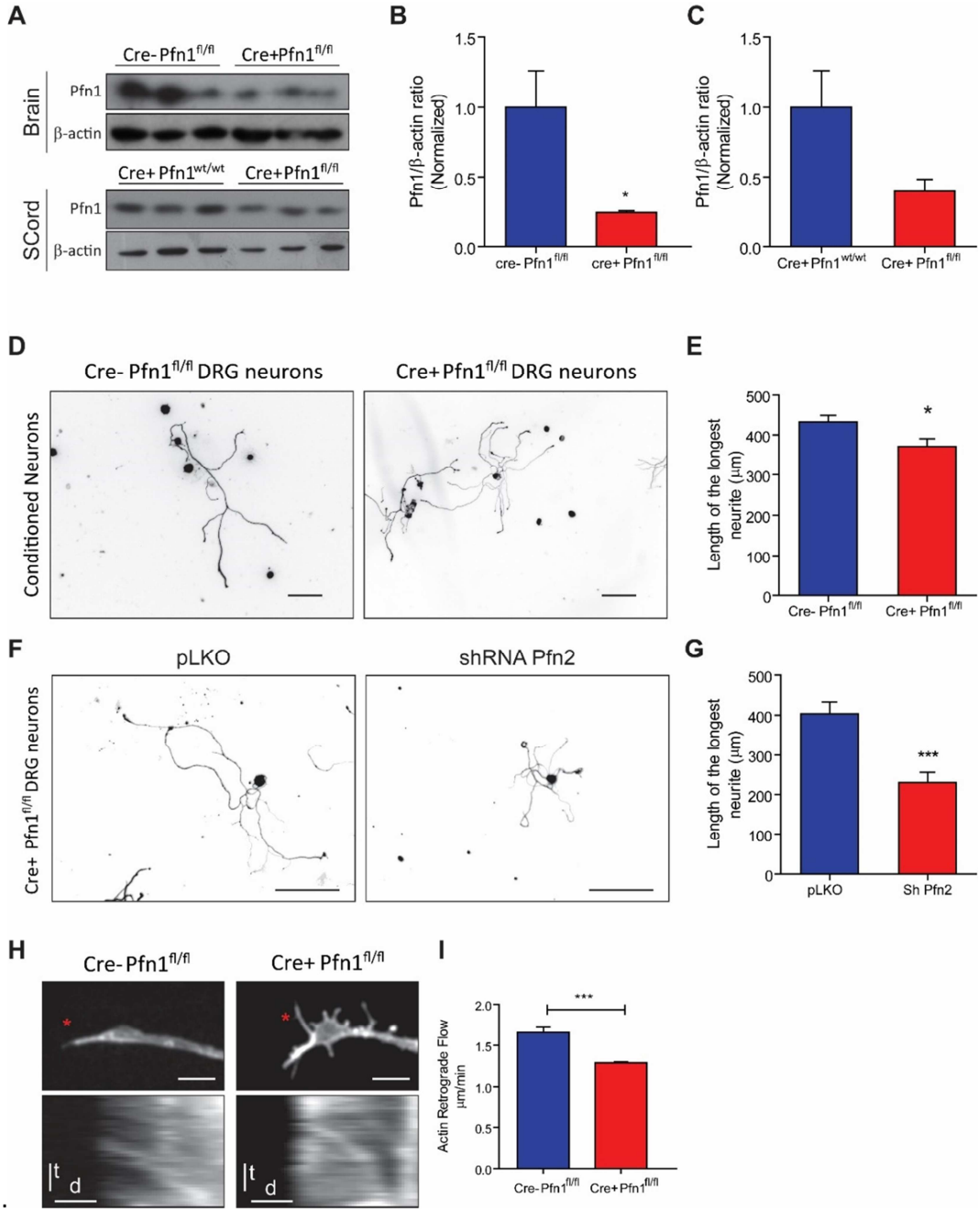

Figure 3**.** The absence of Pfn1 leads to reversion of the conditioning effect and to decreased actin retrograde flow in the growth cone. (A) Western blot against Pfn1 and β-actin of brain and spinal cord (SCord) samples of cre^{+}Pfn1$^{f/f}$ and cre^{+}Pfn1$^{wt/wt}$ mice. (B-C) Quanfication of (A). (D) βIII-tubulin immunofluorescence of cre^{+}Pfn1$^{fl/fl}$ and cre^{-}Pfn1$^{fl/fl}$ conditioned DRG neurons. Scale bar: 100µm. (E) Quantification of the length of the longest neurite in cre^{+}Pfn1$^{fl/fl}$ and cre^{-}Pfn1$^{fl/fl}$ conditioned DRG neurons (D). (F) Representative βIII-tubulin immunofluorescence in cre^{+}Pfn1$^{f/f}$ DRG neurons either transduced with a control lentivirus (pLKO) or with a Pfn2 ShRNA directed lentivirus (ShRNA Pfn2). Scale bar: 100µm. (G) Quantification of the length of the longest neurite in DRG neurons either transduced with a control lentivirus (pLKO) or with a Pfn2 ShRNA directed lentivirus (ShRNA Pfn2). (H) Representative growth cones of lifeAct-RFP transfected cre^{+}Pfn1$^{wt/wt}$ and cre^{+}Pfn1$^{fl/fl}$ DRG neurons (upper) and respective kymographs (lower). Red asterisks highlight the region where kymographs were performed. Upper panel: scale bar:

5µm; Bottom panel: vertical scale bar (time (t)): 50 seconds, horizontal scale bar (distance (d)): 1µm. (I) Quantification of (H). p-value *<0.05 and ***<0.001

In vivo regeneration of peripheral and central DRG axons is diminished in the absence of Pfn1.

To determine whether *in vivo* the absence of Pfn1 results in decreased axon growth, two paradigms that originate a robust axon regeneration were used to compare $cre^{+}Pfn1^{wt/wt}$ and $cre^{+}Pfn1^{fl/fl}$ mice: sciatic nerve injury and the conditioning lesion model (Silver, 2009). Two weeks after sciatic nerve crush, regeneration of myelinated axons was assessed. Of note, using the SlickH cre reporter system most of the axons in the sciatic nerve are YFP^{+} (Figure 4A). $cre^{+}Pfn1^{fl/fl}$ mice had a decreased density of myelinated axons after sciatic nerve crush when compared to $cre^{+}Pfn1^{wt/wt}$ ($cre^{+}Pfn1^{wt/wt}$ n=5 animals; $cre^{+}Pfn1^{fl/fl}$ n=8 animals) (Figure 4B-C), supporting a decreased axon regeneration capacity.

To reinforce the importance of Pfn1 for axon regrowth, an alternative model was used, the conditioning lesion paradigm. In this model, the enhanced regeneration capacity of the dorsal column tract was assessed in animals where a sciatic nerve transection preceded an acute spinal cord lesion. The severed tract was clearly identified by the YFP axonal staining (in green) and the presence of the tracer – CT-B subunit conjugated with Alexa568 (in red) (Figure 4D). Although there was a tendency for a decreased number of dorsal column axons regenerating though the glial scar in $cre^{+}Pfn1^{fl/fl}$ mice, this did not reach statistical significance (Figure 4D and 4E) ($cre^{+}Pfn1^{wt/wt}$: n=5 animals; $cre^{+}Pfn1^{fl/fl}$: n=6 animals). However, the length of the regenerating axons was severely decreased in animals lacking Pfn1 ($Cre^{+}Pfn1^{wt/wt}$: 311.0 µm ±65.4 SD, n=5 animals; $Cre^{+}Pfn1^{fl/fl}$: 185.8 µm ±58.7 SD, n=5 animals) (Figure 4F), further support the importance of Pfn1 in axon growth, including through the inhibitory adult spinal cord injury site.

Taken together, this data strongly support that profilin-1 is essential for axon extension and regeneration and reinforce the role of actin – and actin dynamics – in the conditioning lesion model.

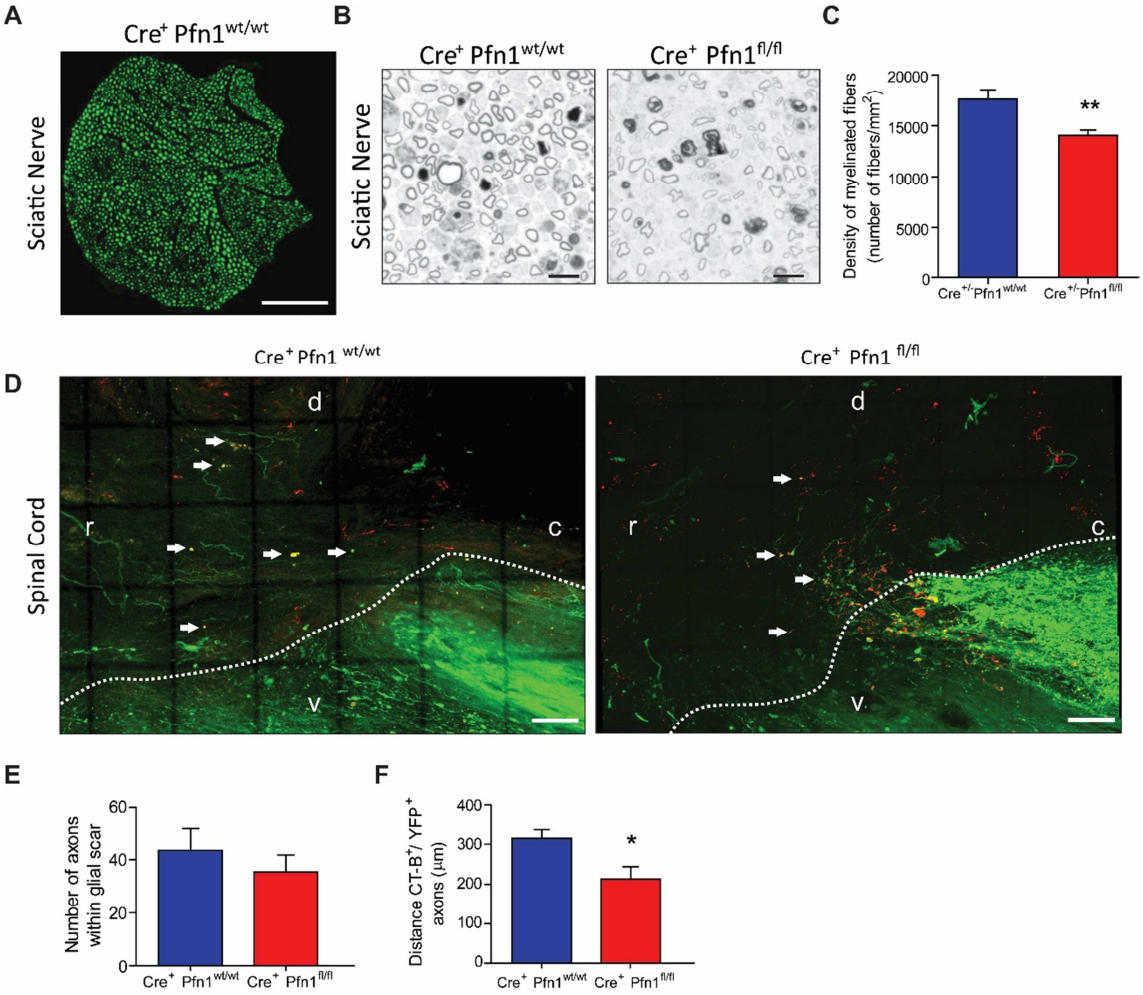

Figure 4. Pfn1 is a key regulator of axon regeneration after injury. (A) Cre^{+} Pfn1$^{wt/wt}$ YFP sciatic nerve section. (B) Representative images of PPD-stained semithin sciatic nerve sections from cre^{+}Pfn1$^{fl/fl}$ and cre^{+}Pfn1$^{wt/wt}$ mice two weeks after sciatic nerve crush; scale bar: 50 µm. (C) Quantification of myelinated axon density in sciatic nerves from cre^{+}Pfn1$^{fl/fl}$ and cre^{-}Pfn1$^{fl/fl}$ mice, 2 weeks after sciatic nerve crush. Error bars are SEM. (D) Representative images of CT-B+ fibers in sagittal spinal cord sections following conditioning lesion in cre^{+}Pfn1$^{wt/wt}$ and cre^{+}Pfn1$^{fl/fl}$ mice. YFP+ axons are shown in green and dorsal column fibers traced with CT-B are labeled in red. The double positive YFP+/CT-B+ axons are highlighted with arrows; scale bar: 100 µm. R: rostral; C: caudal; D: dorsal; V: ventral; Dashed lines label the border of the glial scar. (E) Quantification of the number of CT-B+/YFP+ dorsal column fibers that are able to enter in the glial scar. (F) Quantification of the length of the regenerating axons within the glial scar, from the lesion border. All error bars are SEM. p-value *<0.05, **<0.01

Overexpression of the constitutively active form of Pfn1 S137A increases axon growth

Our data suggests that the regulation of Pfn1 activity is an important event in conditions of increased axon growth. Profilin activity is regulated by phosphorylation of its C-terminal serine residue 137. This phosphorylation, performed by ROCK1 is inhibitory for its activity (Shao et al., 2008). Although the exact mechanism is not fully

understood, it is known that Pfn1 S137A mutant binds actin with higher affinity than WT Pfn1 (Shao et al., 2008). To further assess the importance of Pfn1 regulation, hippocampal neuron cultures were transfected with WT Pfn1 and Pfn1 mutants of the phosphorylatable S137 residue (Figure 5A). Given the known regulation of Pfn1, our expectations were to have increased outgrowth with the overexpression of the constitutively active S137A mutant, and decreased growth capacity with the S173D mutant, which should mimic innactivePfn1 phosphorylated by ROCK. Confirming our hypothesis, overexpression of the constitutively active Pfn1 mutant S137A increased very consistently axon growth (Figure 5B), but not that of dendrites (Figure 5C), whereas the WT and the pseudo-phosphorylatable form of Pfn1 had no significant impact in axon growth.

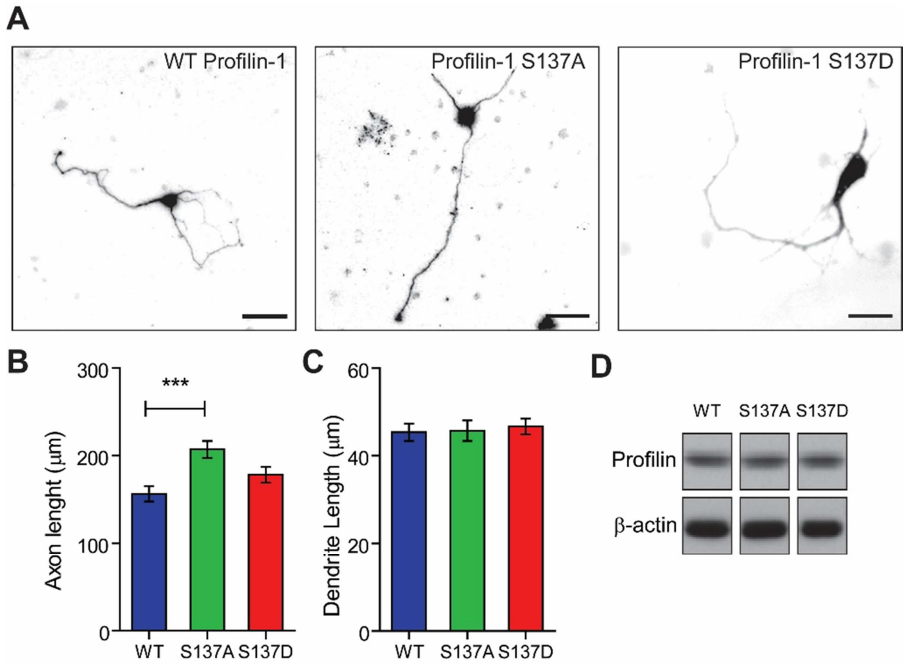

Figure 5. Overexpression of constitutively active profilin leads to increased axon outgrowth. (A) E16.5 hippocampal neurons were co-transfected with pMAX GFP and WT, S137A or S137D profilin and fixed at DIV4. During this period of active axon outgrowth, only the constitutively active form increased growth capacity (B), whereas the effect in the dendrite outgrowth was not observed (C). (D) The overexpression of the WT and profilin mutants was confirmed in CAD cell extracts. Scale bars: 50µm. p-value ***<0.001

Pfn1 overexpression impacts intracellular signaling

Besides its actin-binding activity, Pfn1 binds PIP2 in the cellular membrane (Krishnan and Moens, 2009). Given its PIP2 binding activity, we evaluated a possible effect of Pfn1 overexpression in the PI3K/GSK3β (Figure 6A) pathway using the neuronal CAD cell line overexpressing WT Pfn1 (Figure 6B). Phosphorylated AKT S473 (Figure 6E) was increased by Pfn1 overexpression, and phospho-AKT T308 levels were also increased although this increase did not reach statistic significance (p-value = 0.09) (Figure 6D). The activation of the kinase responsible for the phosphorylation of AKT at T308, PDK1 (Hemmings and Restuccia, 2012), was not significantly altered by Pfn1 overexpression(Figure 6C). These results suggest that the induction of AKT activation by Pfn1 overexpression occurs mostly through S473 phosphorylation, which is regulated by mTORC2 (Hemmings and Restuccia, 2012). The downstream effector of activated AKT, GSK3β was also differently regulated upon Pfn1 overexpression, with a 2 fold increase in the inhibitory phosphorylation at the S9 residue (Figure 6F). Interestingly, GSK3β inactivation increases axon outgrowth (Liz et al., 2014). The GSK3β activator phosphorylation at Y216 was unaltered by Pfn1 overexpression (Figure 6G). These results suggest that Pfn1 modulates not only the actin cytoskeleton but may also impact microtubule regulation, through PI3K/AKT signaling, a central pathway in this context (Read and Gorman, 2009).

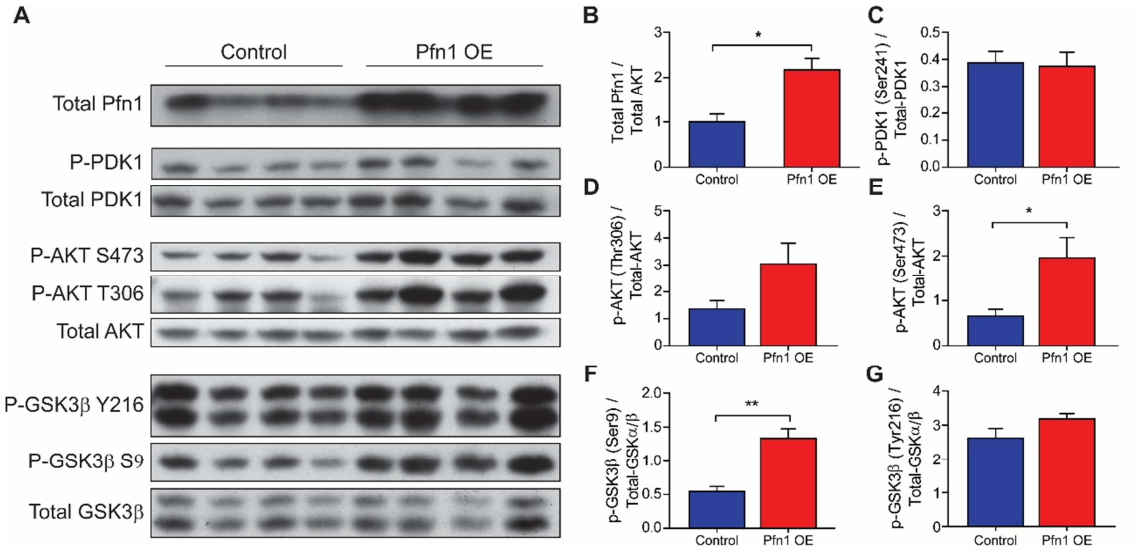

Figure 6. Pfn1 overexpression activates the AKT/GSK3β signaling cascade. (A) Western blot analysis of Pfn1, PDK1 (phosphorylated and total levels), AKT (phosphorylated and total levels) and GSK3β (phosphorylated and total levels) in control CAD cells (control) and CAD cells overexpressing Pfn1 (Pfn1 OE). (B-G) Quantification of A. p-value *<0.05 and **<0.01.

Discussion

The conditioning lesion is a paradigm of enhanced intrinsic regeneration capacity of DRG neurons. These neurons, after a priming injury to their peripheral branch become more competent to regenerate their central branch. The nature of this increased ability to regrow is dependent on the activation of the transcription machinery that leads to the expression of regeneration-associated genes (RAGs) (Hoffman, 2010) and also to the increase in the axonal transport of proteins related to axon outgrowth (Hoffman, 2010; Mar et al., 2014). Here we show that the levels and activity of Pfn1 are crucial in mediating the conditioning effect and actin dynamics during axon growth/regeneration. In an acute depletion model downregulation of Pfn1 generated a striking neuritogenic deficiency in hippocampal neurons. A similar phenotype is found in ADF/Cofilin dKO neurons (Flynn et al., 2012). It is however unlikely that under chronic depletion of Pfn1 such an effect is visible. In fact, in Nestin-cre^{+} Pfn1$^{fl/fl}$ mice, which have decrease levels of Pfn1 from early neuronal differentiation periods (and no Pfn1 at P1) (Kullmann et al., 2012a), development occurs without any obvious and striking impairment, and the only defect found was in the migration of cerebellar granule neurons (CGN) (Kullmann et al., 2012a). It is important to note that in the cerebellum, radial migration occurs late in development (from P4 to P9) and this may be the reason why no defects are seen in other neuron populations as Pfn1 decrease in Nestin-cre^{+} Pfn1$^{fl/fl}$ is observable at E15 and complete at P1. In DRG neurons, however, the phenotype after acute depletion of Pfn1 was not as severe as that observed in hippocampal neurons, and only a decreased neurite outgrowth was observed. The reason underlying the different effect of Pfn1 depletion in different neuron types remains to be established. Besides the acute depletion of Pfn1, we also used Pfn1 conditional KO mice to further dissect the role of this protein in axon growth – namely in the context of *in vivo* axon regeneration. In this model we clearly demonstrate that *in vivo,* in axon regeneration paradigms that are followed by successful axon regeneration, as is the case of sciatic nerve injury and conditioning lesion, Pfn1 is required. In Pfn1 KO animals, compensation by Pfn2 might not be neglectable, as Pfn2 is not only neuronal specific, but also present in increased levels in (CNS) neurons (Pilo Boyl et al., 2007; Witke et al., 1998; Witke et al., 2001). Of note, Pfn2 depletion by ShRNA in a Pfn1 KO background led to a decreased neurite outgrowth. This reinforces the idea of a compensatory mechanism of Pfn2 when Pfn1 is depleted, namely in the chronic depletion model generated by the SLICK-H Pfn1^{fl} mice. The same is observed with ADF/Cofilin-1 (Flynn et al., 2012) and Cofilin-1/Cofilin-2 (Frank Bradke, personal communication, Chile 2015). In this context, it

would be interesting to have a full Pfn1 and Pfn2 KO mice, to further study the importance of profilins for the axon regeneration ability in the absence of any compensatory role. For this, the SLICK-H $Pfn1^{fl}$ x PFN2 KO mice should be generated, since the full Pfn1 KO mice are unviable (Witke et al., 2001) whereas the Pfn2 KO is not (Pilo Boyl et al., 2007).

Our data demonstrates that profilin is fundamental for axon regeneration. But how does Pfn1 exerts its effect? Our analysis suggests that the actin retrograde flow, which is crucial for the proper extension of the axon (Gomez and Letourneau, 2014), is impaired in the absence of Pfn-1. As it was demonstrated before (Lee et al., 2013), profilin is fundamental for the maintenance of the G-actin pool (ATP bound) at the leading edge of the growth cone membranes. In its absence, the G-actin pool is decreased as well as lamellipodia extension (Lee et al., 2013). Therefore, the role of Pfn1 as the exchanger of ADP to ATP bound G-actin monomers and its capacity to be localized at the cell membrane is crucial for the growth cone dynamics.

Interestingly, we show that in the spinal cord lesion site, levels of Pfn1 are increased in conditioned animals but, more strikingly, that the inhibitory phosphorylation of Pfn1 is almost 10-fold decreased. *In vitro*, although overexpression of Pfn1 in hippocampal neurons did not result in increased neurite outgrowth, the constitutively active Pfn1 mutant S137A, that cannot be phosphorylayed by ROCK, increased consistently axon outgrowth. This result strengths the idea of that active Pfn1 is required for optimal axon growth to occur. Interestingly, cofilins are also inhibited through phosphorylation by LIM kinases 1 and 2, which are downstream effectors of the Rho kinases ROCK (Sumi et al., 1999), cdc42 (Garvalov et al., 2007) and Rac (Arber et al., 1998), inhibiting them. Since Rho signaling is a main inhibitory pathway of axonal regeneration in the CNS (Fujita and Yamashita, 2014), it is likely that Cfl1 and Pfn1 are two of the main downstream targets of its action.In summary, in the conditioning lesion model increased regeneration capacity is achieved by increasing the overall pool of Pfn1 and Cfn1 in the lesion site. In the case of Pfn1, not only the absolute amounts of the protein but also severely decreased levels of the inhibited form of the protein are clearly mediating the enhanced growth ability. To further assess the *in vivo* relevance of this mechanism, future experiments should test the delivery of the constitutively active form of Pfn1 to regenerating DRG neurons.

It is important to note that the localization of Pfn1 in the membrane, at the edge of the growth cone, is fundamental for its actin-related role. But, interestingly, actin is not the only cytoskeleton-related protein that Pfn1 (and Pfn2) is able to interact with. Profilins have two additional important domains besides the actin binding domain, that are the

poly-L-proline binding motif (which enables interaction with a large group of ABPs) and the phosphoinositide binding domain (Goldschmidt-Clermont et al., 1990; Lassing and Lindberg, 1988). Through its interaction with PIP2, profilins might regulate the PI3K signaling and can have non-actin related functions with impact in the organization of the microtubule cytoskeleton. To test this hyposthesis, we performed the analysis of the PI3K/AKT pathway in a neuronal cell line overexpressing Pfn1. Our analysis revealed that Pfn1 not only impacts the actin cytoskeleton but may also regulate microtubule dynamics through modulation of GSK3β activity. The inhibition of GSK3β is known to be an important event in the neurite outgrowth process, namely in the conditioning lesion model (Liz et al., 2014). In the future one key experiment will be the analysis of microtubule dynamics in the context of either overexpression or absence of profilin. Together these findings raise new and exciting possibilities, namely that increased activity of Pfn1 might result in increased axon regeneration *in vivo* not only through the regulation of actin dynamics in the growth cone, but also through the modulation of the microtubule cytoskeleton.

Methods

Animals

Mice were handled according European Union and National rules. The protocols described in this work have been approved by the IBMC Ethical Committee and by the Portuguese Veterinarian Board. Mice were bred at the IBMC animal facility, had *ad libitum* access to water and standard rodent food, and were kept on a 12 hour light and dark cycle. Genotyping was performed as described (Bottcher et al., 2009). Floxed Pfn1 mice ($Pfn1^{fl/fl}$, a kind gift from Prof R Fassler, Max Planck Institute of Biochemistry) and Slick-H mice (a kind gift from Dr Guoping Feng, Duke University Medical Center; mice that co-express inducible-Cre^{ERT2} and YFP under the control of the Thy1 promoter (Young et al., 2008)) were used to generate neuronal-specific conditional Pfn1 knockout mice ($cre^{+}Pfn1^{fl/fl}$). For that, $Pfn1^{fl/fl}$ were crossed with Slick-H mice. $cre^{+}Pfn1^{fl/wt}$ were selected and then crossed with $Pfn1^{fl/fl}$ mice and $Pfn1^{wt/wt}$ mice in order to generate $cre^{+}Pfn1^{fl/fl}$ mice and the controls $cre^{+}Pfn1^{wt/wt}$ and $cre^{-}Pfn1^{fl/fl}$. Induction of cre expression was performed by tamoxifen injection at weaning (3-4 weeks of age). In all experiments animals of either sex were used.

Sciatic nerve and spinal cord lesions

Sciatic nerve crush: 7 weeks old mice were anesthetized with 5% isoflurane in a closed chamber, followed by delivery of 2-3% of isofluorane using a mask, which was maintained through the surgery procedure. Crush was done using hemostatic forceps for 2 times during 15 seconds Animals were allowed to recover for two weeks after which nerves were collected for analysis of axon regeneration as detailed below.

Sciatic nerve transection: 8-10 weeks old Wistar rats were anesthetized with ketamine (75mg/Kg) and medetomidine (0.6 mg/Kg) and sciatic nerve transections were performed using a microscissor,. Animals received analgesia (butorphanol) twice a day, for 48 hours.

Spinal cord injury (SCI): 10-12 weeks old Wistar rats, or 8 weeks old mice, were used. Animals were anesthetized with ketamine/medetomidine, as above. The skin was shaved and the spinal cord was exposed at the thoracic level. Laminectomy was performed at the T6-T8 level (in rats), or at the T7-T9 level in mice. Dorsal hemisection was done with a microscissor (in rats) or using a micro-scalpel (in mice) for western blot analysis (rats) and for dorsal column tract analysis (mice). Animals received analgesia (butorphanol) twice a day, for 72 hours and fluid therapy once a day (Duphalyte), for 72 hours. Animals also required manual voiding of the bladder twice a day for the rest of the experimental period. Wet food was placed in the cage floor and water with antibiotic (0.016% Baytril) was supplied in long nipple bottles. The recovery period after spinal cord injury was: i) 1 week for collection of 5mm of the spinal cord injury site (2.5mm rostral and 2.5mm caudal to the lesion site) and analysis by western blot, as detailed below and ii) 4 weeks for dorsal column tract analysis (also detailed below).

Conditioning lesion: sciatic nerve transection was performed as described above and one week later dorsal spinal cord hemisection was conducted, also as described above.

Analysis of axon regeneration

Regeneration of sciatic nerve axons: 7 weeks-old mice (n= 8 $cre^{+}Pfn1^{fl/fl}$ and n= 5 $cre^{+}Pfn1^{wt/wt}$ mice) were subjected to sciatic nerve crush as detailed above. 2 weeks after crush animals were sacrificed and sciatic nerves were collected and fixed for two weeks in 4% glutaraldehyde in 0.1M sodium cacodylate buffer (pH 7.4). After post-fixation with 1% OsO4 in 0.1M sodium cacodylate buffer (pH 7.4) for 2 hours, tissues were dehydrated and embedded in Epon (Electron Microscopy Sciences). In sciatic

nerves, for the assessment of the density of myelinated axons, 1µm-thick nerve sections were stained for 10 minutes with 1% p-phenylenediamine (PPD) in absolute methanol, dried, and mounted on a drop of DPX (Merck). The entire area of the nerve, distally to the lesion site, was photographed using an Olympus optical microscope equipped with an Olympus DP 25 camera and Cell B software, and images were imported into Photoshop (Adobe).

Regeneration of dorsal column axons after conditioning lesion: 8 weeks old $cre^{+}Pfn1^{wt/wt}$ (n=6) and $cre^{+}Pfn1^{fl/fl}$ (n=5) mice were subjected to spinal cord dorsal hemisection and allowed to recover for 4 weeks, as detailed above. Four days prior euthanasia, 2µL of 1% cholera toxin B (CT-B) (List Biologicals, Campbell, CA, USA) was injected in both sciatic nerves. Animals were perfused with formalin, tissues were cryopreserved in sucrose and sectioned at 50µm. Consecutive spinal cord sagittal sections were collected for free floating immunohistochemistry with anti-CT-B (1:30000; List Biologicals, #703). The secondary anti-goat biotinylated antibody Alexa fluor 568 conjugated streptavidin was used to detect the axons from the conditioned DRG neurons (and non-conditioned controls). Image analysis was done with Fiji software. Dorsal column fibers were quantified by counting the total number of axons within the glial scar, in the CT-B positive sections (2-4 sections per animal). The length of the longest CT-B labeled axon found rostrally to the injury site was measured using as the origin a vertical line placed at the rostral end of the dorsal column tract (that is, where CT-B labeling accumulates). Lesion margins were evident under YFP channel visualization and the line corresponding to the lesion site was drawn. For scoring, only double YFP / Texas Red positive axons were considered.

Western blotting

For western blots of rat spinal cord injury sites (for comparison of animals with SCI and CL), 10-15% SDS-PAGE gels with 50 µg of sample were run; for the analysis of Pfn1 overexpression (for 48h) in CAD cells, 15% SDS-PAGE gels and 20-25µg of sample were used; for the brain and spinal cord samples from floxed animals 15% SDS-PAGE gels and 25µg of protein were applied. Gels were transferred for 2 hours in a semi-dry system to a nitrocellulose membrane. Membranes were washed in TBS with 0.1% of Tween-20, blocked in 5% non-fat dried milk (Sigma) in TBS for 1 hour at room temperature, incubated with primary antibody (in either 5% BSA or 5% non-fat dried milk, in TBS) 1 hour at room temperature or overnight at 4ºC. Membranes were then washed and incubated with secondary antibody in 5% non-fat dried milk in TBS for 1

hour at room temperature and then incubated 5 minutes at room temperature with Pierce ECL (Pierce) for development. Chemiluminescence was analyzed by exposure to Amersham Hyperfilm ECL (GE Healthcare).

For western blotting the following primary antibodies were used: rabbit anti-phospho-Akt (S473) (1:1000; Cell Signaling), rabbit anti- phospho-Akt (T308) (1:1000; Cell Signaling), rabbit anti- total-Akt (1:1000; Cell Signaling), rabbit anti- phospho-GSK3β (S9) (1:500; Cell Signaling), rabbit anti- phospho-GSK3β (Y216) (1:500; Santa Cruz), mouse anti-GSK3α/β (1:1000; Santa Cruz), rabbit anti- phospho-PDK1 (S241) (1:1000; Cell Signaling), rabbit anti- total-PDK1 (1:1000; Cell Signaling), mouse anti- total-Pfn1 (1:1000; Santa Cruz Biotechnology), rabbit anti- phospho-Pfn1 (S137) (a kind gift from Dr Jieya Shao, University of California, San Francisco), mouse anti- β-actin (1:5000; Sigma, rabbit anti- cofilin-1 (kindly provided by Dr James Bamburg, Colorado State University, Fort Collins, Colorado, USA); rabbit anti-HPRT, 1:2000 (Santa Cruz Biotechnology). The secondary antibodies were: donkey anti-mouse or donkey anti-rabbit conjugated with HRP, 1:5000 (Jackson). Samples were homogenized in PBS with 0.3%Triton-X100 (Sigma), 1mM sodium orthovanadate (Sigma) and protease inhibitor cocktail (Roche).

DRG and Hippocampal neuron cultures

Briefly, for DRG neuron cultures, the animals used were 8 weeks old when sacrificed. DRGs were collected and digested for 90 minutes with 0.125% collagenase IV-S (C1189, Sigma). DRG were then triturated and passed through a 15% BSA gradient. Cells were counted and plated at a density of 40 cells/mm2 in previously treated 24-well plate coverslips, coated with 20µg/mL poly-L-lysine (P2636, Sigma) and 5µg/mL laminin (L2020, Sigma). Neurons were grown in DMEM:F12 (D8437, Sigma) supplemented with 1x B27 (Gibco), 1% penicillin/streptomycin (Gibco), 2mM L-glutamine (Gibco) and 50ng/mL NGF (01-125, Millipore). For neuronal outgrowth of cre+Pfn1$^{fl/fl}$ and cre+Pfn1$^{wt/wt}$ neurons, only YFP positive neurons were considered. For hippocampal neurons, cultures were performed following the general protocol detailed in the Kaech and Banker protocol (Kaech and Banker, 2006). Briefly, pregnant mice at E16.5 were sacrificed and pups were individually dissected and genotyped. The hippocampus of each pup was digested 15 minutes in 0.06% porcine tryspin solution (T4799, Sigma), triturated and plated at a density of 125 cells/mm2 in 24 well plates containing glass cover slips previously treated with 20µg/mL poly-L-lysine (P2636, Sigma). Neurons were plated in Neurobasal (21103-049, Invitrogen) supplemented

with 1x B27 (Gibco), 1% penicillin/streptomycin (Gibco) and 2mM L-glutamine (Gibco). For neurite outgrowth analysis, neurons were fixed 12 or 96h post plating (for DRG and hippocampal neurons, respectively), and immunofluorescence for βIII-tubulin (Promega, G7121, 1:2000) was performed. The length of the longest neurite was determined using NeuronJ plug-in for ImageJ.

Virus production and gene transduction

For viral production, HEK293T cells were seeded at 90% confluence in T75cm2 flasks and transfected using Lipofectamine (Invitrogen) with packaging plasmids pPAX (6µg) and VSVG (3µg) (a kind gift from Dr. Relvas, IBMC) and a lentiviral vector coding for puromycin resistance and expressing the ShRNA of interest (6µg, Sigma): for Pfn1 TRCN0000011969 and for Pfn2 TRCN0000071642; empty vector (pLKO- Sigma) was used as a control. Forty-eight hours post-transfection, the supernatants were collected, centrifuged at 1000 rpm for 5 minutes at room temperature and filtered through a 0.45µm filter. Viral titration was done by infecting HEK 293T cells with serial dilutions of viral stock and using puromycin selection. The knockdown efficiency of Pfn1 ShRNA was determined by transduction of rat DRG cultures, and selection with 2µg/ml of puromycin for 48h. Transcriptomes were obtained using the RNeasy Lipid Tissue Mini Kit (Qiagen) and expression levels were quantified by qPCR.

DRGs from cre^{+}Pfn1 mice or Wistar Rat, or hippocampal neurons from WT NMRI E16.5 embryos were isolated as mentioned previously. One (for DRG neurons) or 3 days (for hippocampal neurons) after plating, cells were infected with lentivirus (5000 IU per well), produced as described above, for 12–16 hours, and 24 hours later treated with puromycin (5µg/ml for DRG and 0.5µg/ml for hippocampal neurons) for 48 h. For neurite outgrowth assays, cells were trypsinized, replated for 12 h (for DRG) or for 48 hours (for hippocampal neurons), fixed and βIII-tubulin immunocytochemistry (1:1000; Promega) was done. Calculations of the Pfn1 and Pfn2 expression levels in DRG and hippocampal neurons were done by analysis of the Pfn1, Pfn2 and HPRT by qPCR.

Analysis of actin retrograde flow

DRG neurons from 8-weeks-old $cre^{+}Pfn1^{fl/fl}$ and $cre^{-}Pfn1^{fl/fl}$ mice, dissected and cultured as mentioned previously, were nucleofected (4D Nucleofector Amaxa system, Lonza, CU137 program) with either 750 ng LifeAct-mCherry (Riedl et al., 2008) (in the case of $cre^{+}Pfn1^{fl/fl}$ DRG neurons) or 750 ng LifeAct-mCherry plus 150 ng pmaxGFP™ (Lonza) (in the case of $cre^{-}Pfn1^{fl/fl}$ DRG neurons). After transfection, cells were left in

suspension overnight and then plated for 12 hours in a PLL (20µg/mL)/laminin (5µg/mL) coated µ-Dish 35 mm (Ibidi) previously treated with 2M HCl. Twelve hours after plating, time-lapse recordings were performed, in phenol-free DMEM/F12 (Invitrogen) supplemented as mentioned above, for 40 frames every 5 seconds at 37ºC on a Spinning Disk Confocal System Andor Revolution XD (ANDOR Technology, UK) equipped with an iXonEM+ DU-897 camera and with IQ 1.10.1 software (all from ANDOR Technology, UK). Kymographs were made using Kymograph plugin for ImageJ for retrograde flow quantification. Only cells double positive for either YFP (cre^+ neurons) or GFP (cre^- transfected neurons) and RFP (from the lifeact-RFP staining) were considered.

Overexpression of WT and Pfn1 mutants in hippocampal neurons and CAD cells

Residues of Pfn1 were mutated to generate a phospho-resistant Pfn1 (Pfn1S137A) and a phospho-mimetic Pfn1 (Pfn1S137D) mutantby PCR-based site-directed mutagenesis using QuickChange II XL (Agilent Technologies). Hippocampal neurons were cultured, as described above, and co-transfected with 200 ng pmaxGFP™ (Lonza) and 600 ng pCMV-SPORT6 vector coding the full length Pfn1 open reading frame (Addgene, clone IRATp970C034D) or each of the mutant plasmids mentioned above, before plating. Transfected cells were grown for 4 days and then fixed with 4% PFA (30 minutes). Immunofluorescence was done for βIII-tubulin and YFP+/βIII-tubulin+ neurons were selected for neurite outgrowth evaluation. For the analysis of the expression levels of WT Pfn1 and of the above mutants, transfection of the neuronal cell line CAD (Qi et al., 1997) was used. Protein extractions were performed 48 hours after transfection.

Acknowledgements

This work was funded by the International Foundation for Research in Paraplegia (IRP). Leite SC was supported by Fundação para a Ciência e Tecnologia (FCT) (SFRH/BD/72240/2010). We thank the excellent technical support of the IBMC Animal Facility.

References

Alto, L.T., Havton, L.A., Conner, J.M., Hollis, E.R., 2nd, Blesch, A., and Tuszynski, M.H. (2009). Chemotropic guidance facilitates axonal regeneration and synapse formation after spinal cord injury. Nat Neurosci 12, 1106-1113.

Arber, S., Barbayannis, F.A., Hanser, H., Schneider, C., Stanyon, C.A., Bernard, O., and Caroni, P. (1998). Regulation of actin dynamics through phosphorylation of cofilin by LIM-kinase. Nature 393, 805-809.

Bottcher, R.T., Wiesner, S., Braun, A., Wimmer, R., Berna, A., Elad, N., Medalia, O., Pfeifer, A., Aszodi, A., Costell, M., and Fassler, R. (2009). Profilin 1 is required for abscission during late cytokinesis of chondrocytes. EMBO J 28, 1157-1169.

Bradke, F., Fawcett, J.W., and Spira, M.E. (2012). Assembly of a new growth cone after axotomy: the precursor to axon regeneration. Nat Rev Neurosci 13, 183-193.

Da Silva, J.S., Medina, M., Zuliani, C., Di Nardo, A., Witke, W., and Dotti, C.G. (2003). RhoA/ROCK regulation of neuritogenesis via profilin IIa-mediated control of actin stability. J Cell Biol 162, 1267-1279.

Didry, D., Carlier, M.F., and Pantaloni, D. (1998). Synergy between actin depolymerizing factor/cofilin and profilin in increasing actin filament turnover. J Biol Chem 273, 25602-25611.

Flynn, K.C., Hellal, F., Neukirchen, D., Jacob, S., Tahirovic, S., Dupraz, S., Stern, S., Garvalov, B.K., Gurniak, C., Shaw, A.E., et al. (2012). ADF/cofilin-mediated actin retrograde flow directs neurite formation in the developing brain. Neuron 76, 1091-1107.

Fujita, Y., and Yamashita, T. (2014). Axon growth inhibition by RhoA/ROCK in the central nervous system. Front Neurosci 8, 338.

Garvalov, B.K., Flynn, K.C., Neukirchen, D., Meyn, L., Teusch, N., Wu, X., Brakebusch, C., Bamburg, J.R., and Bradke, F. (2007). Cdc42 regulates cofilin during the establishment of neuronal polarity. J Neurosci 27, 13117-13129.

Goldschmidt-Clermont, P.J., Machesky, L.M., Baldassare, J.J., and Pollard, T.D. (1990). The actin-binding protein profilin binds to PIP2 and inhibits its hydrolysis by phospholipase C. Science 247, 1575-1578.

Gomez, T.M., and Letourneau, P.C. (2014). Actin dynamics in growth cone motility and navigation. J Neurochem 129, 221-234.

Hemmings, B.A., and Restuccia, D.F. (2012). PI3K-PKB/Akt pathway. Cold Spring Harb Perspect Biol 4, a011189.

Hoffman, P.N. (2010). A conditioning lesion induces changes in gene expression and axonal transport that enhance regeneration by increasing the intrinsic growth state of axons. Exp Neurol 223, 11-18.

Kaech, S., and Banker, G. (2006). Culturing hippocampal neurons. Nat Protoc 1, 2406-2415.

Krishnan, K., and Moens, P.D.J. (2009). Structure and functions of profilins. 71-81.

Kullmann, J.A., Neumeyer, A., Gurniak, C.B., Friauf, E., Witke, W., and Rust, M.B. (2012a). Profilin1 is required for glial cell adhesion and radial migration of cerebellar granule neurons. EMBO Rep 13, 75-82.

Kullmann, J.A., Neumeyer, A., Wickertsheim, I., Bottcher, R.T., Costell, M., Deitmer, J.W., Witke, W., Friauf, E., and Rust, M.B. (2012b). Purkinje cell loss and motor coordination defects in profilin1 mutant mice. Neuroscience 223, 355-364.

Lassing, I., and Lindberg, U. (1988). Specificity of the interaction between phosphatidylinositol 4,5-bisphosphate and the profilin:actin complex. J Cell Biochem 37, 255-267.

Lee, C.W., Vitriol, E.A., Shim, S., Wise, A.L., Velayutham, R.P., and Zheng, J.Q. (2013). Dynamic localization of G-actin during membrane protrusion in neuronal motility. Curr Biol 23, 1046-1056.

Lewis, T.L., Jr., Courchet, J., and Polleux, F. (2013). Cell biology in neuroscience: Cellular and molecular mechanisms underlying axon formation, growth, and branching. J Cell Biol 202, 837-848.

Liz, M.A., Mar, F.M., Santos, T.E., Pimentel, H.I., Marques, A.M., Morgado, M.M., Vieira, S., Sousa, V.F., Pemble, H., Wittmann, T., et al. (2014). Neuronal deletion of GSK3beta increases microtubule speed in the growth cone and enhances axon regeneration via CRMP-2 and independently of MAP1B and CLASP2. BMC Biol 12, 47.

Mar, F.M., Bonni, A., and Sousa, M.M. (2014). Cell intrinsic control of axon regeneration. EMBO Rep 15, 254-263.

Martin, M., Benzina, O., Szabo, V., Vegh, A.G., Lucas, O., Cloitre, T., Scamps, F., and Gergely, C. (2013). Morphology and nanomechanics of sensory neurons growth cones following peripheral nerve injury. PLoS One 8, e56286.

Michaelsen, K., Murk, K., Zagrebelsky, M., Dreznjak, A., Jockusch, B.M., Rothkegel, M., and Korte, M. (2010). Fine-tuning of neuronal architecture requires two profilin isoforms. Proc Natl Acad Sci U S A 107, 15780-15785.

Moens, P.D. (2008). Protein Reviews. In Actin-Binding Proteins and Disease, C. dos Remedios, and D. Chhabra, eds. (Sydney: Springer), pp. 200-217.

Neuhoff, H., Sassoe-Pognetto, M., Panzanelli, P., Maas, C., Witke, W., and Kneussel, M. (2005). The actin-binding protein profilin I is localized at synaptic sites in an activity-regulated manner. Eur J Neurosci 21, 15-25.

Neumann, S., and Woolf, C.J. (1999). Regeneration of dorsal column fibers into and beyond the lesion site following adult spinal cord injury. Neuron 23, 83-91.

Pilo Boyl, P., Di Nardo, A., Mulle, C., Sassoe-Pognetto, M., Panzanelli, P., Mele, A., Kneussel, M., Costantini, V., Perlas, E., Massimi, M., et al. (2007). Profilin2 contributes to synaptic vesicle exocytosis, neuronal excitability, and novelty-seeking behavior. EMBO J 26, 2991-3002.

Qi, Y., Wang, J.K., McMillian, M., and Chikaraishi, D.M. (1997). Characterization of a CNS cell line, CAD, in which morphological differentiation is initiated by serum deprivation. J Neurosci 17, 1217-1225.

Read, D.E., and Gorman, A.M. (2009). Involvement of Akt in neurite outgrowth. Cell Mol Life Sci 66, 2975-2984.

Riedl, J., Crevenna, A.H., Kessenbrock, K., Yu, J.H., Neukirchen, D., Bista, M., Bradke, F., Jenne, D., Holak, T.A., Werb, Z., et al. (2008). Lifeact: a versatile marker to visualize F-actin. Nat Methods 5, 605-607.

Shao, J., Welch, W.J., Diprospero, N.A., and Diamond, M.I. (2008). Phosphorylation of profilin by ROCK1 regulates polyglutamine aggregation. Mol Cell Biol 28, 5196-5208.

Silver, J. (2009). CNS regeneration: only on one condition. Curr Biol 19, R444-446.

Stiess, M., and Bradke, F. (2011). Neuronal polarization: the cytoskeleton leads the way. Dev Neurobiol 71, 430-444.

Sumi, T., Matsumoto, K., Takai, Y., and Nakamura, T. (1999). Cofilin phosphorylation and actin cytoskeletal dynamics regulated by rho- and Cdc42-activated LIM-kinase 2. J Cell Biol 147, 1519-1532.

Witke, W., Podtelejnikov, A.V., Di Nardo, A., Sutherland, J.D., Gurniak, C.B., Dotti, C., and Mann, M. (1998). In mouse brain profilin I and profilin II associate with regulators of the endocytic pathway and actin assembly. EMBO J 17, 967-976.

Witke, W., Sutherland, J.D., Sharpe, A., Arai, M., and Kwiatkowski, D.J. (2001). Profilin I is essential for cell survival and cell division in early mouse development. Proc Natl Acad Sci U S A 98, 3832-3836.

Wu, C.H., Fallini, C., Ticozzi, N., Keagle, P.J., Sapp, P.C., Piotrowska, K., Lowe, P., Koppers, M., McKenna-Yasek, D., Baron, D.M., et al. (2012). Mutations in the profilin 1 gene cause familial amyotrophic lateral sclerosis. Nature 488, 499-503.

Ylera, B., Erturk, A., Hellal, F., Nadrigny, F., Hurtado, A., Tahirovic, S., Oudega, M., Kirchhoff, F., and Bradke, F. (2009). Chronically CNS-injured adult sensory neurons gain regenerative competence upon a lesion of their peripheral axon. Curr Biol 19, 930-936.

Young, P., Qiu, L., Wang, D., Zhao, S., Gross, J., and Feng, G. (2008). Single-neuron labeling with inducible Cre-mediated knockout in transgenic mice. Nat Neurosci 11, 721-728.

General conclusions and future perspectives

Our work led us to reach interesting conclusions and raises new conceptual perspectives that will need to be tested by future experiments. It is known that actin plays a crucial role in the neuritogenic process and that axon growth and regeneration depends on how efficient is the formation of a new growth-competent growth cone, which is critically dependent of the dynamics of its actin cytoskeleton.

The starting point of this Thesis was to find which actin-related proteins were playing a (important) role in the enhanced axon growth paradigm that the conditioning lesion model provides. It is known that conditioned neurons gain some embryonic-like characteristics, as a preference for extension instead of branching, and also the capacity to be sensitive to neurotrophic gradients, a very distinctive feature of the actin cytoskeleton in the embryonic growth cone. These features suggest a distinctive regulation of the actin cytoskeleton in conditioned neurons. ABPs are therefore very good candidates to be modulating this effect. In our analysis, we found two different ABPs differently regulated in the conditioning lesion model. Interestingly, one being a positive and the other a negative regulator of actin dynamics – Pfn1 and adducin, respectively. Moreover, in conditioned neurons Pfn1 activity was increased whereas adducin activity was inhibited, which reinforces the idea of the need of increased actin dynamics in the growth cone to achieve optimal axon growth.

Our studies with Pfn1 demonstrated that it is a fundamental component of the conditioning effect, which became evident when the double Pfn1 and Pfn2 deletion was performed. Moreover, the effect was not only visible *in vitro* but also *in vivo* when the conditioning lesion was performed in animals depleted of Pfn1 which resulted in decreased growth ability. These results are similar to those obtained using the animal model of ADF/Cofilin depletion, which lack the Pfn1 partner in the actin filament turnover. Contrarily to the Pfn1 depletion, overexpression of the Pfn1 constitutively active form – Pfn1S137A, which cannot be modulated by Rho GTPase signaling – led to increased axon growth capacity. One key future experiment will be the overexpression of this Pfn1 mutant in the DRG *in vivo*, to assess if the increased growth capacity is translated in a physiological context. It is also interesting to find that Pfn1 not only modulates the actin cytoskeleton but might also regulate the microtubule cytoskeleton. Supporting this hypothesis, that needs to be further substantiated by additional experiments, we show that Pfn1 overexpression increases AKT activation that leads to GSK3β inactivation through S9 phosphorylation. The GSK3β inhibition is a

well-known pro-regenerative event that leads to increased axon growth capacity both *in vitro* and *in vivo*.

The other ABP identified as being differently regulated in the conditioning effect was adducin – namely the α and γ forms. Interestingly, adducin KO neurons presented a highly dynamic actin cytoskeleton in the growth cones that led to an increased dynamics of the microtubule cytoskeleton. In culture adducin KO neurons presented increased growth capacity, even in non-permissive substrates, as the ones found in the spinal cord lesion site, as is the case of CSPGs and myelin. Moreover, when we assessed CNS axon regeneration using adducin KO mice, these presented an increased capacity to extend axons through the inhibitory glial scar.

Although the knockdown of adducin appears to be beneficial for CNS regeneration, its absence comes with a price. Adducins are ubiquitous ABPs that present inclusively a neuron (and erythrocyte) specific form, β-adducin. It is known that β-adducin KO mice present a myriad of impairments in the CNS, namely affecting synapse dynamics. Therefore, α-adducin KOs, that lack not only β but also α and γ adducin, could have additional deleterious effects in the nervous system. Our systematic analysis of the nervous system of the α-adducin KO mice revealed a generalized axonopathy, with axon enlargement and axon degeneration both in PNS and CNS tracts. Interestingly, the axon enlargement phenotype, was discovered when a new and revolutionary organization of the actin cytoskeleton – the axon actin rings, was described in neurons. Using a super-resolution method of imaging, a new cortical sub-membranar cytoskeleton was identified, and adducin was one of its three components (alongside actin and spectrin). Our data on adducin KO neurons shows that in the absence of adducin this cortical cytoskeleton can be assembled but that the rings of the adducin KO neurons are enlarged (i.e., they have an increased diameter). This points to a possible link between the absence of one of the components required for the axon actin rings with a phenotype of axon enlargement and degeneration. This finding certainly warrants further research.

Given the above, it is my belief that this work is a contribution to the understanding of the neuronal mechanisms that participate in axon regeneration and axonal stability during nervous system aging. There is still certainly a lot to be done, specifically in what respects the understanding of actin ring assembly and function in physiology and neurodegeneration but step by step is how the whole picture is drawn and understood.